Tackling the vascular heterogeneity issue in tumors: identification of novel targets for tumor therapy

Een wetenschappelijke proeve op het gebied van de Medische Wetenschappen

Proefschrift

ter verkrijging van de graad van doctor
aan de Radboud Universiteit Nijmegen
op gezag van de rector magnificus prof. mr. S.C.J.J. Kortmann,
volgens besluit van het college van decanen
in het openbaar te verdedigen op woensdag 11 november 2009
om 10.30 uur precies

door

Ilse Roodink
geboren op 3 februari 1980
te Ede

Promotor
Prof. dr. J.H.J.M. van Krieken

Copromotor
Dr. W.P.J. Leenders

Manuscriptcommissie
Prof. dr. O.C. Boerman
Prof. dr. W.T.A. van der Graaf
Prof. dr. G. Molema (UMC Groningen)

The studies presented in this thesis were performed at the Department of Pathology, Radboud University Medical Center, Nijmegen, the Netherlands.

This work was financially supported by N.V. Organon, a grant of the Radboud University Nijmegen Medical Centre, grants 5.91898, KUN 2000-2302, KUN 2005-3337 of the Dutch Cancer Society, and grant 14F06(2).03 of the Hersenstichting Nederland.

ISBN 978-90-9024637-6
Cover by De Rooij Art & Design, Velp
Printed by Ipskamp Drukkers B.V., Enschede

Contents

Chapter 1

General introduction

Despite considerable advances in treatment modalities during the last decades, cancer is still the second cause of death in the Western world. Improvements in the traditional approaches to cancer therapy, surgical removal of the tumor, radiotherapy and chemotherapy, have generally led to some improved prognosis of cancer patients. However, the majority of cancer related deaths are due to the occurrence of metastases, which may be too numerous to be treated by surgery, or recurrent tumors which may eventually become resistant to chemotherapeutic or radiotherapeutic treatment. In addition, conventional anti-tumor drugs and radiotherapy often non-selectively interfere with the basic proliferation machinery of cells, resulting in toxicity to non-malignant cells. This along with therapy resistance are major therapy-limiting factors.

Targeted therapy of solid tumors

With the increasing knowledge about the molecular pathways that lead to deranged growth in cancer, targeting of these pathways has also become possible, resulting in a burst of research in the field of targeted tumor therapies (Table 1). Since targeted therapies are directed against particular tumor-specific molecular targets, these are supposed to result in less toxicity compared to conventional anti-tumor therapies.

Tyrosine kinase inhibitors

The discovery that tyrosine kinase (TK) membrane receptors are often dysregulated in tumor cells in several ways has led to inhibitors of TKs as a novel class of therapeutic compounds in oncology.[1] Activation of TKs affects many cellular events involved in tumor progression including cell growth, proliferation, survival, adhesion, and migration. TK receptor signaling can be interrupted by antibodies against these receptors or their ligands. As an example, the humanized anti-EGFR antibody cetuximab inactivates EGFR by preventing the binding of its ligands EGF and TNFα, and promoting its internalization and lysosomal degradation. Another class of TK inhibitors includes small molecules that directly inhibit the catalytic activity of kinases via interference with binding of ATP.

c-KIT

Approximately 85% of the patients with gastrointestinal stromal tumors (GISTs) have activating mutations of the c-KIT TK, the receptor for the cytokine stem cell factor. Imatinib, a small-molecule inhibitor of the TK activities of c-KIT, is approved by the USA Food and Drug Administration (FDA) for treatment of advanced GIST. In a multicenter trial of imatinib in GIST patients that failed conventional therapy more than 80% of these patients showed response to imatinib treatment, although none of them showed complete response.[2] In addition, in 5% of these patients the tumor exhibited primary resistance to imatinib within the first two months.

Platelet-Derived Growth Factor Receptor (PDGFR)

Tumor cells in different malignancies are associated with (mutational) activation of PDGF or its receptors (PDGFR).[3,4] The PDGFRs (α and β) are activated by PDGFs (PDGF-A, -B, -C and -D). Because imatinib is also an inhibitor of PDFGRs, this agent has been evaluated in a number of malignancies in which PDGFR signaling has been implicated.

Due to a translocation that places the PDGF-B gene under control of the collagen 1A1 promoter, which is observed in more than 90% of dermatofibrosarcomas protuberans (DFSP), PDGF-B is up-regulated in these tumors resulting in overactivation of PDGFR-β. In a phase II study of eight patients with locally advanced DFSP treated with imatinib all patients achieved a clinical response, with four complete responses.[5]

Although overexpression of PDGFR-α has been documented in all grades of malignancy in glioma,[6] phase II trials revealed that imatinib had minimal single-agent activity in recurrent gliomas, since a partial response was observed in approximately 5% of the patients.[7,8] Currently, the therapeutic efficacy of imatinib in combination with chemotherapy in glioma patients is evaluated in several clinical trials. A phase II study of patients with recurrent high grade glioma already demonstrated that imatinib plus hydroxyurea had modest activity with a partial radiographic response in only 9% of the patients.[9]

High levels of PDGFR-α and PDGF have been reported in a subset of ovarian carcinomas.[10,11] A phase II trial of patients with recurrent epithelial ovarian or primary peritoneal carcinoma revealed that imatinib had minimal activity as single agent in these patients, although the majority of them had tumors co-expressing imatinib-sensitive receptors c-KIT and PDGFR-β.[12]

Human Epidermal Growth Factor Receptor family

Members of the human Epidermal Growth Factor Receptor (EGFR and HER2) family are overexpressed or mutated in many solid tumors.[13,14] Trastuzumab, a humanized monoclonal antibody which is FDA-approved for treatment of breast cancer, targets the receptor TK HER2, which is overexpressed in approximately 25% percent of invasive breast tumors. In patients with HER2-positive breast tumors addition of trastuzumab to chemotherapy significantly improved median time to progression (7.4 vs. 4.6 months) and median survival (25.1 vs. 20.3 months).[15] However, disease recurrence and trastuzumab resistance are observed in a subset of patients.[15,16]

Targeting EGFR TK signaling has demonstrated clinical activity in many solid tumor types.[13] Promising results in patients with advanced head and neck squamous cell carcinoma[17] and refractory metastatic colorectal cancer[18] led to the approval by the FDA of cetuximab, a chimeric monoclonal antibody to the extracellular domain of EGFR, for these patient populations. In contrast, recent data from a phase III trial of previously untreated metastatic colorectal cancer patients revealed that the addition of cetuximab to

capecitabine, oxaliplatin and bevacizumab resulted in a significantly decreased progression-free survival and inferior quality of life.[19] Of importance, a mutated, constitutively active K-ras bypasses the need for EGFR-mediated K-ras phosphorylation and renders tumors resistant to cetuximab therapy.

Erlotinib, a specific small molecule inhibitor of ATP binding by EGFR, displayed anti-tumor activity in refractory advanced non-small cell lung cancer[20] and advanced pancreatic cancer[21] and is approved by the FDA for treatment of these tumors. Recently, panitumumab, a human monoclonal antibody against EGFR, was approved by the FDA for metastastic colorectal cancer.[22] Although the EGFR gene is amplified in approximately 50% of high grade gliomas[23] only a small percentage of patients showed response to EGFR kinase inhibitors erlotinib or gefitinib, in particular those patients in whom glioma cells co-expressed EGFRvIII, a constitutively active mutant variant of EGFR, and wild-type PTEN.[24] A recent study confirmed the relatively poor therapeutic efficacy of erlotininb and gefitinib in patients with recurrent or progressive high grade glioma. Furthermore, in the responding subpopulation there was no consistent association with EGFRvIII/PTEN co-expression.[25] Very recently, the addition of erlotinib to standard treatment with radiotherapy and temozolomide did not demonstrate additive or synergistic effects in a phase I/II trial of newly diagnosed high grade glioma patients.[26]

Insulin-like Growth Factor Receptor type 1 (IGF-1R)

IGF-1R is frequently overexpressed in a variety of tumor types.[27] Different preclinical studies indicated that IGF-1R signaling, induced by binding of its principal ligand IGF-1, promotes tumor growth and metastasis which can be reduced by interference with IGF-1R-mediated signaling.[28-30] Preclinical testing also revealed that antibodies raised against IGF-1R have, in addition to directly blocking its ability to bind IGF-1, the potential to improve sensitivity and block resistance to other antitumor therapies.[29,30] Currently, various IGF-1R antibodies are evaluated in phase I and II trials. Results from a recent phase I trial of CP-751,871, a human monoclonal antibody against IGF-1R, in different advanced solid tumors suggest that a subset of patients treated with this antibody experience clinical benefit as evidenced by disease stabilization.[31] In addition, early data from different clinical trials support the observation from preclinical studies that targeting IGR-1R enhances the efficacy of cytotoxic cancer therapies.[32] However, due to the body-wide expression of IGF-1R targeting of this receptor might result in serious adverse effects. In addition, as IGF-1R and Insulin Receptor (IR) are nearly identical, compounds with crossreactivity to IR could induce toxicity. Interestingly, specific targeting of IGF-1R/IR hybrid receptors in addition to IGF-1R resulted in increased anti-tumor activity *in vivo*.[33]

Mammalian target of rapamycin (mTOR) inhibitors

mTOR is a cytoplasmic serine-threonine kinase of the phosphatidylinositol 3-kinase (PI3K)/Akt signalling pathway and as such involved in the regulation of cellular metabolism, growth, proliferation, and angiogenesis. Upon stimulation growth factor receptor TKs recruit PI3K leading to activation of Akt, which subsequently phosphorylates mTOR resulting in increased translation rates, enhanced phosphorylation of Akt and effects on actin skeleton.[34,35] In a phase III study patients with newly diagnosed advanced renal cell carcinoma treated with temsirolimus, a specific inhibitor of mTOR kinase, exhibited improved median progression-free and median survival compared with those receiving interferon (3.8 vs. 1.9 months and 10.9 vs. 7.3 months respectively).[36] Despite an objective response rate of 8.6%, these trial results led to the recent approval of temsirolimus by the FDA for treatment of this patient population.

Table 1. Targeted therapies of solid tumors

Compound	Target(s) in solid tumors	FDA approved for	Adverse effects
Imatinib	c-KIT PDGFR	Gastrointestinal stromal tumors	Hemorrhages Diarrhea Edema Fatigue
Trastuzumab	HER2	Breast cancer	Cardiac dysfunction
Cetuximab	EGFR	Advanced head and neck squamous cell carcinoma Metastatic colorectal tumors	Acneiform rash
Erlotinib	EGFR	Refractory advanced non-small cell lung cancer Advanced pancreatic cancer	Rash Diarrhea Stomatitis Infection
Panitumumab	EGFR	Metastastic colorectal cancer	Skin toxicities Diarrhea
Temsirolimus	mTOR	Advanced renal cell carcinoma	Rash Peripheral edema Stomatitis

Antibody-Dependent Cell-Mediated Cytotoxicity

Apart from selective and specific blockade of signaling pathways, clinical efficacy of monoclonal antibodies may also be a result of their ability to activate the immune system, called antibody-dependent cellular cytotoxicity (ADCC), which differentiates them from small molecule compounds.[37] ADCC occurs when tumor cell-bound antibodies interact via their Fc domain with Fcγ receptors (FcγR) on the surface of effector cells, principally natural killer cells, resulting in the release of cytotoxic substances (perphorin) and

subsequent lysis of the target cell. In addition, macrophages also express FcγRs and can induce phagocytosis of antibody-bound tumor cells as well as enhance ADCC through release of proteases and reactive oxygen species.[38] The ability of monoclonal antibodies to induce ADCC depends on their isotype. Whereas IgG1 and IgG3 antibodies bind very well to FcγRs, IgG2 and IgG4 isotypes bind weakly to these receptors.[37,38] Because trastuzumab and cetuximab have a human IgG1 backbone they potentially can provoke immunologic anti-tumor effects. Indeed, ADCC activity was found to play a prominent role in the efficacy of trastuzumab in a mouse xenograft model of breast cancer.[39] In addition, cetuximab is described to induce ADCC activity against different EGFR-expressing tumor cell lines.[40,41]

Pitfalls of targeted tumor therapy

Targeted cancer therapy has been proposed as a promising therapeutic approach in oncology. However, as described above, results from clinical trials demonstrate that most targeted therapies are likely beneficial for only a small subset of cancer patients. Due to the generally heterogeneous nature of cancer, different tumor cells may depend on different specific signaling pathways for progression and display specific antigens, which differ between, or even within various tumor types or within an individual tumor. This calls for tailor-made therapy approaches as pan-tumor cell targets which are present in the majority of cancer patients have not yet been identified.

Another factor limiting efficient targeted therapy in solid tumors is the distribution of targeting agents to tumor cells, which may be inadequate due to elevated tumor interstitial pressure, poor or irregular tumor vascularisation and slow diffusion of large molecules, which all worsen with increasing tumor size. In case of astrocytomas in the brain, the blood brain barrier which is generally intact in large areas of these tumors, precludes efficient delivery of therapeutic compounds. Although specific targeting of malignant cells results in moderate toxicity compared to conventional anti-tumor therapies (Table 1), tumor cells also frequently adjust to targeted tumor therapy, resulting in therapy resistance, also to TK targeted treatments.[1]

Alternatively, the beneficial effects of targeting stroma of solid tumors, including blood vessels, fibroblasts and macrophages, is now widely recognized. An efficient blood supply is crucial for tumor growth and metastasis and already in the early 1970s interference with the tumor blood supply was proposed as an attractive therapeutic option.[42] Unlike tumor cells, tumor endothelial cells are well accessible to intravenously administered compounds and are genetically stable, reducing the risk of therapy resistance. Importantly, therapy directed against tumor vasculature may be effective against a range of tumor types.

Tumor angiogenesis

To grow beyond a size of 1-2 mm^3, solid tumors depend on the formation of new blood vessels from pre-existing ones to supply them with nutrients and oxygen.[43] In addition, tumor angiogenesis propagates tumor progression by increasing the opportunity for tumor cells to enter the circulation and disseminate.

Tumor angiogenesis (figure 1) is orchestrated by a variety of pro- and anti-angiogenic molecules which are secreted by tumor cells and supportive cells, such as tumor-associated endothelial cells, pericytes, smooth muscle cells, fibroblasts, and macrophages. The relative balance of pro- and anti-angiogenic molecules in the tumor micro-environment can switch angiogenesis on or off. When pro-angiogenic factors outbalance the action of anti-angiogenic molecules, the tumor acquires an angiogenic phenotype that leads to the formation of new blood vessels. Different situations, such as hypoxia and metabolic and mechanical stresses, and activation of oncogenes and inactivation of tumor-suppressor genes[44,45] can provoke an unbalanced shift towards pro-angiogenic factors, including Vascular Endothelial Growth Factor (VEGF), Angiopoietins, PDGF and others.

Angiogenesis is a complex, multistep process which starts with VEGF-A-induced vasodilatation and increased vascular permeability of pre-existing capillaries, or post-capillary venules (Fig. 1B). The vascular permeability allows the extravasation of plasma proteins such as fibrinogen, which is subsequently converted to fibrin serving as a provisional matrix for migrating endothelial cells. This is accompanied by Angiopoietin-2 mediated detachment of pericytes (Fig. 1B).[46] To allow endothelial cells to migrate towards chemotactic angiogenic stimuli the vascular basement membrane and extracellular matrix surrounding pre-existing capillaries are degraded by proteases, in particular matrix metalloproteinases, secreted by tumor cells and supporting cells.[47] Subsequently, endothelial cells proliferate, invade the surrounding extracellular matrix and adhere to each other to form hollow tubes (Fig. 1C). This is accompanied by Angiopoietin 1- and PDGF-B-induced recruitment of perivascular cells and basement membrane formation around the newly formed vessels. Finally, blood vessel sprouts fuse with other sprouts to form vascular loops. During physiological angiogenesis, as occurs during embryonic development and the menstruation cycle, the tightly regulated balance of pro- and anti-angiogenic signals results in rapid maturation and stabilization of newly formed microvasculature. However this step is incomplete during tumor-associated angiogenesis leading to formation of tumor vessels that are architecturally different from their normal counterparts (Fig. 1D).[44] They spread without any organization, are tortuous, irregularly shaped, dilated, leaky, and poorly differentiated.[48] Tumor vessels may have thin walls, with only partial endothelial linings, loss of adherence between endothelial junctions, loosely attached or absent perivascular cells and a discontinuous basement

membrane.[49,50] These structural abnormalities contribute to an inefficient and irregular blood flow, which is slow and may be stationary or even exhibit turbulence or a reversal in the direction of flow. In addition, the hyperpermeability of tumor vasculature leads to elevated hydrostatic pressure in the interstitium. Importantly, both the inefficient tumor blood flow and interstitial hypertension reduces efficient delivery of chemotherapy to the tumor.[51]

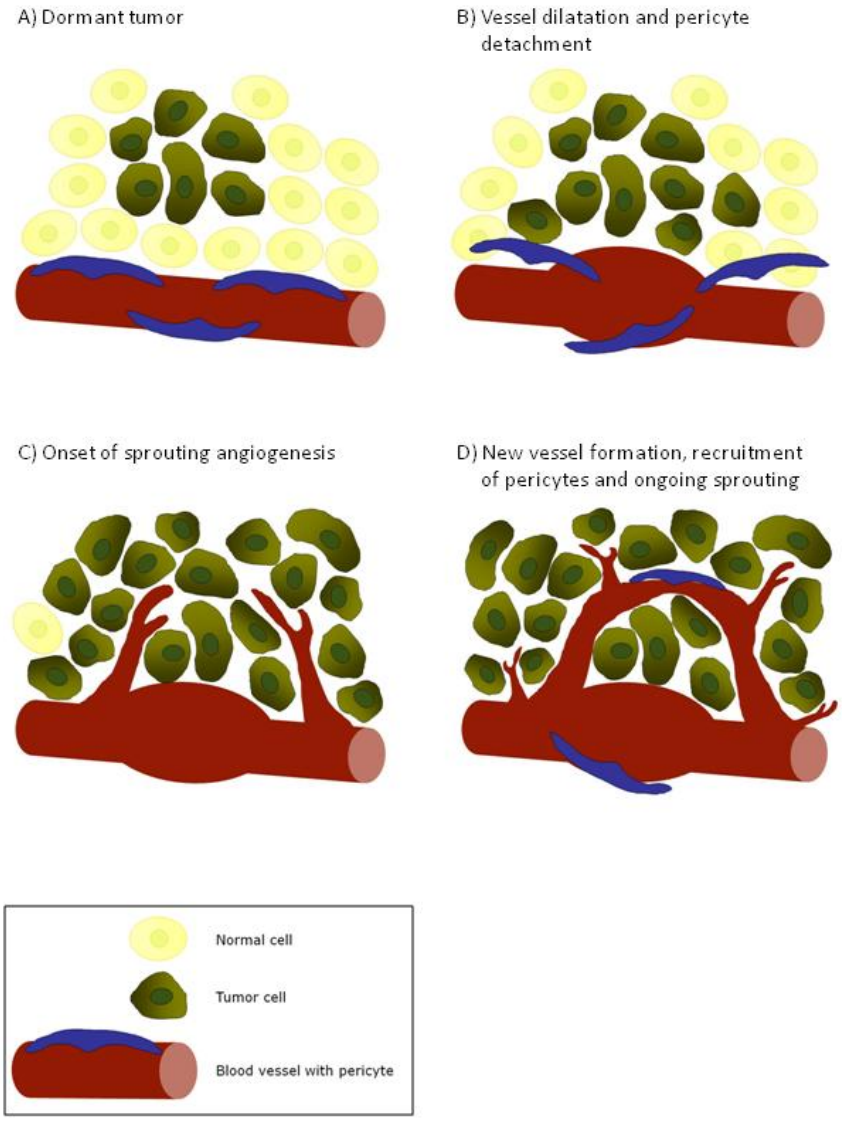

Figure 1. Schematic overview of tumor angiogenesis

Inhibition of angiogenesis

The knowledge that has been gathered in the last decade on the formation of neovasculature in tumors led to the development of compounds that interfere with different pathways of the angiogenic process. In particular, three pathways have received considerable attention, VEGF and its receptor VEGFR2, the angiopoietins and their Tie2 receptor, and PDGF-B and its receptor PDGFR-β.

VEGF-A/VEGFR2 pathway

VEGF-A-mediated signal transduction via its TK receptor VEGFR2 and possibly VEGFR1 and the neuropilin class of receptors leads to a cascade of different signaling pathways, resulting in proliferation and migration of endothelial cells, production of tissue factor and proteases, vascular permeability and deposition of extravascular fibrin which serves as provisional matrix for newly formed endothelial cells.[50,52-54] Alternative splicing yields at least six VEGF-A isoforms, existing of 121, 145, 165, 183, 189 and 206 amino acid residues,[55-57] which differ in their incorporation of exons that determine the degree of cell surface and extracellular matrix association. While VEGF-A_{121} lacks these exons and is able to act at more distal sites because it is freely released from producing cells, the larger isoforms remain more cell and extracellular matrix associated resulting in effects on nearby vessels. Hypoxia, often relevant in the centers of rapidly growing tumors, is an important inducer of VEGF-A expression. In addition, expression of VEGF-A may also be induced by genetic mutations and several cytokines and growth factors.[52,58]

The search for anti-angiogenic strategies for cancer treatment mainly focused on compounds that target the VEGF-A signaling pathway. Many of such agents have been developed and preclinical testing indicated that targeting of the VEGF-A/VEGFR2 pathway resulted in significant inhibition of neovascularization and tumor growth in various mouse xenograft models.[59-63]

Angiopoietin/Tie2 pathway

Despite its requisite role in vascular formation, VEGF-A must work in concert with other factors, among which the angiopoietins. Although angiopoietins are not able to induce tumor angiogenesis, they are involved in the angiogenic process at the level of vessel stabilization and maturation.[64,65] The angiopoietins include angiopoietin-1 (Ang-1) through angiopoietin-4 (Ang-4). The best studied are Ang-1 and Ang-2 which have similar binding affinity for the endothelial cell specific TK receptor Tie2. Whereas binding of Ang-1 to its receptor induces autophosphorylation of Tie2, Ang-2 antagonizes the actions of Ang-1 by competitively binding to Tie2 without activating the receptor (in endothelial cells). Ang-1/Tie2 signaling promotes recruitment of perivascular cells to immature angiogenic vessels and maintenance of the association of endothelial cells with surrounding support

cells and the matrix, resulting in vessel stabilization and maturation. Ang-2 is expressed primarily at sites of vascular remodeling, where it blocks the constitutive stabilizing action of Ang-1/Tie2 signaling, resulting in dissociation of perivascular cells and reduced contact of endothelial cells with the matrix, thereby preventing tumor vessel differentiation and maturation.[46,66] This destabilizing action of Ang-2 facilitates the angiogenic action of VEGF, whereas such destabilization in the absence of VEGF leads to vessel regression.[46] Although blockade of the angiopoietin/Tie2 pathway seems difficult due to the complexity of agonistic and antagonistic ligands for the same receptor, different mouse tumor models revealed that *in vivo* interference with the Tie2 pathway resulted in reduced tumor vascularization and tumor growth.[67-70] In addition, antibodies against Ang-2 were also able to block tumor angiogenesis and tumor growth in preclinical models.[71]

PDGF-B/PDGFR-β pathway

Although above described anti-angiogenic approaches focus on receptor TKs that are selectively expressed within the vascular endothelium, recent data imply that targeting tumor associated pericytes may provide additional benefits. As is clear from the role of the Ang/Tie2 pathway, TK inhibitors reducing pericyte coverage of tumor vessels might have anti-tumor activity, in part by sensitizing them to inhibition of endothelial receptor TKs.[46]

PDGF-B signaling via PDGFR-β, located on pericytes in the tumor stroma, plays a key role in angiogenesis and vessel maturation.[3] PDGFR-β expression by pericytes is necessary for their recruitment to tumor vessels, whereas PDGF-B produced by tumor endothelium is required for the recruitment of adequate numbers of pericytes, as well as for proper integration of pericytes in the vascular wall.[72] Adequate pericyte coverage functionally affects the tumor vasculature by promoting vessel stabilization and maturation thereby enhancing tumor perfusion. Blockade of signaling via PDGFRs in established tumors in transgenic RIP1Tag2 transgenic mice, which spontaneously develop pancreatic carcinomas, resulted in marked detachment of pericytes from tumor vessels and enlargement and distortion of these vessels leading to vascular dysfunction and reduced tumor growth.[73] Treatment of early carcinomas with PDGFR inhibitors did not show an anti-tumor effect. Conversely, blockade of VEGF signaling was effective in the early stages of tumor formation, but not in advanced tumors. Simultaneous inhibition of early angiogenesis and vessel maturation by targeting VEGF and PDGF receptors indeed showed increased anti-tumor activity. Noteworthy, several multitargeted agents inhibit both VEGF and PDGF receptors, and thus inhibition of PDGFRs present on pericytes might contribute to the anti-angiogenic effects of these compounds.[59-61]

Apart from targeting PDGF signaling via PDGFRs on pericytes, a recent study indicated that imatinib-induced blockade of PDGF signaling in carcimona-associated fibroblasts can

reduce tumor progression via down-regulation of fibroblast growth factors, thereby reducing tumor cell proliferation and angiogenesis.[74]

Relevance of tumor micro-environment

The angiogenic switch can occur at different stages of tumor progression, depending not only on the tumor type, but also on the specific tumor microenvironment. It is commonly accepted that most solid tumors originate as small avascular lesions, which initially thrive on pre-existent vessels in their surrounding micro-environment. In the next phase hypoxia arises because proliferating tumor cells outgrow the capacity of the existing vasculature, leading to the localization of tumor cells beyond the maximum oxygen diffusion distance from supplying vessels. As a result, VEGF-A is overexpressed initiating tumor vascularization. However, it is now realized that when tumors arise in vessel dense tissues they do not progress in an angiogenic fashion, but rather associate with and grow preferentially along existing vessels, a process called vessel co-option.[65,75] We showed in a mouse brain metastasis model of human melanoma that in the well vascularized brain Mel57 cells grow to highly infiltrative tumors without the induction of angiogenesis.[76] In this micro-environment tumor cells are able to thrive in the presence of pre-existing brain vasculature without becoming hypoxic by infiltrating the brain parenchyma in the perivascular space. In contrast, after subcutaneous injection these same cells grow to highly necrotic tumors with only a small viable tumor rim. In this point of view it is important to realize that many traditional tumor xenograft models generally involve the inoculation of tumor cells in the essentially avascular subcutaneous space. These experimental tumors are devoid of blood supply, forcing them to induce angiogenesis in order to grow. Interestingly, in the same mouse brain metastasis model of human melanoma we demonstrated that the most frequent VEGF-A isoforms, VEGF-A_{121}, $_{165}$ and $_{189}$, contribute differentially to the process of tumor vascularization. While stably transfected Mel57 cells overexpressing VEGF-A_{165} or VEGF-A_{189} develop to highly angiogenic brain lesions, VEGF-A_{121} overexpression results in profound peritumoral vasodilatation of mature pre-existent vessels thereby increasing the tumor's blood supply, and thus tumor growth, without inducing a true angiogenic response.[77,78]

Altogether these data demonstrate that tumors arising within or metastasizing to vessel-rich tissues can grow along (modulated) pre-existent vessels to form a well vascularized lesion. Prototype clinical tumors which may progress almost exclusively without the induction of angiogenesis are diffuse infiltrative gliomas, the most frequent primary brain tumors, which are aggressive and highly invasive tumors considered to be among the deadliest of human cancers.[79] Diffuse infiltrative gliomas are classified according to their suspected line of differentiation (astrocytic, oligodendroglial, oligoastrocytic) and graded on a scale of I to IV according to their degree of malignancy.[80,81] Diffuse infiltrative gliomas

grow along pre-existing normal brain capillaries and may infiltrate throughout the whole brain parenchyma.[79] In the most malignant manifestation of glioma, glioblastoma multiforme (GBM), rapidly proliferating tumor cells outgrow the capacity of the brain vasculature. In this situation, local hypoxia arises which results in induction of VEGF-A expression and angiogenesis and microvascular proliferations in these areas.[82,83] Due the prominent diffuse infiltrative growth in the surrounding brain tissue, surgery or radiotherapy of gliomas is hardly ever curative. In addition, the intact blood-brain barrier in these diffuse infiltrative areas contributes to a poor response of these tumors to conventional tumor therapies[79,81,82], whereas epigenetic alterations in gliomas result in intrinsic resistance to DNA-alkylating agents further deteriorating the efficacy of chemotherapy.[84] GBM is apart from the most aggressive form of glioma also the most frequent one, accounting for 40% of all primary brain tumors. Despite improvements in the treatment of GBM by surgery, radiotherapy and chemotherapy, the prognosis of patients affected by GBM remains relatively poor, with median overall survival times of 1-2 year. Although angiogenesis inhibition does not affect diffuse infiltrative, co-optive growth, it is yet considered as a suitable anti-tumor approach for GBM patients, given the characteristic areas of prominent angiogenesis and microvascular proliferations in these tumors.[82,83]

Translation to the clinic

Results obtained from preclinical studies indicated that anti-angiogenic agents induced tumor stabilization or even regression in subcutaneous tumor models. As the suboptimal character of subcutaneous tumors for the purpose of studying anti-angiogenic therapy was not recognized at that time, these findings led to the assumption that also in the clinic anti-angiogenic therapy could turn cancer into a chronic disease. This resulted in numerous clinical trials evaluating the beneficial effects of different anti-angiogenic agents. To date three of them are approved by the FDA (Table 2).

Bevacizumab

Bevacizumab (a humanized antibody against all isoforms of VEGF-A[62]) has become part of first line treatment of patients with metastatic colorectal cancer, non-small-cell lung cancer and metastatic breast cancer. As monotherapy, bevacizumab prolonged the time to progression and improved response rates in patients with advanced renal cell carcinoma,[85] epithelial ovarian cancer and peritoneal cancer.[86,87] However, in combination with chemotherapy bevacizumab also increased overall survival in patients with metastatic colorectal cancer[88-90] and non-small-cell lung cancer,[91] while the benefit of bevacizumab therapy for patients with metastatic breast cancer was limited to increased

response rate and prolonged progression-free survival.[92,93] Although GBMs are considered as good candidates for anti-angiogenic therapy, a phase II pilot study of bevacizumab in combination with temozolomide and radiation therapy in patients with newly diagnosed GBM revealed modest therapy efficacy as evidenced by the progression-free survival (>8.8 months).[94] In addition, one study evaluating treatment efficacy of the combination of bevacizumab and irinotecan in 13 patients with recurrent heavily pretreated GBM revealed that 10 patients had a partial response and 3 stable disease. However, after the initial response 8 patients had aggressive patterns of disease progression.[95] It is now well accepted that the initial response which is seen in these patients on contrast-enhanced MRI, may be overestimated due to restoring effects of bevacizumab therapy on the blood brain barrier.[96]

Sorafenib

The small compound multi-targeted receptor TK inhibitor sorafenib, which inhibits among others VEGFR2, and PDGFRβ,[61] has been approved for treatment of metastatic renal cell cancer and advanced hepatocellular carcinoma. Single-agent sorafenib therapy had significant disease-stabilizing activity and prolongs progression-free survival in patients with advanced renal cell carcinoma[97,98] from 2.8 months to 5.5 months[97] and resulted in a 3-month overall survival benefit in patients with advanced hepatocellular carcinoma.[99] Due to its activity against multiple kinases, sorafenib was brought into various trials in different malignancies. Recent results in patients with advanced melanoma and thyroid carcinoma showed promising response rates and progression-free survival improvements of sorafenib therapy,[100-102] while sorafenib had only modest anti-tumor activity in patients with advanced prostate cancer[103,104] and patients with advanced head and neck cancer.[105]

Sunitinib

Sunitinib, like sorafenib a small compound multikinase inhibitor directed against among others VEGFR2, and PDGFRβ,[60] is now approved for treatment of advanced renal cell cancer and gastrointestinal stromal tumors in patients who had been treated unsuccessfully with imatinib. Sunitinib monotherapy in patients with metastatic renal cell carcinoma resulted in improved response rates and a progression-free survival benefit.[106-109] Phase II trials demonstrated that sunitinib is associated with anti-tumor activity in advanced non-small-cell lung cancer,[110] metastatic breast cancer [111] and advanced pancreatic neuroedocrine tumors,[112] whereas its efficacy in advanced carcinoid patients could not be determined.[112] Patients with advanced gastrointestinal stromal tumors withdrawn from imatinib treatment exhibited significantly longer time to tumor progression with sunitinib and improved overall survival.[113] However, these effects may be also attributable to targeting c-KIT which is frequently expressed on tumor cells in GIST.

Table 2. Anti-angiogenic therapies

Compound	Target(s)	FDA approved for	Adverse effects
Bevacizumab	VEGF-A	Metastatic colorectal cancer Non-small-cell lung cancer Metastatic breast cancer	Hypertension Hemorrhages Thrombosis Proteinuria Wound dehiscence Fatigue Headaches
Sorafenib	VEGFR2 and -3 PDGFRβ Flt-3 c-KIT Raf	Metastatic renal cell cancer Advanced hepatocellular carcinoma	Diarrhea Hand–foot syndrome Rash Fatigue Hypertension
Sunitinib	VEGFR2 PDGFRβ Flt-3 c-KIT	Advanced renal cell cancer Gastrointestinal stromal tumors withdrawn from imatinib	Diarrhea Hand-foot syndrome Fatigue Hypertension

Although inhibition of angiogenesis has emerged as an important therapeutic strategy, clinical trials demonstrated that different tumor types respond differently to anti-angiogenic therapy. Strikingly, as single agent therapy all three approved anti-angiogenic compounds have clinical activity in renal cell carcinoma patients. Since the von Hippel-Lindau gene is mutated or silenced in approximately 80% of renal cell carcinomas, leading to constitutive overexpression of VEGF-A, these develop as truely angiogenic tumors. So, anti-angiogenic monotherapy significantly reduces progression of tumors with a truely angiogenic phenotype as also observed in ovarian cancer,[114] whereas in most other, probably not entirely angiogenic tumors the beneficial effects of monotherapy with anti-angiogenic agents are rather disappointing. The prolonged overall survival of patients with metastatic colorectal cancer or non-small-cell lung cancer, seen when bevacizumab is added to chemotherapy is hypothesized to be due to anti-angiogenic treatment-induced vessel normalization.[115] As discussed above, the imbalanced expression of angiogenic factors during tumor-associated angiogenesis leads to a structurally abnormal vasculature which results in impaired blood supply and interstitial hypertension, both interfering with the delivery of therapeutics. Anti-angiogenic therapy inactivates the excess of pro-angiogenic stimuli and is hypothesized to induce morphological changes leading to a more normal vasculature. These normalized vessels would be more regularly shaped, less tortuous and less permeable resulting in increased tumor blood supply and reduced interstitial pressure thereby improving the distribution of therapeutics.

Pitfalls of anti-angiogenic therapy in the clinic

Because preclinical studies indicated that targeting of angiogenic pathways almost without exception resulted in tumor stabilization or even regression,[59-63,67-71,73,116] there is a clear discrepancy with the efficacy of anti-angiogenic therapy in clinical settings. For this, there is a number of possible explanations. As already indicated, preclinical testing of anti-angiogenic compounds is predominantly performed in experimental tumors which grow in the avascular subcutaneous space, forcing them to induce angiogenesis in order to grow. Consequently, this setting leads to the selection of tumors that have the ability to induce angiogenesis and thus will be susceptible to anti-angiogenic therapy. In contrast, clinical tumors frequently grow in tissues with intrinsically high vessel densities, which may, as discussed above, progress independently of angiogenesis via infiltration and incorporation of pre-existing blood vessels.[76,78] Such tumors are less sensitive to anti-angiogenic therapy. Importantly, the aim of anti-angiogenic therapy is to halt progression of otherwise untreatable, mostly disseminated, cancers. However, most metastases are blood-borne and generally grow in vessel dense tissues (e.g. bone, liver, lung and brain). Consequently, metastatic lesions may progress by co-option of pre-existent vasculature, rendering them resistant to anti-angiogenic therapy. In addition, we demonstrated in a brain metastasis model of human melanoma that stably transfected tumor cells overexpressing VEGF-A_{165} which develop to highly angiogenic tumors in the brain parenchyma,[77] do not regress in response to treatment with the angiogenesis inhibitor vandetanib, but rather progress via increased reliance of tumor cells on vessel co-option.[117] This provides tumors in a well vascularized environment with an escape mechanism which makes them partially insusceptible to anti-angiogenic compounds by shifting their phenotype to vessel co-option. Similarly, we and others showed in different orthotopic mouse models of glioma that high grade gliomas do not adequately respond to anti-angiogenic therapy due to progression of tumor cells via co-option of pre-existing brain capillaries.[96,118-121] Importantly, a recent clinical study of bevacizumab in combination with irinotecan in GBM patients revealed that after an initial response the majority of patients indeed experience aggressive patterns of disease progression, including gliomatosis cerebri, which is characterized by its wide diffuse infiltration throughout the brain.[95] In gliomas there is another factor complicating anti-angiogenic therapy. Whereas the beneficial effects of anti-angiogenic therapy in combination with chemotherapy are hypothesized to be attributable to anti-angiogenic treatment-induced vessels normalization in patients with metastatic colorectal cancer or non-small-cell lung cancer, in gliomas normalization of the vascular bed involves restoration of the blood-brain barrier, thereby possibly hampering, instead of enhancing, the delivery of therapeutic compounds to tumor cells.[120,122] However, the reduced vascular permeability also results in decreased interstitial pressure

and cerebral edema thereby improving quality of life of glioma patients treated with anti-angiogenic therapy.[123]

As discussed above, despite improvements in the standard treatment of GBM and several attempts to gain clinical benefit with the addition of therapies specifically targeting tumor cells, treatment efficacy of these tumors is still unsatisfactory. In addition, although high grade gliomas have long been considered as good candidates for anti-angiogenic therapy, preclinical results from orthotopic mouse models of glioma and recent data from clinical studies suggest otherwise. So, there is an urgent need for new approaches to improve treatment efficacy of these fatal tumors. Since gliomas, like other tumor types growing in well vascularized tissues, may progress via vessel co-option, targeting the existing vascular bed, instead of prevention of the formation thereof, seems an attractive approach.

Vascular targeting

Targeting the genetically stable tumor endothelium, which is well accessible after intravenous injection of agents (without hindrance by the blood brain barrier in gliomas), may be a good alternative therapy to disrupt a tumor's blood supply. This approach requires the availability of tumor-vessel specific targeting agents (TVTAs) with high enough specificity for existing tumor vasculature. Few candidate TVTAs have been identified so far. Effective tumor vessel targeting can be achieved with the L19 single chain antibody which is directed against the ED-B fragment of fibronectin, a splice variant which is deposited in the extracellular matrix of newly formed vessels only in actively growing tumors,[124] whereas this single chain antibody was unable to detect quiescent endothelium in low grade malignancies.[125] RGD peptides have been used to successfully target integrin αvβ3 *in vivo*.[126] Receptor-targeted radiotherapy using radiolabeled RGD peptides has been shown to reduce tumor growth in xenograft mouse models.[127,128] However, expression of αvβ3 is restricted to immature vessels. In addition, this integrin is also present on intestinal epithelium. Recombinant fusion proteins of a truncated form of the coagulation-inducing protein tissue factor with vascular cell adhesion molecule 1 (VCAM-1), a luminal tumor endothelial antigen expressed in angiogenic vessels, induced tumor specific blood clotting, tumor necrosis and growth delay in different xenograft models.[129] Since endoglin is strongly expressed in vasculature of different solid tumors it has been proposed as an attractive vascular molecule for targeted therapy, however, this protein is also observed in the vasculature of normal adult tissues, limiting its clinical usefulness.[130]

Outline of this thesis

Tumors obtain their blood supply by the formation of new vasculature or by the incorporation, and possibly subsequent modulation, of pre-existent vessels. Importantly,

vascular targeting, which is at the moment restricted to vessels in early maturation stages, requires that TVTAs with specificity for the entire existing vascular bed, including co-opted vessels, become available.

The overall aim of this thesis was to map vascular heterogeneity between and within different clinical brain tumors and to identify novel vascular targets which may be of clinical use for treatment of these tumors. We set up a powerful platform for the identification of targetable tumor vessel associated markers.

In chapter 2 vascular phenotypes of primary and metastatic clinical brain tumors are correlated with their VEGF-A expression profiles, resulting in a model where constitutively VEGF-A expressing tumors present with different vascular beds than tumors in which VEGF-A is expressed as a response to central hypoxia. Chapter 3 demonstrates the identification of a novel tumor vascular target: Plexin D1. Expression of this protein is examined during tumor angiogenesis in a brain metastasis model of human melanoma. In addition, this chapter describes the expression of Plexin D1 on both tumor vessels and tumor cells in a number of primary and metastatic clinical brain tumors. Furthermore, Plexin D1 recognizing antibodies are isolated and analyzed for their ability to target to melanoma brain metastases in a mouse model. Chapter 4 describes expression of Plexin D1 and one of its ligands, Semaphorin 3E, in a series of cutaneous melanocytic lesions representing different stages of melanoma progression. In addition, functional effects of Semaphorin 3E overexpression on tumor development are examined in a xenograft model of metastatic melanoma. In chapter 5, Plexin D1 expression is further evaluated in a large number of different clinical tumors and non-tumor related human tissues. Chapter 6 describes the isolation of a tumor vessel targeting nanobody by *in vivo* biopanning of a phage display library in an orthotopic mouse model of glioma, the identification of its ligand and the expression of this ligand in different tumor xenograft models and a number of clinical gliomas. In addition, a platform for identification of novel targetable vessel associated markers is introduced. In chapter 7 we have extended our nanobody phage display technology by generating a novel nanobody library from an immunized Llama and subsequent isolation of additional TVTAs by *in vivo* biopanning of this library in orthotopic mouse models of glioma. Chapter 8 summarizes the results and discusses future perspectives.

Chapter 2

Development of the tumor vascular bed in response to hypoxia-induced VEGF-A differs from that in tumors with constitutive VEGF-A expression

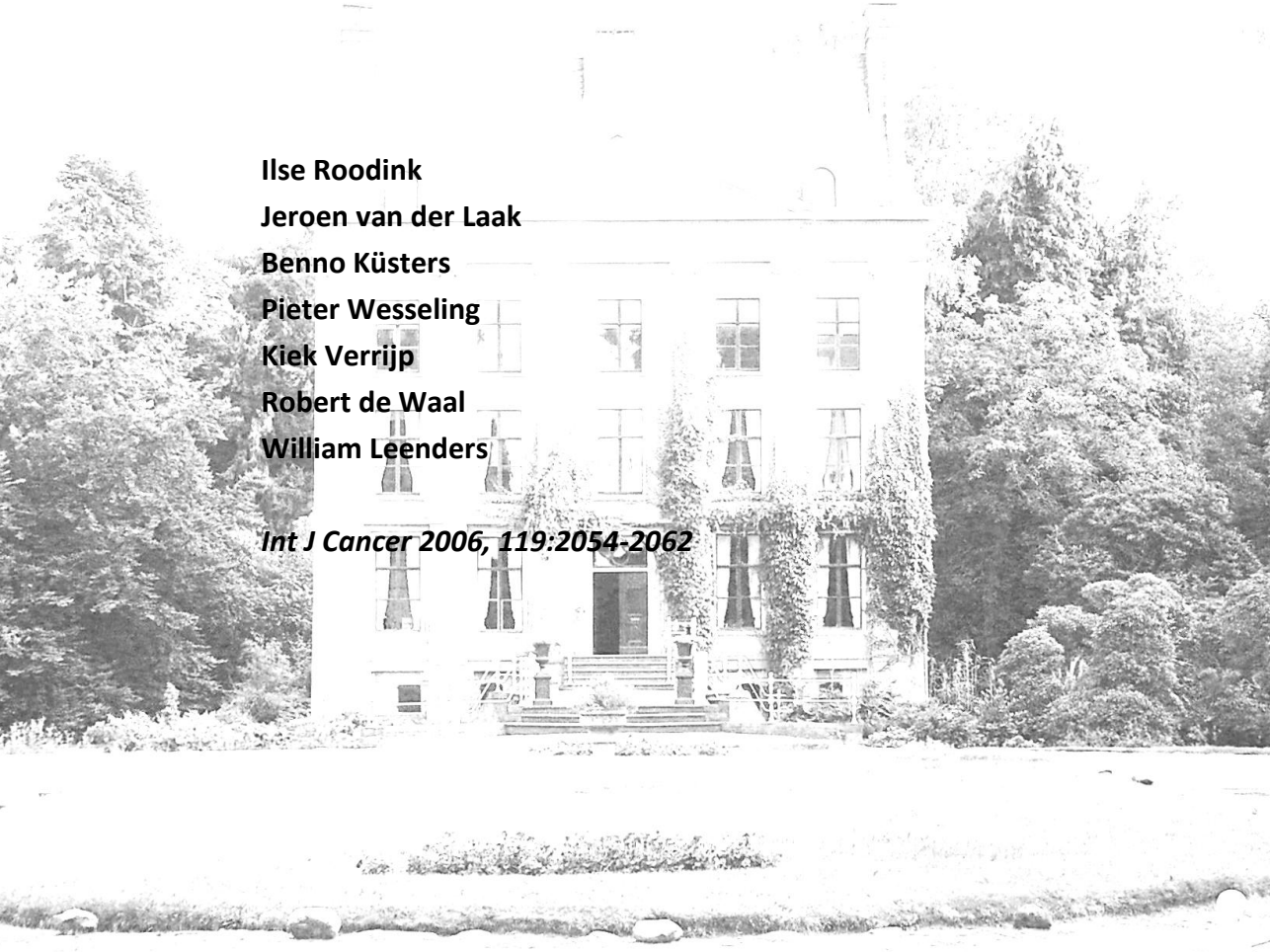

Ilse Roodink
Jeroen van der Laak
Benno Küsters
Pieter Wesseling
Kiek Verrijp
Robert de Waal
William Leenders

Int J Cancer 2006, 119:2054-2062

Abstract

Tumors arise initially as avascular masses in which central hypoxia induces expression of Vascular Endothelial Growth Factor-A (VEGF-A) and subsequently tumor vascularization. However, VEGF-A can also be constitutively expressed as a result of genetic events. VEGF-A is alternatively spliced to yield at least six different isoforms. Of these, VEGF-A_{121} is freely diffusible whereas basically charged domains in the larger isoforms confer affinity for cell surface or extracellular matrix components. We previously reported that in a mouse brain metastasis model of human melanoma, VEGF-A_{121} induced a qualitatively different tumor vascular phenotype than VEGF-A_{165} and $_{189}$: in contrast to the latter ones, VEGF-A_{121} did not induce a neovascular bed but rather led to leakage and dilatation of pre-existent brain vessels.

Here, we correlate vascular phenotypes with spatial VEGF-A expression profiles in clinical brain tumors (low grade gliomas; n=6, melanoma metastases; n=4, adenocarcinoma metastases; n=4, glioblastoma multiforme; n=3, sarcoma metastasis; n=1, renal cell carcinoma metastasis; n=1). We show that tumors that constitutively express VEGF-A present with different vascular beds than tumors in which VEGF-A is expressed as a response to central hypoxia. This phenotypic difference is consistent with a model where in tumors with constitutive VEGF-A expression, all isoforms exert their effects on vasculature, resulting in a classical angiogenic phenotype. In tumors where only central parts express hypoxia-induced VEGF-A, the larger angiogenic isoforms are retained by extracellular matrix, leaving only freely diffusible VEGF-A_{121} to exert its dilatation effects on distant vessels.

Introduction

Except for infiltrative tumors in organs where a high density of capillaries allows co-option of pre-existent vessels,[75,131] tumors cannot grow beyond a minimum size of 3 mm^3 unless they have the capacity to generate a new vasculature via angiogenesis.[132-134] Angiogenesis not only enhances tumor growth by supplying tumor cells with oxygen and nutrients, but also increases the chance of tumor cell intravasation, an obligatory and rate-limiting step in the metastatic process. Indeed, in a number of tumor types positive correlations between vessel density and poor prognosis have been established.[135,136]

Most research on tumor angiogenesis has focused on Vascular Endothelial Growth Factor-A (VEGF-A). *VEGF-A* is a target gene for the transcription factor hypoxia-inducible factor-1 (HIF-1), a dimeric complex of HIF-1α and HIF-1β.[137] Hypoxia, often relevant in the centers of rapidly growing tumors, results in diminished proteasomal degradation of HIF-1α. Consequently, HIF-1 accumulates in the cell which results in enhanced transcription of the VEGF-A gene.[137-140] In tumors, expression of VEGF-A is not always hypoxia-related as it may also be a consequence of genetic events, such as overactivation of proto-oncogenes as k-ras[141] or mutational inactivation of tumor suppressor proteins such as the Von-Hippel-Lindau protein (VHL) and PTEN.[142,143] Finally, VEGF-A expression can also be induced by several cytokines and growth factors.[138,144]

Upon binding of VEGF-A to its tyrosine kinase receptors VEGFR1 and VEGFR2, a cascade of cellular events is initiated, leading to proliferation and migration of endothelial cells, production of tissue factor and proteases, vascular permeability and deposition of extravascular fibrin which serves as provisional matrix for newly formed endothelial cells.[50,53,145] Although VEGFR1 has the higher affinity for VEGF-A, VEGFR2 is tyrosine-phosphorylated more efficiently upon ligand binding and mediates almost all observed endothelial cell responses to VEGF-A[55,146], at least during tumor angiogenesis.

The VEGF-A transcript is alternatively spliced to yield multiple isoforms counting 121, 145, 165, 183, 189 and 206 amino acid residues.[57,147,148] The larger of these isoforms contain basically charged domains, encoded for by exons 6a, 6b and 7, which confer binding affinity towards negatively charged extracellular matrix and cell surface components such as heparan sulphate proteoglycans. Hence, these isoforms are, at least partly, tethered by the extracellular matrix. $VEGF_{121}$ lacks these exons and is freely diffusible. The exon 7-encoded domain in $VEGF_{165}$ results also in binding of this isoform to the non-signaling co-receptor neuropilin-1 (NP-1). Since NP-1 also has affinity for VEGFR2, the hypothesis has been put forward that NP-1 enhances the formation of the VEGF-VEGFR2 complex, explaining the increased potency of $VEGF_{165}$ relative to $VEGF_{121}$ to activate VEGFR2 *in vitro*.[149] NP-1 is essential for angiogenesis: NP-1 knock-out mice, as well as mice expressing solely $VEGF_{120}$ (the mouse VEGF-A isoforms count one amino acid residue less than their

human counterparts) are characterized by a maldeveloped vasculature and die in utero.[150-152] On the other hand, transgenic mice that express $VEGF_{164}$ as the only isoform develop normally.[150,152,153]

Only little information about the *in vivo* activities of the individual isoforms in tumor biology is available, the main reason being that during tumor growth the multiple isoforms are expressed simultaneously. We recently published that, in a mouse model of brain metastases of melanoma which selectively express VEGF-A_{121}, $_{165}$ or $_{189}$, VEGF-A_{165} and VEGF-A_{189} induced angiogenic responses whereas VEGF-A_{121} was unable to do so. This isoform only induced permeability and dilatation of peritumoral pre-existent vessels.[77] Interestingly, despite the absence of angiogenesis, VEGF-A_{121} did induce endothelial proliferation with a potency similar to VEGF-A_{165}, suggesting that endothelial VEGFR2 was equally activated by all isoforms. Importantly, despite the absence of sprouting angiogenesis the "vasomodulation" activities of $VEGF_{121}$ led to increased blood supply and, consequently, higher tumor growth rates.

In clinical practice, tumors present with very heterogeneous vascular beds. Tumors may be homogenously well vascularized, but may also be sparsely vascularized with more or less necrotic regions. The question emerges why the latter tumors fail to mount a proper angiogenic response. Here we approached this question by correlating spatiotemporal expression patterns of distinct VEGF-A-isoforms to vascular phenotypes in a panel of primary and metastatic brain tumors. We show that tumors develop qualitatively different vascular phenotypes, depending on whether VEGF-A expression is constitutive or hypoxia-induced. Our results show that a classical tumor neovascular bed (high density of dilated and sprouting vessels) is characteristic for tumors that constitutively express VEGF-A whereas hypoxia-induced VEGF-A expression results in vasomodulation rather than neovascularization.

Materials and Methods

Tissue samples

Twenty primary and metastatic brain tumors were selected from the archives of the Department of Pathology of the University Medical Centre St Radboud. Tumors consisted of low grade gliomas (n=6), glioblastoma multiforme (n=3), and metastases of melanoma (n=4), adenocarcinoma (n=4), alveolar soft part sarcoma (n=1) and renal cell carcinoma (n=1). Both frozen and formalin-fixed tumor tissues were used for analyses. Tumors were diagnosed by qualified pathologists.

VEGF-A mRNA In Situ Hybridization (ISH)

Single-stranded sense and antisense digoxigenin-labelled VEGF RNA probes were generated by *in vitro* transcription of VEGF-A_{165} cDNA in vector pGEM-T (Promega , Madison, WI) with respectively T7 and Sp6 RNA polymerase (Roche, Almere, The Netherlands) according to the manufacturer´s instructions. Paraffin-embedded tumor sections of 4 µm were dewaxed and treated with proteinase K (Roche) at 37°C for 15 minutes and post-fixed in formaldehyde at room temperature for 30 minutes. Non-specific binding sites were blocked by incubation with acetic anhydride (Sigma Chemical Co., Zwijndrecht, The Netherlands) at room temperature. Overnight hybridization with digoxigenin-labelled RNA probes was performed at 60°C with 100 ng/ml probe. After hybridization and subsequent washing, single stranded non-hybridized RNA was degraded with RNAse T1 (2 units/ml) at 37°C for 30 minutes. After subsequent pre-incubation with normal sheep serum, the slides were incubated with alkaline phosphatase-conjugated sheep anti-digoxigenin antibody (Roche) at room temperature for 1 hour. Alkaline phosphatase was visualized using nitro blue tetrazolium (NBT; Roche) and 5-bromo-4-chloro-3-indolyl phosphate (BCIP; Roche) as substrate. Specificity of hybridisations was always verified by performing control hybridizations with sense probe.

Immunohistochemistry

Immunohistochemical stainings were performed according to standard protocols. In short, sections of 4 µm were prepared from paraffin-embedded brain tumors and immunostained with antibodies against the following antigens: CD31 (to detect endothelial cells, Dako, Glostrup, Denmark), α-SMA (α-smooth muscle actin, to detect activated pericytes, Sigma, Zwijndrecht, The Netherlands), Glut-1 (glucose transporter-1, a brain-endothelial specific protein and a hypoxia marker, Dako), MIB-1 (anti-proliferation antigen Ki67, Dako) and HIF-1α (Chemicon, Temecula, CA). After deparaffinization and blocking of endogenous peroxidase activity, antigen retrieval was performed by boiling in 10 mM citrate buffer, except for the sections stained with anti-αSMA. Non-specific binding sites were blocked by incubation with normal horse or goat serum. Slides were incubated overnight at 4°C with primary antibodies in PBS/1% BSA. After washing, primary antibodies were detected by sequential incubations with biotinylated secondary antibody (Vector, Burlingame, CA) in PBS-BSA and avidin-biotin peroxidase complex (Vector). Finally, the peroxidase was visualized by the 3-amino-9-ethylcarbazole (ScyTek, Utah, USA) peroxidase reaction with hematoxylin as counterstain.

Quantitative analysis of vascular density and morphology, relation to hypoxia

Sections of four representative tumors (sarcoma, renal cell carcinoma and two melanomas) were subjected to extensive quantitative analysis. CD31-stained sections

were analyzed using a digital image analysis system (KS400, Carl Zeiss, Germany), essentially as described before.[154] Numbers of isolated CD31-positive structures were counted as separate vessels. Also, the average diameter was determined for each individual vessel, based on digital distance transforms. In the two melanomas, the mean minimal distance between vessels and VEGF-A-expressing tumor cells (from the ISH analysis) was determined. In the same tumors, the mean minimum distance between vessels and Glut-1-positive hypoxic tumor cells was measured. This was done for twenty six vessels in one of the melanomas. Student T-tests were used for statistical analysis.

Reverse Transcriptase Polymerase Chain Reaction (RT-PCR)

Total RNA was isolated from 30 frozen 20 µm tumor sections using TRIzol Reagent (Life Technologies, Breda, The Netherlands) according to the manufacturer´s protocol. RNA integrity was checked by 1.0% agarose gel electrophoresis. RNA samples (1 µg) were reverse-transcribed at 42°C for 90 minutes using Moloney-mouse-leukemia virus reverse transcriptase (Promega, Leiden, The Netherlands). Two µl of the reaction product were subjected to standard PCR amplification using High Fidelity Taq polymerase (Roche) and VEGF-A-primers 5`-GCA CCC ATG GCA GAA GGA GGA-3` (sense) and 5`-TCA CCG CCT CGG CTT GTC AC-3` (exon 8 specific, antisense). The PCR was made semi-quantitive by first establishing an optimal number of cycles where amplification was in the linear range.
This primer set amplifies all VEGF-A isoforms simultaneously, except VEGF165b. Expected product lengths with this primer set are 367 bp (VEGF-121), 436 bp (VEGF-145), 496 bp (VEGF165) and 568 bp (VEGF189). cDNAs were also subjected to a PCR for PBGD as control house keeping gene. Levels of the individual isoforms relative to PBGD were quantified by densitometry.

Results

Spatial distribution of VEGF-A expression

To investigate the distribution of VEGF-A expression in our panel of tumors, in situ hybridizations (ISH) were performed. We considered VEGF-A expression as hypoxia-induced when ISH profiles correlated with the distribution of HIF-1α and one of its target genes Glut-1[155] in immunohistochemical stainings on serial sections. When VEGF-A expression could be detected in non-hypoxic tumor cells, expression was considered as constitutive.
Three groups could be distinguished. In one group, consisting of the sarcoma and renal cell carcinoma metastases and the glioblastomas (GBM), the majority of viable tumor cells expressed high levels of VEGF-A (Figure 1A,D,G). VEGF-A expression was not related to

hypoxia as no Glut-1 or HIF-1α expression was detected in VEGF-A expressing tumor cells (Figure 1B,E,H, note that the staining in panel B is due to erythrocytes, whereas the Glut-1 staining in panel 1H is partly confined to pre-existent vasculature with a functional blood brain barrier). In GBM, VEGF-A expression was heterogeneous but could not be related to hypoxia. The high VEGF-A expression levels in sarcoma and renal cell carcinoma metastases and parts of the GBM are consistent with the high vascular densities, as indicated by the CD31 staining in Figure 1C,F,I (note that in GBM the high vessel density is seen in the regions that express VEGF-A). Taken together, these results strongly suggest that VEGF-A expression in this group of tumors was the result of a genetic event, rather than hypoxia.

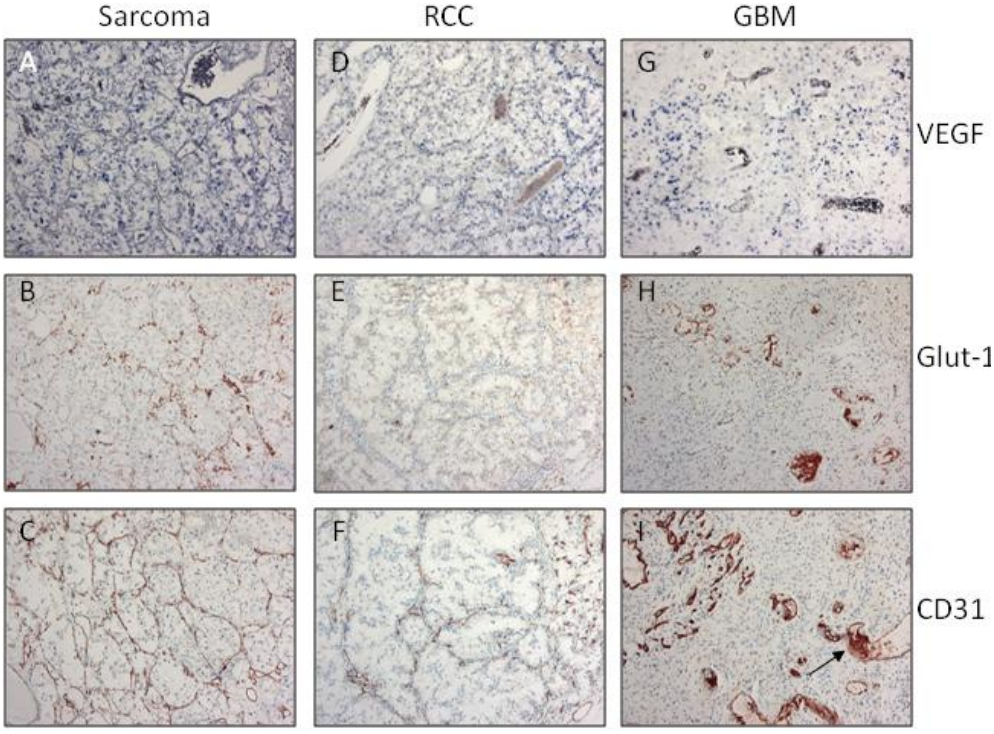

Figure 1. Representative examples of spatial distribution of VEGF-A expression (A,D,G), hypoxia (B,E,H) and blood vessels (C,F,I) in brain metastases of sarcoma (A-C) and renal cell carcinoma (D-F) and in glioblastoma multiforme (G-I). VEGF-A transcripts were highlighted by in situ hybridization with an antisense VEGF-A RNA probe, hypoxia was demonstrated by immunohistochemistry using an anti-Glut-1 antibody, vessels were stained with an antibody against CD31. Note in B, E and H that no Glut-1 positive tumor cells are present. The positivity in these sections is due to erythrocytes in dilated vessels. In the GBM some blood vessels also stain positive, indicating that these are in fact pre-existent capillaries with a functional blood brain barrier. The arrow in I points at a glomeruloid proliferation. These stainings show that in this group of tumors there is no correlation between hypoxia and VEGF-expression.

In the second group, consisting of metastases of adenocarcinoma and melanoma, VEGF-A expression was heterogeneous. In this group, VEGF-A expression co-localized with Glut-1 expression (compare Figure 2A with 2B and 2D with 2E). Especially in melanomas, VEGF-A expression occurred at regular, concentric distances from dilated vessels, exactly the tumor areas that were subject to hypoxia, as revealed by the Glut-1 staining (Figure 2B) and HIF-1α stainings (not shown) suggesting that in these tumor lesions VEGF-A expression was induced by hypoxia. Indeed, the mean distance between vessels and Glut-1 expressing tumor cells and that between vessels and VEGF-A expressing cells did not differ significantly (85±16 µm vs. 78±16 µm, p=0.12), further confirming the hypoxia-induced origin of VEGF-A.

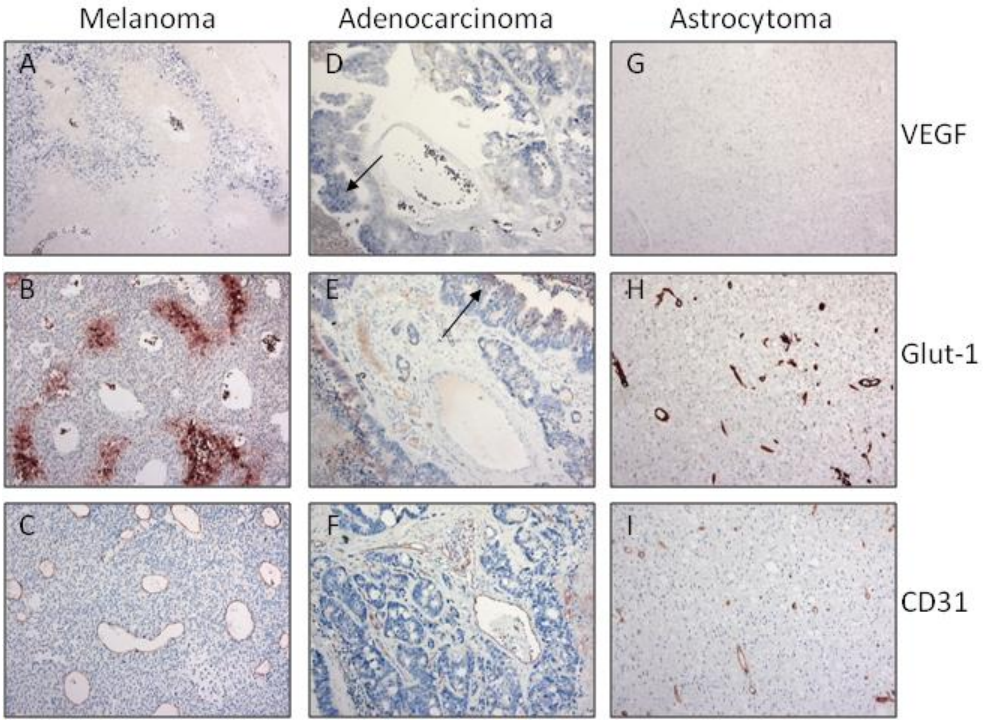

Figure 2. Spatial distribution of VEGF-A expression as determined by VEGF-A ISH (A,D,G), hypoxia (Glut-1 immunostaining, B,E,H) and blood vessels (CD31 immunostaining, C,F,I) in brain metastases of melanoma (A-C), adenocarcinoma (D-F), and in low grade glioma. In melanoma and adenocarcinoma metastases, there is a clear co-localization of Glut-1 expression and VEGF-A expression, suggesting that in these tumor types VEGF-A is expressed as a response to hypoxia. In melanoma the hypoxic areas are confined to concentric regions at regular distances from dilated blood vessels, in the adenocarcinoma metastases the hypoxia and VEGF-A expression occurred primarily in epithelial cells distant from the fibrovascular regions (arrows). The blood vessels in the low grade astrocytoma are positive for Glut-1, indicating that these are pre-existent brain capillaries with a functional blood brain barrier. Note that the sections shown are obtained from the same tumor regions. Due to technical reasons, however, these are not exact serial sections.

VEGF-A mRNA transcripts in adenocarcinoma metastases were predominantly detected distant from the fibrovascular core, and also here VEGF-A expression correlated with Glut-1 expression, again suggesting that VEGF-A was induced as a response to hypoxia.
Finally, in low grade gliomas we only incidently observed low levels of VEGF-A (Figure 2G-I). Hypoxia was not observed in these tumors (see Glut-1 staining in figure 2H), consistent with the infiltrative nature of these tumors which enables the tumors to grow via co-option of pre-existent vessels. Note that these pre-existent blood vessels all express Glut-1, indicative of blood-brain barrier characteristics and, thus, a pre-existent nature.
To examine which isoforms of VEGF-A were expressed by the respective tumors, RT-PCR was performed using a primerset that enables simultaneous detection of the major VEGF-A isoforms. Except for the low grade gliomas, which expressed barely-detectable levels of VEGF-A, all tumors expressed all major VEGF-A isoforms, although the ratios between the isoforms differed between the tumors (Table 1).

Table 1. Levels of the individual VEGF-A isoforms, relative to the house keeping gene PBGD.

	VEGF-121	VEGF-145	VEGF-165	VEGF-189
Low grade gliomas	0.28	n.d.	0.26	0.19
Melanoma metastases	0.47	n.d.	0.39	0.27
Adenocarcinoma metastases	1.92	0.95	1.26	0.76
Glioblastomas Multiforme	2.02	1.34	2.40	1.17
Metastasis of sarcoma/RCC	2.28	1.73	2.98	1.63

The sarcoma metastasis and the GBM expressed the highest levels of VEGF-A, which is consistent with our in situ hybridization data (Figure 3). These tumors expressed predominantly VEGF-A_{165} and VEGF-A_{121}, but significant amounts of the 145 and 189 isoforms were also detected. The renal cell carcinoma showed prominent expression of VEGF-A_{121} and VEGF-A_{165} and less expression of the 145 and 189 aa isoforms.
All four melanoma metastases examined expressed approximately equal levels of the 121 and 165 isoforms. Levels of VEGF-A in these tumors were less than in the GBM, sarcoma and renal cell carcinoma samples. Again, this is consistent with our in situ hybridization data which showed that VEGF-A expression was restricted to relatively small areas of hypoxia. The adenocarcinomas in this study expressed all four isoforms of VEGF-A, but VEGF-A_{165} and VEGF-A_{121} were the most prominent ones.
Finally, in the group of low grade gliomas we could detect in only two samples very low expression levels of the 121 and 165 isoforms. In the other five samples no VEGF-A transcripts could be detected. This is consistent with the absence of detectable angiogenesis in these tumors (see also Figure 2G-I) and lack of VEGF-A transcripts, as observed in the situ hybridization.

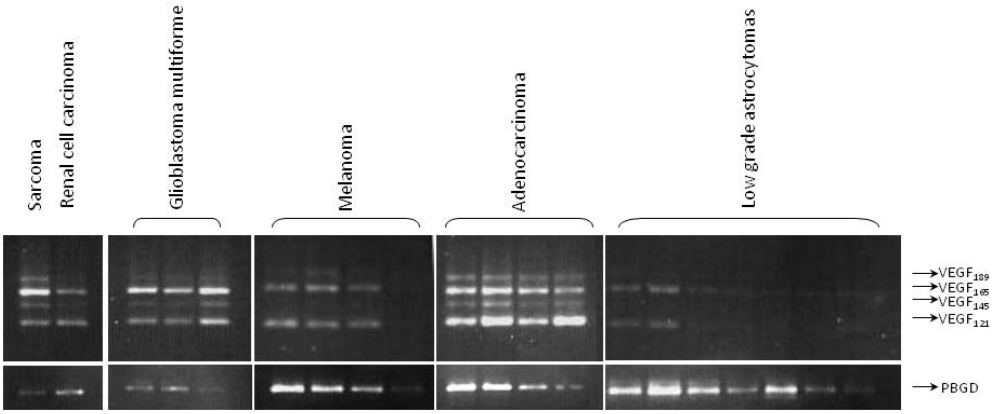

Figure 3. RT-PCR using exon 4 and exon 8 specific VEGF primers, allowing simultaneous detection of the major VEGF-A isoforms (see text). The house keeping gene PBGD was used as a control. The variety in PBGD PCR products is due to the differences in RNA quality of the archival tumor material.

Vascular morphology of brain tumors

Based on immunohistochemical stainings with anti-CD31 and anti-α smooth muscle actin (data not shown) to visualize blood vessels in our panel of brain tumors, we could group the tumors according to VEGF-A expression profiles:

1) constitutive VEGF-A expression

This group of tumors, consisting of the sarcoma and renal cell carcinoma metastases and regions within the GBMs, presented with a high density of dilated and tortuous blood vessels (Figure 1C,F,I and Figure 4A), the classical hallmarks of angiogenic tumors. Vessels were mostly negative for Glut-1 (compare Figure 1C to 1B and 1F to 1E), indicating that they lacked specific characteristics of brain capillaries and were newly formed. A subset of blood vessels in the GBM specimens stained positive for Glut-1. These may represent pre-existent vessels that are co-opted by the tumor cells, but it may also be that the astrocytic nature of GBM induces blood-brain characteristics in some of the tumor vessels.[156] It must be noted that small areas of necrosis within GBM were generally surrounded by hypoxic tumor cells which also expressed VEGF-A (not shown). Therefore, in GBMs a mixture of hypoxia-induced VEGF-A expression and constitutive expression occurs. The vast majority of the tumor vessels stained positive for α-smooth muscle actin, indicative of a high degree of coverage by activated pericytes. In the GBM, regions with glomeruloid microvascular proliferation were observed (see arrow in figure 1I). The GBM was different from the sarcoma and renal cell carcinoma in that VEGF-A expression was heterogeneous

within the tumor. This is also reflected in heterogeneity in vascularization, as shown in Figure 1I.

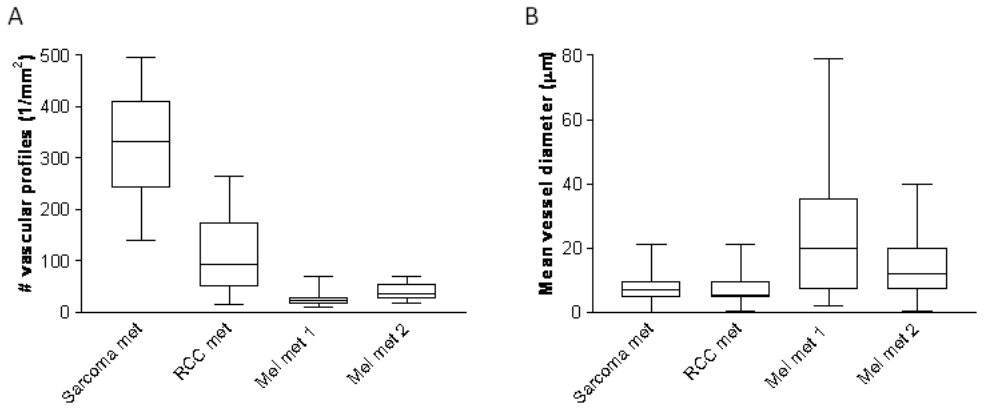

Figure 4. A) Automated analysis of vessels in brain metastases of sarcoma (sarcomas met), renal cell carcinoma (RCC met) and two melanomas (mel met 1 and 2). Note the high vessel densities in sarcoma and renal cell carcinoma, whereas the vessel densities in melanoma metastases are much lower. B) mean vessel diameter in the same tumors. Note that the mean vessel diameter in the melanomas was much higher than in the other tumors, confirming the immunohistochemical stainings in figure 2.

2) hypoxia-mediated VEGF-A expression

The blood vessels in all four melanoma metastases in our study were of a remarkably different phenotype as compared to those in the tumors of the first group. The melanoma lesions presented with regularly dilated vessels, more or less homogeneously distributed throughout the tumors, without indications for sprouting angiogenesis (Fig. 2C and Figure 4B). The majority of these vessels stained positive for α-smooth muscle actin (not shown). In general, these vessels were negative for Glut-1 but occasionally vessels with a mosaic composition of Glut-1-positive and negative endothelial cells could be observed in the tumor periphery (not shown). This suggests that mother endothelial cells (Glut-1 positive and derived from pre-existent brain capillaries) and daughter endothelial cells (Glut-1 negative) co-existed in these vessels, suggesting endothelial cell proliferation in the absence of neo-angiogenesis. Interestingly, similar mosaic vessels were observed in Mel57 melanoma brain lesions, expressing VEGF-A_{121} as the only isoform.[77] Tumor cells located at regular distances from vessels were hypoxic as revealed by Glut-1 staining (Fig. 2B). The blood vessels in the adenocarcinoma metastases were also dilated. Interestingly,

occasionally signs of sprouting angiogenesis were observed in the fibrovascular components of these tumors (Fig. 2F). Again, vessels were predominantly negative for Glut-1, indicating that endothelial cell proliferation had occured in these tumors (Fig. 2E).

3) low to undetectable VEGF-A expression

Finally, in our set of low grade gliomas we observed only occasionally a slight vessel dilatation (Fig. 2H, I). Vessels stained positive for α-smooth muscle actin (α-SMA, not shown) and Glut-1, indicating that these relatively mature vessels had a functional blood-brain-barriere (BBB) and were presumably pre-existent brain vessels. Prominent vascular changes were not detected, nor were hypoxia and necrosis in the examined specimens.

Tumor cell proliferation

Interestingly, we found no correlation between the vascular densities and the proliferation indices of the tumors in this study. The sarcoma metastasis, which was the most vascularized tumor with the highest VEGF-A expression, had a proliferation index of only 1% as indicated by staining for the Ki67 nuclear antigen (Figure 5A), whereas the renal cell carcinoma had a proliferation index of more than 60%. In the GBM samples, MIB staining was heterogeneous, and often proliferating vessel-associated cells, presumably endothelial cells and pericytes, could be observed (arrows in Figure 5F). Whereas the four melanoma metastases in our study showed very similar vascular phenotypes, the MIB proliferation indices varied from less than 1% to more than 80% (Figure 5D and E). The adenocarcinomas also had very high proliferation indices (ranging from 40-90%, see Figure 5C). Finally, in the low grade gliomas Ki67-positivity was limited to less than 5-10% of tumor cells (not shown).

Discussion

We previously reported that in a mouse brain metastases model of the human melanoma cell line Mel57, the VEGF-A isoforms 121, 165 and 189 contribute differentially to the process of tumor vascularisation.[77] Tumors that exclusively expressed VEGF-A_{121} were characterized by a relative absence of intratumoral blood vessels, whereas highly dilated and activated, supposedly pre-existent vessels were concentrated in a peritumoral rim. In sharp contrast, VEGF-A_{165} and VEGF-A_{189} induced the formation of an intratumoral neovascular bed consisting of irregularly dilated and leaky vessels. In VEGF-A_{165} expressing tumors vasodilatation was more prominent as compared to $VEGF_{189}$ tumors. In the

present study we sought to extrapolate these findings to the human situation by comparing expression profiles of distinct VEGF-A-isoforms with tumor vascular phenotypes in a set of human primary and metastatic brain tumors.

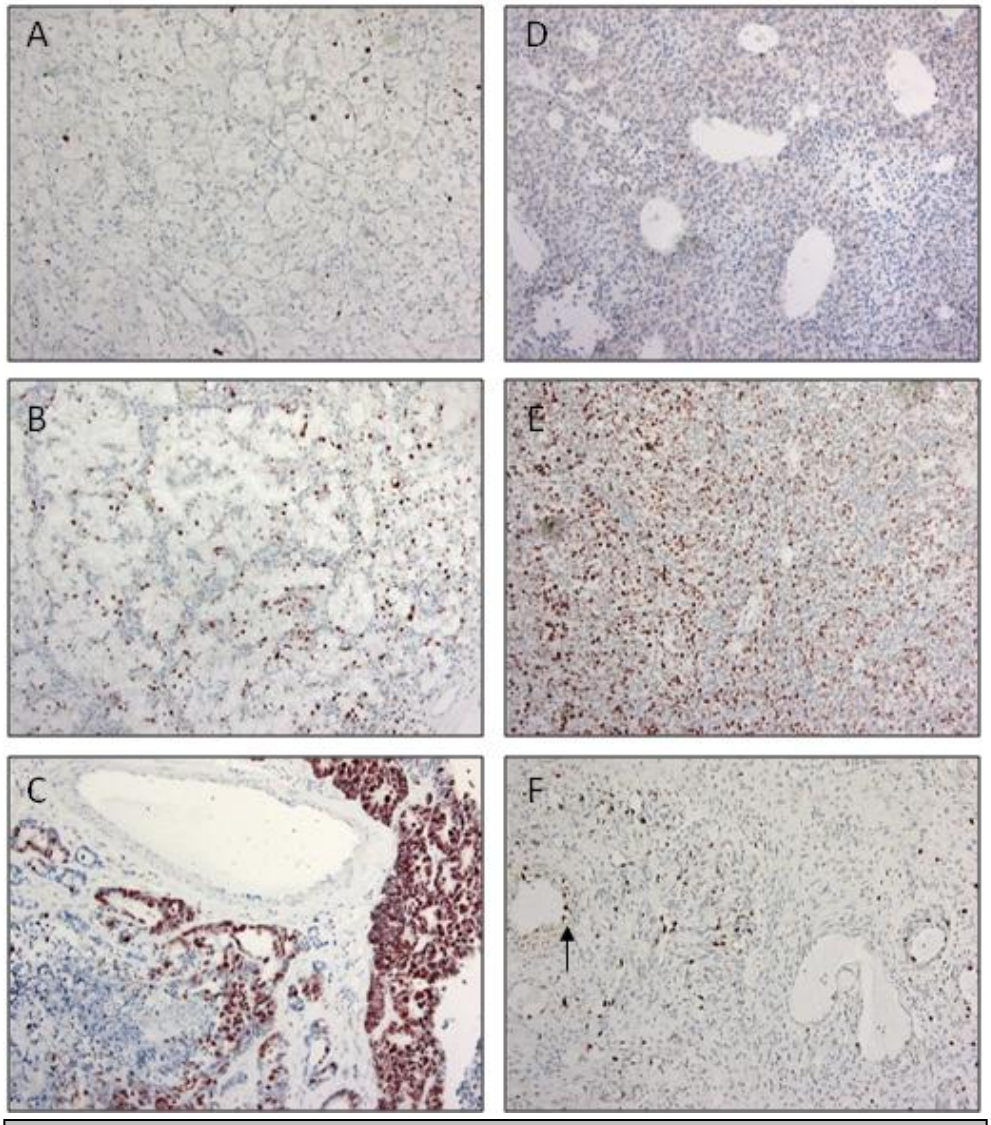

Figure 5. Proliferation indices of tumors as revealed by MIB-1 staining. Shown are brain metastases of sarcoma (A), renal cell carcinoma (B), adenocarcinoma (C), melanoma (D,E) and a GBM (F).

Multiple VEGF-A isoforms were expressed simultaneously in most tumors. In four of the low grade gliomas low VEGF-A expression was detected, both by in situ hybridization and RT-PCR. This is in accordance with the absence of vascular effects in these tumors. Typically, low grade gliomas are infiltrative and slowly growing tumors, which is also apparent from the low proliferation indices.[82] Supposedly, the blood supply from the pre-existent vascular bed in and around these tumors sufficed for growth of these relatively quiescent tumors. This situation is remarkably similar to that in which VEGF-A negative Mel57 melanoma cells are grown in brain.[76] In all other tumors examined in this study, VEGF-A transcripts could be readily detected by RT-PCR. Without exception, VEGF-A_{121} and VEGF-A_{165} were the predominant isoforms, and the occurrence of these was always related to prominent vascular changes. The tumors that presented with the highest expression levels were the metastases of sarcoma, renal cell carcinoma and regions within the GBMs. It has to be realized, however, that these tumors expressed VEGF-A homogeneously throughout the tumor, whereas in the tumors with the relatively lower VEGF-A expression, the melanomas and the adenocarcinomas, expression was confined to hypoxic tumor cells (a subpopulation, estimated to comprise 10% of the total tumor area). Taking this factor into account, it is reasonable to assume that the VEGF-A expression levels per tumor cell are comparable between the different tumors. Only minor differences between the ratios of the isoforms could be detected. The sarcoma metastasis and two of the glioblastomas multiforme were the only tumors in which significantly more VEGF-A_{165} than the other isoforms could be detected. In two of the adenocarcinoma metastases, VEGF-A_{121} dominated over VEGF-A_{165}. These differences were not reflected in the vascular morphologies of these tumors.

Despite the absence of dramatic differences in VEGF-A expression levels and ratios of VEGF-A isoforms between the tumors, the low grade gliomas excluded, there were profound differences between the vascular architectures of the tumors.

In the sarcoma and renal cell carcinoma metastases where VEGF-A was homogeneously distributed throughout the tumor, also in apparently normoxic areas, vessel densities were always high and vessels lacked expression of Glut-1. Apart from being a marker for hypoxic cells, Glut-1 is also expressed on the endothelium of brain capillaries with a functional blood-brain barrier. We already demonstrated in a mouse model of brain metastasis that the absence of Glut-1 on tumor vessels is an indication that such vessels are the product of neovascularization, whereas tumor vessels that do express Glut-1 are actually incorporated pre-existent brain capillaries.[77] Incorporation of pre-existent, Glut-1 positive blood vessels was indeed observed in the grade II gliomas in our study.

Unlike primary brain tumors that have the tendency to show infiltrative growth, metastases in brain generally grow expansively, showing little infiltration in the brain parenchyma.[82] Therefore these tumors can hardly thrive on pre-existent vasculature and

are dependent on neovascularization. Indeed, the vessels in these tumors all lacked Glut-1 expression. In GBM, Glut-1 was expressed on a subset of tumor vessels. High grade astrocytomas are characterized by the presence of necrotic areas, areas of active angiogenesis, but also areas of infiltration.[82] It is therefore possible that the Glut-1 positive vessels that we detected were indeed incorporated pre-existent vessels. However, since the blood-brain barrier is induced by contacts between astrocytes and brain capillaries, we can not exclude the possibility that these vessels are actually newly formed, and that the astrocytic tumor cells induced expression of Glut-1.[156]

In the melanoma- and adenocarcinoma metastases, VEGF-A expression was induced by hypoxia, as revealed by the colocalization of VEGF-A mRNA and the hypoxia-marker Glut-1. In these tumors the vasculature was less tortuous and more organized. This was especially evident in the melanoma metastases which presented with a low density of highly dilated vessels with no signs of sprouting angiogenesis. Interestingly, these vessels sometimes had a mosaic phenotype for Glut-1, a phenomenon that we previously described in brain lesions of transgenic melanoma cells expressing VEGF-A_{121}. We propose that these vessels are modulated, pre-existent vessels in which endothelial proliferation results in Glut-1-positive mother cells and Glut-1-negative daughter cells.

How can the differences between vascular phenotypes between the groups of tumors be explained when similar levels of similar VEGF-A isoforms are expressed by tumor cells? From the results of this study we hypothesize that the mechanism underlying VEGF-A expression, i.e. hypoxia-induced or constitutive, is responsible for the vascular phenotype in brain tumors. When VEGF-A expression occurs in tumor cells that have become hypoxic because during growth the distance to the most nearby vessels has become too large, a situation develops where multiple isoforms are expressed but only the freely diffusible VEGF-A_{121} may be able to make contact to distant endothelial cells and activate these. The larger isoforms are tethered by the extracellular matrix and are thus physically unable to activate the endothelial cells in distant vessels (figure 6A). Our previous results on VEGF-A_{121} -expressing Mel57 brain lesions cells would then predict that vessel activation and dilatation, rather than neovascularization, occurs. This is indeed what we observe in tumors with hypoxia-induced VEGF-A expression (melanoma and adenocarcinoma metastases), where a relatively low density of highly dilated blood vessels is present.

This situation is fundamentally different from that in which tumor cells constitutively express multiple VEGF-A isoforms. Upon extravasation, tumor cells in the early stages of outgrowth will be in direct contact with blood vessels, and therefore all isoforms will be capable of inducing vascular effects. Because we know from our animal work that VEGF-A_{165} and VEGF-A_{189} induce a neovascular bed, it is anticipated that in such cases highly angiogenic phenotypes are observed. The continuous angiogenesis during tumor growth

explains the absence of hypoxia and necrosis in these tumors. This concept is illustrated in figure 6B.

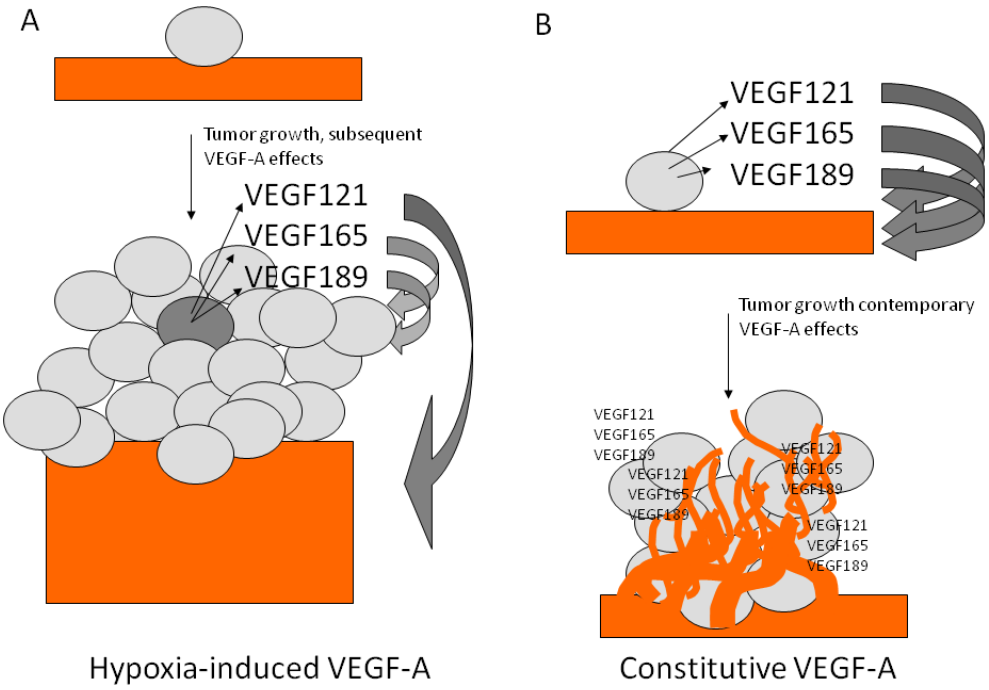

Figure 6. Proposed model of development of vascular phenotypes in tumors which express VEGF-A in response to hypoxia (A) or constitutively (B). In the former situation, only the small molecular weight isoforms (VEGF-A_{121} or proteolytic cleavage products of the larger isoforms) can exert their effects on the vasculature, whereas in tumors that constitutively express VEGF-A, all isoforms can exert their effects on blood vessels, resulting in classical angiogenesis. Hypoxic cells are indicated as dark grey.

It is commonly accepted that ECM-bound VEGF-A_{165} and VEGF-A_{189} act as a biological reservoir of growth factors which can be quickly released on demand by proteolytic digestion with metalloproteinases or plasmin.[157,158] Digestion results in the release of aminoterminal fragments of 113 and 110 amino acids, which contain all receptor binding domains. A recent paper by Lee *et al.*[159] described that the aminoterminal VEGF-A fragments induced receptor activation and endothelial proliferation, giving rise to endothelial sheets in 3D *in vitro* cell cultures, whereas VEGF-A_{165} induced endothelial proliferation and migration, resulting in tubular structures. These activities could be translated to vessel dilatation and sprouting angiogenesis, respectively, in the *in vivo*

situation, very similar to what we previously described in our mouse model of VEGF-A transgenic brain metastasis. In fact, we have also been able to show that a truncated VEGF-A_{110} protein induced a tumor vascular phenotype similar to VEGF-A_{121} (manuscript in preparation). Thus, soluble VEGF-A isoforms, whether in the form of VEGF-A_{121} or proteolytic digests of larger isoforms that are tethered in the tumor center, act as vasodilators and have little potency to induce sprouting angiogenesis.

In the adenocarcinomas we found moderate expression of VEGF-A_{145}, an isoform which is also tethered in the extracellular matrix.[56] Whether VEGF-A_{145} is also a substrate for plasmin or MMPs has not been investigated. At this moment there is no reason to assume that VEGF-A_{145} would behave differently from the other large VEGF-A- isoforms.

The underlying reasons for the differential angiogenic potencies of VEGF-A_{121} and VEGF-A_{165} are poorly understood. NP-1 binding by VEGF-A_{165} may be a factor. However, NP- involvement is contradicted by the fact that a novel VEGF-A splice variant, VEGF-A_{165b} lacks significant angiogenic activity despite the presence of an intact exon 7 and all receptor binding domains.[160] Another explanation may be the higher affinity of VEGF-A_{165} for matrix components, resulting in higher local concentrations and consequently increased potency. It has been proposed that matrix-bound VEGF-A promotes endothelial cell adhesion and migration through an integrin-dependent (α3β1 and αvβ3) pathway.[161] Obviously, this would require a direct association of matrix-bound VEGF-A and blood vessels, a situation that is not expected to occur in tumors in which VEGF-A expression is induced by hypoxia, distant from vessels.

Central hypoxia in tumors has generally been considered as the major factor leading to VEGF-A expression. Surprisingly, we found here that in tumors where VEGF-A expression is the result of central hypoxia, a vascular phenotype develops which does not conform to the hallmarks of angiogenesis. Instead, prototype tumor vascular beds with tortuous, dilated and highly branched vessels were only observed in tumors where VEGF-A expression was constitutive. The specific genetic defects in our panel of tumors which resulted in VEGF-A expression was not subject of this investigation. It is however well known that over 80% of renal cell carcinomas are relelated to mutations in the Von Hippel Lindau (VHL) protein, resulting in attenuated breakdown and accumulation of the VEGF-A transcription factor HIF-1α.[142] In GBMs, PTEN mutations or EGFR amplifications are frequently found that result in high VEGF-A expression levels.[143]

It must be noted here that there may be distinct differences in hypoxia-sensitivity of tumor cells. Sensitive cells will start expressing VEGF-A at relatively higher pO_2 (i.e. at shorter distances from the most nearby vessels) and may therefore deliver more VEGF-A_{165} to where the action is needed, generating a more angiogenic phenotype. Whether the melanoma and adenocarcinoma metastases in our study are exceptionally hypoxia-insensitive is however unlikely: hypoxia-induced Glut-1 expression was always detected at

approximately 100 µm from the tumor vessels, the diffusion distance of oxygen through tissues.[162]

Our findings may have therapeutic consequences. Both vasomodulation in the tumors with hypoxia-induced VEGF-A and neo-angiogenesis in the constitivtively-expressing tumors are dependent on the interaction between VEGF-A with VEGF receptors. Anti-angiogenic therapies, directed at interference with VEGF and its receptors would therefore likely inhibit both processes. However, specific interference with the interaction between VEGF-A_{165} and neuropilin, for example by exon 7-derived peptides,[163] would probably prevent neo-angiogenesis by inhibiting endothelial migration, but not the small-isoforms-induced vasomodulation. These issues have to be taken into account when developing future therapies.

Chapter 3

Plexin D1 expression is induced on tumor vasculature and tumor cells: a novel target for diagnosis and therapy?

Ilse Roodink
Jos Raats
Bert van der Zwaag
Kiek Verrijp
Benno Küsters
Hans van Bokhoven
Marianne Linkels
Robert de Waal
William Leenders

Cancer Res 2005, 65:8317-8323

Abstract

We previously reported that during mouse embryogenesis, plexin D1 (*plxnD1*) is expressed on neuronal and endothelial cells. Endothelial cells gradually loose *plxnD1* expression during development. Here we describe, using in situ hybridization, that endothelial *plxnD1* expression is regained during tumor angiogenesis in a mouse model of brain metastasis. Importantly, we found PLXND1 expression also in a number of human brain tumors, both of primary and metastatic origin. Apart from the tumor vasculature, abundant expression was also found on tumor cells. Via panning of a phage display library, we isolated two phages that carry single domain antibodies with specific affinity towards a PLXND1-specific peptide. Immunohistochemistry with these single domain antibodies on the same tumors that were used for in situ hybridization, confirmed PLXND1 expression on the protein level. Furthermore, both these phages and the derived antibodies specifically homed to vessels in brain lesions of angiogenic melanoma in mice after intravenous injection.
These results show that PLXND1 is a clinically relevant marker of tumor vasculature that can be targeted via intravenous injections.

Introduction

It is commonly accepted that, to grow beyond a size of 2-3 mm^3, tumors have to recruit a neovasculature via angiogenesis.[42,132] Tumors accomplish this via expression of Vascular Endothelial Growth Factor-A (VEGF-A), either induced by hypoxia in the tumor centre[57] or as a result of malfunctioning tumor suppressor gene products or activated proto-oncogenes.[143,164] A number of compounds that target the VEGF-A signaling pathway has been developed with the aim to inhibit angiogenesis and, consequently, tumor growth.[165] Although such anti-angiogenic therapies have been effective in animal tumor models[63,116], translation to the clinical level has so far proven to be less successful.[166]

For this, there is a number of possible explanations. In clinically relevant situations, tumors may have been growing for months or even years at the time of diagnosis, and a significant proportion of the vasculature may be more or less mature and thus insensitive to angiogenesis inhibition. This situation is in sharp contrast to that in most animal models in which, as a rule, aggressive, fast-growing tumors are studied. Furthermore, patients that are candidates for anti-angiogenic therapy are typically patients with disseminated, uncontrollable cancer. We and others described that growth of metastases may not always be strictly dependent on angiogenesis.[75,167,168] Because most metastases are blood-borne, they grow out in organs with intrinsically high vessel densities like liver, lung and brain where they can grow in an angiogenesis-independent fashion by co-option of pre-existent vessels.[75,76,78] We have recently reported that an angiogenesis inhibitor that very effectively inhibits tumor growth in a number of subcutaneous tumor models,[63] does not inhibit growth of infiltrative tumors in mouse brain. Moreover, upon treatment of mice carrying highly angiogenic brain tumors, angiogenesis inhibition resulted again not in tumor inhibition, but rather in a phenotypic shift towards co-option and infiltration.[117] These results imply that anti-angiogenic therapy should, ideally, be supplemented by vascular targeting therapies in which the existing tumor vascular bed is attacked, resulting in secondary tumor cell death due to disruption of the tumor's blood supply.[166] To accomplish effective vascular targeting therapy, markers have to be identified that have specificity for tumor vasculature. Much effort has already been put in this, but with varying success. Effective vascular tumor targeting has been accomplished using single chain antibodies, directed against the fibronectin ED-B domain, which is selectively expressed and deposited in the extracellular matrix of newly formed vessels in angiogenic tumors.[124,125] Targeting of $\alpha_v\beta_3$-integrin (the expression of which is restricted to immature vessels) using Vitaxin yielded disappointing results,[169] whereas endoglin-expression was not specific for tumor blood vessels.[130]

Plexins comprise a family of membrane proteins that are receptors for the semaphorins, a family of secreted and membrane-bound Ligands.[170] Class 3 semaphorins are potent axon

repellants and are as such involved in morphogenesis of the nervous system (for review, see[171,172]). These semaphorins activate plexins via binding of neuropilins in a multicomponent complex.[173]

We previously identified and characterized plexin D1 (*plxnD1*) as a plexin which is not only expressed in neuronal cells, but also in the vasculature during early stages of development.[174] In adult vasculature, *plxnD1* is absent. Recently, proof for a functional role of *plxnD1* during vascular and cardiovascular morphogenesis was provided using zebrafish mutants and knock-out mice.[175,176] PlxnD1 is a receptor for Semaphorin 3E, and, unlike other members of the plexin family, does not require neuropilins for Semaphorin 3E-mediated signaling.[177]

The high expression levels of *plxnD1* in angiogenic vessels during embryogenesis, led us to investigate whether this protein is also expressed during tumor-associated angiogenesis. We found that *plxnD1* was indeed expressed at high levels in tumor vessels of intracerebral Mel57-VEGF-A tumors,[77] but not in unaffected brain vessels. Importantly, human tumors of different origin also expressed the protein in their vessels indicating that *PLXND1* expression is not restricted to early stages of angiogenesis. Interestingly, tumor cells also frequently express *PLXND1*, making this protein a unique candidate for tumor targeting therapies as it is expected to target both vessels and tumor cells. Intravenous injection of M13 phages displaying anti-*PLXND1* single domain antibodies (sdabs) or the respective soluble sdabs, led to accumulation on tumor vessels but not on normal brain vessels. Thus, PLXND1 may be a promising target for anti-vascular and anti-tumor therapies.

Materials and Methods

Phage display

A phage display library was constructed by RT-PCR from Llama B-lymphocytes essentially as described.[178,179] VHH-single domain antibody (sdab) fragments were ligated into phagemid vector pHENIXHis8VSV (Raats, unpublished results), resulting in a fusion product with a 8*His-tag and a VSV-G-tag at the C-terminus.[180] After electroporation in *E. coli* TG1 cells, ampicillin-resistant colonies were collected and pooled. The library had a complexity of $8x10^8$ clones. Eighty percent of plasmids contained full-length sdab insert as determined by PCR analysis and immunological dot-blot-detection of the VSV-G-tag in sdabs (see below). The phage library was propagated as phagemids in *E. coli* TG1 bacteria. Phage particles were rescued by infection with trypsin sensitive helper phage M13K07.[181] Phages were purified and concentrated from the culture supernatant by precipitation with 20% PEG-2.5 M NaCl as described.[182]

Selection of PLXND1-binding phage-sdab

Immunotubes (Nunc, Roskilde, Denmark) were coated overnight at 4°C with 5 µg/mL KLH-conjugated peptide (H_2N-ALEIQRRFPSPTPTNC-$CONH_2$, corresponding to amino acids 1-16 of the mature human PLXND1 protein, accession no. AY116661) in 50 mM $NaHCO_3$ (pH 9.6). Of note, the glutamic acid on position 3 in this peptide is a lysine in the mouse sequence, the remaining amino acids are homologous to mouse plxnd1. After washing with PBS/0.05% Tween 20 (PBST), non-specific binding sites were blocked with 5% marvel in PBST (MPBST, 1 hr at room temperature (RT)) and 10^{13} phage particles from the library stock were incubated with the immobilized peptide for 90 min at RT. After rigorous washing with PBST and PBS, bound phages were eluted by trypsin treatment (10 mg/ml, 30 min RT). After trypsin inactivation with 1% newborn calf serum, the eluate was used to infect log-phase TG1 cells to amplify PLXND1-binding phages and calculate number of binders.

To enrich for binding phages, four rounds of selection were performed. From the second round on, selections were performed against unconjugated peptides, immobilized on DNA-binding plates (Costar) to prevent selection of KLH-binders.

Analysis of phage specificity by ELISA

Individual PLXND1-binding phages with PCR-confirmed full-length sdab inserts were tested for specificity. Wells of DNA-binding plates or immunoplates (Nunc) were coated overnight at 4°C with PLXND1-peptide or an irrelevant peptide (1 µg/well in PBS/0.5 M NaCl pH 9.0), BSA (1 µg/well in 50 mM $NaHCO_3$ pH 9.6) or human IgG (1 µg/well in 50 mM $NaHCO_3$ pH 9.6). After blocking non-specific binding sites with MPBST, wells were incubated with phages in MPBST for 1 hr at RT and non-bound phages removed by rigorous washing. Bound phages were detected using HRP-conjugated anti-M13 (Amersham Pharmacia Biotech, Piscataway, NJ, USA) and tetramethylbenzidine (TMB; BioMérieux B.V., Netherlands). The reaction was terminated with 2M H_2SO_4 and enzymatic activity quantified by measuring absorbance at 450 nm using an ELISA reader.

Soluble sdab expression of Plexin D1 specific clones

Expression of soluble sdabs was induced in log-phase TG1 cells by culturing at 30°C in 2xTYA medium/1 mM IPTG. Sdabs were collected by osmotic lysis using ice-cold TES buffer (200mM TrisHCl, 0.5 mM EDTA, 500 mM sucrose) containing a protease inhibitor cocktail (Roche, Basel, Switzerland). Sdab concentrations were estimated via dot-blot analysis using the mouse monoclonal anti-VSV-G P5D4, alkaline phosphatase-conjugated rabbit anti-mouse immunoglobulin (Dako, Denmark) and NBT/BCIP staining. Sdabs were tested in ELISA for PLXND1-peptide specificity.

BIAcore analysis

A BIAcore 2000 (Uppsala, Sweden) biosensor was used to determine binding affinities of the sdabs. The sensor chip and protein coupling chemicals were purchased from Biacore AB. PLXND1-peptide-KLH conjugate (27 µg/ml in Na-Acetate, pH 4.0) or BSA (1 µg/ml in Na-Acetate, pH 5.0) was coupled to activated CM5 surfaces using *N*-ethyl-*N'*-(dimethylaminopropyl) carbodiimide, *N*-hydroxysuccinimide, under conditions recommended by the manufacturer. Unreacted groups were inactivated by 1 M ethanolamine, pH 8.5. Kinetic measurements were performed at 25^{o}C with a flow rate of 10 µl/min in HBS-EP buffer (10 mM Hepes, pH 7.4, 150 mM NaCl, 3 mM EDTA, 0.005% surfactant P20). Six concentrations of Ni-affinity-purified sdabs (in the range of 1 mM to 50µM) were used to determine the dissociation constants (K_d values) of the interaction with the PLXND1-peptide. After each experiment, regeneration of the sensor surface was performed with 10 mM NaOH. Specific binding, defined by binding to a PLXND1-surface minus binding to a control BSA-surface, was analyzed using the BIAevaluation 4.1 software and a 1:1 Langmuir binding model.

In situ hybridization (ISH)

Generation of dig-labelled sense and antisense mouse *plxnD1* RNA probes was described before.[174] A 600 bases human sense and antisense *PLXND1* RNA probe, located in the 3'-untranslated region, was generated by transcription from a PCR product which was flanked by T7 and T3 promoters. Hybridizations were performed using standard protocols.

Immunohistochemistry

Four µm sections of archival, paraffin-embedded or frozen brain tumor tissue of different origin (glioblastoma multiforme and brain metastases of melanoma and sarcoma) were immunostained with anti-*PLXND1* sdabs. Also cerebral mouse xenografts of the human melanoma cell line Mel57-VEGF-A[77] were stained with these sdabs. Following deparaffinization, endogenous peroxidase activity was blocked by incubation with 3% H_2O_2. Antigen retrieval was performed by treatment with pronase according to standard protocols. Subsequently, slides were pre-incubated with normal horse or goat serum (to block non-specific binding sites in sections of human and mouse tissues, respectively), followed by incubation with sdabs for 1 hr. Sdabs were detected by sequential 1 hr incubations with a mouse or rabbit anti-VSV-G antiserum (Sigma-Aldrich Chemie B.V., Zwijndrecht, The Netherlands), biotinylated anti-mouse or anti-rabbit antibody as appropriate (Vector, Burlingame, CA), and avidin-biotin peroxidase complex (Vector, Burlingame, CA). Finally, peroxidase was visualized by the 3-amino-9-ethylcarbazole (ScyTek, Utah, USA) peroxidase reaction with haematoxylin as counterstain. All steps were performed at RT. The blood vessel origin of PLXND1 expression was confirmed by

performing stainings on serial sections with sdabs and anti-human or anti-mouse (as appropriate) anti-CD31 antibody (DAKO, Glostrup, Denmark (anti-human CD31), Hycult Uden, The Netherlands (anti-mouse CD34)).

Animal experiments

All experiments were approved by the Animal Experiment Committee of the Nijmegen University. The hematogenous brain metastasis protocol has been described previously.[183] In short, $2x10^5$ stably transfected Mel57 cells expressing the VEGF-A_{165} isoform were microsurgically injected into the right internal carotid artery of BALB/C nude mice. After 18 days, when animals showed neurological symptoms, CE-MRI was routinely performed to confirm presence of tumor.[77] Mice were used 1 day later for intravenous injections of phages or single domain antibodies.

In vivo homing of plxnd1-binding phages and corresponding sdabs

10^{12} *PLXND1*-binding phages of clones A12, F8 or non-relevant phages were injected in the tail vein of nude mice, carrying established Mel57-VEGF-A_{165} brain metastases (n=2 for A12, n=4 for F8, n=3 for control phage). In two other groups of mice, we intravenously injected 30 µg sdab F8 or a control sdab (n=2 for each group). After 5 minutes, mice were anesthesized using isoflurane, the chests were opened, and non-bound phages were washed from the system by cardiac perfusion with 15 ml of phosphate buffered saline (PBS). Then, mice were sacrificed by cervical dislocation, and parts of brains, hearts, lungs, livers, spleens and kidneys were snap frozen in liquid nitrogen. Other parts were fixed in formalin to be paraffin-embedded. After short hematoxylin staining, tumors were dissected from 10 µm brain sections using laser capture dissection microscopy. Equivalent areas were dissected from unaffected brain, contralateral to the tumor. Subsequently, TG1 cells were infected with phages, eluted by trypsin treatment from dissected samples. Numbers of colony-forming phages were counted and used as a measure of tumor homing. To qualitatively assess tumor homing by phages or sdabs, 4 µm sections were stained with anti-M13 p8 antibody (Abcam Limited, Cambridge, UK) to detect bound phages, or anti-VSV-G antibodies (Sigma-Aldrich) to detect single domain antibodies.

Results

PLXND1 RNA expression in animal and human tumors

To explore whether endothelial *plxnD1* expression is a common feature of activated endothelial cells or is restricted to developing vasculature during embryogenesis as we described previously,[174] we subjected brains of mice, carrying highly angiogenic Mel57-

VEGF-A lesions, to ISH analysis using a mouse *plxnD1*-specific probe. Vessels in these lesions, but not in unaffected brain tissue, expressed high levels of the transcript (Figure 1A, inset shows a CD34 staining). To explore the clinical relevance of this finding, we subjected a number of different human brain tumors and normal brain to ISH using a human-specific *PLXND1* probe. Vessels in brain metastasis of sarcoma (Figure 1B) and melanoma (Figure 1C), as well as a number of other tumor types (not shown), expressed high levels of *PXLND1* RNA.

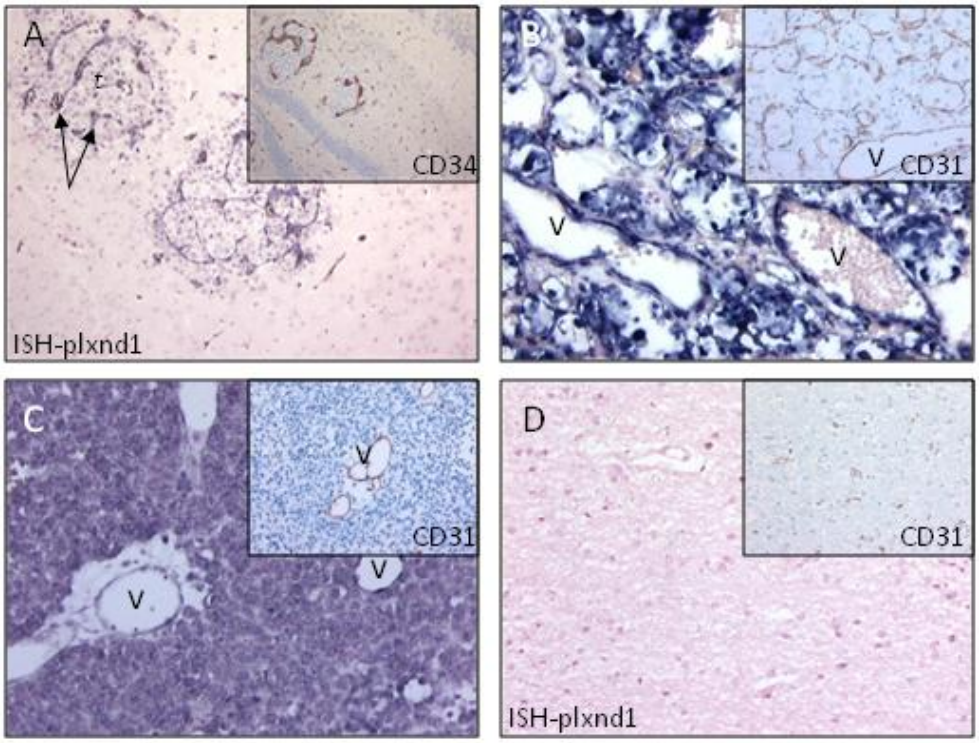

Figure 1. A) ISH analysis of a cerebral Mel57-VEGF lesion using a mouse-specific *plxnd1* RNA probe.
Note the strong positivity of tumor vessels (arrows) whereas brain capillaries, distant from the lesions, are negative (compare the ISH profile with the CD34 staining in the inset). B-D) Human PLXND1-specific ISH analyses of a brain metastasis of sarcoma (B), melanoma (C) and normal brain (D). Insets show
CD31 stainings of serial sections. Control ISH using sense probes were negative (not shown). Note in B and C that *PLXND1* expression is not confined to the blood vessels: also in tumor cells high levels of the *PLXND1* transcript are found. *t*=tumor, V=vessel
In normal human brain, no vessel-associated expression of *PLXND1* was detected (Figure 1D). ISH revealed that tumor cells themselves also were often strongly positive for PLXND1 (compare ISH profiles with the CD31 stainings in the insets in Figure 1B and 1C). Also primary brain tumors were found to be positive for *PLXND1* both on blood vessels and tumor cells (not shown).

Isolation of anti-PLXND1-sdabs

To confirm expression of *PLXND1* on the protein level, we first selected PLXND1-binding VHH-single domain antibodies (sdabs) from a pHENIXHis8VSV-vector-based Llama phage display library. During the four consecutive rounds of selection, a gradual enrichment of phages with PLXND1 affinity (up to 1,400-fold) was observed, indicating that specific binders were present (not shown). Ultimately, 100 individual phages were analyzed for binding to unconjugated PLXND1-peptide in an ELISA-based assay. Seven independent clones, as revealed by *Bst*N1 fingerprinting (not shown), showed specific affinity for the PLXND1-peptide. Phages A12 and F8 were chosen for further analysis because the derived sdabs recognized PLXND1 in immunohistochemical stainings better than the other sdabs (see below). Sequence analysis revealed that A12 and F8 were independent clones, with homology in the CDR1 to CDR3 domains of approximately 40%. These phages, but not an irrelevant sdab-phage or M13 helper phage, bound specifically to *PLXND1*-peptide but not BSA, IgG or an irrelevant peptide (Figure 2A). Furthermore, soluble sdabs derived from these phages also bound specifically to the *PLXND1*-peptide (figure 2B).

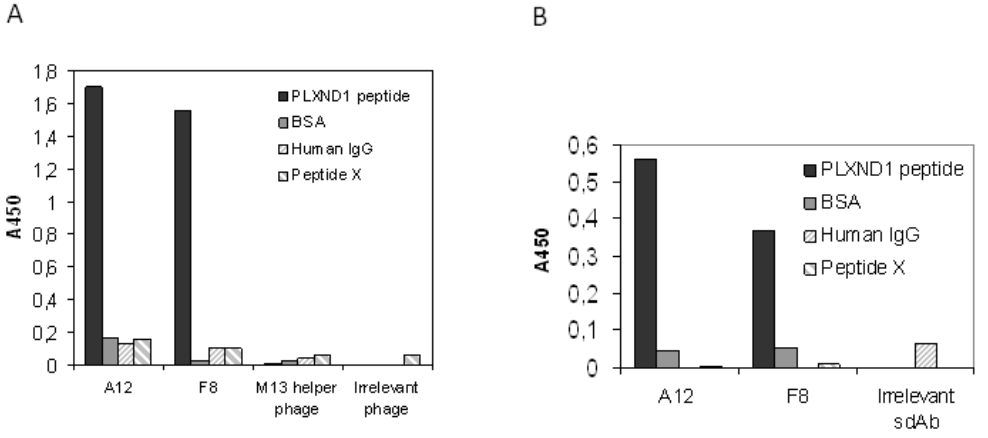

Figure 2. Specificity of phages (A) and corresponding sdabs (B) A12 and F8 for peptide H_2N-ALEIQRRFPSPTPTNC-$CONH_2$. In A, 10^{10} phages were allowed to bind to PLXND1-peptide, BSA, human IgG or irrelevant peptide as described in the text. After rigorous washing, bound phages were detected using an anti-M13 antibody. In B, similar incubations were performed but now with soluble sdabs. After washing, bound sdabs were detected and semi-quantified via the VSV-G-tag.

The binding kinetics of the sdabs/*PLXND1*-peptide interactions were determined by BIAcore analysis. Analysis of the binding data with the 1:1 Langmuir binding model showed a good fit for the sdab binding to the PLXND1-peptide consistent with a 1:1 binding interaction (data not shown). The K_d values of the sdabs were found to be 2.4×10^{-8} M and 3.9×10^{-8} M for sdabs A12 and F8, respectively.

Immunohistochemical analysis

To confirm that sdabs A12 and F8 specifically recognize PLXND1 not only *in vitro* as a peptide, but also in immunohistochemical stainings, we first stained mouse embryos of different developmental stages, in which *plxnd1* expression was previously analyzed by *ISH*.[174] ISH and immunohistochemistry grossly correlated to each other. Especially in the growth plate of trabecular bone, a site of active angiogenesis, blood vessels stained strongly positive both in ISH and immunohistochemistry using *plxnD1*-recognizing sdabs (Figure 3A, the inset shows corresponding plxnd1- ISH).

We went on to use sdabs A12 and F8 for immunohistochemistry on different mouse and human tumors. Indeed, immunostainings with sdabs A12 and F8 confirmed the ISHs shown in Figure 1. Vessels and, to a lesser extent, tumor cells in cerebral angiogenic Mel57 tumors stained positive (figure 3B and not shown). Also in the human sarcoma and melanoma brain metastases (Figures 3C and D), vessels as well as tumor cells stained positive with sdab A12. Interestingly, and consistent with the imperfect homology between the human peptide used for antibody selection and its mouse equivalent, sdabs appeared more efficient in detecting human than mouse plxnD1 (compare Figures 3B with C and D). Furthermore, sdab F8 was more efficient than A12 in detecting mouse *plxnd1*.

The positivity of the tumor cells in Mel57-VEGF-A tumors prompted us to investigate expression of PLXND1 in cultured Mel57-VEGF-A cells. Both by RT-PCR using PLXND1 specific primers and immunostainings with sdab A12, we found that tumor cells expressed the protein *in vitro* also (not shown).

The presence of PLXND1 on tumor- but not normal vessels suggests that this protein may be a suitable target for *in vivo* delivery of diagnostic and therapeutic compounds to tumors. To test this, we injected mice, carrying established Mel57-VEGF-A brain tumors, with 10^{12} colony forming units of phage A12, F8 or a non-relevant phage in the tail vein, and washed non-bound phages from the circulation by cardiac perfusion. After removal and snap-freezing of part of the brains, areas containing tumor or unaffected brain tissue from the contralateral hemisphere were dissected using a laser-capture dissection microscope and analyzed for phage content.

As illustrated in Figure 4D, after intravenous injection of phage F8, significantly more phages were eluted from brain lesions than from comparable areas of normal brain tissue. Consistent with the apparently higher affinity of sdab F8 towards mouse *plxnD1*, more F8 than A12 phages were eluted from tumor. Immunostaining of frozen sections of the same brains with anti-M13 antibodies confirmed the presence of blood vessel-bound phages in tumor but not in normal brain (compare the anti-M13 staining in Figure 4A with the anti-CD31 staining of a serial section in Figure 4B, arrows point at a plxnd1-negative, normal vessel). Upon intravenous injection of an irrelevant phage, no vessel-associated phages could be detected (inset in Figure 4A).

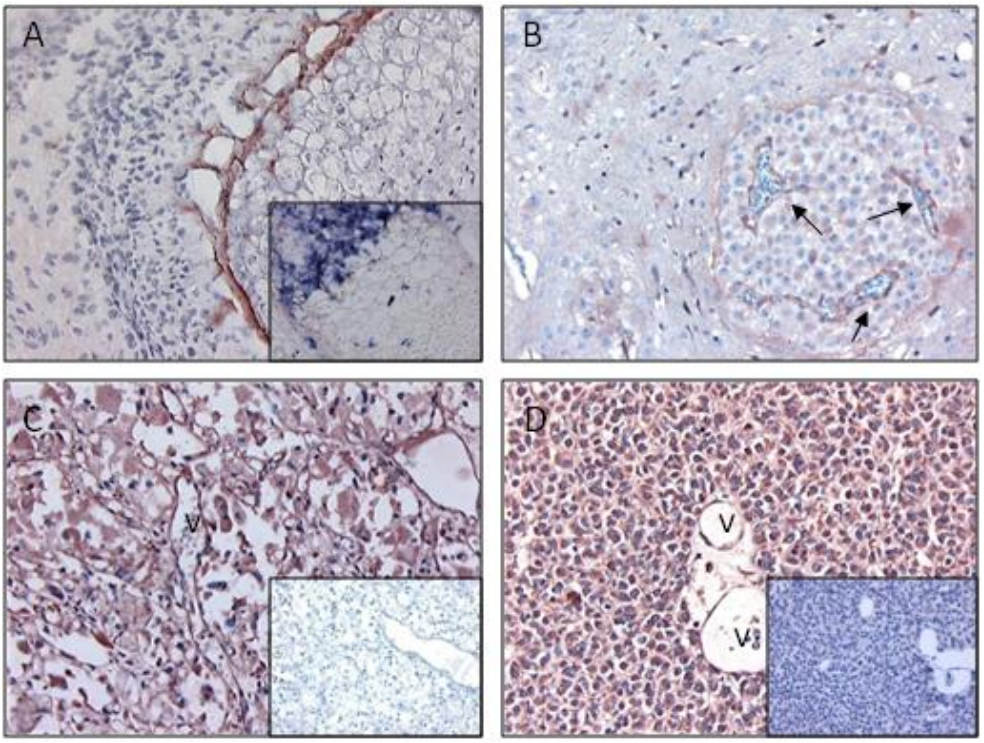

Figure 3. Immunohistochemistry using sdab A12 and F8. A) Growth plate of a trabecular bone in a mouse embryo (E16.5), stained with sdab A12. Note the immunoreactivity in the blood vessels which is consistent with ISH for *plxnd1* (inset). B) Immunostaining with sdab F8 of a Mel57-VEGF-A_{165} lesion in mouse brain. A similar expression profile is seen as in the ISH depicted in figure 1A. Vessels stain positive (arrows) while tumor cells are moderately positive. C) and D) show immunostainings with sdab A12 of the sarcoma (C) and melanoma (D) brain metastases, of which *PLXND1* ISHs are shown in Figure 1. The insets in C and D show control stainings with anti-VSV antibody only. V=vessel.

Tumor targeting by phages is clinically less relevant. Therefore we continued by testing whether purified sdabs are also able to target tumor vasculature *in vivo*. After intravenous injection of sdab F8, this antibody could be detected on tumor vessels by anti-VSV-G immunostaining (Figure 4C). Importantly, no non-specific homing to normal brain vessels could be observed (not shown). Upon intravenous injection of an irrelevant sdab, no vessel-associated sdabs could be detected. However, we observed some staining in the interstitium of Mel57-VEGF-A tumors (inset in Figure 4C). This is to be expected because the leaky tumor vessels are permeable to the small-sized sdabs.

Previous work already revealed that small amounts of the *plxnD1* transcript can be detected in adult normal tissues, especially heart, lung and liver. To investigate targeting of these organs by sdab F8, we performed anti-VSV-G immunostainings of frozen sections. No sdabs could be found associated with normal heart, kidney, liver, spleen and lung (not shown).

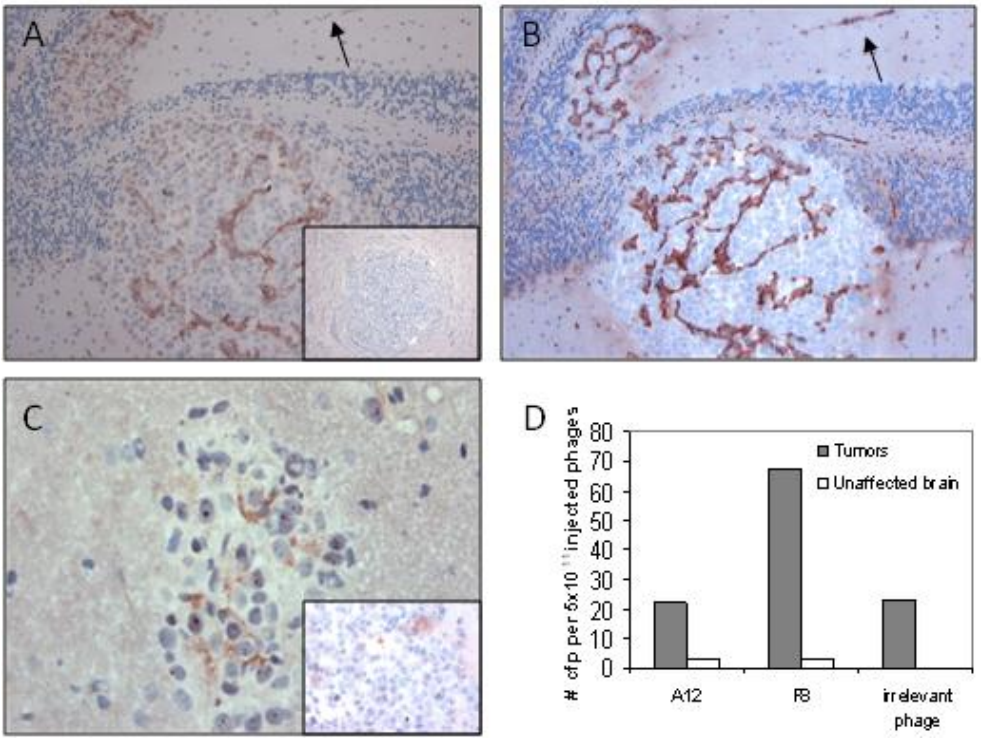

Figure 4. *In vivo* targeting: homing of phage A12, F8 or an irrelevant phage to Mel57-$VEGF_{165}$ brain lesions. Tumor-bearing mice were injected with 10^{12} phages in the tail vein as described in the text. Mice were sacrificed, brains removed and frozen sections were analyzed for phage content and distribution. A) M13 staining of a frozen section of brain Mel57-$VEGF_{165}$ lesions. Phages are clearly vessel-associated, as evidenced by the anti-CD31 immunostaining on a serial section, shown in B). The arrows point at a CD34-positive vessel, distant from the lesion, which is not highlighted by anti-M13 staining. The inset in (A) shows a control experiment where an irrelevant phage was injected. C) Distribution of sdab F8 after intravenous injection in tumor bearing mice. Sdabs are visualized by immunohistochemistry using an anti-VSV antibody. Note that the sdab is detected in tumor vessels but not in normal brain capillaries. The inset shows the control experiment where an irrelevant sdab was injected. An interstitial localization was observed, consistent with the leaky nature of the vessels in these tumors. D) Quantification of phage homing. Tumor tissue was dissected from 10 µm frozen sections using laser capture dissection microscopy. Number of colony-forming phages (cfp) were counted after infection of TG1 cells. Twenty-fold more F8 phages were eluted from tumors than from comparable areas of unaffected brain tissue.

Discussion

In previous work we described *plxnd1* expression in a subset of neuronal cell types and in endothelial cells during developmental angiogenesis.[174] Very recently, plxnD1 knock-down in mice and zebrafish has been described to result in maldevelopment of the vasculature.[175,176] These data suggest a role for plxnD1 in vascular patterning, analogous to that of other plexin family members in axonal patterning (for review, see[172,184]). Here we demonstrate that endothelial expression of *plxnD1* is not restricted to vasculature during development but also occurs in the vascular bed of tumors. Intriguingly, we found that *PLXND1* is also frequently expressed at high levels in tumor cells in a variety of tumor types. This expression profile makes *PLXND1* a potentially powerful target for diagnostic and therapeutic purposes in oncology. To our knowledge, this is the first example of a protein that is specifically expressed on both tumor vessels and tumor cells, allowing simultaneous targeting of different tumor compartments. Indeed, we could show that phages carrying single domain antibodies against *PLXND1* on their surface effectively and specifically homed to cerebral melanoma metastases in mice after i.v. injection. These phages were all vessel-associated. When single domain antibodies were injected we found accumulation in the tumor vasculature, and to a lesser extent also in the tumor interstitium. This interstitial localization could be partly attributed to non-specific extravasation of the small-sized sdabs from leaky tumor vessels, since irrelevant control sdabs showed a similar localization. Importantly, the tumor vessel-association of anti-PLXND1 sdabs was specific, since control sdabs did not accumulate in vasculature. Anti-PLXND1 antibodies may be suitable vehicles to deliver cytotoxic agents to tumors, especially since leaky tumor vessels will allow extravasation of targeting antibodies, thereby enabling a second wave of action against the *PLXND1*-expressing tumor cells themselves. In order to be efficient tumor vessel-targeting vehicles, affinity of anti-PLXND1 antibodies should be as high as possible, whereas targeting of the tumor cell compartment may be more efficient with smaller, lower affinity antibodies with predicted high tumor penetrance.[185] Whether the K_d values of our sdabs of 20-30 nM allow therapeutic targeting of either tumor compartment is not known at the moment. It is however expected that mouse monoclonal targeting antibodies will be more succesful for these purposes. These are currently under development.

The rather disappointing results with anti-angiogenic compounds in clinical trials, which may be related to angiogenesis-independent tumor growth in vessel-dense organs,[117] suggest that vascular targeting therapies may be more effective than anti-angiogenic therapies. This stresses the importance of identifying molecular beacons that are specifically expressed in a wide range of tumors. Few of such molecules have been identified so far. An alternatively spliced fibronectin molecule is deposited in the

basement membrane of newly formed vessels, and single chain antibodies against this protein have been succesfully used to detect clinical tumors in whole body scintigraphs.[124] RGD-motif containing peptides have been used to target integrin $\alpha_v\beta_3$,[127,186] resulting in endothelial apoptosis and anti-tumor activity in animal models, but expression of this integrin is restricted to early stages of angiogenesis. Since mature tumor vessels may therefore be less sensitive to such targeting, it may be more relevant to identify target markers that fulfil the prerequisite of being expressed in mature human tumors. PLXND1 appears to be such a marker. In a number of brain tumors, both primary tumors and metastases, the protein is abundantly expressed. In fact, we have not yet been able to identify a PLXND1-negative tumor. Nevertheless, a more extensive analysis of *PLXND1*-expression and distribution in a variety of human tumor types will be needed to make more rigorous statements about the usefulness of PLXND1 as a tumor marker in the clinic.
A functional role of PLXND1 in developmental angiogenesis is now well established.[175,176] Whether PLXND1 is functionally involved in vessel morphogenesis during tumor angiogenesis as well, is an intriguing question. If so, targeting of this protein may well lead to a functional blockade and consequently an anti-angiogenic effect. This aspect is currently under investigation in our lab. Whether PLXND1 on tumor cells is functionally important, is also not known. Intriguingly, Gu et al. recently published that Semaphorin 3E is a ligand for PLXND1.[177] Since Semaphorin 3E has been identified in microarray experiments as a protein involved in tumor invasion and metastasis,[187] this opens up the interesting possibility that a PLXND1/Semaphorin 3E loop is involved in aggressive tumor behaviour. In this context, neutralization of PLXND1 may directly inhibit tumor invasion and metastasis.
PLXND1-expression is not absolutely tumor-specific. We and others have previously shown that low levels of the PLXND1 transcript can be found in normal adult heart, liver and testis.[174] Immunohistochemical analysis and in situ hybridization revealed that the cells that are responsible for these expression levels are mostly macrophages. Interestingly, these cells are characterized by their migratory potential. Taken together, this opens up the possibility that PLXND1 has a more general function in cell migration.
In conclusion, we have demonstrated that *plxnD1* is expressed in tumor- but not normal vasculature, as well as tumor cells in a wide range of tumor types. The expression patterns, and emerging data on PLXND1 function in vascular morphogenesis and possibly tumor cell behavior, highlight this protein as a potentially powerful tool for future diagnosis and therapy in oncology.

Chapter 4

Semaphorin 3E expression correlates inversely with Plexin D1 during tumor progression

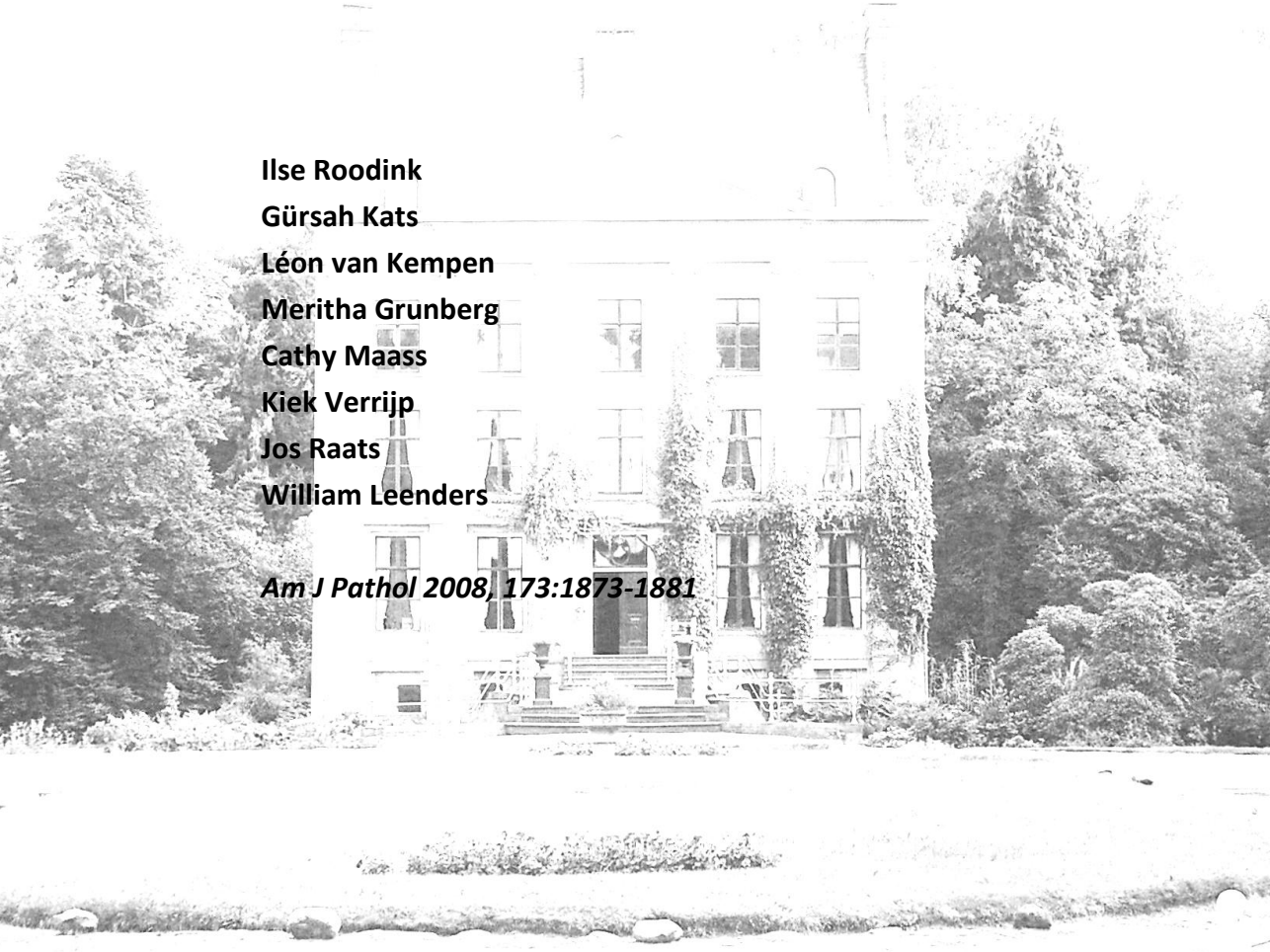

Ilse Roodink
Gürsah Kats
Léon van Kempen
Meritha Grunberg
Cathy Maass
Kiek Verrijp
Jos Raats
William Leenders

Am J Pathol 2008, 173:1873-1881

Abstract

Plexin D1 (PLXND1) is ubiquitously expressed on tumor vessels and tumor cells in a number of human tumor types. If and how PLXND1 expression functionally contributes to tumor development is not known. Expression of semaphorin 3E (Sema3E), one of the ligands for PLXND1, has previously been described to correlate with invasive behaviour and metastasis, suggesting that the PLXND1-Sema3E couple is responsible for tumor progression. Here we investigated PLXND1 and Sema3E expression during tumor progression in melanoma. PLXND1 was not expressed by melanocytic cells in naevi and melanomas *in situ*, whereas expression increased with invasion level according to Clark. Furthermore, 89% of the metastatic melanomas showed membranous PLXND1-staining of tumor cells. Surprisingly, expression of Sema3E was inversely correlated with tumor progression, with predominantly no detectable staining in melanoma metastasis. To functionally assess the effects of Sema3E expression on tumor development, we overexpressed Sema3E in a xenograft model of metastatic melanoma. Sema3E expression dramatically decreased metastatic potential. These results show that PLXND1 expression during tumor development is strongly correlated to invasive behaviour and metastasis, but exclude Sema3E as an activating ligand.

Introduction

Cutaneous melanoma is a highly malignant tumor derived from pigment-producing melanocytes in the epidermis. Melanoma frequently develops in a sequence of steps from benign proliferative naevi to atypical naevi, non-invasive *in situ* melanomas (lesions confined to the epidermis), invasive melanomas and finally to metastases. Clinically, melanomas begin as pigmented lesions that enlarge along an imaginary radius of an imperfect circle, the so-called radial growth phase (RGP).[188] At the time of diagnosis many melanomas have progressed to the next phase of progression or vertical growth phase (VGP) that is characterized by invasion of the papillary and reticular dermis.[188] Whereas the relatively indolent RGP melanomas rarely give rise to metastases, VGP melanomas do have the tendency to metastasize.[189] Furthermore, progression from RGP to VGP melanoma is accompanied by angiogenesis.[190,191] Stage of disease is usually determined histopathologically by both the maximum vertical tumor thickness (Breslow index) and tumor invasion level (Clark classification).[192]

Many studies focused on the identification of differentiation markers to distinguish naevi from melanomas. These include mostly non-specific markers related to cell survival, cell adhesion and extracellular matrix changes,[193-196] general processes that contribute to tumor growth and metastasis.

Plexins encode large transmembrane proteins that are receptors for neuropilins and semaphorins, a family of secreted or membrane-associated proteins.[170,197] Class 3 semaphorins have been mostly studied in the developing nervous system, where they regulate axonal guidance via activation of plexin/neuropilin complexes.[171,173,184,198] The widespread expression of both plexins and semaphorins during embryogenesis, also outside the nervous system, suggests a more general role in physiological and pathological processes.[199,200] We previously demonstrated that Plexin D1 (PLXND1) is expressed by vascular endothelial cells during developmental angiogenesis.[174] Loss of PLXND1 function in mice and zebrafish leads to lethality, due to maldevelopment of the cardiovascular system, indicating a functional role of PLXND1 in vascular patterning.[175,176] Recently we demonstrated that PLXND1 is also specifically expressed on vascular endothelium during tumor-associated angiogenesis in both animal tumor models and a number of human brain tumors, both of primary and metastatic origin.[201] Interestingly, in the examined metastatic brain tumors, including a melanoma metastasis, we observed abundant specific expression of PLXND1 on tumor cells too.[201] PLXND1 contains in its intracellular domain consensus motifs for Rho-guanine nucleotide exchange factors (GEFs). A predicted effect of PLXND1 activation is therefore induction of cytoskeletal rearrangements, translating into cellular migration and invasion. These processes are fundamental in both

angiogenesis and tumor metastasis, suggesting that PLXND1 is functionally involved in tumor development in multiple ways.

Three candidate ligands for PLXND1 have been identified. Semaphorin 3C (Sema3C) binds with high affinity to a Neuropilin-1/PLXND1 complex,[176] whereas binding of semaphorin 3E (Sema3E) or semaphorin 4A (Sema4A) to PLXND1 does not require the presence of neuropilin.[177,202] Interestingly, Sema3E was identified from array analyses as a protein involved in tumor invasion, progression and metastasis.[187] Collectively, these data suggest an involvement of a PLXND1/Sema3E complex in tumor angiogenesis, tumor cell invasion and metastasis.

Here we have addressed this hypothesis in two independent ways. First, we analyzed PLXND1 and Sema3E expression by immunohistochemistry on a series of cutaneous melanocytic lesions representing different stages of melanoma progression. Secondly, we examined the effects of overexpression of Sema3E in a melanoma metastasis model.

Our results show that PLXND1 expression correlates with tumor invasion level and metastasis in a melanoma progression series. In contrast, Sema3E expression showed a negative association with melanoma progression. This inverse correlation was corroborated in functional studies, which revealed that Sema3E expression, in contrast to Sema3C, resulted in an altered tumor vascular phenotype and significantly reduced metastatic potential.

Materials and Methods

Tissue samples

Formalin-fixed, paraffin-embedded tissue specimens were obtained from the archive of the Department of Pathology of the Radboud University Nijmegen Medical Centre. This study included naevocellular naevi (n=19), dysplastic naevi (n=10), melanomas *in situ* (n=5), primary cutaneous melanomas (n=22) and disseminated melanomas, including skin (n=4), lymph node (n=9), brain (n=5) and lung (n=1) metastases. All primary melanomas were classified by qualified pathologists and graded according to Clark's criteria (II, n=7; III, n=5; IV, n=10) and Breslow thickness.

Immunohistochemistry

Tissue sections (4 µm) were dewaxed and endogenous peroxidase activity was quenched with 3% H_2O_2 in PBS. Antigen retrieval was performed by digestion with pronase for 9 minutes at 37°C. Subsequently, tissues were pre-incubated with normal horse serum to block non-specific binding sites, followed by incubation for 1 hr with single domain antibody A12, which was previously selected against a PLXND1-specific peptide.[201] Single

domain antibodies were detected by sequential incubations with the mouse monoclonal anti-VSV antibody P5D4, biotinylated anti-mouse IgG (Vector, Burlingame, CA), and avidin-biotin peroxidase complex (Vector) for 1 hr, 30 minutes and 45 minutes respectively. Peroxidase was visualized by the 3-amino-9-ethylcarbazole (ScyTek, Logan, UT) peroxidase reaction and counterstained with haematoxylin. All incubations were performed at room temperature.

Fifty of the 75 human melanocytic lesions analyzed for PLXND1 expression were immunostained for Sema3E according to standard protocols. In short, antigen retrieval was performed by boiling in 10 mM citrate buffer. Non-specific binding sites were blocked by incubation with normal horse serum. Slides were incubated overnight at 4°C with goat anti-Sema3E (Abcam Limited, Cambridge, UK), and subsequently detected by sequential incubations with biotinylated anti-goat IgG antibody (Vector) and avidin-biotin peroxidase complex (Vector).

For immunohistochemical analysis of experimental tumors, tissues (tumor, lung) were formalin fixed and used for (immuno)histological analysis using rat anti-mouse CD34 (Hycult Biotechnology, Uden, The Netherlands), rabbit anti-mouse Ki-67 (Dianova, Hamburg, Germany), rabbit anti-laminin (Dako, Glostrup, Denmark), rabbit anti-GFP (a kind gift of Huib Croes, Department of Cell Biology, Radboud University Nijmegen Medical Center, The Netherlands) and mouse anti-thrombospondin (Abcam Limited).

To determine metastatic deposits in lungs of mice carrying subcutaneous tumors, lungs were cut in five to six slices and arranged in tissue blocks in such a way that in one section a representative overview through the lungs is obtained. Numbers of metastases were counted in H&E stained sections. Differences in metastatic load between tumor groups were studied using Mann-Whitney U test. Statistics were performed using SPSS software (SPSS Inc, Chicago, Il, USA).

Cell lines and transfections

Mel57 human melanoma cells were cultured in DMEM (Cambrex Bioscience, Verviers, Belgium) supplemented with 10% fetal calf serum (Cambrex), 100 U/ml penicillin and 100 µg/ml streptomycin (Cambrex) at 37°C at 5% CO_2. cDNA encoding VEGF-A_{165} (human origin) was cloned in pIREShyg essentially as described.[76] Human Sema3E cDNA was obtained by RT-PCR on glioblastoma RNA, using primers *Hpa*I-Sema3E (5'-CGTTAACAGGGCTTGGACGG–3') and *Bst*X1-Sema3E (5'-CCAGCACACTGGTCAGGAGTCCAGCGT-3') and cloned in the *Eco*RV/*Bst*XI sites of vector pIRESneo (Clontech, Palo Alto, CA) to generate plasmid pIRESneoSema3E. In parallel, Sema3C was PCR cloned in pIRESneo. Mel57 melanoma cells, stably transfected with pIREShyg-VEGF-A_{165} were supertransfected with plasmid pIRESneoSema3E or pIRESneoSema3C using Fugene reagent (Roche, Almere, The Netherlands). Two days after transfection, cells were put under hygromycin and

neomycin selection pressure until colonies could be expanded. Similarly, double transfectants of Mel57 were generated expressing VEGF-A_{165} and EGFP as control. The presence of recombinant VEGF-A, Sema3E and Sema3C in conditioned medium was confirmed by Western blot analysis using VEGF-A20 antibody (Santa Cruz Biotechnology, Santa Cruz, CA), goat anti-Sema3E antibody (Abcam Limited) and sheep anti-Sema3C antibody (R&D Systems, Oxon, UK) respectively.

Animals

All animal experiments were approved by the Animal Experiment Committee of the Radboud University. Specific pathogen-free, male BALB/c nude mice, 6–8 weeks of age were housed under specific pathogen-free conditions (five mice/cage, temperature 20–24°C; relative humidity 50–60%; 15 air changes per hour; light–dark periods 14 h/10 h). Water and food (RMH, Hope Farms, the Netherlands) were available to the animals ad libitum.

Metastasis model

Groups of mice were injected subcutaneously in the flank with $2x10^6$ Mel57-VEGF-A/Sema3E cells (n=9), Mel57-VEGF-A/Sema3C cells (n=9) or Mel57-VEGF-A/EFGP cells (n=8) in 200 µl PBS, essentially as described.[203] To be able to analyze mono- or multicellular origin of metastases, we tagged the tumors by co-injecting $4x10^5$ Mel57-EGFP cells. Tumor growth was monitored twice weekly and volumes calculated as height x depth x width. Mice were sacrificed after development of severe cachexia owing to tumor load, which was 28 and 37 days post subcutaneous injection of Mel57-VEGF-A/EGFP and Mel57-VEGF-A/Sema3(C/E) cells respectively. One out of nine animals carrying a Mel57-VEGF-A/Sema3E tumor had to be sacrificed two days earlier because of severe ascites and tumor deposits on the peritoneum. Before sacrifice, blood plasma was collected for determination of circulating VEGF-A levels by an in house developed ELISA.[204]

Expression of extracellular matrix and adhesion molecules

Total RNA was isolated from 30 frozen 20 µm sections of subcutaneous Mel57-VEGF-A (n=5) and Mel57-VEGF-A/Sema3E (n=5) tumors using TRIzol reagent (Invitrogen, Carlsbad, CA) according to the manufacturer's protocol and treated with DNaseI (NEB, Ipswich, MA). RNA samples (1 µg) were reverse transcribed using MMLV reverse transcriptase (Promega, Leiden, The Netherlands) according to the manufacturer's instructions. In each individual sample, cDNA quality was assessed by PCR for β-actin and VEGF-A . Of each tumor group, cDNAs were pooled and subjected to the Human Extracellular Matrix and Adhesion Molecules RT^2 Profiler Array™ (Superarray Bioscience Corporation, Frederick, MD). Amplification was performed in a volume of 25 µl containing 1 µl of template cDNA,

12.5 µl of RT^2 Real-Time SYBR Green/ROX PCR master mix, 10.5 µl of H_2O, and 1 µl RT^2 primer set. Amplification was carried out for 40 cycles (95°C for 15 seconds, 60°C for 1 minute) on an ABI 7000 Real-Time PCR System (Applied Biosystems). For data analysis the $2^{-\Delta\Delta Ct}$ method[205] was used with normalization of raw data to the housekeeping gene glyceraldehyde-3-phosphate dehydrogenase (GAPDH). Fold change values are presented as difference in expression due to Sema3E-overexpression in Mel57-VEGF xenografts. Cut off values for significant up- or downregulation were chosen as 3 and 0.3, respectively.

Results

PLXND1 and Sema3E expression in human melanocytic lesions

(Dysplastic) naevi

We analyzed PLXND1 and Sema3E expression in benign melanocytic lesions, primary melanomas of different stage and melanoma metastases to determine if this receptor/ligand couple could be involved in tumor progression.

As shown by immunohistochemistry with single domain antibody A12, PLXND1 expression was absent in melanocytes in both naevocellular naevi and dysplastic naevi (Figure 1A and B respectively). Furthermore, no vessel-associated PLXND1 expression was observed in naevi. In the majority of naevi we observed immunoreactivity on cells which appeared to be subsets of macrophages (arrow in figure 1A) as determined by CD68 staining (not shown) and fibroblast-like cells (arrowhead in figure 1A). Whereas PLXND1 was not expressed by melanocytes, Sema3E was abundantly expressed in melanocytes in approximately 80% and 75% of the naevocellular (Fig. 1C) and dysplastic (Fig. 1D) naevi respectively. The vasculature in all but one dysplastic naevi also stained positive for Sema3E (arrows in figure 1D).

Primary cutaneous melanoma

Tumor cells in melanomas *in situ* were negative for PLXND1 (Table 1). However, 73% of the primary cutaneous melanomas exhibited membranous PLXND1 expression by tumor cells. The PLXND1 expression pattern varied per tissue sample from focal to homogeneous throughout the tumor. PLXND1 expression by tumor cells increased during progression from Clark II to IV (Table 1), with 43% of Clark II melanomas (Fig. 2A) and 100% of Clark IV melanomas (Fig. 2B) showing tumor cell-associated PLXND1 to some extent. Also within tumors, the percentage of PLXND1-positive melanoma cells increased with Clark level (Table 1). In 40% of Clark IV primary cutaneous melanomas, all tumor cells expressed PLXND1 (Fig. 2B).

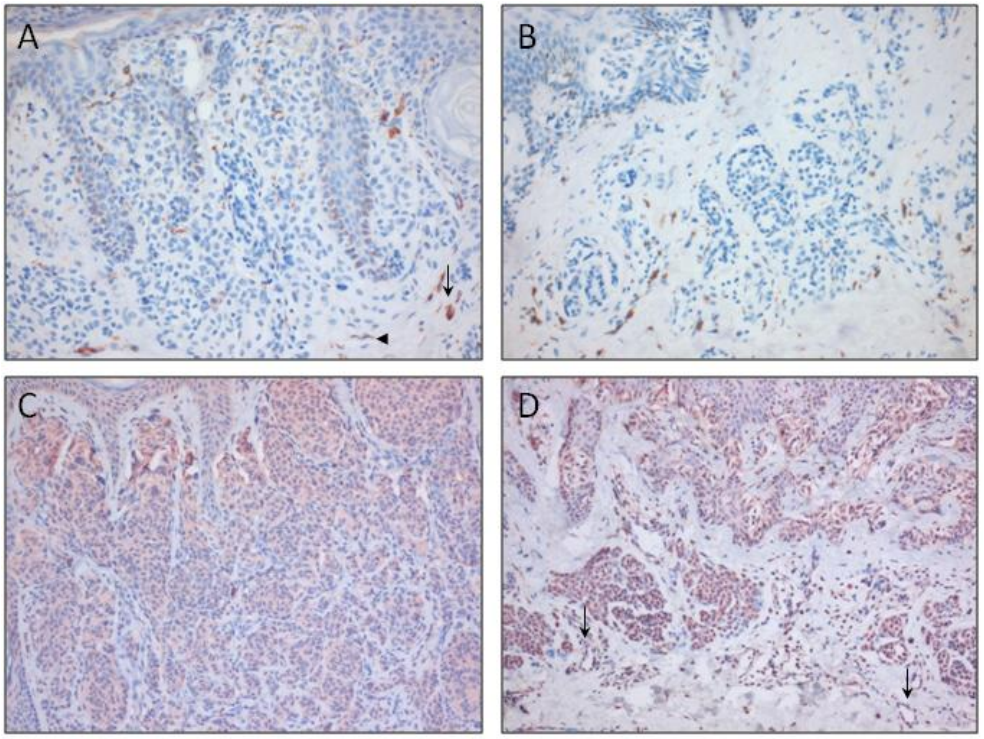

Figure 1. Immunohistochemical analysis of PLXND1 and Sema3E expression in naevi. PLXND1 is not detected in melanocytes in naevocellular (A) and dysplastic (B) naevi. Note the PLXND1-positivity of macrophage- (arrow in A) and fibroblast-like (arrowhead in A) cells. Melanocytes in naevocellular (C) and dysplastic (D) naevi abundantly express Sema3E. Note that vessels in a dysplastic naevus express Sema3E (arrows in D).

Whereas PLXND1 expression on tumor cells correlated with Clark level, we did not find a correlation between tumor cell PLXND1 expression and tumor thickness according to the Breslow index. However, vascular expression of PLXND1 did increase with tumor thickness. PLXND1-positive tumor vessels were absent in primary cutaneous melanoma thinner than 2 mm, while 83% of the lesions (Clark IV melanomas) thicker than 2 mm showed PLXND1-positive tumor vessels (Table 2). The arrows in figure 2B point at PLXND1-positive tumor vessels in a Clark IV melanoma with a Breslow thickness of 3.2 mm. Even in a Clark IV melanoma with a Breslow thickness of 0.65 mm, tumor vessels were negative (arrow in figure 2C).

Table 1. Membranous PLXND1 expression in melanocytic cells in benign naevi, primary cutaneous melanomas, and melanoma metastases

% Positive melanocytic cells	Naevi naevocellularis	Dysplastic naevi	Melanomas *in situ*	Primary Melanomas			Melanoma metastases			
				Clark II	Clark III	Clark IV	Skin	Lymph node	Brain	Lung
0	19	10	5	4	2		1	1		
1-25					2	2				
26-50						2		1		
51-75				1		1				
76-99				2	1	1				
100						4	3	7	5	1
N^+/N_t*	0/19	0/10	0/5	3/7	3/5	10/10	3/4	8/9	5/5	1/1
%	0%	0%	0%	43%	60%	100%	75%	89%	100%	100%

* Number of PLXND1 positive lesions (N^+) per total number of examined lesions (N_t)

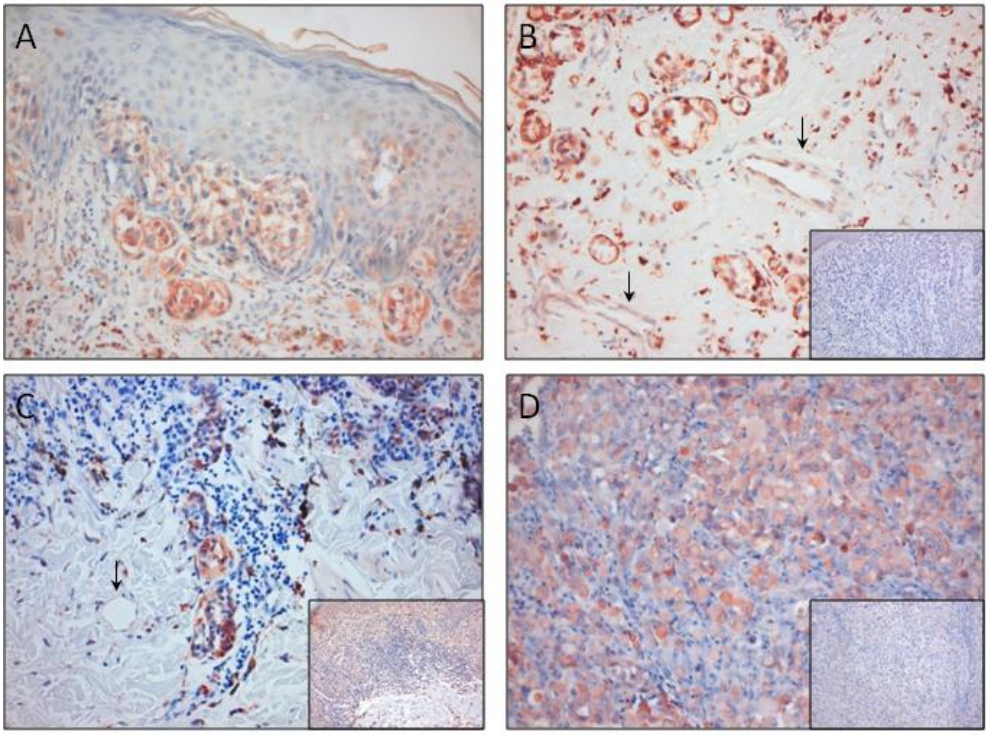

Figure 2. PLXND1 expression in primary melanomas and a melanoma metastasis as revealed by immunostaining with single domain antibody A12. Shown are PLXND1 positive tumor cells in a Clark II melanoma (A), Clark IV melanomas (B and C) and a lymph node metastasis (D). Note in B that tumor vessels in a melanoma with a Breslow thickness of 3.2 mm express PLXND1 (arrows), while PLXND1 is absent in the vasculature of a Clark IV melanoma with a Breslow thickness of 0.65 mm (arrow in C). The insets in B, C and D show Sema3E staining in a Clark IV melanoma (B), a Clark II melanoma (C) and a lymph node metastasis (D).

Table 2. PLXND1 expression in Clark IV melanomas

	Breslow thickness	
	< 2 mm	≥ 2 mm
Melanoma cells	4	6
Tumor vasculature	0	5

The increase in PLXND1 expression was not paralleled by Sema3E expression which was not significantly different between Clark II, III and IV melanomas (Table 3). The inset in Figure 2B shows an example of a PLXND1-positive Clark IV melanoma in which no Sema3E expression is detected. Interestingly, blood vessels in Clark II (inset in Fig. 2C) and Clark III melanomas stained positive for Sema3E, whereas in Clark IV lesions Sema3E-negative vessels were present too.

Melanoma metastases

Approximately 90% of the melanoma metastases showed PLXND1 immunoreactivity (Table 1). A homogeneous expression pattern on all melanoma cells was observed in 75% and 78% of the skin and lymph node (Fig. 2D) metastases respectively, while only one lymph node metastasis showed focal PLXND1 expression by tumor cells (not shown).

Consistent with our earlier observations, PLXND1 was abundantly expressed by both melanoma cells and tumor vessels in brain and lung metastases. In contrast, both the number of melanoma metastases expressing Sema3E and the percentage of Sema3E-positive melanoma cells in individual lesions were reduced compared to primary cutaneous melanomas (Table 3). Only 36% of the melanoma metastases in our series exhibited tumor cell expression of Sema3E, which furthermore was restricted to only a small number of melanoma cells in 60% of these metastases. In 64% of the melanoma metastases, blood vessels were negative for Sema3E whereas in the remaining 36%, Sema3E was expressed in less than 25% of the tumor vessels.

Sema3E inhibits VEGF-A induced micronodular growth in subcutaneous angiogenic melanoma xenografts

The unexpected inverse correlation between PLXND1 expression and its ligand Sema3E in melanoma progression series prompted us to examine whether expression of Sema3E functionally affects tumor development and metastatic behaviour of VEGF-A-expressing subcutaneous Mel57 melanoma xenografts.[203] In these xenografts, tumor cells stain positive with our anti-PLXND1 single domain antibody (Fig. 3A). In addition we analyzed the effects of expression of Sema3C, the Neuropilin-1 dependent PLXND1 ligand, on tumor development and metastasis of these subcutaneous xenografts. Mel57-VEGF-A/Sema3E and Mel57-VEGF-A/Sema3C xenografts showed similar growth rates and developed somewhat delayed as compared to control Mel57-VEGF-A/EGFP xenografts (Fig 3B). Mice were sacrificed when tumors had reached comparable sizes.

All mice exhibited comparable elevated VEGF-A levels in their plasma (3-5 ng/ml) suggesting that effects on tumor growth, morphology and metastatic phenotype were due to Sema3 expression and not to low VEGF-A production by the tumor cells.

Table 3. Sema3E expression in melanocytic cells in benign naevi, primary cutaneous melanomas, and melanoma metastases

% Positive melanocytic cells	Naevi naevocellularis	Dysplastic naevi	Melanomas *in situ*	Primary Melanomas			Melanoma metastases		
				Clark II	Clark III	Clark IV	Skin	Lymph node	Brain
0	2	1		1	1	1	2	5	2
1-25				1		2	2	1	
26-50						1		1	1
51-75									
76-99	1			1					
100	8	3	4	3	3	3			
N^+/N_t^*	9/11	3/4	4/4	5/6	3/4	6/7	2/4	2/7	1/3
%	82%	75%	100%	83%	75%	86%	50%	29%	33%

* Number of Sema3E positive lesions (N^+) per total number of examined lesions (N_t)

In addition, VEGF-A expression in the xenografts was confirmed by mRNA in situ hybridization (not shown). Sema3E and Sema3C expression was determined by immunostainings on Mel57-VEGF-A/Sema3E (inset in Fig. 3C) and -/Sema3C (inset in Fig. 3E) xenografts respectively. Whereas VEGF-A expressing Mel57 xenografts grew with a characteristic micronodular phenotype,[203] the architecture of these tumors was remarkably different when Sema3E was co-expressed (Fig. 3C). Mel57-VEGF-A/Sema3E xenografts consisted of a well vascularized rim of viable tumor cells (Fig. 3D), while centrally these tumors were sparsely vascularized with numerous necrotic areas. This phenotype was not observed when Sema3C instead of Sema3E was co-expressed (Fig. 3E and F). Staining for the proliferation marker Ki-67 with mouse Ki67-specific antibodies revealed that, although Sema3E reduced tumor angiogenesis, VEGF-A-induced proliferation of vascular cells in the tumor rim was unaffected in Mel57-VEGF-A xenografts co-expressing Sema3E (not shown).

Sema3E reduces metastatic potential of subcutaneous Mel57-VEGF-A xenografts

We previously established that Mel57-VEGF-A tumors metastasize by shedding multicellular tumor fragments, surrounded by vessel wall elements, into the circulation which eventually grow to large lung tumors, initially in pulmonary arteries.[203] The multicellular origin of these metastases was assessed by tagging tumor xenografts with EGFP-expressing tumor cells. This principle was also applied in the current experiments.

To investigate whether Sema3E affects metastatic capacity of Mel57 xenografts, we analyzed metastatic burden, composition and localization of lung lesions. In mice carrying subcutaneous Mel57-VEGF-A/Sema3E xenografts, metastatic load in the pulmonary vessels was significantly reduced compared to Mel57-VEGF-A/EGFP ($p=0.022$) and -/Sema3C tumors ($p=0.006$) (Fig. 4A). Whereas Mel57-VEGF-A/Sema3C xenografts exhibited the typical metastatic features previously described for Mel57-VEGF-A tumors[203] (Fig. 4B), such phenotype was observed in only one mouse carrying a Mel57-VEGF-A/Sema3E xenograft. In two mice of the Sema3E group, small lung lesions in the tip of the lungs were detected (Fig. 4C), which in contrast to lung metastases derived from Mel57-VEGF-A/Sema3C xenografts, lacked coverage by the vessel wall elements laminin (not shown) and endothelial cells (inset in Fig. 4C).

Because we co-injected EGFP-tagged Mel57 cells, we could judge whether metastases were of multicellular or monoclonal origin. EGFP immunostainings revealed that the composition of most lung lesions derived from Mel57-VEGF-A/Sema3C xenografts was polyclonal with both Mel57-VEGF-A/Sema3C and Mel57-EGFP cells (Fig. 4D) whereas the two Mel57-VEGF-A/Sema3E derived lesions located in the lung tip were composed of EGFP negative tumor cells (Fig. 4E), suggesting that these originated from clonal expansion of single tumor cells rather than tumor emboli.

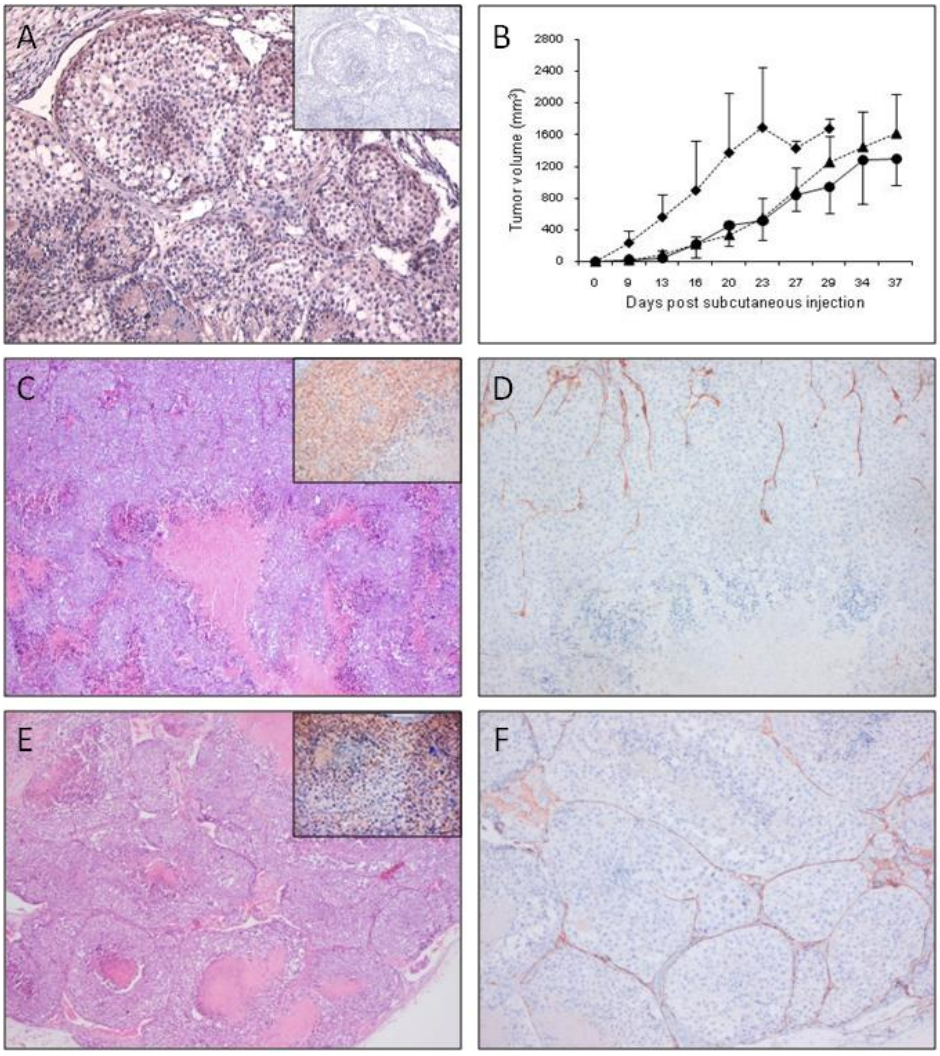

Figure 3. Analysis of subcutaneous Mel57-VEGF-A xenografts co-expressing Sema3E or Sema3C. A) shows PLXND1 expression in subcutaneous Mel57-VEGF-A xenografts as revealed by immunohistochemistry using single domain antibody A12. Both Mel57-VEGF-A cells and endothelium express PLXND1 (the inset shows a negative control staining with anti-VSV-G antibody). B) Tumor growth curves of Sema3E (●) and Sema3C(▲)-expressing Mel57-VEGF-A xenografts and control Mel57-VEGF-A/EGFP lesions (◆). Tumor volumes are calculated as height x depth x width. Note that the xenografts co-expressing Sema3(C/E) show comparable growth rates. Histological analysis of subcutaneous Mel57-VEGF-A/Sema3E and -/Sema3C tumors by H&E staining (C and E) and anti-CD34 staining (D and F). Note the absence of micronodular transformation in Sema3E-expressing tumors (C and D), while Mel57-VEGF-A/Sema3C xenografts show the typically VEGF-A induced micronodular growth pattern (E and F). In contrast to Mel57-VEGF-A/Sema3C xenografts, Sema3E-expressing tumors only show a well vascularized tumor rim. The insets in C and E show Sema3E and Sema3C immunostainings on Mel57-VEGF-A/Sema3E (C) and -/Sema3C (E) xenografts respectively.

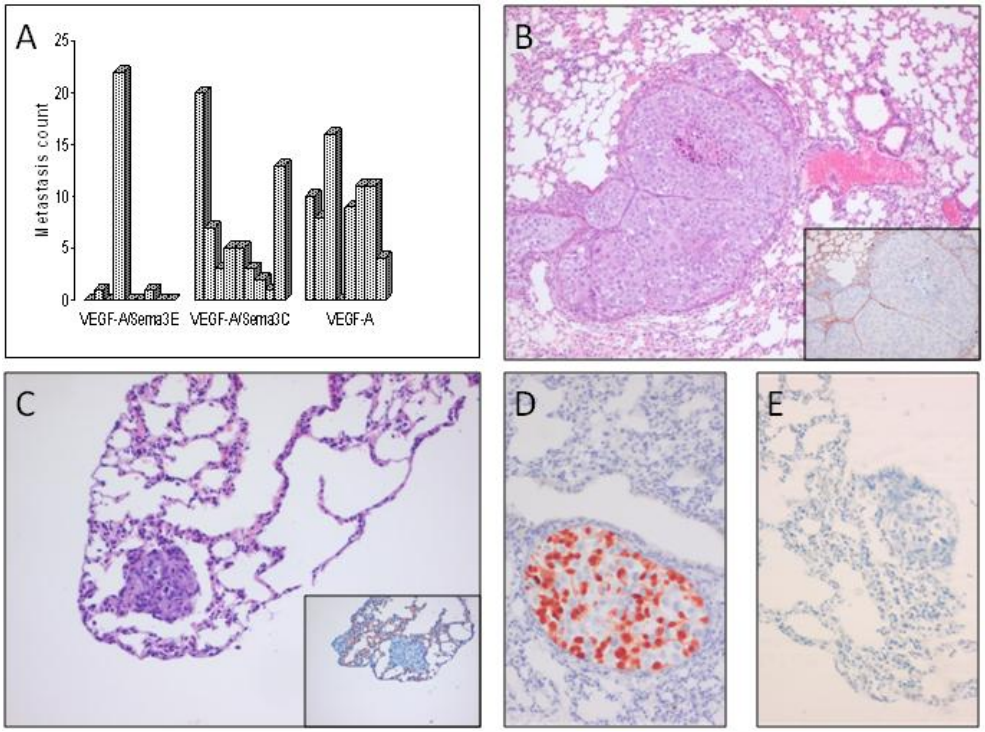

Figure 4. Analysis of metastatic burden, localization and composition. A) Metastasis count of mice carrying different subcutaneous Mel57-VEGF-A xenografts. Lung lesions were counted after H&E staining. Note that in mice carrying subcutaneous Mel57-VEGF-A/Sema3E xenografts metastatic burden is significantly reduced compared to Mel57-VEGF-A/EGFP (p=0.022) and -/Sema3C tumors (p=0.006). In contrast, metastatic load in mice carrying Sema3C expressing tumors is not significantly different from Mel57-VEGF-A/EGFP xenografts (p=0.289). Histochemical analysis of lung metastases by H&E staining (B and C) and anti-CD34 staining (insets) show that lung metastases derived from Mel57-VEGF-A/Sema3C xenografts (B) are predominantly located in the larger branches of the pulmonary vessels. Note in C that the small lesion in the tip of the lung derived from a Mel57-VEGF-A/Sema3E tumor is not surrounded by endothelial cells (inset in C). EGFP immunostainings on lung metastases derived from Mel57-VEGF-A/Sema3C (D) and -/Sema3E (E) xenografts tagged with EGFP-expressing tumor cells. Note that most lung metatases derived from Mel57-VEGF-A/Sema3C xenografts are of multicellular origin with both Mel57-VEGF-A/Sema3C and Mel57-EGFP cells (D), while the EGFP-negative lung lesion in a mice carrying a subcutaneous Mel57-VEGF-A/Sema3E xenograft likely originates from clonal expansion of a single tumor cell (E).

Subcutaneous Mel57-VEGF-A/Sema3E xenografts display down-regulated expression of Thrombospondin 1 and Extracellular matrix protein 1

Both angiogenesis and metastasis highly depend on extracellular matrix remodeling and establishing and disrupting cell-cell interactions. We therefore compared expression profiles of a number of extracellular matrix and adhesion molecules in Mel57-VEGF-A and

Mel57-VEGF-A/Sema3E tumors using the Superarray RT^2 profiler kit. Detectable PCR products, defined as requiring <30 cycles, were obtained for 41 out of 83 genes analyzed. Neither of the tested genes were significantly upregulated in tumors expressing Sema3E as compared to Mel57-VEGF-A tumors. However, we found that thrombospondin 1 (THBS1) and Extracellular matrix protein 1 (ECM1) were expressed at significantly lower levels (respectively 3.8- and 3.6-fold lower as compared to Mel57-VEGF-A xenografts, Figure 5A). To validate the RT-PCR array results we examined THBS expression at the protein level using immunohistochemistry on frozen sections of Mel57-VEGF-A and Mel57-VEGF-A/Sema3E tumors. In accordance with our array data these immunostainings revealed that THBS is abundantly expressed in Mel57-VEGF-A xenografts (Fig. 5B), while this protein is hardly detectable in Mel57-VEGF-A/Sema3E tumors (Fig. 5C). Note that our staining protocol, using a mouse monoclonal THBS antibody, inevitably also results in aspecifical staining of mouse IgG in necrotic areas in both tumors (see negative control stainings with anti-mouse secondary antibody only, insets). Comparison with these control staining clearly shows that THBS is associated with the network of vessel wall elements in Mel57-VEGF-A lesions. Importantly, in these xenografts THBS is expressed by Mel57-VEGF-A cells (magnification in B), while tumors cells overexpressing Sema3E lack THBS expression (magnification in C).

Discussion

Previous studies have suggested a functional role of PLXND1 in developmental angiogenesis.[175,176] In later stages of embryonic development, endothelial cells loose PLXND1 expression and expression is absent in adult endothelial cells.[174] We demonstrated that PLXND1 is re-expressed on vasculature during tumor-associated angiogenesis in both animal tumor models and a number of human brain tumors.[201] Here we show that PLXND1 is expressed by the tumor vasculature in primary melanomas thicker than 2 mm. Transition from micro- to deeply invasive melanoma is accompanied by angiogenesis[190,191] which augments vascular invasion of melanoma cells.[206] Thus, our findings confirm our previous observation that PLXND1 is expressed on angiogenic endothelium and not in quiescent vasculature. PLXND1 was also abundantly expressed by tumor cells, including metastatic melanoma cells. The presence of consensus motifs for Rac-Rho signaling in the intracellular domain of PLXND1[174] is consistent with a possible regulatory role in cellular migration and, thus, tumor progression. Here we show using a single domain antibody against the most aminoterminal part of PLXND1 that expression of this protein in melanocytic lesions is indeed correlated with malignancy stage, being absent in benign lesions and ubiquitous in metastatic cancer.

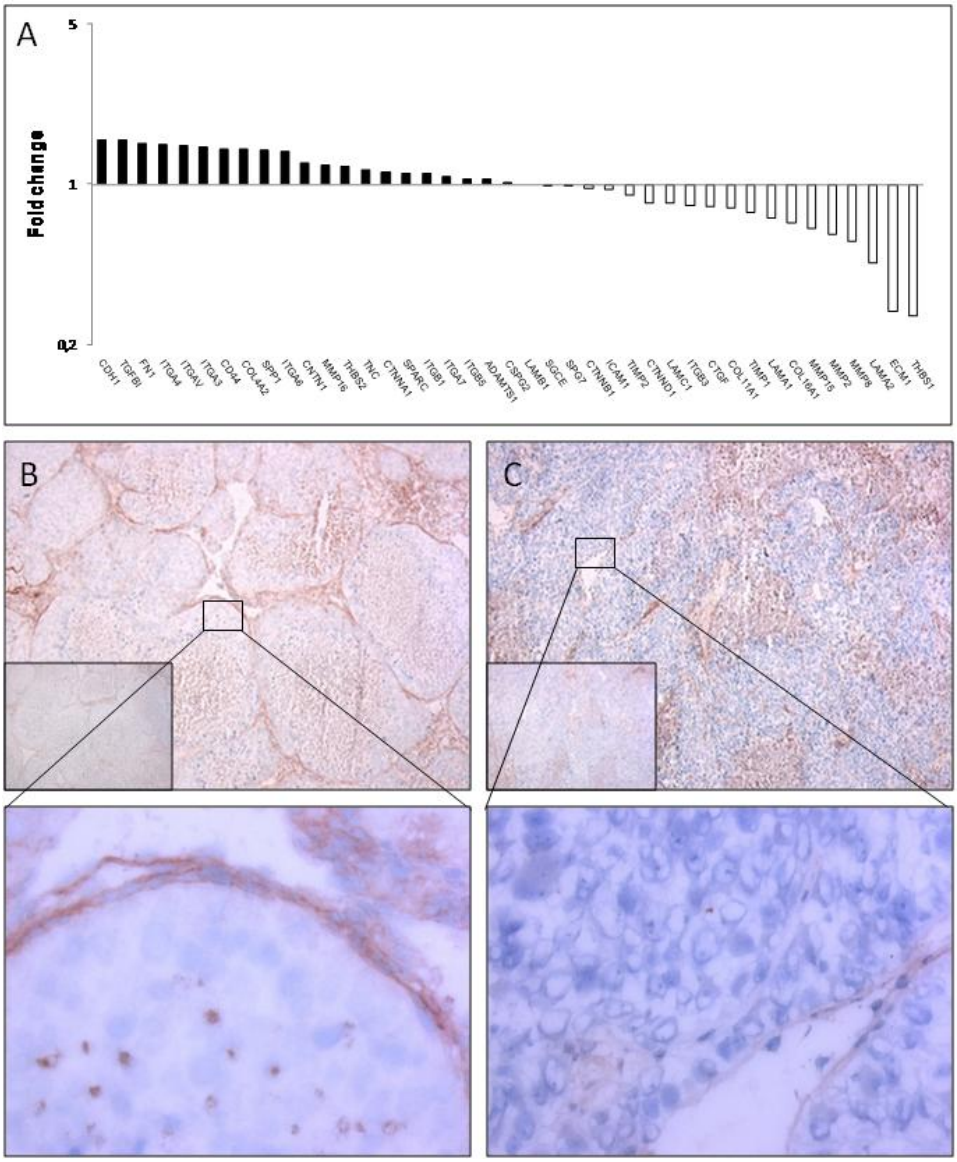

Figure 5. Fold-changes in mRNA expression of extracellular matrix and adhesion molecules in Sema3E overexpressing tumors relative to the control subcutaneous Mel57-VEGF-A lesions as revealed by RT-PCR array analysis (A). Columns represent fold changes in expression in Sema3E-expressing tumors relative to subcutaneous Mel57-VEGF-A lesions. Upper columns (>1.00) represent molecules whose mRNA expression is up-regulated, lower columns (<1.00) molecules whose expression is down-regulated. Immunohistochemical analysis of THBS expression in subcutaneous Mel57-VEGF-A (B) and Mel57-VEGF-A/Sema3E xenografts (C). In contrast to Mel57-VEGF-A/Sema3E lesions THBS is abundantly expressed in Mel57-VEGF-A tumors (the insets show negative control stainings with anti-mouse antibody). Note in B that THBS expression is clearly associated with the network of vessel wall elements and tumor cells.

An inverse relationship was observed with Sema3E, one of the PLXND1 ligands, which was largely absent in metastatic lesions. The hypothesis that emerges from these data, that Sema3E expression is linked to decreased metastatic potential could be validated in a functional melanoma metastasis assay.

The role of Sema3E in tumor biology has been matter of debate in the literature. Originally this protein was discovered via array-analyses as being correlated to metastatic mamma carcinoma.[187] In a follow-up study Christensen *et al*. showed by RT-PCR that Sema3E was expressed by 69% of human mamma carcinoma metastases and overexpression resulted in increased tumor growth in lungs.[207] It has to be realized however, that in these experiments tumor cells were injected directly in the circulation. The initial and possibly rate-limiting steps of metastasis, invasive growth in extracellular matrix and entry into the vasculature, were thus lacking in these experiments.

An inhibitory role of Sema3E for cell migration has also been described. Sema3E acts via PLXND1 to serve as a chemorepellant for endothelial cells[177,202] and inhibits neoangiogenesis *in vivo*.[202] Sema4A, which binds to the same region of PLXND1 as Sema3E, suppresses VEGF-A-mediated angiogenesis by downregulating Rac-GTP-dependent cytoskeletal rearrangement[202] and it is conceivable that Sema3E has a similar mode of action. This notion is supported by our finding that Mel57 xenografts overexpressing Sema3E and VEGF-A, display large areas of central necrosis, consistent with poor angiogenesis. Yet, in vasculature in vital parts of Mel57 VEGF-A/Sema3E xenografts proliferating endothelial cells were observed, indicating that VEGF-A was still able to activate VEGF receptors on endothelial cells. We previously showed that metastasis from Mel57-VEGF-A xenografts develop by bulging of tumor nodules into dilated vessels, a process which is accompanied by gradual coverage of these nodules by endothelial cells.[203] For this process, both endothelial proliferation and migration are indispensable. Our data are therefore consistent with a model in which lack of metastasising capacity is due to impaired migration of endothelial cells.

The dualistic chemorepellant/chemo-attractant properties which are contained within Sema3E appear to be controlled by proteolytic processing, converting a repelling full length Sema3E into an inducer of invasiveness.[207] The antibody used in our current study recognizes both full length Sema3E and the p61 degradation product. The absence of any immunoreactivity in metastatic cancer cells thus places doubt on whether similar proteolytic mechanisms are relevant for regulating Sema3E activity in melanoma. It has recently been described that the presence or absence of neuropilin may also be an important factor, determining the guidance properties of the Sema3E/PLXND1 complex.[208] Interestingly, immunostainings on our melanoma progression series revealed that membranous expression of Neuropilin-1 was almost exclusively observed in melanoma

metastases and to a much lesser extent in primary melanomas (not shown), ruling out an involvement for Neuropilin-1 in regulating Sema3E activity.

To obtain more insight in the underlying mechanisms of angiogenesis and metastasis inhibition by Sema3E, we examined expression levels of a series of genes involved in extracellular matrix remodelling and cell adhesion. THBS1 and ECM1 were significantly down-regulated in Sema3E overexpressing xenografts. It must be noted that we examined gene expression in tumor xenografts consisting of a mix of tumor and stromal cells. Although we can therefore not determine to which cell types the differences in gene expression can be attributed, validation of the array results by immunohistochemistry revealed that Sema3E overexpression results in lack of THBS expression by Mel57 cells. THBS is a secreted protein which interacts with different types of collagen[209,210] and laminin[210]. These matrix proteins are major components of the vascular network surrounding Mel57-VEGF-A tumor noduli[203] which explains the localization of THBS in Mel57-VEGF-A xenografts. Thus, our observations are in agreement with a model in which THBS is secreted by Mel57-VEGF-A cells followed by retention by vessel wall elements generating a bioreservoir of THBS. It remains to be established which mechanisms underly downregulation of THBS by Sema3E on the cellular level.

The role of THBS1 in tumor progression is controversial. Whereas this protein is generally presented as an angiogenesis inhibitor, it has also been reported that THBS1 promotes melanoma invasiveness and metastasis via modulation of melanoma-matrix interactions (for review, see[211]). Interestingly, in clinical cutaneous melanomas, THBS1 expression correlates with microvessel density, tumor thickness and the presence of vascular invasion.[212] Our results are thus in agreement with a pro-angiogenic and pro-metastatic effect of THBS1 in melanoma progression. We also found ECM1 to be down-regulated in Sema3E expressing Mel57 tumors. Expression of ECM1 is closely associated with early stages of angiogenesis during embryonic development and this protein has also been shown to be expressed by tumor cells.[213,214] Concordant with our results, ECM1 expression is associated with metastatic behaviour.[214]

Several other class 3 semaphorins and plexins have been found to affect tumor growth and invasion. Whereas Sema3A, 3B and 3F are described to be functional inhibitors of tumorigenesis and involved in inhibition of tumor cell spread,[215-217] binding of Sema4D to its high affinity receptor plexin B1 contributes to invasive tumor growth and metastasis via activation of Met and Ron receptors.[218,219] Although we showed here that PLXND1 expression is correlated with tumor invasion and metastasis in melanoma progression series, we could not reveal which of its ligands functionally contributes to tumor progression and metastasis. Overexpression of Sema3C, one of the other PLXND1 ligands, did not affect metastasis of Mel57 xenografts. In addition, immunostainings on a number of human melanocytic lesions revealed that Sema3C was equally expressed in both benign

and malignant tissue samples (not shown). Taken together, based on our data we consider it unlikely that binding of Sema3C to a Neuropilin-1/PLXND1 complex contributes to tumor progression.

The correlation between PLXND1 expression and level of melanoma invasion makes this protein a potentially valuable diagnostic marker. PLXND1 can aid to distinguish primary cutaneous melanomas from naevi with a sensitivity of 73%. The observation that PLXND1 is expressed in both tumor vessels and tumor cells in melanoma metastases may also have therapeutic relevance since the protein may be used for simultaneous targeting of different tumor compartments of metastatic melanomas, i.e. melanoma cells and the tumor vasculature.[201]

In conclusion, PLXND1 expression correlates with malignancy grade in tumors but the ligand responsible for PLXND1 activation still has to be identified. Sema3E expression inhibits angiogenesis and metastasis in melanoma, possibly via downregulation of matrix-associated proteins such as thrombospondin 1 and extracellular matrix protein-1. It remains to be elucidated whether Sema3E exerts its effect by competitive inhibition of as yet unknown activating PLXND1 ligands.

Chapter 5

Plexin D1 is ubiquitously expressed on tumor vessels and tumor cells in solid malignancies

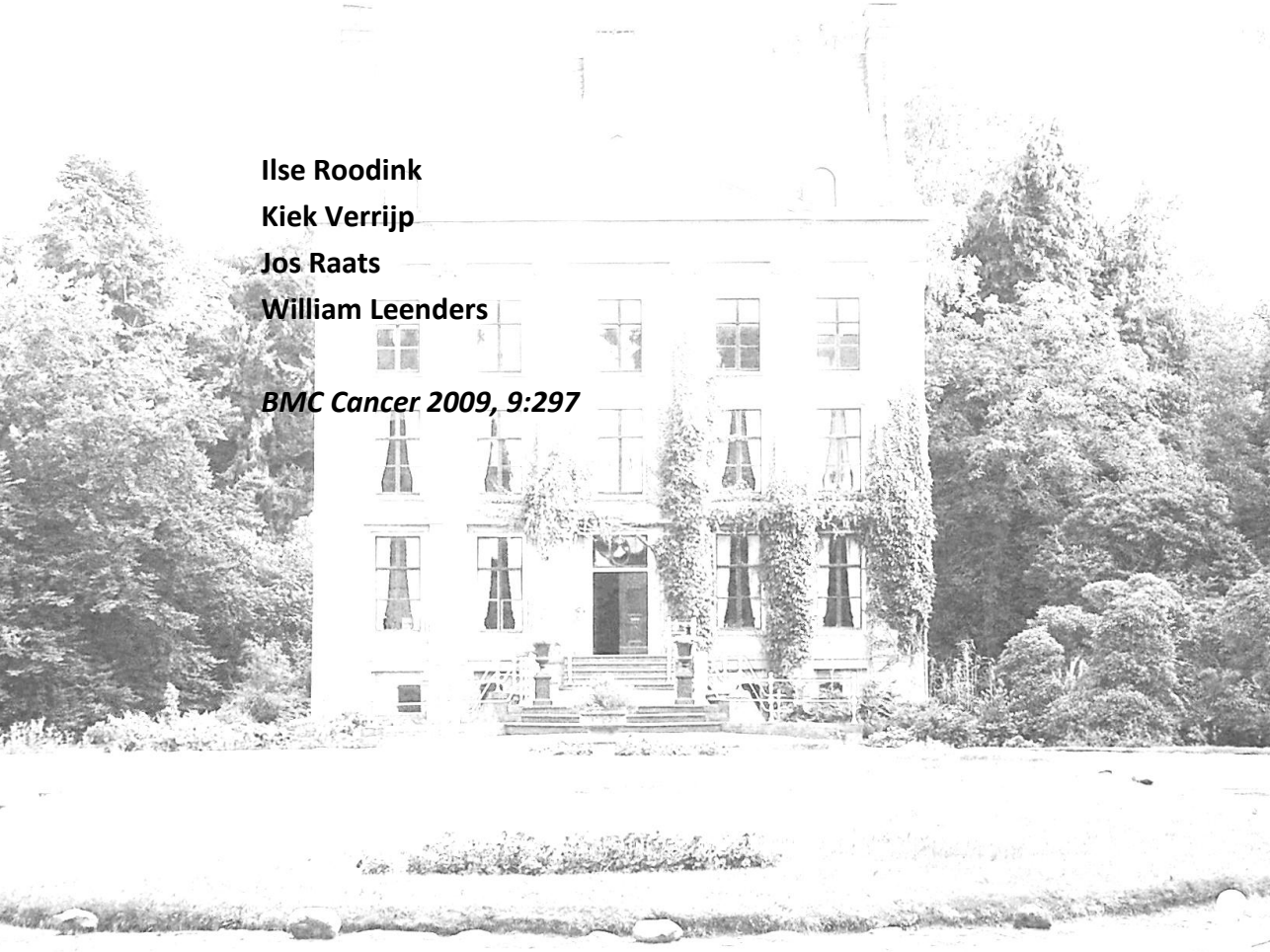

Ilse Roodink
Kiek Verrijp
Jos Raats
William Leenders

BMC Cancer 2009, 9:297

Abstract

Plexin D1 is expressed on both tumor-associated endothelium and malignant cells in a number of clinical brain tumors. Recently we demonstrated that Plexin D1 expression is correlated with tumor invasion level and metastasis in a human melanoma progression series. Here we examined Plexin D1 expression in clinical solid tumors (n=77) of different origin, a selection of pre-malignant lesions (n=29) and a variety of non-tumor related tissues (n=52) by immunohistochemistry. Signals were verified in a selection of tissues via mRNA *in situ* hybridization. Plexin D1 is abundantly expressed on both activated established tumor vasculature and malignant cells in the majority of primary and metastatic clinical tumors, as well as on macrophages and fibroblasts. Importantly, in non-tumor related tissues Plexin D1 expression is restricted to a subset of, presumably activated, fibroblasts and macrophages. This expression profile highlights Plexin D1 as a potentially valuable therapeutic target in clinical solid tumors, enabling simultaneous targeting of different tumor compartments.

Introduction

Interference with a tumor's blood supply is an attractive approach to inhibit tumor growth and dissemination. Thereto, many research focused on targeting the angiogenic process via inhibition of the Vascular endothelial Growth Factor (VEGF-A) pathway.

Despite promising results in animal tumor models in which anti-VEGF therapy translates into potent anti-tumor effects,[60-62] implementation of these therapies for a number of tumor types in the clinic has now learned that they, either or not in combination with chemotherapy, do increase quality of life or modestly prolong survival,[108,220-222] but lack curative effects.[123,166] This discrepancy may be partly due to the high heterogeneity of the vasculature[223-225]: in established clinical tumors all possible maturation stages may be represented, only a small fraction of which may be susceptible to VEGF inhibition.[73] This situation contrasts that in fast growing animal tumors in which the entire population of tumor vessels may be in a synchronized maturation stage. In addition, we and others described that in organs with intrinsically high vessel densities, tumors and metastases are able to grow in an angiogenesis-independent fashion via co-option of pre-existing blood vessels.[75,76,78,167,168] This provides tumors with a route of escape which makes them (partially) unsusceptible to anti-angiogenic compounds. Even more, anti-angiogenesis may drive a shift in brain tumors from an angiogenic to a co-opting phenotype.[117,120,226] Therefore, vascular targeting therapy in which the existing tumor vascular bed, angiogenic or pre-existent, is attacked with the aim to induce acute tumor-specific coagulation may be an attractive additional approach to deprive a tumor from blood supply. To apply vascular targeting therapies, targetable markers that discriminate tumor vessels from normal vasculature are needed. We previously described that Plexin D1 (PLXND1) could be such a target.[201]

PLXND1 belongs to a family of large transmembrane proteins that are receptors for neuropilins and semaphorins.[170,197] Plexins are involved in regulation of axonal patterning during embryonic development.[171,173,184,198] Apart from neuronal cells, PLXND1 is also expressed by vascular endothelial cells during embryogenesis[174] and is of pivotal importance for vascular patterning, as illustrated by the fact that PLXND1 knock-down in mice and zebrafish results in abnormal development of the cardiovascular system.[175,176,227]

We previously demonstrated that PLXND1 is also specifically expressed on vascular endothelium during tumor-associated angiogenesis in a mouse xenograft model of cerebral melanoma metastasis and in a number of human brain tumors, both of primary and metastatic origin.[201] Importantly, expression of this protein was also found on tumor cells in these tumors,[201] and this expression correlates with malignancy grade in a human melanoma progression series: whereas PLXND1 is abundantly expressed in both invasive primary and disseminated melanomas, both in the vasculature and in tumor cells, its

expression was absent in benign melanocytic lesions and melanomas *in situ*, except for expression on macrophages and fibroblasts.[228]

PLXND1 contains in its intracellular domain consensus Rac/RhoA signalling motifs,[174] suggestive of a role in cytoskeletal rearrangements and cell motility, processes which are fundamental for both tumor angiogenesis and metastasis. PLXND1 may thus be functionally involved in tumor development in multiple ways.

The expression profile of PLXND1 suggests that it may be a valuable tumor target for established solid tumors, allowing simultaneous targeting of different tumor compartments, i.e. vessels and tumor cells. To examine whether PLXND1 might be clinically useful as a pan-tumor vessel and pan-tumor cell target in solid tumors we analyzed PLXND1 expression in a wide range of human tumors of different origin and various pre-malignant and non-tumor related tissues by immunohistochemistry and mRNA *in situ* hybridization.

Methods

Tissue samples

Primary and metastatic tumor tissues of different origin (n=77), among them 15 paired samples of human primary and metastatic lesions and various pre-malignant lesions (n=29), were selected from the archives of the Department of Pathology and Radiology of the Radboud University Nijmegen Medical Centre. Furthermore, non-tumor related tissues (n=52) were obtained.

Immunohistochemistry

After deparaffinization and blocking of endogenous peroxidase activity, antigen retrieval was performed by treatment with pronase according to standard protocols.[228] Non-specific binding sites were blocked by incubation with 20% normal horse serum. Slides were incubated for 1 hr with single domain antibody A12, which was previously selected against a PLXND1-specific peptide.[201] A12 was detected by sequential incubations with the mouse anti-VSV-G P5D4, biotinylated anti-mouse IgG (Vector, Burlingame, CA), and avidin-biotin peroxidase complex (Vector). Peroxidase was visualized by the 3-amino-9-ethylcarbazole (ScyTek, Logan, UT) peroxidase reaction, with haematoxylin as counterstain. All incubations were performed at room temperature. Blood vessel origin was confirmed by endothelial stainings on serial sections with anti-human CD31 antibody (DAKO, Glostrup, Denmark).

In a selection of tissues, macrophage identity was confirmed by double staining for PLXND1 and CD68. In short, the above mentioned avidin-biotin peroxidase procedure was

used to detect PLXND1 via rabbit anti-VSV-G antiserum (Sigma Chemical Co., Zwijndrecht, The Netherlands). Following visualization, avidin-biotin was blocked according to standard protocols. Slides were successively incubated with normal horse serum, mouse anti-human CD68 antibody (DAKO) overnight at 4^{o}C, biotinylated anti-mouse IgG (Vector) and avidin-biotin alkaline phosphatase (AP) complex (Vector) at RT. AP was visualized with a mixture of naphthol phosphate (Sigma), levamisole (Sigma), and Fast Blue (Sigma).

PLXND1 mRNA In Situ Hybridization

To explore whether the PLXND1 transcript is also specifically present in malignant tissues, we performed mRNA *in situ* hybridizations on 28 of the 158 paraffin-embedded tissues analyzed by immunohistochemistry (malignant lesions, n=15; benign samples, n=13) as previously described.[201] In brief, digoxigenin-labelled sense and antisense human PLXND1 RNA probes, located in the 3'-untranslated region, were generated by *in vitro* transcription from a PLXND1 PCR product which was flanked by T7 and T3 promoters as described.[174] Following deparaffinization, 4 µm tumor sections were treated with proteinase K (Roche, Almere, The Netherlands) at 37°C for 15 minutes and post-fixed in formaldehyde. Non-specific binding sites were blocked by incubation with acetic anhydride (Sigma) at room temperature. Tissues were hybridized with digoxigenin-labelled RNA probes at 63°C with 200 ng/ml probe. Single stranded non-hybridized RNA was degraded with RNAse T1 (2 units/ml) at 37°C for 30 minutes. After subsequent pre-incubation with normal sheep serum, the slides were incubated with alkaline phosphatase-conjugated sheep anti-digoxigenin antibody (Roche) at room temperature for 1 hour. Alkaline phosphatase was visualized using nitro blue tetrazolium (NBT; Roche) and 5-bromo-4-chloro-3-indolyl phosphate (BCIP; Roche) as substrate with nuclear fast red as counterstain. Specificity of hybridizations was verified by performing control hybridizations with sense probe.

Results

To explore whether PLXND1 may be clinically useful as a pan-tumor endothelium and a pan-tumor cell target we examined the expression profile of this protein in a large variety of human tissue samples. As summarized in Table 1, PLXND1 is abundantly expressed in both the vasculature and malignant cells in the majority of clinical tumors, whereas in pre-malignant lesions the protein is present at lower levels or, like in benign tissues, almost completely absent (Table 2).

Table 1. Plexin D1 expression in solid malignancies

Malignant tissue	PLXND1 expression				Remarks
	Endothelial cells	*Tumor cells*	*Subset of macrophages*	*Subset of fibroblasts*	
Paired samples					
• Medullary breast carcinoma (n=1)	-	-	+	+	Plasma cells also positive
Lymph node metastasis (n=1)	Subset	-	+	n.d.	
• Ductal breast carcinoma (n=8)	+	+	+	+	Some plasma cells also positive
Lymph node metastasis (n=8)	+	+	+	+	
• Adenocarcinoma of colon (n=4)	+	+	+	+	
Liver metastasis (n=4)	+	+	+	+	
• Alveolar soft part sarcoma of femur (n=1)	+	+	n.d.	n.d.	
Brain metastasis (n=1)	+	+	n.d.	n.d.	
• Renal cell carcinoma (n=1)	+	+	n.d.	n.d.	
Brain metastasis (n=1)	+	+	n.d.	n.d.	
Non-paired samples					
Adenocarcinoma of coecum (n=1)	+	+	+	-	
Adenocarcinoma of oesophagus (n=1)	+	+	+	-	
Adenocarcinoma of ovary (n=1)	Subset	+	+	+	
Adenocarcinoma of prostate (n=1)	+	+	-	-	
Adenocarcinoma of rectum (n=5)	+	+	+	+	
Brain metastasis of adenocarcinoma (n=4)	+	+	n.d.	n.d.	
Liver metastasis of adenocarcinoma colon (n=8)	+	+	+	+	
Ovary metastasis of adenocarcinoma colon (n=1)	-	+	-	-	
Low grade astrocytoma (n=2)	Subset	Subset	n.d.	n.d.	
Glioblastoma Multiforme (n=3)	+	+	n.d.	n.d.	
Medulloblastoma (n=1)	+	+	n.d.	n.d.	
Neuro-endocrine tumor of lung (n=2)	+	+	+	n.d.	
Medullary breast carcinoma of (n=4)	+	+	+	+	2 samples negative vessels and tumor cells
Lymph node metastasis of ductal breast carcinoma (n=1)	Subset	+	-	-	
Squamous cell carcinoma of cervix (n=5)	Subset	+	+	-	1 sample negative vessels and tumor cells
Squamous cell carcinoma of vulva (n=5)	-	-	+	+	
Urothelial cell carcinoma of prostate (n=2)	+	+	+	-	

+, corresponding cell type expresses PLXND1
-, PLXND1 expression is absent in corresponding cell type
n.d., corresponding cell type is not detected

Table 2. Plexin D1 expression in pre-malignant and non-tumor related tissues

Tissue	PLXND1 expression			Remarks
	Endothelial cells	*Subsets of macrophages*	*Subsets of fibroblasts*	
Pre-malignant samples				
Ductal carcinoma *in situ* of breast (n=5)	+	+	+	Weak staining of tumor cells
Lobular carcinoma *in situ* of breast (n=3)	Weak	+	+	Weak staining of tumor cells
Vulvar intraepithelial neoplasia (VIN)				
• Classic VIN III, HPV negative (n=5)	-	+	+	
• Classic VIN III, HPV positive (n=8)	-	+	+	
• Differentiated VIN III (n=8)	-	+	n.d.	
Non-tumor related samples				
Bladder (n=1)	-	+	-	
Blood vessel				
• Atherosclerosis (n=6)	-	+	-	
• Fatty streaks (n=1)	-	+	-	
Bone marrow (n=2)	n.d.	-	-	
Brain				
• Cortex (n=1)	-	n.d.	n.d.	Some neurons perinuclear staining
• Alzheimer and CAA (n=1)	-	n.d	n.d.	
• Multiple Sclerosis (n=2)	-	n.d	n.d.	
Breast				
• Normal breast (n=2)	-	-	-	Some epithelial cells perinuclear staining
• Ductal hyperplasia (n=1)	-	+	-	Focal epithelial cells perinuclear staining
Endometrium				
• Proliferation phase (n=5)	Subset (n=3)	+	n.d.	
• Secretion phase (n=4)	-	+	n.d.	
• Secretion/menstruation phase (n=1)	-	+	n.d.	
• Endometriosis interna (n=1)	-	+	n.d.	
Heart (n=1)	-	n.d	n.d	Myocytes perinuclear staining
Large intestine (n=1)	-	+	+	Some epithelial cells perinuclear staining
Liver (n=1)	-	+	n.d.	Some hepatocytes perinuclear staining
Lung (n=2)	-	+	n.d.	
Oesophagus (n=1)	-	+	-	
Pancreas (n=1)	-	n.d	n.d.	Perinuclear staining in Islets of Langerhans
Pituitary gland (n=1)	-	n.d.	n.d.	Some epithelial cells perinuclear staining
Prostate (n=1)	-	-	n.d.	Some epithelial cells perinuclear staining
Small intestine (n=1)	-	+	+	Some epithelial cells perinuclear staining
Spleen (n=1)	-	+	n.d.	
Thyroid gland (n=1)	-	+	n.d.	Some epithelial cells perinuclear staining
Vulva				
• Normal vulva (n=6)	-	+	+	
• Lichen sclerosus (n=6)	-	+	+	

+, corresponding cell type expresses PLXND1
-, PLXND1 expression is absent in corresponding cell type
n.d., corresponding cell type is not detected

Figure 1 shows vascular (arrows) and tumor cell expression of PLXND1 in representative samples of brain metastasis of adenocarcinoma (A), glioblastoma multiforme (B), neuro-endocrine lung tumor (C), ovarian adenocarcinoma (D), and prostatic urothelial cell carcinoma (E). The insets in A and B show corresponding *in situ* hybridization signals. Vascular and tumor cell-associated PLXND1 expression was absent in 3 out of 5 medullary breast carcinomas, one out of 5 cervical squamous cell carcinomas, and all examined vulvar squamous cell carcinomas (Table 1). A representative sample of vulvar squamous cell carcinoma is shown in figure 1F. In addition, two low grade astrocytomas showed infrequent vascular and tumor cell-associated PLXND1 expression (Table 1).

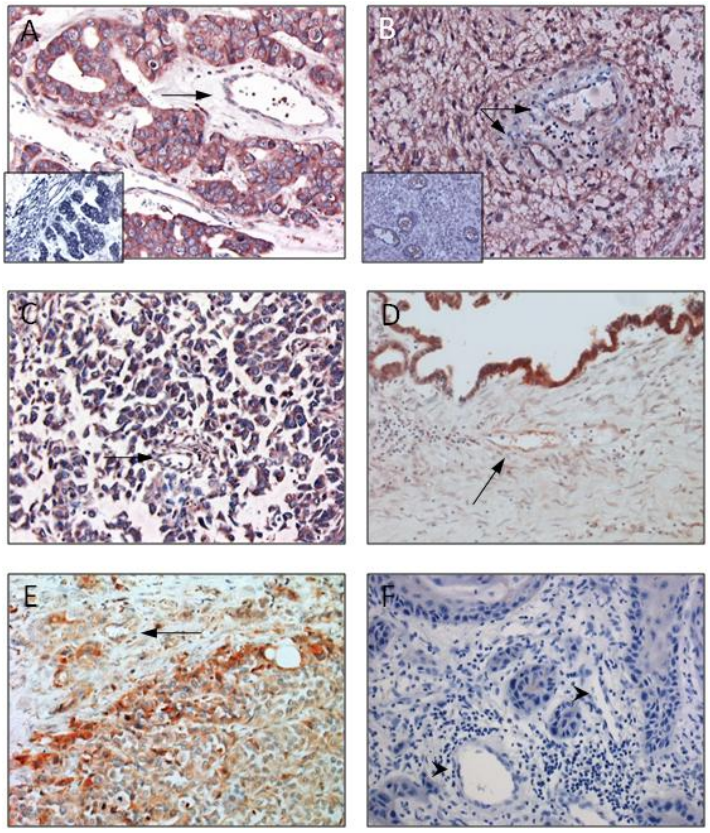

Figure 1. Immunohistochemical analysis of PLXND1 expression in representative clinical tumor samples. PLXND1 is abundantly expressed in adenocarcinoma brain metastases (A), glioblastomas multiforme (B), neuro-endocrine lung tumors (C), an ovarian adenocarcinoma (D), and prostatic urothelial cell carcinomas (E). The arrows point at PLXND1-positive vasculature. PLXND1 is absent in both tumor vasculature (arrowheads) and tumor cells in vulvar squamous cell carcinomas (F). The insets in A and B show corresponding PLXND1 mRNA *in situ* hybridization analyses.

As shown in figure 2A through F no significant differences in staining pattern and intensity of vascular structures (arrows) and malignant cells could be observed between primary ductal breast carcinoma (A) and a corresponding lymph node metastasis (B), colon adenocarcinoma (C) and a corresponding liver metastasis (D) and renal cell carcinoma (E)

and a corresponding brain metastasis (F, the inset shows corresponding *in situ* hybridization signal).

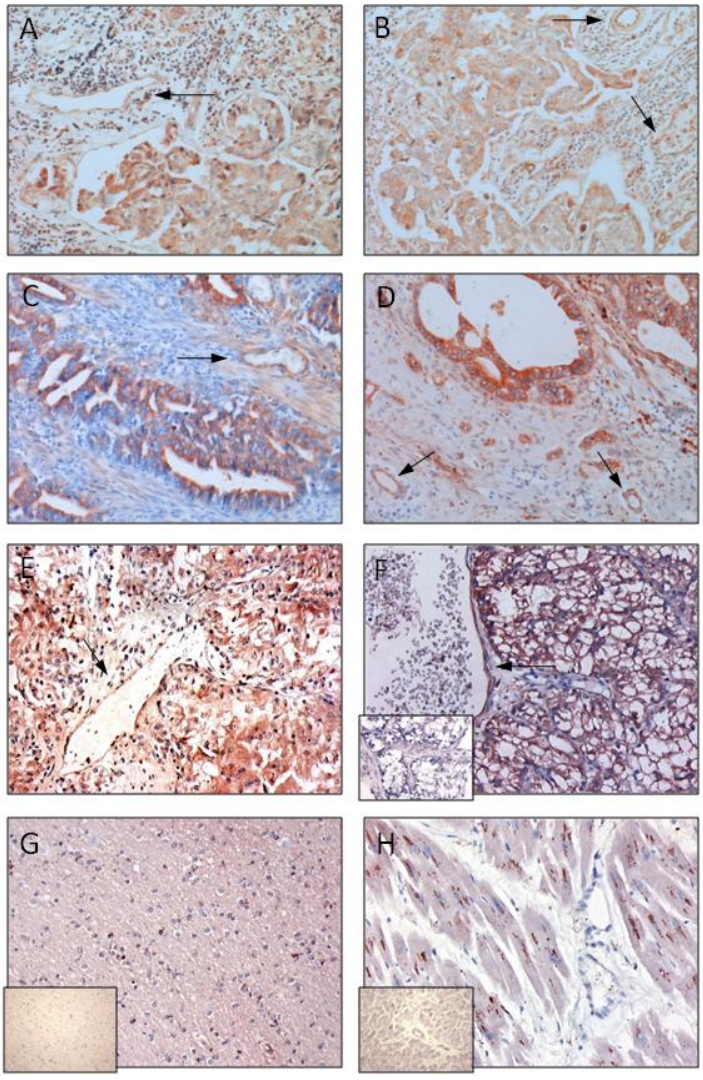

Figure 2. Immunohistochemical analysis of PLXND1 expression in representative clinical tumor samples. PLXND1 is expressed at high levels in primary ductal breast carcinomas (A) and corresponding lymph node metastases (B), colon adenocarcinomas (C) and corresponding liver metastases (D) and a renal cell carcinoma (E) and corresponding brain metastasis (F). The arrows point at PLXND1-expressing tumor vessels. PLXND1 is not detected in normal human cerebral cortex (G) and heart (H) tissue samples. The insets in F, G and H show corresponding PLXND1 mRNA *in situ* hybridization analyses.

To examine whether PLXND1 is expressed on angiogenic vessels under physiological conditions, we also investigated expression in endometrium. In 3 out of 5 proliferative phase endometria some vessels stained positive for PLXND1 (Table 2). Figure 2G and H show lack of PLXND1 protein and transcript (insets) in normal human cerebral cortex and heart tissue. The granular staining pattern in cerebral neurons (G) and cardiac myocytes

(H) is presumably due to aspecific binding of single domain antibodies to lipofuscine as this is observed with other non-related single domain antibodies too (not shown).
Apart from tumor-associated endothelium and tumor cells, PLXND1 expression was also observed in subsets of fibroblast- and macrophage-like cells in both tumor samples and pre-malignant and non-tumor related tissues. Identity of macrophages was confirmed by double staining a selection of analyzed tissues for PLXND1 and CD68 (not shown).

Discussion

In previous work we showed that PLXND1 is expressed in endothelial cells during developmental and tumor-associated angiogenesis.[174,201] Besides vascular expression, high PLXND1 expression was also found on tumor cells in cerebral melanoma metastases. Whereas a role of PLXND1 in vessel patterning during development is well established,[175,176,227] the functional consequences of PLXND1 expression on tumor cells and vessels are less clear. We recently demonstrated that PLXND1 expression is correlated with tumor invasion and metastasis in a human melanoma progression series.[228] However, the PLXND1 ligands Semaphorin 3E and 4A inhibit, rather than promote, (tumor) angiogenesis.[202,228] Moreover, Semaphorin 3E even exhibits anti-tumor and anti-metastatic properties.[228,229]
Here we show that PLXND1 is expressed at high levels on activated established tumor vasculature in a variety of primary and metastatic human malignancies, whereas in benign tissues PLXND1 expression is restricted to a subset of, presumably activated, fibroblasts and macrophages. These results are in agreement with our previous observations in clinical brain tumors of different origin[201] and a series of cutaneous melanocytic lesions representing different stages of melanoma progression.[228] So, for subsets of tumor types in which vessel activation has occurred, PLXND1 may be a valuable candidate protein for vascular targeting approaches. Indeed, the anti-PLXND1 single domain antibody A12 homes to and accumulates in tumor vessels.[201]
Successful vascular targeting has also been achieved with agents directed against molecules of which expression is restricted to vessels in early stages of angiogenesis. Examples are the L19 single chain antibody, directed against the ED-B fragment of fibronectin which targets vasculature in actively growing tumors,[124] whereas this single chain antibody is unable to detect quiescent endothelium in low grade malignancies.[125] Targeted radiotherapy with radiolabeled RGD peptides, recognizing integrin αvβ3 on newly formed endothelial cells, led to reduced growth of xenografts in mouse models of cancer.[126-128] Furthermore, chimeric proteins, consisting of antibodies against the tumor vessel marker vascular cell adhesion molecule 1 (VCAM-1), fused to soluble Tissue Factor,

induced tumor specific blood clotting, tumor necrosis and growth delay in different xenograft models.[129]

Due to vessel heterogeneity in tumors[223-225,230] it is unlikely that one single marker will behave as a targetable pan-tumor-endothelial antigen, but appropriate mixtures of different tumor vessel targeting agents, including anti-PLXND1 antibodies, may allow specific targeting of the majority of tumor vessels. For instance, to effectively starve tumors like low grade gliomas, which (partly) thrive on quiescent vasculature, targeting agents that recognize co-opted vessels in infiltrative tumor areas need to be developed. It remains to be seen whether such targets can be identified and, if so, whether such strategy holds promise for treatment of brain tumors, as it will include some toxicity for interspersed normal brain in infiltrative tumor areas.

Apart from vascular PLXND1 expression in tumors, the protein is also abundantly expressed on tumor cells in a wide range of clinical solid tumors which reinforces this membrane protein as a tumor target, since it allows simultaneous targeting of different tumor compartments with one compound. Since all tumor metastases tested, except for one lymph node metastasis of a medullary breast carcinoma, expressed high levels of this protein, both on vessels and tumor cells, a PLXND1-directed seek-and-destroy strategy may therefore indeed be feasible.

Despite its abundant expression in many different tumor types PLXND1 was not expressed on tumor cells and vessels in a subset of medullary breast carcinomas. Interestingly, these relatively rare tumors generally have a favorable prognosis.[231] It is tempting to speculate that PLXND1 expression is generally correlated with increased malignancy grade. The only other tumor type in our series which lacked vascular and tumor cell-associated PLXND1 expression was vulvar squamous cell carcinoma. Because the increased microvessel density in these tumors suggests angiogenesis,[232] the lack of PLXND1 on vessels in these tumors was unexpected.[201] Whether a lack of PLXND1 expression on these vessels is related to a more mature state can only be speculated upon. Physiological angiogenesis in proliferative phase endometria has been described to occur mainly in a non-sprouting fashion via vessel elongation[233] which may explain the appearance of vascular PLXND1 in only a small subset of vessels in such tissue.

We demonstrated that PLXND1 is in general ubiquitously expressed in tumor but not normal vasculature, as well as in malignant cells in a wide range of human (tumor) tissues. This expression pattern warrants further investigation towards PLXND1 as a therapeutic target in oncology.

Chapter 6

Dynactin-1-p150^{glued} as a specific and targetable marker on tumor endothelial cells

Ilse Roodink
Ronald Roepman
Erwin van Wijk
Stef Letteboer
Roel Hermsen
Geert Frederix
Kiek Verrijp
Jos Raats
William Leenders

Submitted for publication

Abstract

Vasculature in clinical tumors is generally heterogeneous with glioblastoma multiforme as an extreme example. In these tumors, areas of angiogenesis exist next to large areas in which tumor cells diffusely infiltrate the brain. This latter tumor component thrives on pre-existent vessels and is not sensitive to angiogenesis inhibition. Therefore, induction of coagulation in these pre-existent tumor vessels is an attractive adjuvant approach to anti-angiogenesis to deprive tumor cells from blood. This requires that tumor specific vascular targeting agents (TVTAs) become available. Here we describe a novel TVTA, nanobody C-C7, which was isolated by *in vivo* biopanning of a phage display library in the E98 orthotopic mouse model of glioma. Using C-C7 as a bait in yeast two hybrid screens, we identified dynactin-1-p150^{glued} as its binding partner. This protein is specifically expressed on subsets of blood vessels in cerebral and subcutaneous tumor xenografts of different origin, but not on normal brain vessels. C-C7 also recognizes human dynactin-1-p150^{glued} in vessels in clinical glioma. In conclusion, nanobody phage display in combination with yeast-2-hybrid screening is a powerful technique to identify novel targetable tumor vessel markers. The heterogeneity of tumor vasculature suggests that cocktails of anti-vascular targeting agents are needed. Anti-p150^{glued} antibodies are candidate to be included in such cocktails.

Introduction

In order to grow and disseminate, tumors depend on an adequate blood supply.[132] Interference with the tumor vasculature is therefore a promising anti-tumor therapy. Many research focused on inhibition of angiogenesis using antibodies against Vascular Endothelial Growth Factor-A (VEGF-A), the most potent angiogenic factor, or tyrosine kinase inhibitors which specifically interfere with angiogenic receptor signalling. A number of clinical trials on different tumor types have now shown beneficial effects of such therapies, either or not in combination with chemotherapy, on patient performance and progression free survival[234] and culminated in registration of anti-VEGF compounds for treatment of multiple tumor types. However, it is now well recognized that anti-angiogenesis does not cure cancer nor turns cancer into chronic disease.[235] One of the underlying causes is tumor vessel heterogeneity which is especially prominent in glioblastoma multiforme (GBM), a highly malignant astrocytic brain tumor.[82] One hallmark of GBM is the presence of large areas of diffuse infiltrative growth in which tumor cells thrive on pre-existent vessels (co-option) without the need for angiogenesis. One of the other characteristics of GBM is however prominent focal angiogenesis and this has been the rationale for preclinical and clinical testing of anti-VEGF therapy for recurrent GBM as well. Such studies have shown effective inhibition of angiogenesis, however without affecting tumor progression in areas of diffuse infiltrative growth.[120,226,236] This growth pattern thus provides tumors with a route of escape from anti-angiogenic therapies.[123,234]
Anti-angiogenic therapies may be improved by combination with vascular targeting strategies, which aim at destruction of endothelial cells in tumor vessels and subsequent coagulation. Such approach requires that tumor vascular targeting agents (TVTAs) are developed with high enough specificity for tumor vasculature. Available TVTAs [e.g. RGD peptides targeting endothelial αvβ3 integrin,[237] the L19 single chain antibody that targets the ED-B fragment of fibronectin,[124] anti-V-CAM antibodies,[129] anti-plexinD1 antibodies[201]] are directed against newly formed vessels and do not target tumor vessels in more matured stages of development.
Biopanning of peptide or single chain-antibody phage display libraries is a powerful technique which allows identification and isolation of tumor endothelium binding partners.[238-240] Nanobodies® are recombinant antibodies, cloned from cameloid IgG2 and 3 heavy chain antibodies (V-HH) and consist of a single polypeptide chain, making this class of antibodies suitable for display on phages without significant loss of affinity.[241] Their small size (15-18 kDa) and stability make nanobodies to an attractive class of diagnostic and therapeutic compounds. Nanobodies against epidermal growth factor receptor (EGFR) or carcinoembryonic antigen (CEA) have already successfully been used for *in vivo* diagnosis and therapy.[242,243]

In a search for relevant nanobody-based TVTAs we performed *in vivo* biopannings with a nanobody phage display library in mice carrying orthotopic xenografts of the human glioma xenograft line E98.[121] We here describe nanobody C-C7 which specifically binds to tumor vessels in mouse and human gliomas. The C-C7 target was identified as the p150^{glued} subunit of dynactin-1 in yeast two hybrid (Y2H) screens.

Materials and Methods

Tumor models

The E98 glioma xenograft line is maintained as subcutaneous tumors in Balb/c nude mice.[121] E98 tumor homogenates were injected in the cerebrum essentially as previously described.[121] Characteristically, after approximately 21 days mice start to display weight loss and neurological symptoms due to tumor growth. When tumor-related symptoms were apparent, mice were used for *in vivo* biopanning.

In vivo selection of tumor vessel binding phages in mouse cerebral E98 xenografts

All experiments were approved by the Animal Experiment Committee of the Radboud University Nijmegen. Two hundred µl of phosphate buffered saline (PBS) containing 10^{12} phages of a nanobody-displaying phage library (cloned from lymphocytes of Llama glama in phagemid pHENIX-HIS-VSV[201]) were injected in the tail vein of nude mice, carrying cerebral E98 tumors (n=2). Phages were allowed to circulate for 15 minutes. Mice were subsequently put under deep anaesthesia with a mixture of isoflurane/N_2O and chests were opened. Cardiac perfusion was performed with 10 ml sterile 0.9% NaCl solution to remove unbound phages from the circulation. Brains were removed and snap frozen in liquid nitrogen. Sections of 4 µm were stained with anti-M13 p8 antibody (Abcam Limited, Cambridge, UK) to assess phage distribution. Using a laser dissection microscope (Leica AS LMD, Wetzlar, Germany) tumor areas were dissected from 10 µm brain sections and collected. Phages were eluted by incubation with trypsin (10 mg/ml in PBS) for 30 min at room temperature. Following infection in 10 ml of log-phase E. coli TG1 culture, bacteria were plated on 2xTY plates containing 100 mg/L ampicillin and 2% glucose. After overnight incubation, individual clones were picked and analyzed via colony-PCR for the presence of full-length nanobody insert using flanking primers M13fw (5`-TCA CAC AGG AAA CAG CTA TGA-3`) and M13rev (5`-GTA ACG ATC TAA AGT TTT GTC G-3`). Subsequently, PCR products were digested with the 4-cutter restriction enzyme *Bst*NI to analyze the diversity of the phage population. Expression of soluble nanobodies by independent clones was induced in log-phase TG1 cells by culturing at 30^{o}C in 2xTY medium, containing 100 mg/L ampicillin and 1 mmol/L IPTG.

Expression of nanobodies was verified by dot blot analysis of medium using anti-VSV antibodies, as previously described.[201] Based on combined data of full length PCR, *Bst*NI restriction and dotblot analysis, clones were selected for high-yield expression and subsequent immunohistochemical stainings. For that purpose, expression of nanobodies was induced in 200 ml log-phase TG1 cells with 1 mmol/L IPTG for 2 hours after which antibodies were isolated from the periplasm by osmotic lysis as described previously.[201]

Immunohistochemistry

Nanobodies were tested in immunostainings on 4 µm sections of paraffin-embedded tissue sections. Following deparaffinization, endogenous peroxidase activity was blocked by incubation with 3% H_2O_2. Antigen retrieval was performed by boiling in 10 mmol/L citrate buffer. Sections were pre-incubated with normal goat serum to block non-specific binding sites, followed by overnight incubation with nanobody at 4^0C. Detection was performed by sequential incubations with rabbit anti-VSV-G antibody (Sigma-Aldrich Chemie B.V., Zwijndrecht, The Netherlands), biotinylated anti-rabbit antibody (Vector, Burlingame, CA) and avidin-biotin peroxidase complex (Vector, Burlingame, CA). Peroxidase was visualized with 3-amino-9-ethylcarbazole (ScyTek, Utah, USA) with haematoxylin as counterstain. Tumor vessels in serial sections were visualized with anti-mouse anti-CD34 antibody (Hycult, Uden, The Netherlands).

Tumor vessel specificity of selected nanobodies was assessed by staining on normal mouse tissues (heart, kidney, liver, lung and spleen) and tumor xenografts of different origin (intracerebral E98 and U87 gliomas, brain metastases of Mel57-$VEGF_{165}$ melanoma,[117] subcutaneous xenografts of these tumor lines and of the colon carcinoma cell lines C26 and C38[244]). Primary human brain tumors, classified as grade II (n=2) and grade IV (n=7) gliomas, as well as normal brain tissue (n=2) from the archive of our department were also stained. In that case, nanobodies were detected via mouse monoclonal antibody anti-VSV-G P5D4.

Dynactin-1-$p150^{glued}$ expression was verified by immunohistochemistry with a rabbit anti-dynactin-1 antibody (Abcam, Cambridge, UK).

Y2H screens

All cloning steps were performed using the Gateway System (Invitrogen, Carlsbad, CA). The cDNA encoding nanobody C-C7 (without pelB leader) was flanked by attB sites via PCR and cloned in vector pDONR201 before transfer into destination vector pBD-GAL4-CAM/DEST, generating a fusion protein with the GAL4 DNA binding domain. After sequence-verification this vector was transfected into yeast strain PJ69 (A-mating type) using standard protocols.[245] Generation of a randomly primed bovine retina cDNA library in pAD-GAL4, transfected in PJ69 (α-mating type, $2x10^6$ clones) has been described

before.[245] The yeast strain containing pBD-GAL4-C-C7 was mated with this library and diploid cells in which C-C7-prey interactions led to functional GAL4 transcription factor, were selected based on histidine and adenine prototrophy and transactivation of ß-galactosidase activity. Production of ß-galactosidase by activation of the LacZ reporter gene was detected by a filter-lift assay.[245] From positive yeast clones, pAD-GAL4 library expression plasmids were rescued and amplified in E.coli. Plasmids were sequenced using flanking forward and reverse primers. Sequences were blasted (http://www.ncbi.nlm.nih.gov/blast/Blast.cgi) and aligned with multalin software (http://bioinfo.genotoul.fr/multalin/multalin.html). All sequenced clones contained intact reading frames in fusion with the GAL4-activation domain.

Verification of the C-C7-dynactin-1 interaction

The carboxyterminal part of dynactin-1-p150^{glued} was RT-PCR cloned from human glioblastoma cDNA using primers attB1-dyn 2532 (5'-AAA AAG CAG GCT TCA CCA TGG CAG CTG CTG CTG CC-3', sense) and attB2-dyn 3837 (AGA AAG CTG GGT GTT AGG AGA TGA GGC GAC TGT G-3', antisense). attB1 and attB2 sites were extended in a second PCR and products were cloned via pDONR201 in p3xflg-CMV (Invitrogen) to generate p3xflg-CMV-dyn 2532-3837. Plasmid was transfected into COS1 cells in eight-well glass slides (Lab-Tek™ Chamber Slide™ System, Nunc, Roskilde, Denmark). Forty-eight hours later, cells were fixed with acetone and incubated with nanobody C-C7 for 1 hr, followed by sequential incubations with mouse anti-VSV and goat-anti-mouse FITC (Invitrogen, Carlsbad, CA). After washing, slides were stained with rabbit-anti-dynactin-1 which was detected with donkey-anti-rabbit TRITC (Invitrogen, Carlsbad, CA). Images were processed on a Leica Discovery Fluorescence Microscope and a Leica confocal microscope. Image processing was performed with Leica software.

RT-PCR

To examine levels of the dynactin-1 p150^{glued} transcript or its splice variant p135^{glued}, PCR was performed with Phusion DNA polymerase (Bioké, Leiden, The Netherlands) with primer pairs dyn-801fw (ATGGCACAGAGCAAGAG)/dyn-1421rev (GACTGCTCCAGGAGAGG) (detecting p150) or the exon 6A specific primer dyn6Afw (ATGATGAGACAGGCACC)/dyn-1421rev (detecting p135) yielding PCR products of 620 and 280 bp respectively. RT-PCR for β-actin served as housekeeping gene control. Conditions were as follows 94^{o}C, 10sec; 58^{o}C, 30 sec; 72^{o}C 60 sec for 30 or 35 cycles.

Results

In vivo selection of tumor vessel binding phages in cerebral E98 xenografts

A nanobody-displaying phage library[201] was intravenously injected in mice carrying intracerebral E98 xenografts and irrelevant phages were removed from the circulation by cardiac perfusion. Already after the first round of biopanning, anti-M13 immunostainings demonstrated a surprisingly tumor-specific vessel localization of phages (compare anti-M13 with anti-CD31 immunostaining in Figure 1A and 1B respectively). After collection of tumor areas from brain sections by laser capture dissection microscopy and subsequent trypsin treatment, a total of 453 colony-forming phages was rescued of which 192 clones were randomly picked and analysed for full length nanobody expression and diversity. Dot blot analysis revealed that 95% of clones expressed nanobodies and restriction enzyme finger print analysis resulted in five different restriction patterns (not shown). Due to the small variation on the nucleotide level between nanobodies, sequence differences within these groups may still be expected. Therefore, we arbitrarily chose to analyze from each group the 30% of clones with highest nanobody expression levels.

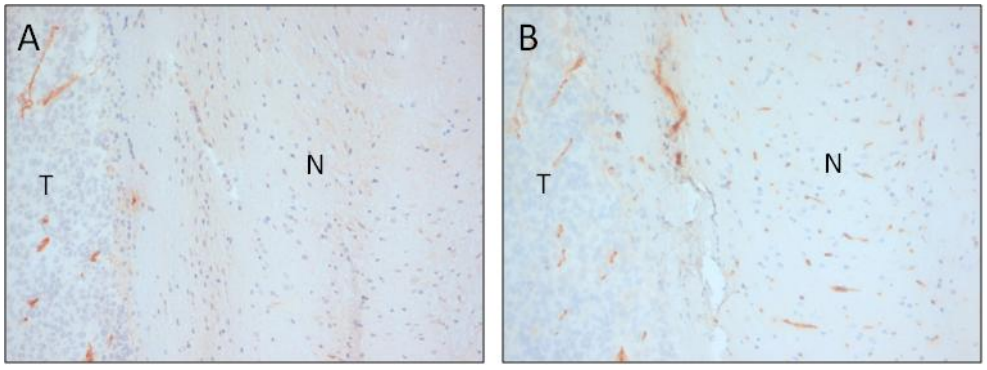

Figure 1. Phage distribution in orthotopic glioma xenografts after *in vivo* biopanning. Procedures are described in Materials and Methods. After sacrifice, brains were removed and serial frozen sections of E98 glioma xenografts were analyzed for phage distribution by anti-M13 (A) or anti-CD31 (B) immunostaining. Note that phages are clearly more associated with tumor vasculature than normal vessels. N=normal, T=tumor

Immunohistochemistry

Immunohistochemical stainings were performed on sections of intracerebral E98 xenografts to select for nanobodies which specifically recognize tumor vessels. Because evaluation of vessel staining requires optimal morphology, we chose to perform immunostainings on sections of formalin-fixed, paraffin-embedded tissues and accepted

that potentially interesting nanobodies (recognizing conformational epitopes that are disrupted during formalin fixation) were lost during analyses. Positive staining of tumor vessels was observed with 27 of the 39 analysed nanobodies of which 10 also recognized unaffected mouse brain vessels. The remaining 17 stained subsets of tumor vessels (not shown). Of these, C-C7 showed most prominent staining of tumor vasculature in E98 xenografts and was analyzed in more detail. As illustrated in Figure 2, C-C7 stained both small and medium sized tumor vessels in the diffuse infiltrative component (Fig. 2A), but also the (neo)vasculature in the compact tumor areas (not shown). Interestingly, not all tumor associated vessels were recognized (compare the C-C7 staining patterns with the anti-CD34 staining of serial sections in the inset in Fig. 2A). Nanobody C-C7 did not stain normal vasculature in mouse brain (Fig. 2B), heart, kidney, liver, lung and spleen (not shown). The observation that C-C7 stained only a subset of tumor vessels prompted us to further characterize C-C7 by immunohistochemistry in other mouse tumor models.

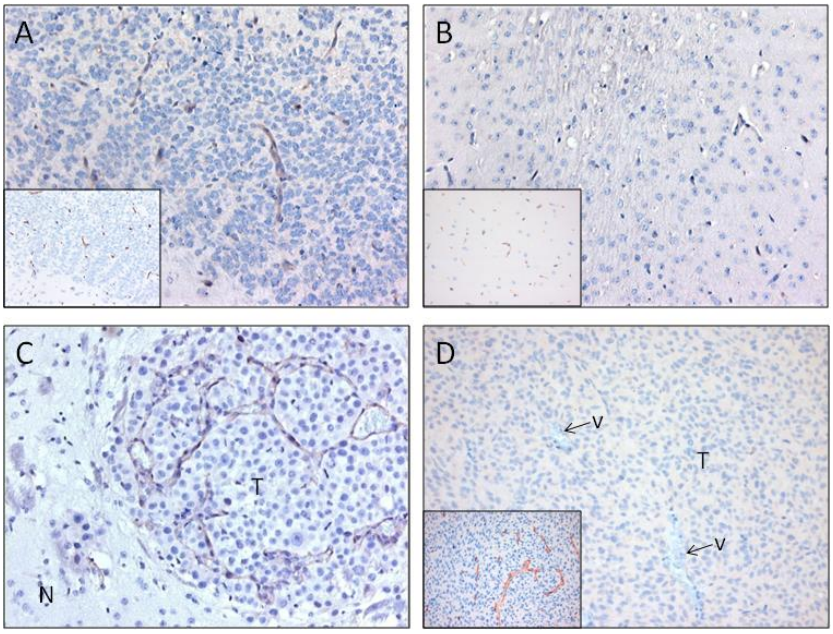

Figure 2. Immunohistochemical analysis of nanobody C-C7 reactivity in cerebral E98 xenografts (A), unaffected mouse brain parenchyma (B), a brain metastasis of Mel57-VEGF$_{165}$ melanoma (C) and a cerebral U87 xenograft (D). C-C7 recognizes subsets of tumor vessels in both diffuse infiltrative E98 tumor, while normal mouse brain vessels and the vasculature of intracerebral U87 glioma are negative. Insets in A, B and D show CD34 immunostainings of serial sections. N=normal, T=tumor, V=vessel.

Whereas the nanobody showed prominent staining of the vasculature in angiogenic brain metastases of the human melanoma cell line Mel57-VEGF$_{165}$[77] (Fig 2C), intracerebral

mouse xenografts of the human glioma cell line U87 did not show any staining (Fig. 2D, the inset in this panel shows a CD34 vascular staining). To examine whether or not vascular expression of the C-C7 target is restricted to brain tumors, we also immunostained subcutaneous xenografts of glioma (U87 and E98), melanoma (Mel57-$VEGF_{165}$) and colon carcinoma (C26 and C38[244]). Consistent with the absence of C-C7 immunoreactivity in intracerebral U87 tumors, vessels in subcutaneous U87 xenografts were negative (not shown). The vasculature of subcutaneous Mel57-$VEGF_{165}$, E98, C26 and C38 xenografts did show expression of the C-C7 ligand (not shown). These data illustrate that reactivity towards C-C7 is not limited to blood vessels in brain tumors.

To investigate whether nanobody C-C7 might have clinical relevance, we proceeded by staining a number of clinical samples of grade II and grade IV astrocytomas as well as unaffected human brain with this nanobody. A subset of tumor vessels in GBMs (see representative example in Fig. 3A) and one low grade glioma (Fig. 3B) was recognized. We could not detect C-C7 reactivity in the other low grade glioma (Fig. 3C), nor did C-C7 stain normal human brain vessels (Fig. 3D).

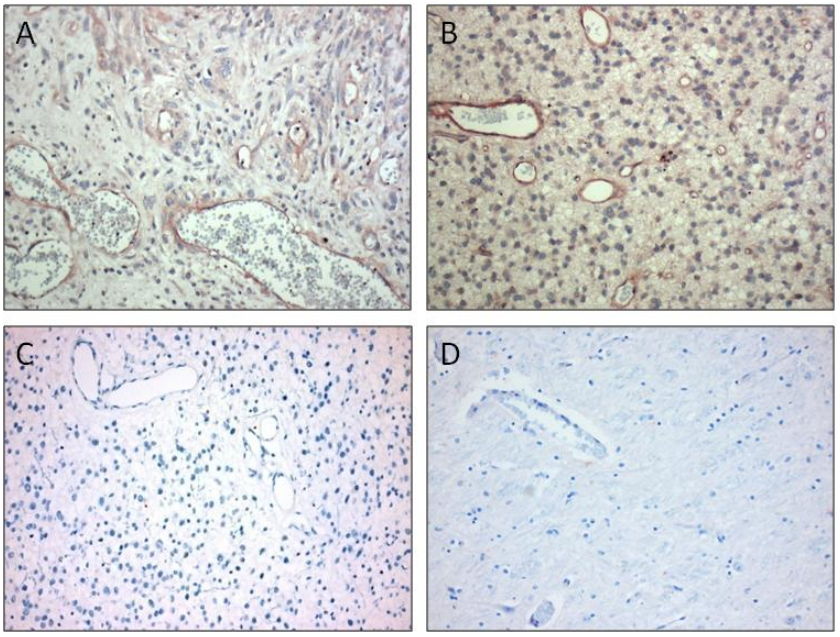

Figure 3. C-C7 also recognizes human tumor blood vessels. Shown are immunostaining with nanobody C-C7 of human GBM (A), low grade glioma (B,C) and normal brain (D). Subsets of vessels are strongly positive for C-C7 (A-B), while C-C7 reactivity is absent in the vasculature of a low grade glioma (C) and normal brain endothelium (D).

C-C7 can be used as TVTA

To confirm the ability of C-C7 to target tumor vasculature, we injected monoclonal phages displaying C-C7 in mice carrying orthotopic E98 xenografts, using the *in vivo* biopanning protocol which was used for its selection. Figure 4 shows that phages displaying C-C7 accumulate in subsets of vessels in E98 xenografts, but not in normal brain blood vessels (compare the phage localization in Fig. 4A with the anti-CD31 staining of a serial section in Fig. 4B). Control phages did not show such specific tumor vessel localization (not shown).

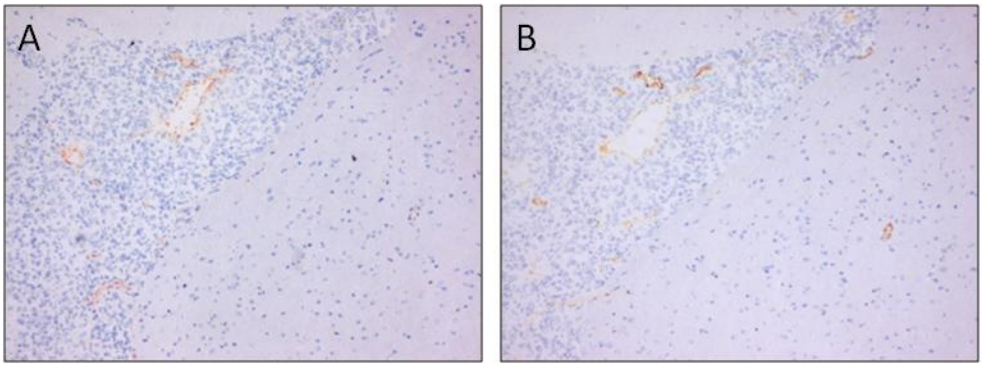

Figure 4. *In vivo* targeting of phages displaying C-C7 to cerebral E98 xenografts. Monoclonal C-C7 phages were injected in mice with orthotopic E98 xenografts and phage distribution analyzed by M13 staining after cardiac perfusion. (A) Frozen brain sections stained for M13 phages. Phages displaying C-C7 home to a subset of tumor vessels in E98 xenografts, but not to normal brain vessels, as evidenced by the anti-CD31 immunostaining on a serial section (B).

C-C7 recognizes an endothelial protein of 150 kDa

To identify the C-C7 ligand, we first prepared western blots of RIPA extracts of the rat brain endothelial cell line GP8.[246] Staining of these blots with C-C7 (Figure 5A, lane 3), but not irrelevant nanobodies (lanes 1 and 2) revealed that it recognized a protein of approximately 150 kDa. Attempts to immunoprecipitate the ligand for standard proteomic analysis were unsuccessful, possibly due to a relatively low number of C-C7 binding sites in cultured endothelial cells and tumor extracts.

C-C7 recogizes the carboxyterminal domain of dynactin-1-p150^{glued}

To unravel the identity of its interacting ligand, we used C-C7 as bait in a Y2H screen against an expression library of bovine retina, using histidine (HIS3), adenine and β-galactosidase (LacZ) as reporter genes.[245] Six positive interactors were identified. Sequence analysis and blast searches revealed that 3 of these represented the carboxyterminal part of the p150^{glued} subunit of dynactin-1. Clones 21 and 26 were

composed of the carboxyterminal 432 amino acids of dynactin-1 (aa 808-1240) and included 150 nucleotides of the 3'-untranslated region, while another one, clone 22, spanned aa 890-1238 of the bovine sequence (Figure 5B). A comparison of bovine dynactin-1-p150^{glued} with the human homologue revealed 96% sequence identity in this region.

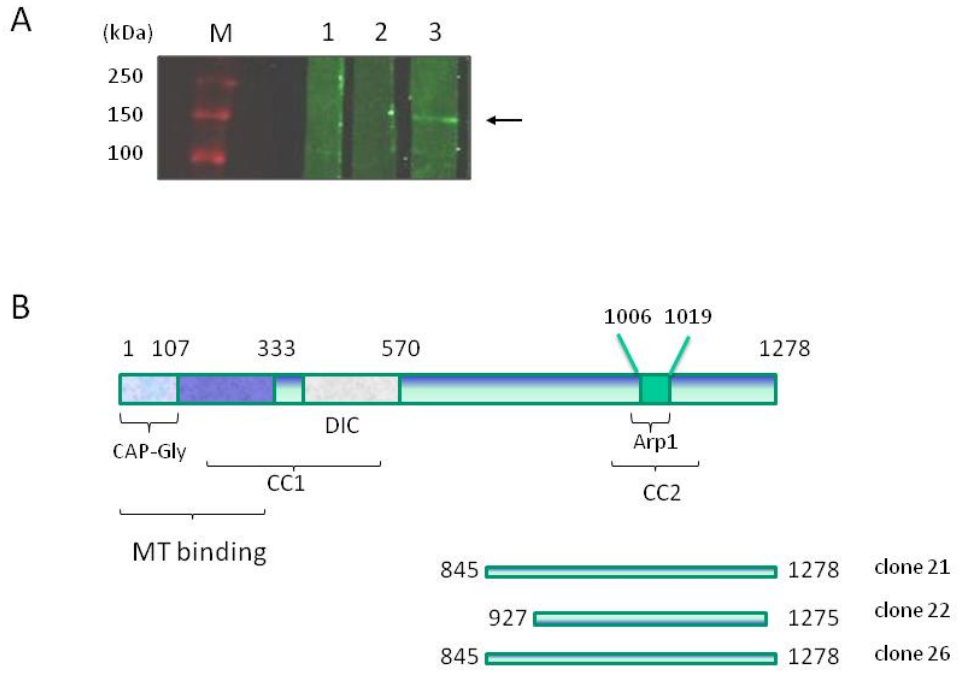

Figure 5. Identification of dynactin-1 p150^{glued} as the C-C7 ligand. A) Western blot analysis of GP8 cell extract with C-C7. Nanobody C-C7 (lane 3) but not two irrelevant single domain antibodies (lanes 1 and 2) recognizes an endothelial protein of approximately 150 kDa (arrow). B) Structural domains in p150^{glued} and recognized domains of C-C7. The aminoterminal domains contain a CAP-Gly domain and and a coiled-coil domain which are responsible for microtubule (MT) binding and dynein binding (DIC=dynein intermediate chain). A second coiled-coil domain, encompassing a binding site for Arp1, is present in the carboxyterminal part of the protein and mediates binding to membrane components.

To validate p150^{glued} as the C-C7 target, we proceeded by staining E98 tumor xenografts and clinical glioma samples with a commercially available anti-human dynactin-1-p150^{glued} antibody. In all tumors examined, this antibody gave a similar staining profile as nanobody C-C7 (see figure 6 for a representative example of staining with anti-dynactin (A) and C-C7 (B).

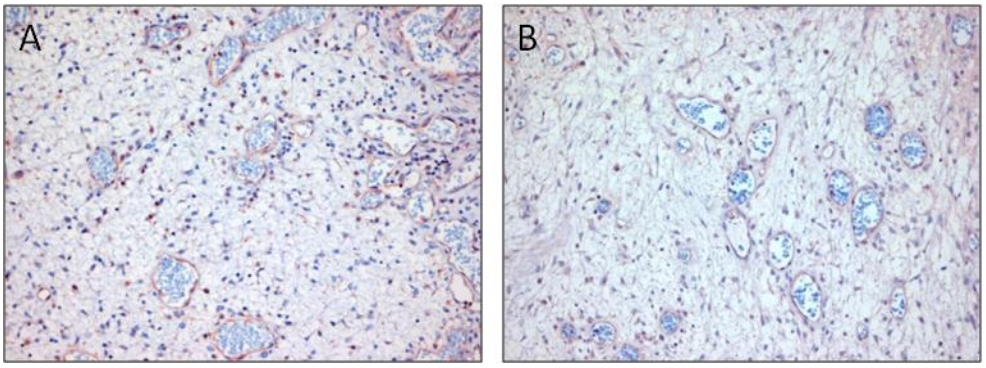

Figure 6. Comparative immunohistochemistry with a commercial anti-dynactin-1-p150^{glued} antibody (A) and C-C7 (B) on serial sections of a high grade glioma. Note that both antibodies react similarly in these tissues. Control stainings were negative (not shown).

To further confirm the interaction between C-C7 and human dynactin-1-p150^{glued}, the region encompassing aa 816-1278 (human numbering) was RT-PCR-cloned from human glioblastoma tissue and transiently expressed in COS-1 cells. Confocal microscopy of transfected cells, costained with C-C7 (visualized using FITC) and anti-dynactin-1 (visualized using TRITC) showed that both antibodies co-localized to cytoplasmic vesicular structures (Fig. 7).

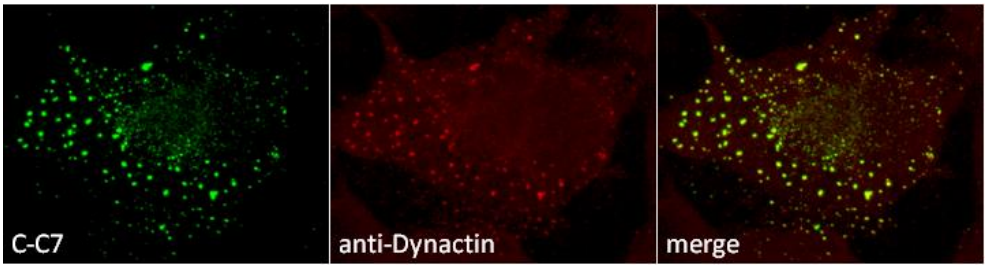

Figure 7. Immunolocalization of the carboxyterminal domain of dynactin-1-p150^{glued} in transfected COS-1 cells, as illustrated by costaining with C-C7 (green) and commercial anti-dynactin (red). Cells were transiently transfected with p3xflg-CMV-dyn-2532-3837 and analysed two days later with a confocal microscope. Both antibodies colocalize as shown in the merged figure.

Expression of dynactin-1-p150^{glued} in tumors and tissues is not ubiquitous

Dynactin-p150^{glued} has been proposed to function in microtubule-guided transport of vesicles,[247] organization of microtubule-organizing centres during mitosis,[248] establishment of gap junctions[249] and has been proposed to be involved in organization of Weibel-Palade bodies in endothelial cells[250] and disruption of the endothelial barrier and vessel

leakage.[251] The functional involvement in such basic cellular processes suggests possibly ubiquitous expression patterns which appears to be not concordant with the tumor-vessel specific immunostaining profiles which we observed. Therefore, we performed RT-PCR for p150^{glued} and its recently described splice variant p135^{glued}[252] in a set of normal tissues and tumors. Consistent with previous reports, we found detectable expression levels in a 30-cycle PCR of both p150 and p135 transcripts in brain,[253] whereas in other normal tissues expression was negligible (not shown). Low expression levels of p150^{glued}, which required 35 PCR cycles to be detected, were found in ovary, thyroid gland, kidney, lung, uterus, and liver (Figure 8). Except for brain, p135 was not detected in normal tissues. Low but detectable levels of p150^{glued} expression were observed in 2/4 astrocytomas, 8/10 adenocarcinomas and 3/3 renal cell carcinomas. p135 was observed in only one glioblastoma.

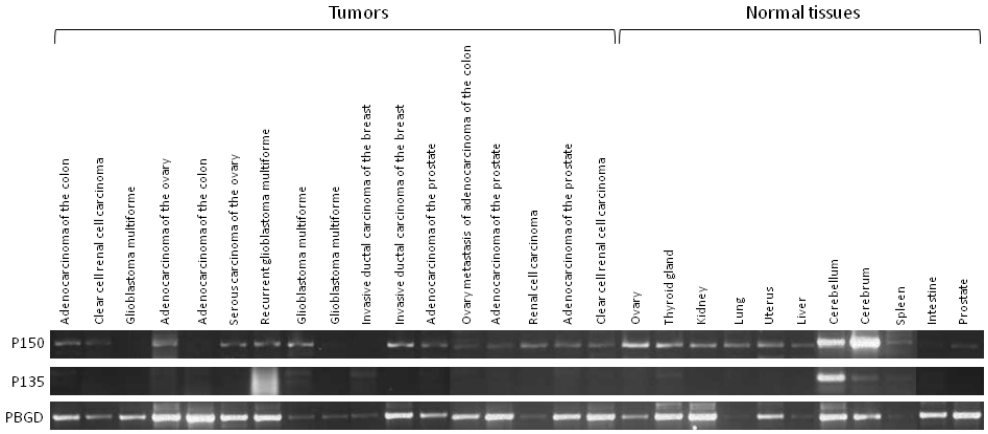

Figure 8. p150 and p135 expression in tumors and normal tissues. Most prominent expression is found in brain, probably neurons. Thirty-five cycles of PCR were needed to detect p150^{glued} in other normal tissues and tumors.

These results show that, under normal conditions, the p135 and p150 proteins are not ubiquitously expressed and confirm our immunohistochemical stainings with C-C7 and other anti-p150^{glued} antibodies. We attribute the low expression levels in tumors to the relatively limited number of endothelial cells in tumors.

Discussion

In human tumors the vasculature is in general highly heterogeneous with vessels in different stages of maturation or, in vessel dense tissues, co-opted vessels.[75,223] Prototype tumors with heterogeneous vasculature are high grade gliomas which partly grow by infiltration along pre-existent vessels or along white matter tracts, whereas areas with abundant angiogenesis are also present.[82] The diffuse infiltrative growth of human gliomas and the intact blood brain barrier in these areas contribute to their poor response to conventional tumor therapies.[81,82] In addition, it was previously demonstrated that in animal models of orthotopic GBM, such tumors do not adequately respond to anti-angiogenic therapies because diffuse infiltrative progression does not strictly depend on angiogenesis[120,226] a result which was recently corroborated in clinical studies.[123,236] Therefore, a combination of different vascular targeting strategies aimed at complete destruction of the tumor's vascular bed is probably needed to effectively deprive these tumors from blood. However, the possibility for vascular targeting is at the moment restricted to vessels in early maturation stages and targeting agents that recognize more matured vessels are needed.

Here we show that TVTAs can be effectively isolated by means of *in vivo* biopanning of nanobody phage display libraries in animal models of cancer. Furthermore, we show for the first time that nanobodies can be used as bait in Y2H screens to identify their interacting ligands. Since the library that we used in this work, a bovine retina expression library, may be considered less relevant for this purpose it is envisioned that in future studies, Y2H screens with human glioma prey libraries have an even higher chance on success.

Our *in vivo* biopanning approach resulted in the isolation of a set of nanobodies of which 44 percent specifically recognized tumor blood vessels, indicating tumor-specific enrichment in only one round of biopanning. Since we stained paraffin sections, this percentage is probably an underestimate because antibodies against conformational epitopes which are disrupted during formalin fixation, are not included. These results suggest that during the *in vivo* selection procedure, phages which bind to the surplus of common epitopes on quiescent endothelial cells in the circulation are competitively depleted. *In vivo* biopanning of phage display libraries therefore appears to be a relatively quick and efficient method to identify targeting nanobodies.

In this study we concentrated on C-C7 because it proved to be the most suitable for immunostainings on formalin-fixed tissues. Since this nanobody also recognized tumor vessels in clinical samples of glioma, it may be a proper candidate for further development for human application. The framework of llama nanobodies is highly homologous to the human V-H III gene family[254] reducing the need for extensive antibody humanization.

We found that C-C7 is directed against the carboxyterminus of dynactin-1-p150^{glued}, a protein which is involved in vesicular trafficking along microtubules, mitotic spindle assembly and cell migration.[247,255] There are several arguments which indicate that the identification of dynactin-1-p150^{glued} as the C-C7 ligand is not an artifact. First, different independent clones with overlapping dynactin-1 regions were identified in our yeast-two-hybrid screen, and this protein was not picked up in screens with other nanobodies (not shown) indicating that it is not an aspecific abundant interactor. Secondly, C-C7 recognizes a protein of 150 kDa on a western blot of endothelial cell extracts which conforms to the molecular weight of dynactin-1-p150^{glued}. Thirdly, C-C7 and a commercial antibody against dynactin-1 react similarly on mouse and human tumor tissues. Finally, C-C7 specifically stains COS-1 cells overexpressing the recombinant carboxyterminal domain of p150^{glued} and colocalizes with a validated commercial anti-p150 antibody in transfected cells. Interestingly, the immunolocalization of the transfected p150 fragment was similar to that, previously observed for the p150^{glued} G59S mutant[252] which lacks microtubule binding activity. Indeed, this was expected as the microtubule-binding region is localized in the N-terminal part which was not included in our construct (see Figure 5B).

The relevance and functional significance of expression of dynactin-1 by tumor endothelial cells is not known at this moment. Dynactin-1 is a membrane associated protein complex and interacts with dynein, a motor protein which is involved in vesicle trafficking from Golgi to endoplasmic reticulum. Vascular permeability, one of the most prominent effects brought about by VEGF,[78] may involve the formation of transcellular membrane channels via directed fusion of vesiculo-vacuolar organelles (VVOs).[256] Combined with reports on a functional role of p150^{glued} in regulating endothelial cell permeability,[251] it is tempting to speculate that dynactin-1-p150^{glued} is involved in organization of vesicles into VVOs.

Whatever its function, the subcellular localization of the dynactin-1 protein complex is expected to be cytoplasmic, which does not concur with the *in vivo* targeting properties of C-C7 phages. At this moment it is enigmatic which mechanisms are involved in establishing the extracellular localization of p150^{glued}. This situation is not unique; unexpected membranous expression of other cytoplasmic proteins in tumors has been described previously.[257] One example is tissue transglutaminase which is involved in establishing cell-matrix interactions.[258] Of interest, it has been described that microvesicles, released from endothelial progenitor cells, are integrated in cell membranes of activated endothelium.[259] As such microvessels are likely to be coated with dynactin, re-integration in the membrane may indeed result in an extracellular localization. These issues are under investigation.

Levels of p150^{glued} transcripts were low in our series of tumors. We attribute this to 1) the low percentage of endothelial cells in tumors, and 2) heterogeneity of expression, since not all tumor vessels are recognized by C-C7. While in certain clinical and preclinical

tumors (glioblastoma and VEGF-expressing melanoma) all tumor vessels showed reactivity with C-C7, we also identified tumors (e.g. U87 xenografts) which were entirely negative.

Tissue- and tumor-specific heterogeneity of the vascular proteome is now widely recognized.[260] A tumor specific vascular signature, composed of distinct surface proteins, can aid to design an appropriate mix of different and complementary TVTAs which in combination are able to target a significant proportion of tumor blood vessels. Nanobody C-C7 may be a good candidate to be included in such a TVTA-cocktail, once p150^{glued} expression can be verified in individual tumors, e.g. in tumor biopsies. Technology platforms have been and still are being developed to use TVTAs to specifically deliver anti-tumor drugs in high concentrations to the tumor. RGD-conjugated liposomes have been successfully used for delivery of dexamethasone to angiogenic endothelial cells.[261] Furthermore, targeting antibodies conjugated to soluble tissue factor, induce tumor-specific blood clotting, tumor necrosis and growth delay.[129,262] A chimeric nanobody against carcinoembryonic antigen (CEA) fused to β-lactamase accumulated in CEA-positive tumor xenografts and was successfully used as a therapeutic prodrug.[242] Additional studies are needed to resolve whether similar conjugates of nanobodies against tumor vasculature are effective therapeutics.

In conclusion, *in vivo* biopanning of phage nanobody-display libraries in animal models of cancer in combination with Y2H technology represents a powerful platform to identify novel TVTAs and their interacting ligands. We identified C-C7 as a targeting nanobody against dynactin-1-p150^{glued} and show that this protein is expressed on tumor vessels. Future studies should resolve whether C-C7 conjugates have anti-tumor effects.

Chapter 7

Isolation of targeting nanobodies against co-opted tumor vasculature

Ilse Roodink
Maarten Franssen
Malou Zuidscherwoude
Kiek Verrijp
Tom van der Donk
Jos Raats
William Leenders

In press, Lab Invest

Abstract

Tumor vasculature is in general highly heterogeneous. This characteristic is most prominent in high grade gliomas which present with areas of angiogenic growth, next to large areas of diffuse infiltrative growth in which tumor cells thrive on pre-existent brain vasculature. This limits the effectiveness of anti-angiogenic compounds as these will not affect more matured and co-opted vessels. Therefore, additional destruction of existing tumor vasculature may be a promising alternative avenue to effectively deprive tumors from blood. This approach requires the identification of novel tumor vascular targeting agents which have broad tumor vessel specificities, i.e. are not restricted to newly formed vessels.

Here we describe the generation of a phage library displaying nanobodies which were cloned from lymphocytes of a Llama which had been immunized with clinical glioma tissue. *In vivo* biopanning with this library in the orthotopic glioma xenograft models E98 and E434 resulted in the selection of various nanobodies which specifically recognized glioma vessels in corresponding glioma xenografts. Of importance, also nanobodies were isolated which discriminated incorporated pre-existent vessels in highly infiltrative cerebral E434 xenografts from normal brain vessels.

Our results suggest that generation of nanobody-displaying immune phage libraries and subsequent *in vivo* biopanning in appropriate animal models is a promising approach for identification of novel vascular targeting agents.

Introduction

High grade gliomas (WHO grade IV astrocytomas, glioblastoma multiforme [GBM]) are aggressive primary brain tumors considered to be among the deadliest of human cancers. These tumors are generally characterized by a necrotic core, surrounded by an angiogenic rim.[82,83] Importantly, these cancers always present also with large areas of diffuse infiltrative growth, in which tumor cells migrate along white matter tracts or blood vessels. This diffuse infiltrative phenotype strongly limits the effectiveness of surgery and radiotherapy. In addition, the blood-brain barrier in diffuse infiltrative areas is generally intact, contributing to the poor response of these tumors to chemotherapies.[79,81,82]

The occurrence of angiogenesis in GBM has been rationale for extensive testing of angiogenesis inhibitors. However, a number of phase II studies have now revealed that, despite inducing a radiological response, these inhibitors do not prolong overall survival and allow disease progression,[95,123] likely because diffuse infiltrative growth is angiogenesis-independent and provides a mechanism of escape from anti-angiogenic therapies.[79,95,96,118-121,123]

The phenotypic differences which exist in GBM are reflected in the vasculature, which is highly heterogeneous.[223] Vessels may be angiogenic as well as more mature or co-opted, and the latter ones may be unsusceptible to anti-angiogenic therapy.[117] To bypass resistance to anti-angiogenic therapies, additional vascular targeting therapy in which the existing tumor vascular bed is attacked with the aim to acutely deprive tumors from blood supply may be an attractive option. So far, identified targets with specificity for tumor vasculature are restricted to vessels in early stages of maturation.[124,125,201] Thus, there is a need for additional tumor vascular targeting agents which recognize tumor vessels in more mature stages.

One technique which allows for isolation of such targeting agents is biopanning, the procedure of contacting libraries of binding agents with epitopes of interest, and selecting and isolating those agents with significant affinity.[17] *In vivo* biopannings with peptide phage display libraries have been successfully used to obtain organ-specific vascular targeting peptides in animal models.[18,19] In addition, we previously provided proof of concept that via *in vivo* biopanning of phage antibody-display libraries in orthotopic E98 glioma xenografts,[121,226] antibodies can be isolated that recognize subsets of tumor vessels (submitted). In that work we used a nanobody phage display library, cloned from lymphocytes of an immune-naive Llama.[201] Nanobodies are composed of the variable domains of cameloid heavy-chain antibodies which lack a light chain. Because these consist of a single polypeptide chain, nanobodies can be cloned and displayed in a phage context without significant loss of affinity compared to the originating heavy-chain

antibody, making them to an attractive class of compounds.[263] Nanobodies against EGFR have already been successfully used for *in vivo* tumor targeting purposes.[242,243,264]
By *in vitro* biopannings, we previously isolated from our immune-naive library, nanobodies Plexin D1 specific with affinities in the range of 10^{-8}-10^{-9} M which suffice for immune stainings,[201] but are possibly of too low affinity for effective *in vivo* applications. Matured nanobodies, cloned from immunized animals, will obviously have the advantage of higher affinity. Here we describe the construction of a phage library, displaying IgG2 and IgG3 isotype specific nanobodies which were cloned from lymphocytes after immunization of a Llama glama with a homogenate of surgically obtained GBM. We performed *in vivo* biopanning of this phage library in the orthotopic glioma xenograft model E98 and the oligodendroglioma xenograft line E434. E98 was used because it displays angiogenic as well as co-optive growth,[121] whereas E434 is a hallmark example of a xenograft which exclusively displays diffuse infiltrative growth with no apparent sprouting angiogenesis.[121] This approach resulted in the isolation of a number of tumor vessel recognizing nanobodies, also against non-angiogenic blood vessels in diffuse infiltrative tumor areas.

Materials and Methods

Llama immunization

All animal experiments were approved by the Animal Experiment Committee of the Nijmegen University and informed consent was obtained from patients with newly diagnosed GBM who did not receive prior treatment for use of tumor material. A Llama glama was immunized with a homogenate of three surgically obtained clinical GBMs, after confirmation of absence of reactivity in preserum, as determined by immunohistochemical stainings on frozen sections of the same GBMs. GBMs were selected that showed only minimal necrosis, as was determined by H&E staining. A total of 90 mg glioma tissue was homogenized in 2.5 ml sterile 0.9% NaCl solution. The homogenate was aliquoted in 500 µl portions and stored at -80°C. For primary immunization and boosts, 500 µl homogenate was mixed with 625 µl Stimune™ adjuvant (Cedi Diagnostics, Lelystad, The Netherlands). This suspension was injected intramuscularly into a Llama. Boost immunizations were performed at day 28, 42, 70, 98 days after the initial immunization. Serum and blood samples were isolated prior to each boost and 126 days after the first immunization. At each time point, leukocyte RNA was isolated using the LeukoLOCK™ Total RNA Isolation System (Ambion, Austin, TX) according to the manufacturer's protocol. In addition, to verify immune responses, 4 µm frozen clinical GBM sections were immunostained with the sera obtained at each time point, according to standard protocols. In short, tissues were pre-incubated with normal goat

serum to block non-specific binding sites, followed by overnight incubation at 4°C with Llama immune serum or pre-immune serum as control. Llama IgG was detected by incubation with horseradish peroxidase conjugated goat anti-Llama IgG antibody (Bethyl Laboratories Inc., ITK Diagnostics, Uithoorn, The Netherlands). Peroxidase was visualized by the 3-amino-9-ethylcarbazole (ScyTek, Logan, UT) peroxidase reaction and sections were counterstained with haematoxylin.

Llama phage display library construction

Llama nanobodies were RT-PCR cloned in phagemid pHENIX as follows. Total leukocyte RNA samples (2 µg) isolated on day 28 after the last boost were reverse-transcribed at 42°C for 90 minutes using Moloney-mouse-leukemia virus reverse transcriptase (Promega, Leiden, The Netherlands). Subsequently, V_{HH} antibody fragments were amplified by PCR using Phusion polymerase (Finnzymes, Bioké, Leiden, The Netherlands), forward primer FR1 (5'-GAG GTB CAR ***CTG CAG*** GAS TCY GG-3') (*Pst*I restriction site shown in bold italic) and hinge specific reverse primers LH49 (AAC AGT TAA GCT TCC GCT T**GC GGC CGC** TGG TTG TGG TTT TGG TGT CTT GGG-3') and SH48 (5'-AAC AGT TAA GCT TCC GCT T**GC GGC CGC** GGA GCT GGG GTC TTC GCT GTG GTC CG-3') (*Not*I restriction sites shown in bold) which assured separate amplification of IgG2- and IgG3-encoding V_{HH} fragments respectively.[265] Amplified V_{HH} products were agarose gel purified and digested with *Pst*I (New England Biolabs, Westburg, Leusden, The Netherlands) and *Not*I (New England Biolabs). Fragments were ligated into pHENIX *Pst*I-*Not*I vector using Quick Ligase (New England Biolabs). This results in V_{HH} chimeras with a His8-VSV-G- tag at the C-terminus.[180] The phagemid library was transformed in electrocompetent *E. coli* TG1 bacteria. Individual clones were picked and analyzed for the presence of full-length insert by standard colony PCR using forward primer pHEN-fw (5'-TCA CAC AGG AAA CAG CTA TGA-3') and reverse primer pHEN-rev (5'-GTA ACG ATC TAA AGT TTT GTC G-3'). Full-length insert ratio was determined after running PCR products on a 1.0% agarose gel.

Phages were grown from this library by infection with the trypsin sensitive helper phage M13K07[181] and purified from the culture supernatant by precipitation with 20% PEG-2.5 M NaCl as previously described.[182]

In vivo selection of tumor vessel binding nanobodies via biopanning of phage display libraries

To grow intracerebral E98 and E434 tumors Balb/c nude mice were transcranially injected with the glioblastoma xenograft line E98 (n=2) or the oligodendroglioma line E434 (n=2) essentially as previously described.[121] In short, a mouse carrying a subcutaneous E98 tumor and one carrying a cerebral E434 xenograft were killed. The tumors were sterile removed, minced to small pieces and filtered through a 70 µm mesh nylon filter. The

resulting single cell suspensions were subsequently injected through the skull of nude mice under deep anesthesia. After respectively 3 and 7 weeks, when mice carrying E98 and E434 xenografts displayed signs of tumor growth (discomfort, weight loss and neurological symptoms), *in vivo* biopanning was performed as follows: 10^{12} GBM nanobody-phages were intravenously injected. Nanobody-displaying phages were allowed to circulate and bind to their targets for 15 minutes. Subsequently, mice were anaesthetized using 1.3% isoflurane/N_2O/O_2 and cardiac perfusion was performed with 15 ml sterile 0.9% NaCl solution to remove unbound phages from the circulation. Mice were then sacrificed by decapitation and brains were collected. A small part was formalin-fixed and paraffin-embedded, the remainder was snap frozen in liquid nitrogen. Paraffin-embedded sections (4 µm) were stained with anti-M13 p8 antibody (Abcam Limited, Cambridge, UK) to investigate phage distribution in the tumor. In case of E98, tumor areas were dissected from 16 frozen brain sections (10 µm) using a laser dissection microscope (Leica AS LMD, Wetzlar, Germany), whereas excessive unaffected brain parenchyma was scratched manually from 18 frozen E434 brain sections (30 µm). The remaining E434 tumor areas were collected in a tube. Phages were eluted from the obtained tumor areas by trypsin treatment (10 mg/ml, 30 min RT) and infected in 10 ml of log-phase TG1 culture.

Ninety-four randomly selected individual clones were picked and analyzed for the presence of full-length insert as described above. To prevent analysis of duplicate clones, fingerprint analysis was performed by digesting full-length PCR products with the four-cutter enzymes *Bst*NI and *Bst*U1 followed by electrophoresis on 4% nusive agarose gels. In addition, these clones were used for small scale IPTG-induced nanobody production by overnight induction with 1 mM IPTG. Nanobody expression levels in the culture supernatant were determined via dotblot analysis using the mouse monoclonal anti-VSV-G P5D4 and alkaline phosphatase-conjugated rabbit anti-mouse immunoglobulin (Dako, Glostrup, Denmark). Alkaline phosphatase was visualized using nitro blue tetrazolium (NBT; Roche, Almere, The Netherlands) and 5-bromo-4-chloro-3-indolyl phosphate (BCIP; Roche) as substrate. Based on the collective data, clones were selected for further analysis by immunohistochemistry. High level expression of soluble nanobodies was induced in log-phase TG1 cells by culturing at 30^{o}C in 2xTYA/1 mM IPTG. Nanobodies were collected by osmotic lysis as described.[201]

Immunohistochemistry

Soluble nanobodies, obtained via osmotic lysis of TG1 cells, were tested in immunostainings on 4 µm sections of paraffin-embedded cerebral mouse xenografts (E98 or E434). Following deparaffinization, endogenous peroxidase activity was blocked by incubation with 3% H_2O_2. Antigen retrieval was performed by boiling in 10 mM citrate

buffer for 10 minutes, using a microwave oven set at 180 Watt. Slides were pre-incubated with normal goat serum to block non-specific binding sites, followed by overnight incubation with nanobodies at 4°C. Subsequently, detection was performed by the following incubations at room temperature: 1 hr rabbit anti-VSV-G antiserum (Sigma-Aldrich, Zwijndrecht, The Netherlands), 30 minutes biotinylated anti-rabbit antibody (Vector, Burlingame, CA), and 45 minutes avidin-biotin peroxidase complex (Vector). Finally, visualization was performed by the 3-amino-9-ethylcarbazole (ScyTek) peroxidase reaction with haematoxylin as counterstain.

Results

Immunohistochemical evaluation of Llama immune response

Sera obtained at five different time points after initial immunization of a Llama with a homogenate of clinical GBM tissues were tested on the same GBM tissues used for immunization. Whereas preserum was completely negative, after each immunization boost increasing immunoreactivity was seen on tumor cells and extracellular matrix components of the GBMs with optimal responses after the fourth boost (not shown). Therefore, leukocyte RNA isolated after this boost immunization, was used for generation of a nanobody phage display library. The combined IgG2 and IgG3 nanobody library had a size of 10^7 clones of which 88 percent contained a full length insert (data not shown).

In vivo selection of tumor vessel binding phages in cerebral E98 and E434 mouse xenografts

A suspension of 10^{12} phages was intravenously injected in tumor-bearing mice for *in vivo* biopanning and irrelevant phages were washed from the circulation by cardiac perfusion, after allowing relevant phages to bind for a period of 10 minutes. Figure 1 shows anti-M13 immunostainings on intracerebral E98 (a) and E434 (b) xenografts. These stainings show a prominent tumor vessel localization of phages (arrowheads in figure 1a and 1b). We observed almost no phages associated with normal brain vessels (compare the phage localizations with the anti-CD34 staining of serial sections of E98 and E434 xenografts in Fig. 1c and d respectively). The arrows in figure 1c and 1d point at vessels which are not highlighted by anti-M13 staining. Approximately 2800 and 3400 colony-forming phages were rescued from tumor sections from mice carrying E98 and E434 xenografts respectively. From the phage populations which were rescued from each xenograft, 94 individual clones were randomly picked for fingerprint analysis and nanobody production. Remaining colonies were collected and pooled and stored as sub-libraries for future rounds of *in vivo* biopanning. Fingerprint analyses identified 20 and 15 distinct groups of

nanobodies, binding to E98 and E434 vasculature, respectively (Table 1). From each group, one clone was selected for nanobody production and immunohistochemical analysis on sections of the corresponding glioma xenografts.

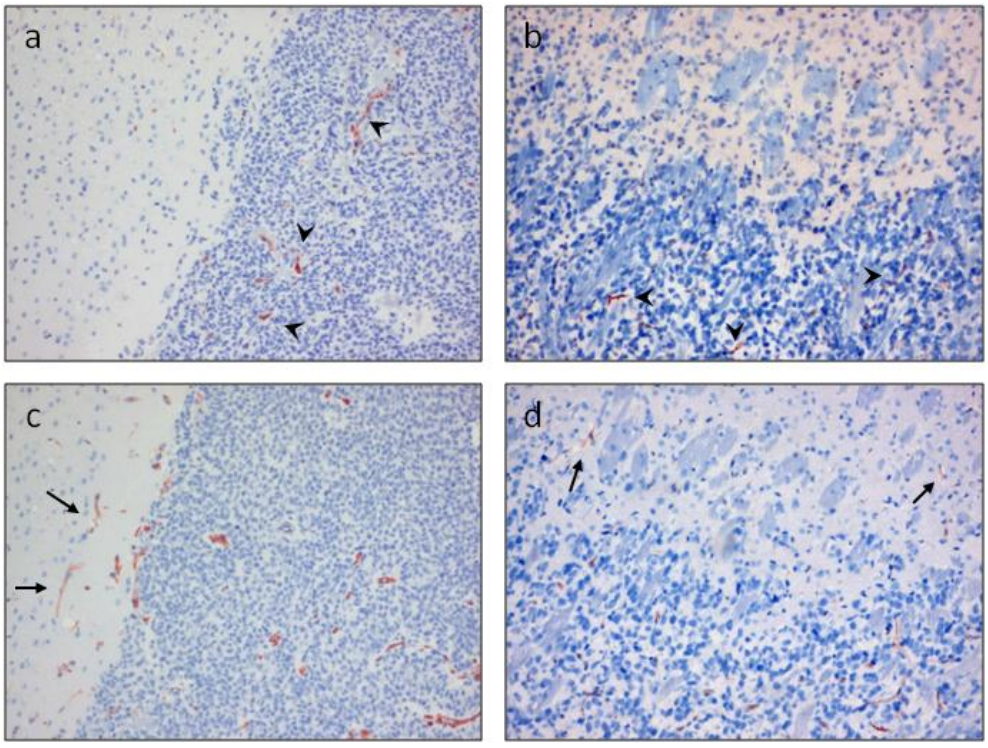

Figure 1. Phage distribution in cerebral glioma xenografts after *in vivo* biopanning of an immune Llama phage library. Paraffin-embedded sections of E98 (a) and E434 (b) xenografts were analyzed for phage localization by M13 immunostainings. As evidenced by anti-CD34 immunostainings on serial sections of E98 (c) and E434 (d) xenografts phages are clearly associated with the tumor vasculature (arrowheads in figure 1a and 1b), whereas vessels in unaffected brain parenchyma are not highlighted by anti-M13 staining (arrows in figure 1c and 1d). Note the CD34 up-regulation on tumor-associated endothelial cells compared to normal brain capillaries (c and d).

Immunohistochemistry

Because evaluation of vessel staining requires optimal morphology, we performed immunostainings with nanobodies on paraffin-embedded sections of cerebral E98 or E434 mouse xenografts. We accepted here that potentially interesting nanobodies, reactive against epitopes which are lost during fixation, were lost during analyses. Of the 20 nanobodies which were rescued from the E98 biopanning experiments, 15 (75%) showed positive staining of subsets of tumor vessels in E98 xenografts. Figure 2 shows

representative immunostainings with clones obtained from group A (a) and D (b). Similarly, 8 of the 15 nanobodies (53%), isolated from *in vivo* biopanning on E434 xenografts, stained positive on E434 vasculature (Fig. 2c and d for clones obtained from group IX and VIII respectively). As shown in the insets in figure 2 these nanobodies did not stain vessels in unaffected brain areas.

Table 1. Percentage E98 and E434 vessel binding clones per restriction pattern of full length PCR products

Glioma xenograft model	Restriction pattern	% Clones with restriction pattern
E98	A	28%
	B	5%
	C	2%
	D	5%
	E	5%
	F	3%
	G	2%
	H	2%
	I	3%
	J	13%
	K	11%
	L	2%
	M	2%
	N	3%
	O	3%
	P	3%
	Q	2%
	R	2%
	S	2%
	T	3%
434	I	2%
	II	12%
	III	4%
	IV	14%
	V	22%
	VI	8%
	VII	8%
	VIII	2%
	IX	8%
	X	8%
	XI	2%
	XII	2%
	XIII	2%
	XIV	2%
	XV	2%

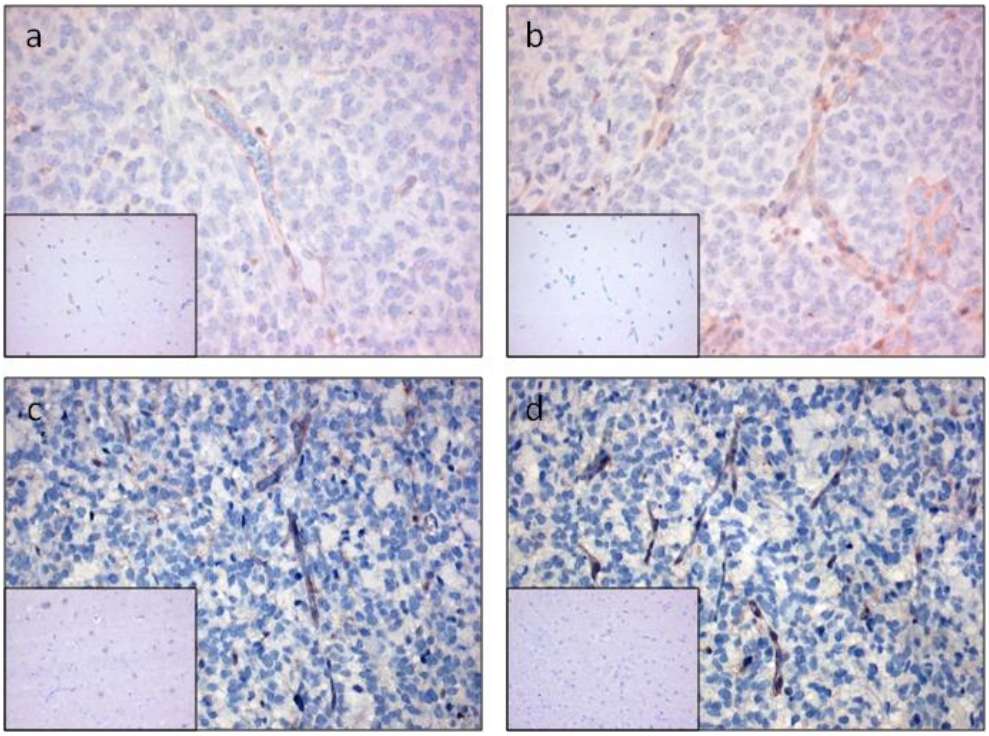

Figure 2. Immunohistochemical analysis of the reactivity of selected nanobodies in glioma xenografts. Clones obtained from group A (a) and D (b) are representative for nanobodies which specifically recognized subsets of glioma vessels in immunostainings on paraffin-embedded sections of E98 xenografts. Nanobodies produced by clones from group IX (c) and VIII (d) demonstrate representative immunoreactivity on E434 vasculature. Note the absence of immunoreactivity on vessels in unaffected brain areas (insets).

Discussion

The diffusely infiltrative growth of human gliomas and the predominantly intact blood brain barrier in these areas contribute to the poor response of human gliomas to conventional tumor therapies[81,82,118] and at the same time allow escape from anti-angiogenic therapy.[76,78,95,96,118-121,123] Although gliomas are certainly at the extreme end of a spectrum with respect to infiltrative growth, it was recently shown that targeting of the angiogenic pathway also in subcutaneous xenografts leads to enhanced invasive growth and metastases.[266,267] Such adverse effects are not expected to occur when directing therapy against the existing tumor vasculature. So far, tumor vascular targeting has focused on markers which are specifically expressed on newly formed vessels, among others the ED-B domain of fibronectin, VCAM-1 and αvβ3 integrin. Targeting of newly

formed vessels with agents directed against such molecules has already been shown to result in potent anti-tumor effects in preclinical models of subcutaneous xenografts.[126-129] However, these results can not be translated directly to clinically relevant situations: in subcutaneous xenografts the vasculature is more or less synchronized and will be homogeneously susceptible to targeting of angiogenic vessels. In contrast, the vasculature of clinical tumors is composed of a heterogeneous population of vessels[223] which requires that clinically relevant anti-vascular therapies combine targeting of newly formed vessels with targeting of more mature or co-opted vessels.

The E434 orthotopic glioma model is an extreme example of an angiogenesis-independent tumor which grows exclusively via incorporation of pre-existent brain vessels, as evidenced by their positivity for glucose transporter-1, which is expressed on brain endothelium with a functional blood-brain barrier.[121] Despite a lack of sprouting angiogenesis in these tumors, the vasculature is activated as exemplified by more prominent staining for the vessel marker CD34.[121] In addition, our data show that these vessels display specific proteins which are distinct from those expressed on normal vessels, and that these differences in proteome can be used for targeting purposes. The concept of therapeutic targeting of incorporated pre-existent tumor vasculature is probably applicable to all tumors which grow in vessel dense tissues and which may progress via co-option. Obviously, especially in brain tumors, therapy directed against incorporated pre-existent vessels carries a particular risk of toxicity due to micro-infarctions which may have effects beyond the tumor. So, this requires thorough examination in relevant tumor models. In other tissues this issue may be less relevant as some anoxic tissue necrosis may be tolerable, as long as a proper inflammation response can be induced that cleans up the necrotic debris.

In accordance with previous *in vivo* biopanning experiments in mice carrying cerebral E98 xenografts in our lab in which we used an immune-naive nanobody phage display library (submitted) we ended up with nanobodies that specifically reacted with tumor vessels of corresponding cerebral glioma xenografts after only one round of biopanning. We propose that using this *in vivo* biopanning protocol, phages against common endothelial surface proteins are depleted from the circulation by the excess of normal mouse endothelium. Importantly, following the same *in vivo* biopanning procedure we rescued six times more interacting phages from E98 xenografts using our immune Llama phage library compared to the immune-naive Llama phage library. This suggests that, as expected, nanobodies against tumor vessel epitopes are more represented in our immune library than in the immune-naive library. In addition, although *in vivo* biopanning in mouse glioma models resulted in the isolation of nanobodies against mouse endothelium, it is reasonable to assume that they also recognize their human counterparts since they are derived from a

Llama after immunization with clinical GBM tissues. Preliminary immunostainings on clinical GBM indeed suggests that this is the case.

The aim of the present work was to select nanobodies which can be further developed into tumor vessel targeting agents. Identification of the ligands which are recognized by our nanobodies is ongoing in our lab.

In conclusion, we showed that triggering the immune system of a Llama with a homogenate of clinical GBM tissues provoked an immune response against all components present in these tissues. Our phage library displaying nanobodies which were cloned from lymphocytes of this Llama is a potential source of targeting agents against different glioma components. Importantly, *in vivo* biopanning using this phage library in well characterized mouse glioma models led to selection of various tumor vessel recognizing nanobodies, among them ones which discriminated incorporated pre-existent vessels from normal brain vessels. Overall, construction of nanobody-displaying immune phage libraries and subsequent *in vivo* biopanning in appropriate animal models is a very promising approach for future identification of novel molecular tools for targeting vascular beds.

Chapter 8

Summarizing discussion and future perspectives

In recent years targeted tumor therapies which aim at the interaction with tumor cell-specific molecular targets have made a firm entry in oncology practice. Unfortunately, such therapies appear beneficial for only subsets of cancer patients and the ultimate goal of these therapies, which obviously is cure, is very seldomly, if ever, achieved. Targeting the genetically stable tumor endothelium, which is well accessible after intravenous injection of agents is an attractive alternative approach to accomplish tumor regression via disruption of the tumor's blood supply. Targeting tumor blood vessels may be accomplished by anti-angiogenesis, which prevents formation of new vasculature, or anti-vascular therapies, which aim at acute regression of existent tumor vasculature. Despite promising results in preclinical studies in which anti-angiogenic therapy translates into potent anti-tumor effects, implementation of these therapies in clinical settings has learned that beneficial effects in the patient are less pronounced. Therefore, adjuvant anti-vascular therapy, targeting the existing vascular bed with the aim to induce tumor-specific coagulation, seems to be an attractive approach to deprive a tumor from blood supply.

This thesis focused on the identification of novel vascular targeting agents directed against tumor endothelium, in particular brain tumor vasculature, and the expression patterns of their targets in (clinical) tumor samples. In addition, a powerful platform for the identification of novel targetable tumor vessel associated markers is presented.

Vascular heterogeneity

As described in chapter 2 various primary and metastatic clinical brain tumors present with different vascular phenotypes. These differences can be explained by a model which incorporates both isoform specific vascular effects and the trigger for VEGF-A expression. The VEGF-A_{165} and $_{189}$ isoforms are capable of inducing a true angiogenic response.[77,78] However, due to their strong cell surface and extracellular matrix binding they only exert effect on vessels in the direct neighborhood of the VEGF-A secreting cells. Therefore, in tumors with constitutive VEGF-A expression all isoforms are able to exert their effects on nearby vessels, resulting in a classical angiogenic phenotype. In contrast, in tumors where only central parts express hypoxia-induced VEGF-A, the larger isoforms are retained by extracellular matrix, leaving only freely diffusible VEGF-A_{121} which is not able to induce a neovascular bed but rather modulates and dilates pre-existent vessels.[77,78] This results in a phenotypically different vasculature, despite the expression of truely angiogenic VEGF-A isoforms. We previously demonstrated in a mouse brain metastasis model of human melanoma that tumor cells are able to thrive in the presence of pre-existing brain vasculature without becoming hypoxic by infiltrating the brain parenchyma in the perivascular space.[76] Similarly, clinical low grade gliomas are able to grow by means of

infiltration and incorporation of pre-existing blood vessels without the need for angiogenesis (chapter 2).

Vascular targeting

Thus, tumors obtain their blood supply by the formation of new vasculature and/or by the incorporation, and possibly subsequent modulation, of pre-existent vessels. As a consequence, tumor vasculature is generally highly heterogeneous, not only between tumor types but even within individual tumors.[225,230,268] This vascular heterogeneity has clinical implications for anti-tumor therapies which aim at interference with a tumor's blood supply. Since VEGF-A-targeting results in inhibition of only the early stages of angiogenesis, vessels in more matured stages are not affected[73] and this may in part explain the limited clinical effects of such therapies. With this in mind, additional vascular targeting therapy in which the existing tumor vascular bed is attacked with the aim to induce acute coagulation seems to be an attractive approach to effectively deprive tumors from blood supply. Clearly, this approach requires the availability of specific tumor vascular targeting agents that recognize the entire heterogeneous tumor vasculature. However, currently available tumor vessel targeting agents are directed against molecules of which expression is restricted to vessels in early stages of angiogenesis, leaving incorporated or more matured tumor vasculature unaffected. In addition, since we can rule out the possibility that one single marker will behave as a targetable pan-tumor-endothelial antigen there is a need for appropriate mixtures of different tumor vessel targeting agents that, in combination, specifically target a tumor's vascular bed.

Tumor vessel targeting agents (TVTAs)

As demonstrated in chapter 3 we identified Plexin D1 as a tumor vascular target. Plexin D1 is a member of the Plexin-family consisting of large transmembrane proteins that are receptors for Neuropilins and Semaphorins[170,197] and as such are involved in regulation of axonal patterning during embryonic development.[171,173,184,198] Apart from its expression by neuronal cells, Plexin D1 is also expressed by vascular endothelial cells during embryogenesis[174] and is of pivotal importance for vascular patterning, as illustrated by the fact that Plexin D1 knock-down in mice and zebrafish results in maldevelopment of the cardiovascular system.[175,176,227] Via panning of an immune naive Llama phage display library against a Plexin D1-specific peptide we isolated nanobodies against Plexin D1 and showed that expression of Plexin D1 is also prominent during tumor-associated angiogenesis. Furthermore we demonstrated that these nanobodies were able to specifically target tumor blood vessels in mice carrying brain lesions of angiogenic melanoma. Although Plexin D1 is expressed during developmental and tumor-associated angiogenesis, in malignant tissues its expression is not restricted to vessels in early

maturation stages. This membrane protein is also abundantly expressed on a subset of established activated tumor vessels and tumor cells of both primary and metastatic clinical brain tumors (chapter 3). Whereas a role of Plexin D1 in vessel patterning during development is well established, the functional consequences of Plexin D1 expression on tumor cells and vessels are less clear. As described in chapter 4 we demonstrated that Plexin D1 expression by tumor cells is correlated with tumor invasion and metastasis in a human melanoma progression series. Nevertheless, the Neuropilin-independent ligands of Plexin D1, Semaphorin 3E and 4A inhibit, rather than promote, (tumor) angiogenesis (chapter 4).[202] Moreover, Semaphorin 3E even exhibits anti-tumor and anti-metastatic properties,[229] whereas overexpression of Semaphorin 3C, which binds with high affinity to a Neuropilin-1/Plexin D1 complex, does not affect tumor angiogenesis and metastasis (chapter 4). However, the presence of consensus motifs for Rac-Rho signaling in the intracellular domain of Plexin D1[174] is consistent with a possible regulatory role in cellular migration and invasion. These processes are fundamental in both angiogenesis and tumor metastasis, indeed suggesting that Plexin D1 may be functionally involved in tumor development in multiple ways. Irrespective of a potential function in tumor biology, we show in chapter 5 that Plexin D1 is a pan-tumor target due to its abundant expression on both angiogenic and activated co-opted tumor vasculature, as well as on tumor cells in a wide range of clinical solid tumors of different origin. This expression profile suggests that Plexin D1 may be a valuable tumor target for established solid tumors in which vessel activation has occurred, allowing simultaneous targeting of different tumor compartments, i.e. vessels and tumor cells. Importantly, non-tumor related tissues lack Plexin D1 expression, except for some expression by subsets of fibroblasts and macrophages (chapter 4 and 5). The effects of targeting of these stromal cells are currently not known and should be thoroughly investigated. It should also be realized that Plexin D1 expression is absent in a subset of matured tumor vessels and quiescent tumor-associated endothelium (chapter 4 and 5) and will therefore probably not suffice for effective therapy as single agent.

Therefore, in order to identify additional TVTAs we performed *in vivo* biopanning experiments using phage display libraries in orthotopic mouse xenograft models of glioma which display vessel heterogeneity, similar to human tumors.[121] As described in chapter 6 we identified nanobody C-C7 as a specific TVTA by *in vivo* biopanning of an immune naive Llama phage display library in mice carrying E98 glioma xenografts.[121] Nanobody C-C7 specifically recognizes a target on a subpopulation of activated tumor vessels and also in clinical glioma specimens. Unfortunately, expression of the C-C7 target is less prominent in quiescent tumor vessels. To identify the target of C-C7, this nanobody was introduced in a yeast-two-hybrid system as a GAL4-DNA binding domain-fused bait and screened against a GAL4-activation domain-bovine retina expression prey library. From this screen the C-C7

target was identified as the p150^{glued} subunit of dynactin, a dynein-microtubule-associated protein complex which is involved in intracellular membrane trafficking.[255]

As stated above the heterogeneity of vasculature in brain tumors requires the identification of additional antibodies which, as mixture, target the entire tumor vasculature. Since immune-specific phage display libraries exhibit the advantage of displaying antibodies with higher affinity and specificity the use of such libraries seems to be a promising approach to select for high affinity antibodies. In chapter 7 we describe the construction of nanobody-displaying phage libraries cloned from lymphocytes of a Llama after immunization with a mixture of three homogenates from surgically obtained clinical high grade gliomas. Subsequent *in vivo* biopanning of these phage display libraries in orthotopic mouse models of glioma E98 and E434[121] resulted in the isolation of various glioma vessel recognizing nanobodies, also against non-angiogenic blood vessels in diffuse infiltrative tumor areas.

Nanobodies

In the biopanning experiments described in this thesis we used nanobody-displaying phage libraries since recombinant nanobodies (the antigen binding parts of cameloid heavy-chain antibodies (figure 1)), have distinct advantages over the, more regularly used, single chain antibodies (Fig. 1B).[254,269] The latter are composed of a variable heavy (V_H) and light (V_L) chain, connected via a flexible linker. This generally affects affinity and makes them more susceptible to proteolytic cleavage. Also the chance that corresponding V_H and V_L chains are ligated during library preparation is infinitely small. We previously constructed a phage library expressing these single chain antibodies cloned from a chicken after successful immunization with a homogenate of clinical glioblastoma multiforme tissues (unpublished results). However, isolated single chain antibodies obtained via *in vivo* biopanning in the E98 mouse model of glioma were predominantly negative in immunostainings. Nanobody libraries constitute a greater chance on success because these antibody fragments consist of a single polypeptide chain, which can be cloned in phagemid vectors in one step. In a phage-context, conformation and binding properties of nanobodies are therefore optimally resembling the characteristics of the original single domain antibody. Furthermore, we experienced that yields of nanodies expressed in *E. coli* are 10 to 100 times higher than single chain antibodies.

Although the studies described in this thesis mainly focused on tumor endothelial cell-specific nanobodies, our Llama nanobody-phage display libraries are also a potential source of nanobodies against tumor cells. Importantly, the immune nanobody-phage display libraries described in chapter 7 contain antigen-binding fragments raised against all tumor components, allowing isolation of tumor cell recognizing nanobodies which have several advantages over conventional antibodies with respect to *in vivo* targeting of tumor

cells. Due to their low molecular weight nanobodies more rapidly diffuse into the tumor tissue after extravasation from leaky tumor vessels and rapidly clear from the circulation and non-target tissues.[270] In addition, their small size may allow access to epitopes which are inaccessible or barely antigenic to conventional antibodies.[271] Although our anti-Plexin D1 nanobodies exhibit relatively good affinities (K_d = 2-4 x 10^{-8} M), binding properties of conventional antibodies are generally in the low nanomolar range. However, targeting of the tumor cells may be more efficient with lower affinity antibodies due to higher tumor penetrance compared to high affinity antibodies.[185]

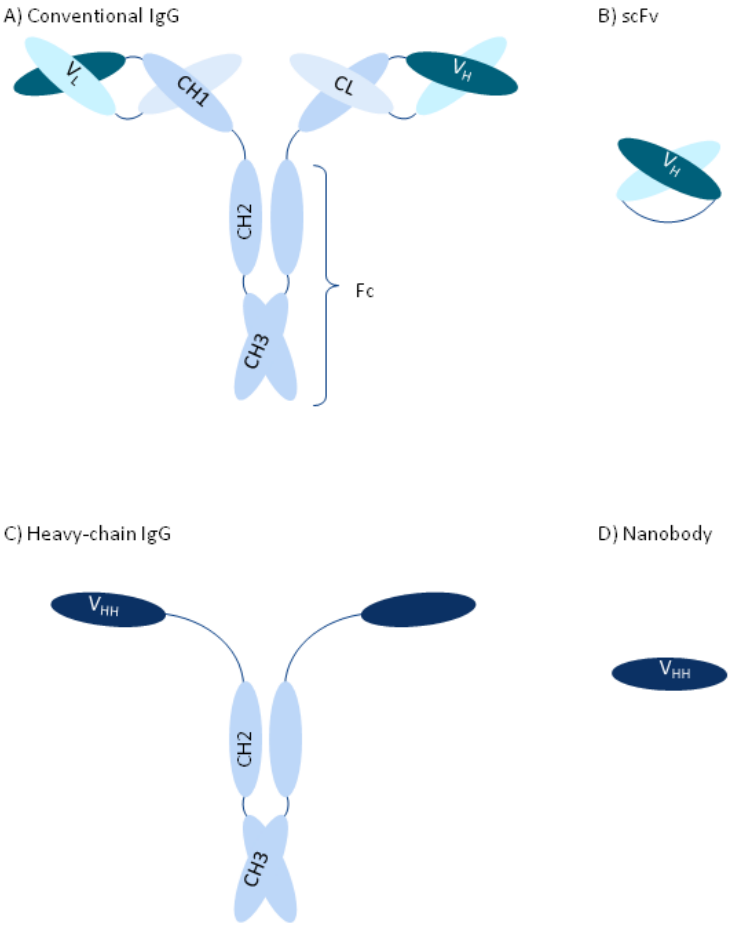

Figure 1. Schematic overview of conventional (A) and heavy-chain (C) antibodies and their corresponding antigen binding fragments in B and D respectively. Note the absence of the light chain and CH1 domain in heavy-chain antibodies.

In general, nanobodies exhibit a higher conformational stability compared to conventional antibody fragments[272-274] and can, due to their monomeric nature, be easily genetically manipulated facilitating their development into therapeutic or diagnostic compounds. From this point of view simultaneous targeting of different tumor compartments via a mixture of nanobodies targeting existing tumor vasculature and ones enabling a second wave of action against tumor cells is an attractive approach. Importantly, the nanobody framework shares high homology with the human V_H III region,[275] reducing immunogenicity when applied in humans. Interestingly, nanobodies have already effectively been used for *in vivo* diagnosis and therapy.[242,243]

Nanobody conjugations

As described in this thesis anti-Plexin D1 nanobody A12, nanobody C-C7 and various nanobodies described in chapter 7 recognize their respective targets in clinical tumor specimens suggesting that these nanobodies can be further developed for future clinical application once their therapeutic and/or diagnostic value is determined in preclinical studies. Of interest, pre-therapy immunohistochemical analyses on tumor biopsies with the targeting nanobodies may allow for proper selection of patients which are amenable to therapy with the respective nanobodies, and this concept may be extended to staining with other tumor-cell targeting nanobodies, resulting in a tailor-made therapeutic approach for individual cancer patients. Conjugation of nanobodies to diagnostic or therapeutic compounds is facilitated by the single domain nature of these antibodies. Introduction of conjugatable tags allows directional conjugation of e.g. N-hydroxy-succimidyl to free ε-NH_2 groups in lysines or maleimide to free SH groups in cysteines. This provides a platform in which nanobodies can be turned into therapeutic or diagnostic compounds, e.g. via conjugation to cytotoxic agents or radioisotopes. In case of vessel targeting, cytotoxic therapy is expected to result in endothelial cell death, followed by coagulation and an avalanche of tumor cell death in the tumor area supplied by these vessels. Alternatively, nanobodies fused to truncated tissue factor can be used to target this initiator of the coagulation cascade to the tumor vasculature in order to introduce tumor embolization.[129]

Besides these therapeutic applications, nanobodies can also be used to deposit imaging agents to tumor vasculature, which has high diagnostic relevance in gliomas. Whereas the disrupted blood brain barrier in regions of prominent angiogenesis allows MRI-based detection of high grade gliomas by extravasation and accumulation of contrast agents in the interstitial spaces,[120] diffuse infiltrative tumor growth, in which the blood brain barrier is intact, is often missed in conventional magnetic resonance imaging leading to a significant underestimation of the actual glioma load. Noteworthy, anti-angiogenic

therapy further deteriorates contrast agent extravasation in these tumors by inducing vessel normalization and closure of the blood brain barrier.[96]

Conclusions

Anti-angiogenic therapies have not fulfilled the initial expectations of turning cancer into chronic disease, and patients may benefit from additional anti-vascular therapies. To target the heterogeneous tumor vasculature there is a need for appropriate mixtures of different TVTAs that, in combination, recognize the majority of tumor vessels. Since endothelial cells in different tissues and tumors display specific antigens,[224,225,239,268] it is assumable that also quiescent tumor endothelial cells will be subject to tumor-derived factors and hence have alterations in their proteomes which can be targeted. In this thesis we have shown that the use of immune nanobody phage libraries, in combination with appropriate animal models of disease, and yeast-two-hybrid screens with appropriate prey libraries, is a very powerful platform for the identification of novel tumor vessel targeting agents and their ligands.

Chapter 9

Nederlandse samenvatting

Hoewel in de afgelopen decennia veel vooruitgang is geboekt in de behandeling van kankerpatiënten is deze ziekte voor een aanzienlijk deel van hen nog steeds dodelijk. Doordat er steeds meer duidelijk wordt welke eiwitten betrokken zijn bij het ontstaan en de groei van kanker zijn er therapieën ontwikkeld die zulke eiwitten remmen. In **hoofdstuk 1** wordt een overzicht gegeven van dergelijke targeted therapieën die momenteel gebruikt worden bij de behandeling van kankerpatiënten. Naast het remmen van de werking van eiwitten die betrokken zijn bij de ontwikkeling van kanker heeft een deel van de targeted therapieën (tevens) anti-tumor effecten door middel van een antilichaam-gemedieerde immuunrespons tegen de tumorcellen. Hoewel targeted therapieën die gericht zijn tegen tumorcel specifieke eiwitten kunnen bijdragen aan een verbeterde progressievrije overleving zijn dergelijke therapieën slechts gunstig voor subgroepen kankerpatiënten. Hiernaast hebben targeted therapieën die zich richten tegen tumorcellen in solide tumoren een verminderde werking doordat intraveneus toegediende antilichamen tumorcellen lastig kunnen bereiken. Het aanvallen van het vaatbed van tumoren ten einde hun bloedvoorziening te verstoren is een goede oplossing om dergelijke beperkende factoren van targeted tumortherapieën te omzeilen. Immers, de endotheelcellen die de vaatwand aan de binnenkant bekleden zijn genetisch stabiel en goed te bereiken zijn na intraveneuze injectie. Tumoren worden van bloed voorzien door vaten die nieuw aangelegd worden onder invloed van een tumor (angiogenese) en/of door het reeds bestaande vaatbed (vaatcoöptie), welke al dan niet onder invloed van de tumor gemoduleerd wordt. Hierdoor zijn er in verschillende tumoren, maar zelfs ook binnen één tumor, diverse soorten vaten aanwezig. Deze vaatheterogeniteit heeft implicaties voor het gebruik van kankertherapieën die er op gericht zijn te interfereren met de bloedvoorziening van een tumor. Aangezien het tegengaan van de nieuwvorming van vaten (anti-angiogene therapie) enkel leidt tot remming van de vroege stadia van angiogenese worden meer volwassen vaten niet getroffen, waardoor de effectiviteit van anti-angiogene therapieën aanzienlijk beperkt is. Derhalve lijkt het tevens aanvallen van het bestaande vaatbed (vasculaire targeting) een aantrekkelijke toevoeging om tumoren effectief af te snijden van bloed.

Hoofdstuk 2 beschrijft de verschillen in kenmerken van het vaatbed (vasculaire fenotype) en expressieprofielen van de belangrijkste factor die angiogenese teweegbrengt, Vascular Endothelial Growth Factor A (VEGF-A), in verscheidene primaire hersentumoren en hersenmetastasen. De verschillen in vasculaire fenotypes kunnen verklaard worden aan de hand van een model welke de specifieke effecten van verschillende VEGF-A varianten (isovormen) combineert met de impuls die leidt tot VEGF-A expressie. Hoewel de VEGF-A_{165} en $_{189}$ isovormen in staat zijn om een echte angiogene respons teweeg te brengen, hebben deze isovormen een sterke binding aan celoppervlakken en structuren in het

omliggende weefsel (extracellulaire matrix) waardoor ze enkel effect hebben op vaten in de directe omgeving van de tumorcellen die VEGF-A maken en uitscheiden. Zodoende kunnen in tumoren die vanaf hun ontstaan VEGF-A maken (constitutieve expressie) alle isovormen effect hebben op nabij gelegen vaten wat resulteert in een echt angiogeen fenotype. Daarentegen worden in tumoren waar VEGF-A wegens een tekort aan zuurstof (hypoxie) slechts in centrale gebieden wordt gemaakt de grotere isovormen vastgehouden door extracellulaire matrix. Hierdoor kan alleen de vrij verspreidbare VEGF-A_{121} isovorm welke niet in staat is angiogenese op te roepen maar slechts verwijding van reeds bestaande (pre-existente) vaten, effect op het verder gelegen vaatbed uitoefenen. Dit resulteert in een fenotypisch ander vaatbed, ondanks de gelijktijdige expressie van de VEGF-A isovormen 165 en 189. Tevens kunnen tumorcellen in goed doorbloede weefsels zoals de hersenen doorgroeien zonder een tekort aan zuurstof door middel van infiltratie in het hersenweefsel en gebruik te maken van de reeds bestaande hersenvaten (vaatcoöptie), zoals waargenomen wordt in gliomen. Aangezien endotheelcellen in verschillende weefsels en tumoren specifieke eiwitten presenteren, is het aannemelijk dat ook endotheelcellen in gecoöpteerde vaten onderhevig zijn aan invloeden van de tumor en zodoende veranderingen in hun eiwitprofiel laten zien die specifiek aangevallen kunnen worden.

Om tumoren effectief af te snijden van bloedvoorziening zijn stoffen nodig die specifieke merkers (tumorvat targets) op het volledige heterogene tumorvaatbed herkennen. In **hoofdstuk 3** wordt Plexine D1 gepresenteerd als een nieuwe tumorvat target. Plexine D1 behoort tot een familie van transmembraan eiwitten die functioneren als receptoren voor Neuropilines en Semaphorines en als zodaning betrokken zijn bij de vorming van het zenuwstelsel en vaatbed tijdens de embryonale ontwikkeling. Zoals beschreven in dit hoofdstuk komt Plexine D1 eveneens tot expressie op nieuwe vaten in tumoren. Tevens is dit eiwit uitgebreid aanwezig op een deel van de bestaande geactiveerde tumorvaten en op tumorcellen in verscheidene primaire hersentumoren en hersenmetastasen. Met behulp van de faagdisplay technologie zijn er antilichaamfragmenten (nanobodies) geselecteerd tegen Plexine D1. Na injectie van deze nanobodies in de bloedbaan van muizen met hersenmetastasen van melanoom binden deze nanobodies specifiek aan het nieuwe gevormde vaatbed in deze uitzaaiingen.

Hoewel bekend is dat Plexine D1 een centrale rol speelt in de ontwikkeling van het vaatbed, is de functie van Plexine D1 expressie op tumorcellen een stuk minder duidelijk. Omdat Plexine D1 alle karakteristieken heeft van een eiwit dat betrokken is bij de voortbeweging van cellen, lijkt het aannemelijk dat Plexine D1 betrokken is bij de uitgroei van tumoren in het omliggende weefsel (invasie) en het uitzaaien naar verderop gelegen

plekken in het lichaam (metastaseren). In **hoofdstuk 4** wordt inderdaad aangetoond dat Plexine D1 expressie gecorreleerd is met tumorinvasie en metastasering in verschillende ontwikkelingsstadia van melanoom. Plexine D1 is afwezig in de pigmentvormende (melanocytaire) cellen in moedervlekken (naevi) en in lesies waarbij de tumorcellen enkel nog gelegen zijn in de opperhuid (*in situ* melanomen), terwijl in primaire melanomen tumorcelexpressie toeneemt met de mate van invasie en bijna alle melanoom metastasen tumorcelexpressie van Plexin D1 tonen. Semaphorine 3E, een eiwit dat aan Plexine D1 bindt en als zodanig betrokken is bij het functioneren van Plexine D1, laat echter een omgekeerde correlatie met tumorprogressie zien, met zo goed als geen waarneembaar Semaphorine 3E in melanoommetastases. Functionele analyse van Semaphorine 3E overexpressie in een muis model voor metastaserend melanoom toont aan dat Semaphorine 3E de nieuwvorming van tumorvaten tegengaat en het vermogen van tumorcellen om uit te zaaien aanzienlijk doet afnemen. Gebaseerd op de resultaten beschreven in dit hoofdstuk kan Semaphorine 3E uitgesloten worden als activerend ligand voor Plexine D1.

Hoofdstuk 5 beschrijft Plexine D1 expressie in solide tumoren van verschillende oorsprong en niet-tumor gerelateerde weefsels. Plexine D1 is uitgebreid aanwezig op zowel nieuw gevormde en geactiveerde gecoöpteerde tumorvaten als op tumorcellen. In niet-tumor gerelateerde weefsels is Plexine D1 slecht aanwezig op een kleine groep cellen, vermoedelijk geactiveerde fibroblasten en macrofagen. Dit expressieprofiel suggereert dat Plexine D1 een belangrijk tumor target kan zijn voor solide tumoren waarin vaat-activatie heeft plaatsgevonden, aangezien het de mogelijkheid biedt om tegelijkertijd tumorcellen en tumorvaten aan te pakken.

Teneinde de bloedtoevoer naar tumoren die (tevens) gebruik maken van reeds bestaande vaten te blokkeren is het noodzakelijk extra stoffen te identificeren die samen het gehele heterogene vaatbed van een tumor kunnen aanvallen. Dergelijke stoffen kunnen geïsoleerd worden met behulp van de biopanning techniek, waarvan een *in vivo* toepassing wordt beschreven in **hoofdstuk 6**. Door middel van biopanning van een naïeve Llama faagbank in een muis model voor hoog gradig glioom (E98) is nanobody C-C7, welke specifiek tumorvaten herkent in E98 tumoren, verkregen. Het ligand van C-C7 is met behulp van de gist-2-hybride techniek geïdentificeerd als dynactin-1-p150^{glued}, een eiwit dat betrokken is bij het membraan verkeer binnenin cellen. Dynactin-1-p150^{glued} is specifiek aanwezig op een deel van de geactiveerde tumorvaten in verscheidene muis tumormodellen, echter, in enkele tumormodellen is dit eiwit afwezig op het vaatbed. Aangezien nanobody C-C7 eveneens de menselijke tegenhanger van dynactin-1-p150^{glued} op vaten van gliomen herkent, kan het een geschikte kandidaat zijn om opgenomen te

worden in een mengsel van stoffen die gezamenlijk het hele tumorvaatbed kunnen aanvallen.

In **hoofdstuk 7** is de procedure om nieuwe stoffen (nanobodies) te isoleren die tumorvaten herkennen verder uitgewerkt. Dit hoofdstuk beschrijft de constructie van een nanobody-faagbank, gecloneerd uit lymfocyten van een Llama na immunisatie met weefsel van hoog gradige gliomen. Deze bank bevat fagen met op hun oppervlak nanobodies die gericht zijn tegen alle weefselcomponenten in hoog gradige gliomen, inclusief bloedvaten. Door middel van *in vivo* biopanning van deze faagbank in glioommodellen met verschillende vasculaire fenotypes zijn verscheidene nanobodies geïsoleerd die tumorvaten herkennen in de corresponderende glioommodellen, waaronder ook nanobodies die geïncorporeerde reeds bestaande vaten in infiltratieve tumorgebieden kunnen onderscheiden van normale hersenvaten.

Teneinde tumoren effectief af te snijden van bloedvoorziening zijn er geschikte mengsels van stoffen nodig die gezamenlijk het gehele heterogene vaatbed herkennen. In dit proefschrift is aangetoond dat de combinatie van *in vivo* biopanning van immuun nanobody-faagbanken in geschikte tumormodellen en gist-2-hybride analyses met juiste prooibanken een krachtig platform vormt voor de identificatie van nieuwe nanobodies die gericht zijn tegen het tumorvaatbed en hun bijbehorende targets.

References

1. Krause DS and Van Etten RA. Tyrosine kinases as targets for cancer therapy. *N Engl J Med* 2005, 353:172-187

2. Demetri GD, von Mehren M, Blanke CD, Van den Abbeele AD, Eisenberg B, Roberts PJ, Heinrich MC, Tuveson DA, Singer S, Janicek M, Fletcher JA, Silverman SG, Silberman SL, Capdeville R, Kiese B, Peng B, Dimitrijevic S, Druker BJ, Corless C, Fletcher CD, Joensuu H. Efficacy and safety of imatinib mesylate in advanced gastrointestinal stromal tumors. *N Engl J Med* 2002, 347:472-480

3. Ostman A. PDGF receptors-mediators of autocrine tumor growth and regulators of tumor vasculature and stroma. *Cytokine Growth Factor Rev* 2004, 15:275-286

4. Board R and Jayson GC. Platelet-derived growth factor receptor (PDGFR): a target for anticancer therapeutics. *Drug Resist Updat* 2005, 8:75-83

5. McArthur GA, Demetri GD, van Oosterom A, Heinrich MC, biec-Rychter M, Corless CL, Nikolova Z, Dimitrijevic S, Fletcher JA. Molecular and clinical analysis of locally advanced dermatofibrosarcoma protuberans treated with imatinib: Imatinib Target Exploration Consortium Study B2225. *J Clin Oncol* 2005, 23:866-873

6. Hermanson M, Funa K, Koopmann J, Maintz D, Waha A, Westermark B, Heldin CH, Wiestler OD, Louis DN, von Deimling A, Nister M. Association of loss of heterozygosity on chromosome 17p with high platelet-derived growth factor alpha receptor expression in human malignant gliomas. *Cancer Res* 1996, 56:164-171

7. Raymond E, Brandes AA, Dittrich C, Fumoleau P, Coudert B, Clement PM, Frenay M, Rampling R, Stupp R, Kros JM, Heinrich MC, Gorlia T, Lacombe D, van den Bent MJ. Phase II study of imatinib in patients with recurrent gliomas of various histologies: a European Organisation for Research and Treatment of Cancer Brain Tumor Group Study. *J Clin Oncol* 2008, 26:4659-4665

8. Wen PY, Yung WK, Lamborn KR, Dahia PL, Wang Y, Peng B, Abrey LE, Raizer J, Cloughesy TF, Fink K, Gilbert M, Chang S, Junck L, Schiff D, Lieberman F, Fine HA, Mehta M, Robins HI, DeAngelis LM, Groves MD, Puduvalli VK, Levin V, Conrad C, Maher EA, Aldape K, Hayes M, Letvak L, Egorin MJ, Capdeville R, Kaplan R, Murgo AJ, Stiles C, Prados MD. Phase I/II study of imatinib mesylate for recurrent malignant gliomas: North American Brain Tumor Consortium Study 99-08. *Clin Cancer Res* 2006, 12:4899-4907

9. Reardon DA, Egorin MJ, Quinn JA, Rich JN, Gururangan S, Vredenburgh JJ, Desjardins A, Sathornsumetee S, Provenzale JM, Herndon JE, Dowell JM, Badruddoja MA, McLendon RE, Lagattuta TF, Kicielinski KP, Dresemann G, Sampson JH, Friedman AH, Salvado AJ, Friedman HS. Phase II study of imatinib mesylate plus hydroxyurea in adults with recurrent glioblastoma multiforme. *J Clin Oncol* 2005, 23:9359-9368

10. Matei D, Chang DD, Jeng MH. Imatinib mesylate (Gleevec) inhibits ovarian cancer cell growth through a mechanism dependent on platelet-derived growth factor receptor alpha and Akt inactivation. *Clin Cancer Res* 2004, 10:681-690

11. Matei D, Emerson RE, Lai YC, Baldridge LA, Rao J, Yiannoutsos C, Donner DD. Autocrine activation of PDGFRalpha promotes the progression of ovarian cancer. *Oncogene* 2006, 25:2060-2069

12. Schilder RJ, Sill MW, Lee RB, Shaw TJ, Senterman MK, Klein-Szanto AJ, Miner Z, Vanderhyden BC. Phase II evaluation of imatinib mesylate in the treatment of recurrent or persistent epithelial ovarian

or primary peritoneal carcinoma: a Gynecologic Oncology Group Study. *J Clin Oncol* 2008, 26:3418-3425

13. Rocha-Lima CM, Soares HP, Raez LE, Singal R. EGFR targeting of solid tumors. *Cancer Control* 2007, 14:295-304

14. Mendelsohn J and Baselga J. The EGF receptor family as targets for cancer therapy. *Oncogene* 2000, 19:6550-6565

15. Slamon DJ, Leyland-Jones B, Shak S, Fuchs H, Paton V, Bajamonde A, Fleming T, Eiermann W, Wolter J, Pegram M, Baselga J, Norton L. Use of chemotherapy plus a monoclonal antibody against HER2 for metastatic breast cancer that overexpresses HER2. *N Engl J Med* 2001, 344:783-792

16. Nanda R. Targeting the human epidermal growth factor receptor 2 (HER2) in the treatment of breast cancer: recent advances and future directions. *Rev Recent Clin Trials* 2007, 2:111-116

17. Bonner JA, Harari PM, Giralt J, Azarnia N, Shin DM, Cohen RB, Jones CU, Sur R, Raben D, Jassem J, Ove R, Kies MS, Baselga J, Youssoufian H, Amellal N, Rowinsky EK, Ang KK. Radiotherapy plus cetuximab for squamous-cell carcinoma of the head and neck. *N Engl J Med* 2006, 354:567-578

18. Cunningham D, Humblet Y, Siena S, Khayat D, Bleiberg H, Santoro A, Bets D, Mueser M, Harstrick A, Verslype C, Chau I, Van Cutsem E. Cetuximab monotherapy and cetuximab plus irinotecan in irinotecan-refractory metastatic colorectal cancer. *N Engl J Med* 2004, 351:337-345

19. Tol J, Koopman M, Cats A, Rodenburg CJ, Creemers GJ, Schrama JG, Erdkamp FL, Vos AH, van Groeningen CJ, Sinnige HA, Richel DJ, Voest EE, Dijkstra JR, Vink-Borger ME, Antonini NF, Mol L, van Krieken JH, Dalesio O, Punt CJ. Chemotherapy, bevacizumab, and cetuximab in metastatic colorectal cancer. *N Engl J Med* 2009, 360:563-572

20. Shepherd FA, Rodrigues PJ, Ciuleanu T, Tan EH, Hirsh V, Thongprasert S, Campos D, Maoleekoonpiroj S, Smylie M, Martins R, van Kooten M, Dediu M, Findlay B, Tu D, Johnston D, Bezjak A, Clark G, Santabarbara P, Seymour L. Erlotinib in previously treated non-small-cell lung cancer. *N Engl J Med* 2005, 353:123-132

21. Moore MJ, Goldstein D, Hamm J, Figer A, Hecht JR, Gallinger S, Au HJ, Murawa P, Walde D, Wolff RA, Campos D, Lim R, Ding K, Clark G, Voskoglou-Nomikos T, Ptasynski M, Parulekar W. Erlotinib plus gemcitabine compared with gemcitabine alone in patients with advanced pancreatic cancer: a phase III trial of the National Cancer Institute of Canada Clinical Trials Group. *J Clin Oncol* 2007, 25:1960-1966

22. van Cutsem E, Peeters M, Siena S, Humblet Y, Hendlisz A, Neyns B, Canon JL, Van Laethem JL, Maurel J, Richardson G, Wolf M, Amado RG. Open-label phase III trial of panitumumab plus best supportive care compared with best supportive care alone in patients with chemotherapy-refractory metastatic colorectal cancer. *J Clin Oncol* 2007, 25:1658-1664

23. Maher EA, Furnari FB, Bachoo RM, Rowitch DH, Louis DN, Cavenee WK, DePinho RA. Malignant glioma: genetics and biology of a grave matter. *Genes Dev* 2001, 15:1311-1333

24. Mellinghoff IK, Wang MY, Vivanco I, Haas-Kogan DA, Zhu S, Dia EQ, Lu KV, Yoshimoto K, Huang JH, Chute DJ, Riggs BL, Horvath S, Liau LM, Cavenee WK, Rao PN, Beroukhim R, Peck TC, Lee JC, Sellers WR, Stokoe D, Prados M, Cloughesy TF, Sawyers CL, Mischel PS. Molecular determinants of the response of glioblastomas to EGFR kinase inhibitors. *N Engl J Med* 2005, 353:2012-2024

25. Preusser M, Gelpi E, Rottenfusser A, Dieckmann K, Widhalm G, Dietrich W, Bertalanffy A, Prayer D, Hainfellner JA, Marosi C. Epithelial Growth Factor Receptor Inhibitors for treatment of recurrent or progressive high grade glioma: an exploratory study. *J Neurooncol* 2008, 89:211-218

26. Brown PD, Krishnan S, Sarkaria JN, Wu W, Jaeckle KA, Uhm JH, Geoffroy FJ, Arusell R, Kitange G, Jenkins RB, Kugler JW, Morton RF, Rowland KM, Jr., Mischel P, Yong WH, Scheithauer BW, Schiff D, Giannini C, Buckner JC. Phase I/II Trial Erlotinib and Temozolomide With Radiation Therapy in the Treatment of Newly Diagnosed Glioblastoma Multiforme: North Central Cancer Treatment Group Study N0177. *J Clin Oncol* 2008,

27. Hartog H, Wesseling J, Boezen HM, van der Graaf WT. The insulin-like growth factor 1 receptor in cancer: old focus, new future. *Eur J Cancer* 2007, 43:1895-1904

28. Yakar S, Leroith D, Brodt P. The role of the growth hormone/insulin-like growth factor axis in tumor growth and progression: Lessons from animal models. *Cytokine Growth Factor Rev* 2005, 16:407-420

29. Rowinsky EK, Youssoufian H, Tonra JR, Solomon P, Burtrum D, Ludwig DL. IMC-A12, a human IgG1 monoclonal antibody to the insulin-like growth factor I receptor. *Clin Cancer Res* 2007, 13:5549s-5555s

30. Cohen BD, Baker DA, Soderstrom C, Tkalcevic G, Rossi AM, Miller PE, Tengowski MW, Wang F, Gualberto A, Beebe JS, Moyer JD. Combination therapy enhances the inhibition of tumor growth with the fully human anti-type 1 insulin-like growth factor receptor monoclonal antibody CP-751,871. *Clin Cancer Res* 2005, 11:2063-2073

31. Haluska P, Shaw HM, Batzel GN, Yin D, Molina JR, Molife LR, Yap TA, Roberts ML, Sharma A, Gualberto A, Adjei AA, de Bono JS. Phase I dose escalation study of the anti insulin-like growth factor-I receptor monoclonal antibody CP-751,871 in patients with refractory solid tumors. *Clin Cancer Res* 2007, 13:5834-5840

32. Chitnis MM, Yuen JS, Protheroe AS, Pollak M, Macaulay VM. The Type 1 Insulin-Like Growth Factor Receptor Pathway. *Clin Cancer Res* 2008, 14:6364-6370

33. Pandini G, Wurch T, Akla B, Corvaia N, Belfiore A, Goetsch L. Functional responses and in vivo anti-tumour activity of h7C10: a humanised monoclonal antibody with neutralising activity against the insulin-like growth factor-1 (IGF-1) receptor and insulin/IGF-1 hybrid receptors. *Eur J Cancer* 2007, 43:1318-1327

34. Dancey JE. Therapeutic targets: MTOR and related pathways. *Cancer Biol Ther* 2006, 5:1065-1073

35. Thomas GV. mTOR and cancer: reason for dancing at the crossroads? *Curr Opin Genet Dev* 2006, 16:78-84

36. Hudes G, Carducci M, Tomczak P, Dutcher J, Figlin R, Kapoor A, Staroslawska E, Sosman J, McDermott D, Bodrogi I, Kovacevic Z, Lesovoy V, Schmidt-Wolf IG, Barbarash O, Gokmen E, O'Toole T, Lustgarten S, Moore L, Motzer RJ. Temsirolimus, interferon alfa, or both for advanced renal-cell carcinoma. *N Engl J Med* 2007, 356:2271-2281

37. Yan L, Hsu K, Beckman RA. Antibody-based therapy for solid tumors. *Cancer J* 2008, 14:178-183

38. Strome SE, Sausville EA, Mann D. A mechanistic perspective of monoclonal antibodies in cancer therapy beyond target-related effects. *Oncologist* 2007, 12:1084-1095

39. Barok M, Isola J, Palyi-Krekk Z, Nagy P, Juhasz I, Vereb G, Kauraniemi P, Kapanen A, Tanner M, Vereb G, Szollosi J. Trastuzumab causes antibody-dependent cellular cytotoxicity-mediated growth inhibition of submacroscopic JIMT-1 breast cancer xenografts despite intrinsic drug resistance. *Mol Cancer Ther* 2007, 6:2065-2072

40. Kurai J, Chikumi H, Hashimoto K, Yamaguchi K, Yamasaki A, Sako T, Touge H, Makino H, Takata M, Miyata M, Nakamoto M, Burioka N, Shimizu E. Antibody-dependent cellular cytotoxicity mediated by cetuximab against lung cancer cell lines. *Clin Cancer Res* 2007, 13:1552-1561

41. Kawaguchi Y, Kono K, Mimura K, Sugai H, Akaike H, Fujii H. Cetuximab induce antibody-dependent cellular cytotoxicity against EGFR-expressing esophageal squamous cell carcinoma. *Int J Cancer* 2007, 120:781-787

42. Folkman J. Tumor angiogenesis: therapeutic implications. *N Engl J Med* 1971, 285:1182-1186

43. Folkman J. What is the evidence that tumors are angiogenesis dependent? *J Natl Cancer Inst* 1990, 82:4-6

44. Carmeliet P and Jain RK. Angiogenesis in cancer and other diseases. *Nature* 2000, 407:249-257

45. Kerbel R and Folkman J. Clinical translation of angiogenesis inhibitors. *Nat Rev Cancer* 2002, 2:727-739

46. Holash J, Maisonpierre PC, Compton D, Boland P, Alexander CR, Zagzag D, Yancopoulos GD, Wiegand SJ. Vessel cooption, regression, and growth in tumors mediated by angiopoietins and VEGF. *Science* 1999, 284:1994-1998

47. Werb Z, Vu TH, Rinkenberger JL, Coussens LM. Matrix-degrading proteases and angiogenesis during development and tumor formation. *APMIS* 1999, 107:11-18

48. Bergers G and Benjamin LE. Tumorigenesis and the angiogenic switch. *Nat Rev Cancer* 2003, 3:401-410

49. Hobbs SK, Monsky WL, Yuan F, Roberts WG, Griffith L, Torchilin VP, Jain RK. Regulation of transport pathways in tumor vessels: role of tumor type and microenvironment. *Proc Natl Acad Sci U S A* 1998, 95:4607-4612

50. Dvorak HF, Nagy JA, Feng D, Brown LF, Dvorak AM. Vascular permeability factor/vascular endothelial growth factor and the significance of microvascular hyperpermeability in angiogenesis. *Curr Top Microbiol Immunol* 1999, 237:97-132

51. Jain RK. Normalizing tumor vasculature with anti-angiogenic therapy: a new paradigm for combination therapy. *Nat Med* 2001, 7:987-989

52. Ferrara N and Davis-Smyth T. The biology of vascular endothelial growth factor. *Endocr Rev* 1997, 18:4-25

53. Dvorak HF. Vascular permeability factor/vascular endothelial growth factor: a critical cytokine in tumor angiogenesis and a potential target for diagnosis and therapy. *J Clin Oncol* 2002, 20:4368-4380

54. van Hinsbergh V, Collen A, Koolwijk P. Role of fibrin matrix in angiogenesis. *Ann N Y Acad Sci* 2001, 936:426-437

55. Robinson CJ and Stringer SE. The splice variants of vascular endothelial growth factor (VEGF) and their receptors. *J Cell Sci* 2001, 114:853-865

56. Poltorak Z, Cohen T, Sivan R, Kandelis Y, Spira G, Vlodavsky I, Keshet E, Neufeld G. VEGF145, a secreted vascular endothelial growth factor isoform that binds to extracellular matrix. *J Biol Chem* 1997, 272:7151-7158

57. Neufeld G, Cohen T, Gengrinovitch S, Poltorak Z. Vascular endothelial growth factor (VEGF) and its receptors. *FASEB J* 1999, 13:9-22

58. Dvorak HF, Brown LF, Detmar M, Dvorak AM. Vascular permeability factor/vascular endothelial growth factor, microvascular hyperpermeability, and angiogenesis. *Am J Pathol* 1995, 146:1029-1039

59. Wood JM, Bold G, Buchdunger E, Cozens R, Ferrari S, Frei J, Hofmann F, Mestan J, Mett H, O'Reilly T, Persohn E, Rosel J, Schnell C, Stover D, Theuer A, Towbin H, Wenger F, Woods-Cook K, Menrad A, Siemeister G, Schirner M, Thierauch KH, Schneider MR, Drevs J, Martiny-Baron G, Totzke F. PTK787/ZK 222584, a novel and potent inhibitor of vascular endothelial growth factor receptor tyrosine kinases, impairs vascular endothelial growth factor-induced responses and tumor growth after oral administration. *Cancer Res* 2000, 60:2178-2189

60. Mendel DB, Laird AD, Xin X, Louie SG, Christensen JG, Li G, Schreck RE, Abrams TJ, Ngai TJ, Lee LB, Murray LJ, Carver J, Chan E, Moss KG, Haznedar JO, Sukbuntherng J, Blake RA, Sun L, Tang C, Miller T, Shirazian S, McMahon G, Cherrington JM. In vivo antitumor activity of SU11248, a novel tyrosine kinase inhibitor targeting vascular endothelial growth factor and platelet-derived growth factor receptors: determination of a pharmacokinetic/pharmacodynamic relationship. *Clin Cancer Res* 2003, 9:327-337

61. Wilhelm SM, Carter C, Tang L, Wilkie D, McNabola A, Rong H, Chen C, Zhang X, Vincent P, McHugh M, Cao Y, Shujath J, Gawlak S, Eveleigh D, Rowley B, Liu L, Adnane L, Lynch M, Auclair D, Taylor I, Gedrich R, Voznesensky A, Riedl B, Post LE, Bollag G, Trail PA. BAY 43-9006 exhibits broad spectrum oral antitumor activity and targets the RAF/MEK/ERK pathway and receptor tyrosine kinases involved in tumor progression and angiogenesis. *Cancer Res* 2004, 64:7099-7109

62. Presta LG, Chen H, O'Connor SJ, Chisholm V, Meng YG, Krummen L, Winkler M, Ferrara N. Humanization of an anti-vascular endothelial growth factor monoclonal antibody for the therapy of solid tumors and other disorders. *Cancer Res* 1997, 57:4593-4599

63. Wedge SR, Ogilvie DJ, Dukes M, Kendrew J, Chester R, Jackson JA, Boffey SJ, Valentine PJ, Curwen JO, Musgrove HL, Graham GA, Hughes GD, Thomas AP, Stokes ES, Curry B, Richmond GH, Wadsworth PF, Bigley AL, Hennequin LF. ZD6474 inhibits vascular endothelial growth factor signaling, angiogenesis, and tumor growth following oral administration. *Cancer Res* 2002, 62:4645-4655

64. Yancopoulos GD, Davis S, Gale NW, Rudge JS, Wiegand SJ, Holash J. Vascular-specific growth factors and blood vessel formation. *Nature* 2000, 407:242-248

65. Holash J, Wiegand SJ, Yancopoulos GD. New model of tumor angiogenesis: dynamic balance between vessel regression and growth mediated by angiopoietins and VEGF. *Oncogene* 1999, 18:5356-5362

66. Hanahan D. Signaling vascular morphogenesis and maintenance. *Science* 1997, 277:48-50

67. Lin P, Buxton JA, Acheson A, Radziejewski C, Maisonpierre PC, Yancopoulos GD, Channon KM, Hale LP, Dewhirst MW, George SE, Peters KG. Antiangiogenic gene therapy targeting the endothelium-specific receptor tyrosine kinase Tie2. *Proc Natl Acad Sci U S A* 1998, 95:8829-8834

68. Siemeister G, Schirner M, Weindel K, Reusch P, Menrad A, Marme D, Martiny-Baron G. Two independent mechanisms essential for tumor angiogenesis: inhibition of human melanoma xenograft growth by interfering with either the vascular endothelial growth factor receptor pathway or the Tie-2 pathway. *Cancer Res* 1999, 59:3185-3191

69. Stratmann A, Acker T, Burger AM, Amann K, Risau W, Plate KH. Differential inhibition of tumor angiogenesis by tie2 and vascular endothelial growth factor receptor-2 dominant-negative receptor mutants. *Int J Cancer* 2001, 91:273-282

70. Popkov M, Jendreyko N, McGavern DB, Rader C, Barbas CF, III. Targeting tumor angiogenesis with adenovirus-delivered anti-Tie-2 intrabody. *Cancer Res* 2005, 65:972-981

71. Oliner J, Min H, Leal J, Yu D, Rao S, You E, Tang X, Kim H, Meyer S, Han SJ, Hawkins N, Rosenfeld R, Davy E, Graham K, Jacobsen F, Stevenson S, Ho J, Chen Q, Hartmann T, Michaels M, Kelley M, Li L, Sitney K, Martin F, Sun JR, Zhang N, Lu J, Estrada J, Kumar R, Coxon A, Kaufman S, Pretorius J, Scully S, Cattley R, Payton M, Coats S, Nguyen L, Desilva B, Ndifor A, Hayward I, Radinsky R, Boone T, Kendall R. Suppression of angiogenesis and tumor growth by selective inhibition of angiopoietin-2. *Cancer Cell* 2004, 6:507-516

72. Abramsson A, Lindblom P, Betsholtz C. Endothelial and nonendothelial sources of PDGF-B regulate pericyte recruitment and influence vascular pattern formation in tumors. *J Clin Invest* 2003, 112:1142-1151

73. Bergers G, Song S, Meyer-Morse N, Bergsland E, Hanahan D. Benefits of targeting both pericytes and endothelial cells in the tumor vasculature with kinase inhibitors. *J Clin Invest* 2003, 111:1287-1295

74. Pietras K, Pahler J, Bergers G, Hanahan D. Functions of paracrine PDGF signaling in the proangiogenic tumor stroma revealed by pharmacological targeting. *PLoS Med* 2008, 5:e19

75. Leenders WP, Kusters B, de Waal RM. Vessel co-option: how tumors obtain blood supply in the absence of sprouting angiogenesis. *Endothelium* 2002, 9:83-87

76. Kusters B, Leenders WP, Wesseling P, Smits D, Verrijp K, Ruiter DJ, Peters JP, van der Kogel AJ, de Waal RM. Vascular endothelial growth factor-A(165) induces progression of melanoma brain metastases without induction of sprouting angiogenesis. *Cancer Res* 2002, 62:341-345

77. Kusters B, de Waal RM, Wesseling P, Verrijp K, Maass C, Heerschap A, Barentsz JO, Sweep F, Ruiter DJ, Leenders WP. Differential effects of vascular endothelial growth factor A isoforms in a mouse brain metastasis model of human melanoma. *Cancer Res* 2003, 63:5408-5413

78. Leenders W, Kusters B, Pikkemaat J, Wesseling P, Ruiter D, Heerschap A, Barentsz J, de Waal RM. Vascular endothelial growth factor-A determines detectability of experimental melanoma brain metastasis in GD-DTPA-enhanced MRI. *Int J Cancer* 2003, 105:437-443

79. Claes A, Idema AJ, Wesseling P. Diffuse glioma growth: a guerilla war. *Acta Neuropathol* 2007, 114:443-458

80. Louis DN, Ohgaki H, Wiestler OD, Cavenee WK, Burger PC, Jouvet A, Scheithauer BW, Kleihues P. The 2007 WHO classification of tumours of the central nervous system. *Acta Neuropathol* 2007, 114:97-109

81. Kleihues P, Louis DN, Scheithauer BW, Rorke LB, Reifenberger G, Burger PC, Cavenee WK. The WHO classification of tumors of the nervous system. *J Neuropathol Exp Neurol* 2002, 61:215-225

82. Wesseling P, Ruiter DJ, Burger PC. Angiogenesis in brain tumors; pathobiological and clinical aspects. *J Neurooncol* 1997, 32:253-265

83. Plate KH, Breier G, Weich HA, Risau W. Vascular endothelial growth factor is a potential tumour angiogenesis factor in human gliomas in vivo. *Nature* 1992, 359:845-848

84. Hau P, Stupp R, Hegi ME. MGMT methylation status: the advent of stratified therapy in glioblastoma? *Dis Markers* 2007, 23:97-104

85. Yang JC, Haworth L, Sherry RM, Hwu P, Schwartzentruber DJ, Topalian SL, Steinberg SM, Chen HX, Rosenberg SA. A randomized trial of bevacizumab, an anti-vascular endothelial growth factor antibody, for metastatic renal cancer. *N Engl J Med* 2003, 349:427-434

86. Burger RA, Sill MW, Monk BJ, Greer BE, Sorosky JI. Phase II trial of bevacizumab in persistent or recurrent epithelial ovarian cancer or primary peritoneal cancer: a Gynecologic Oncology Group Study. *J Clin Oncol* 2007, 25:5165-5171

87. Cannistra SA, Matulonis UA, Penson RT, Hambleton J, Dupont J, Mackey H, Douglas J, Burger RA, Armstrong D, Wenham R, McGuire W. Phase II study of bevacizumab in patients with platinum-resistant ovarian cancer or peritoneal serous cancer. *J Clin Oncol* 2007, 25:5180-5186

88. Hurwitz HI, Fehrenbacher L, Hainsworth JD, Heim W, Berlin J, Holmgren E, Hambleton J, Novotny WF, Kabbinavar F. Bevacizumab in combination with fluorouracil and leucovorin: an active regimen for first-line metastatic colorectal cancer. *J Clin Oncol* 2005, 23:3502-3508

89. Giantonio BJ, Catalano PJ, Meropol NJ, O'Dwyer PJ, Mitchell EP, Alberts SR, Schwartz MA, Benson AB, III. Bevacizumab in combination with oxaliplatin, fluorouracil, and leucovorin (FOLFOX4) for previously treated metastatic colorectal cancer: results from the Eastern Cooperative Oncology Group Study E3200. *J Clin Oncol* 2007, 25:1539-1544

90. Hurwitz H and Saini S. Bevacizumab in the treatment of metastatic colorectal cancer: safety profile and management of adverse events. *Semin Oncol* 2006, 33:S26-S34

91. Sandler A, Gray R, Perry MC, Brahmer J, Schiller JH, Dowlati A, Lilenbaum R, Johnson DH. Paclitaxel-carboplatin alone or with bevacizumab for non-small-cell lung cancer. *N Engl J Med* 2006, 355:2542-2550

92. Miller KD, Chap LI, Holmes FA, Cobleigh MA, Marcom PK, Fehrenbacher L, Dickler M, Overmoyer BA, Reimann JD, Sing AP, Langmuir V, Rugo HS. Randomized phase III trial of capecitabine compared with bevacizumab plus capecitabine in patients with previously treated metastatic breast cancer. *J Clin Oncol* 2005, 23:792-799

93. Miller K, Wang M, Gralow J, Dickler M, Cobleigh M, Perez EA, Shenkier T, Cella D, Davidson NE. Paclitaxel plus bevacizumab versus paclitaxel alone for metastatic breast cancer. *N Engl J Med* 2007, 357:2666-2676

94. Lai A, Filka E, McGibbon B, Nghiemphu PL, Graham C, Yong WH, Mischel P, Liau LM, Bergsneider M, Pope W, Selch M, Cloughesy T. Phase II pilot study of bevacizumab in combination with temozolomide and regional radiation therapy for up-front treatment of patients with newly diagnosed glioblastoma multiforme: interim analysis of safety and tolerability. *Int J Radiat Oncol Biol Phys* 2008, 71:1372-1380

95. Ali SA, McHayleh WM, Ahmad A, Sehgal R, Braffet M, Rahman M, Bejjani G, Friedland DM. Bevacizumab and irinotecan therapy in glioblastoma multiforme: a series of 13 cases. *J Neurosurg* 2008, 109:268-272

96. Claes A, Gambarota G, Hamans B, van Tellingen O, Wesseling P, Maass C, Heerschap A, Leenders W. Magnetic resonance imaging-based detection of glial brain tumors in mice after antiangiogenic treatment. *Int J Cancer* 2008, 122:1981-1986

97. Escudier B, Eisen T, Stadler WM, Szczylik C, Oudard S, Siebels M, Negrier S, Chevreau C, Solska E, Desai AA, Rolland F, Demkow T, Hutson TE, Gore M, Freeman S, Schwartz B, Shan M, Simantov R, Bukowski RM. Sorafenib in advanced clear-cell renal-cell carcinoma. *N Engl J Med* 2007, 356:125-134

98. Ratain MJ, Eisen T, Stadler WM, Flaherty KT, Kaye SB, Rosner GL, Gore M, Desai AA, Patnaik A, Xiong HQ, Rowinsky E, Abbruzzese JL, Xia C, Simantov R, Schwartz B, O'Dwyer PJ. Phase II placebo-controlled randomized discontinuation trial of sorafenib in patients with metastatic renal cell carcinoma. *J Clin Oncol* 2006, 24:2505-2512

99. Llovet JM, Ricci S, Mazzaferro V, Hilgard P, Gane E, Blanc JF, de Oliveira AC, Santoro A, Raoul JL, Forner A, Schwartz M, Porta C, Zeuzem S, Bolondi L, Greten TF, Galle PR, Seitz JF, Borbath I, Haussinger D, Giannaris T, Shan M, Moscovici M, Voliotis D, Bruix J. Sorafenib in advanced hepatocellular carcinoma. *N Engl J Med* 2008, 359:378-390

100. Flaherty KT, Schiller J, Schuchter LM, Liu G, Tuveson DA, Redlinger M, Lathia C, Xia C, Petrenciuc O, Hingorani SR, Jacobetz MA, Van Belle PA, Elder D, Brose MS, Weber BL, Albertini MR, O'Dwyer PJ. A phase I trial of the oral, multikinase inhibitor sorafenib in combination with carboplatin and paclitaxel. *Clin Cancer Res* 2008, 14:4836-4842

101. McDermott DF, Sosman JA, Gonzalez R, Hodi FS, Linette GP, Richards J, Jakub JW, Beeram M, Tarantolo S, Agarwala S, Frenette G, Puzanov I, Cranmer L, Lewis K, Kirkwood J, White JM, Xia C, Patel K, Hersh E. Double-blind randomized phase II study of the combination of sorafenib and dacarbazine in patients with advanced melanoma: a report from the 11715 Study Group. *J Clin Oncol* 2008, 26:2178-2185

102. Gupta-Abramson V, Troxel AB, Nellore A, Puttaswamy K, Redlinger M, Ransone K, Mandel SJ, Flaherty KT, Loevner LA, O'Dwyer PJ, Brose MS. Phase II Trial of Sorafenib in Advanced Thyroid Cancer. *J Clin Oncol* 2008, 26:4714-4719

103. Dahut WL, Scripture C, Posadas E, Jain L, Gulley JL, Arlen PM, Wright JJ, Yu Y, Cao L, Steinberg SM, ragon-Ching JB, Venitz J, Jones E, Chen CC, Figg WD. A phase II clinical trial of sorafenib in androgen-independent prostate cancer. *Clin Cancer Res* 2008, 14:209-214

104. Steinbild S, Mross K, Frost A, Morant R, Gillessen S, Dittrich C, Strumberg D, Hochhaus A, Hanauske AR, Edler L, Burkholder I, Scheulen M. A clinical phase II study with sorafenib in patients with progressive hormone-refractory prostate cancer: a study of the CESAR Central European Society for Anticancer Drug Research-EWIV. *Br J Cancer* 2007, 97:1480-1485

105. Elser C, Siu LL, Winquist E, Agulnik M, Pond GR, Chin SF, Francis P, Cheiken R, Elting J, McNabola A, Wilkie D, Petrenciuc O, Chen EX. Phase II trial of sorafenib in patients with recurrent or metastatic squamous cell carcinoma of the head and neck or nasopharyngeal carcinoma. *J Clin Oncol* 2007, 25:3766-3773

106. Motzer RJ, Michaelson MD, Redman BG, Hudes GR, Wilding G, Figlin RA, Ginsberg MS, Kim ST, Baum CM, DePrimo SE, Li JZ, Bello CL, Theuer CP, George DJ, Rini BI. Activity of SU11248, a multitargeted inhibitor of vascular endothelial growth factor receptor and platelet-derived growth factor receptor, in patients with metastatic renal cell carcinoma. *J Clin Oncol* 2006, 24:16-24

107. Motzer RJ, Rini BI, Bukowski RM, Curti BD, George DJ, Hudes GR, Redman BG, Margolin KA, Merchan JR, Wilding G, Ginsberg MS, Bacik J, Kim ST, Baum CM, Michaelson MD. Sunitinib in patients with metastatic renal cell carcinoma. *JAMA* 2006, 295:2516-2524

108. Motzer RJ, Hutson TE, Tomczak P, Michaelson MD, Bukowski RM, Rixe O, Oudard S, Negrier S, Szczylik C, Kim ST, Chen I, Bycott PW, Baum CM, Figlin RA. Sunitinib versus interferon alfa in metastatic renal-cell carcinoma. *N Engl J Med* 2007, 356:115-124

109. Rini BI, Michaelson MD, Rosenberg JE, Bukowski RM, Sosman JA, Stadler WM, Hutson TE, Margolin K, Harmon CS, DePrimo SE, Kim ST, Chen I, George DJ. Antitumor activity and biomarker analysis of sunitinib in patients with bevacizumab-refractory metastatic renal cell carcinoma. *J Clin Oncol* 2008, 26:3743-3748

110. Socinski MA, Novello S, Brahmer JR, Rosell R, Sanchez JM, Belani CP, Govindan R, Atkins JN, Gillenwater HH, Pallares C, Tye L, Selaru P, Chao RC, Scagliotti GV. Multicenter, phase II trial of sunitinib in previously treated, advanced non-small-cell lung cancer. *J Clin Oncol* 2008, 26:650-656

111. Burstein HJ, Elias AD, Rugo HS, Cobleigh MA, Wolff AC, Eisenberg PD, Lehman M, Adams BJ, Bello CL, DePrimo SE, Baum CM, Miller KD. Phase II study of sunitinib malate, an oral multitargeted tyrosine kinase inhibitor, in patients with metastatic breast cancer previously treated with an anthracycline and a taxane. *J Clin Oncol* 2008, 26:1810-1816

112. Kulke MH, Lenz HJ, Meropol NJ, Posey J, Ryan DP, Picus J, Bergsland E, Stuart K, Tye L, Huang X, Li JZ, Baum CM, Fuchs CS. Activity of sunitinib in patients with advanced neuroendocrine tumors. *J Clin Oncol* 2008, 26:3403-3410

113. Demetri GD, van Oosterom AT, Garrett CR, Blackstein ME, Shah MH, Verweij J, McArthur G, Judson IR, Heinrich MC, Morgan JA, Desai J, Fletcher CD, George S, Bello CL, Huang X, Baum CM, Casali PG. Efficacy and safety of sunitinib in patients with advanced gastrointestinal stromal tumour after failure of imatinib: a randomised controlled trial. *Lancet* 2006, 368:1329-1338

114. Schoenfeld A, Levavi H, Breslavski D, Amir R, Ovadia J. Three-dimensional modelling of tumor-induced ovarian angiogenesis. *Cancer Lett* 1994, 87:79-84

115. Jain RK. Normalization of tumor vasculature: an emerging concept in antiangiogenic therapy. *Science* 2005, 307:58-62

116. Boehm T, Folkman J, Browder T, O'Reilly MS. Antiangiogenic therapy of experimental cancer does not induce acquired drug resistance. *Nature* 1997, 390:404-407

117. Leenders WP, Kusters B, Verrijp K, Maass C, Wesseling P, Heerschap A, Ruiter D, Ryan A, de Waal R. Antiangiogenic therapy of cerebral melanoma metastases results in sustained tumor progression via vessel co-option. *Clin Cancer Res* 2004, 10:6222-6230

118. Kunkel P, Ulbricht U, Bohlen P, Brockmann MA, Fillbrandt R, Stavrou D, Westphal M, Lamszus K. Inhibition of glioma angiogenesis and growth in vivo by systemic treatment with a monoclonal antibody against vascular endothelial growth factor receptor-2. *Cancer Res* 2001, 61:6624-6628

119. Rubenstein JL, Kim J, Ozawa T, Zhang M, Westphal M, Deen DF, Shuman MA. Anti-VEGF antibody treatment of glioblastoma prolongs survival but results in increased vascular cooption. *Neoplasia* 2000, 2:306-314

120. Claes A, Wesseling P, Jeuken J, Maass C, Heerschap A, Leenders WP. Antiangiogenic compounds interfere with chemotherapy of brain tumors due to vessel normalization. *Mol Cancer Ther* 2008, 7:71-78

121. Claes A, Schuuring J, Boots-Sprenger S, Hendriks-Cornelissen S, Dekkers M, van der Kogel AJ, Leenders WP, Wesseling P, Jeuken JW. Phenotypic and genotypic characterization of orthotopic human glioma models and its relevance for the study of anti-glioma therapy. *Brain Pathol* 2008, 18:423-433

122. Claes A and Leenders W. Vessel normalization by VEGF inhibition. A complex story. *Cancer Biol Ther* 2008, 7:1014-1016

123. Narayana A, Kelly P, Golfinos J, Parker E, Johnson G, Knopp E, Zagzag D, Fischer I, Raza S, Medabalmi P, Eagan P, Gruber ML. Antiangiogenic therapy using bevacizumab in recurrent high-grade glioma: impact on local control and patient survival. *J Neurosurg* 2009, 110:173-180

124. Santimaria M, Moscatelli G, Viale GL, Giovannoni L, Neri G, Viti F, Leprini A, Borsi L, Castellani P, Zardi L, Neri D, Riva P. Immunoscintigraphic detection of the ED-B domain of fibronectin, a marker of angiogenesis, in patients with cancer. *Clin Cancer Res* 2003, 9:571-579

125. Castellani P, Borsi L, Carnemolla B, Biro A, Dorcaratto A, Viale GL, Neri D, Zardi L. Differentiation between high- and low-grade astrocytoma using a human recombinant antibody to the extra domain-B of fibronectin. *Am J Pathol* 2002, 161:1695-1700

126. Schraa AJ, Kok RJ, Moorlag HE, Bos EJ, Proost JH, Meijer DK, de Leij LF, Molema G. Targeting of RGD-modified proteins to tumor vasculature: a pharmacokinetic and cellular distribution study. *Int J Cancer* 2002, 102:469-475

127. Janssen ML, Oyen WJ, Dijkgraaf I, Massuger LF, Frielink C, Edwards DS, Rajopadhye M, Boonstra H, Corstens FH, Boerman OC. Tumor targeting with radiolabeled alpha(v)beta(3) integrin binding peptides in a nude mouse model. *Cancer Res* 2002, 62:6146-6151

128. Dijkgraaf I, Kruijtzer JA, Frielink C, Corstens FH, Oyen WJ, Liskamp RM, Boerman OC. Alpha v beta 3 integrin-targeting of intraperitoneally growing tumors with a radiolabeled RGD peptide. *Int J Cancer* 2007, 120:605-610

129. Dienst A, Grunow A, Unruh M, Rabausch B, Nor JE, Fries JW, Gottstein C. Specific occlusion of murine and human tumor vasculature by VCAM-1-targeted recombinant fusion proteins. *J Natl Cancer Inst* 2005, 97:733-747

130. Balza E, Castellani P, Zijlstra A, Neri D, Zardi L, Siri A. Lack of specificity of endoglin expression for tumor blood vessels. *Int J Cancer* 2001, 94:579-585

131. de Waal RM and Leenders WP. Sprouting angiogenesis versus co-option in tumor angiogenesis. *EXS* 2005,65-76

132. Folkman J. Angiogenesis in cancer, vascular, rheumatoid and other disease. *Nat Med* 1995, 1:27-31

133. Folkman J. Angiogenesis and angiogenesis inhibition: an overview. *EXS* 1997, 79:1-8

134. Grunstein J, Roberts WG, Mathieu-Costello O, Hanahan D, Johnson RS. Tumor-derived expression of vascular endothelial growth factor is a critical factor in tumor expansion and vascular function. *Cancer Res* 1999, 59:1592-1598

135. Uzzan B, Nicolas P, Cucherat M, Perret GY. Microvessel density as a prognostic factor in women with breast cancer: a systematic review of the literature and meta-analysis. *Cancer Res* 2004, 64:2941-2955

136. Folkerth RD. Histologic measures of angiogenesis in human primary brain tumors. *Cancer Treat Res* 2004, 117:79-95

137. Harris AL. Hypoxia--a key regulatory factor in tumour growth. *Nat Rev Cancer* 2002, 2:38-47

138. Mukhopadhyay D and Datta K. Multiple regulatory pathways of vascular permeability factor/vascular endothelial growth factor (VPF/VEGF) expression in tumors. *Semin Cancer Biol* 2004, 14:123-130

139. Goldberg-Cohen I, Furneauxb H, Levy AP. A 40-bp RNA element that mediates stabilization of vascular endothelial growth factor mRNA by HuR. *J Biol Chem* 2002, 277:13635-13640

140. Damert A, Machein M, Breier G, Fujita MQ, Hanahan D, Risau W, Plate KH. Up-regulation of vascular endothelial growth factor expression in a rat glioma is conferred by two distinct hypoxia-driven mechanisms. *Cancer Res* 1997, 57:3860-3864

141. Okada F, Rak JW, Croix BS, Lieubeau B, Kaya M, Roncari L, Shirasawa S, Sasazuki T, Kerbel RS. Impact of oncogenes in tumor angiogenesis: mutant K-ras up-regulation of vascular endothelial growth factor/vascular permeability factor is necessary, but not sufficient for tumorigenicity of human colorectal carcinoma cells. *Proc Natl Acad Sci U S A* 1998, 95:3609-3614

142. Harris AL. von Hippel-Lindau syndrome: target for anti-vascular endothelial growth factor (VEGF) receptor therapy. *Oncologist* 2000, 5 Suppl 1:32-36

143. Zundel W, Schindler C, Haas-Kogan D, Koong A, Kaper F, Chen E, Gottschalk AR, Ryan HE, Johnson RS, Jefferson AB, Stokoe D, Giaccia AJ. Loss of PTEN facilitates HIF-1-mediated gene expression. *Genes Dev* 2000, 14:391-396

144. Claffey KP and Robinson GS. Regulation of VEGF/VPF expression in tumor cells: consequences for tumor growth and metastasis. *Cancer Metastasis Rev* 1996, 15:165-176

145. van Hinsbergh V, Collen A, Koolwijk P. Role of fibrin matrix in angiogenesis. *Ann N Y Acad Sci* 2001, 936:426-437

146. Kanno S, Oda N, Abe M, Terai Y, Ito M, Shitara K, Tabayashi K, Shibuya M, Sato Y. Roles of two VEGF receptors, Flt-1 and KDR, in the signal transduction of VEGF effects in human vascular endothelial cells. *Oncogene* 2000, 19:2138-2146

147. Park JE, Keller GA, Ferrara N. The vascular endothelial growth factor (VEGF) isoforms: differential deposition into the subepithelial extracellular matrix and bioactivity of extracellular matrix-bound VEGF. *Mol Biol Cell* 1993, 4:1317-1326

148. Nakamura M, Abe Y, Tokunaga T. Pathological significance of vascular endothelial growth factor A isoform expression in human cancer. *Pathol Int* 2002, 52:331-339

149. Soker S, Miao HQ, Nomi M, Takashima S, Klagsbrun M. VEGF165 mediates formation of complexes containing VEGFR-2 and neuropilin-1 that enhance VEGF165-receptor binding. *J Cell Biochem* 2002, 85:357-368

150. Carmeliet P, Ng YS, Nuyens D, Theilmeier G, Brusselmans K, Cornelissen I, Ehler E, Kakkar VV, Stalmans I, Mattot V, Perriard JC, Dewerchin M, Flameng W, Nagy A, Lupu F, Moons L, Collen D, D'Amore PA, Shima DT. Impaired myocardial angiogenesis and ischemic cardiomyopathy in mice lacking the vascular endothelial growth factor isoforms VEGF164 and VEGF188. *Nat Med* 1999, 5:495-502

151. Maes C, Carmeliet P, Moermans K, Stockmans I, Smets N, Collen D, Bouillon R, Carmeliet G. Impaired angiogenesis and endochondral bone formation in mice lacking the vascular endothelial growth factor isoforms VEGF164 and VEGF188. *Mech Dev* 2002, 111:61-73

152. Mattot V, Moons L, Lupu F, Chernavvsky D, Gomez RA, Collen D, Carmeliet P. Loss of the VEGF(164) and VEGF(188) isoforms impairs postnatal glomerular angiogenesis and renal arteriogenesis in mice. *J Am Soc Nephrol* 2002, 13:1548-1560

153. Stalmans I, Ng YS, Rohan R, Fruttiger M, Bouche A, Yuce A, Fujisawa H, Hermans B, Shani M, Jansen S, Hicklin D, Anderson DJ, Gardiner T, Hammes HP, Moons L, Dewerchin M, Collen D, Carmeliet P, D'Amore PA. Arteriolar and venular patterning in retinas of mice selectively expressing VEGF isoforms. *J Clin Invest* 2002, 109:327-336

154. van der Laak JA, Westphal JR, Schalkwijk LJ, Pahlplatz MM, Ruiter DJ, de Waal RM, de Wilde PC. An improved procedure to quantify tumour vascularity using true colour image analysis. Comparison with the manual hot-spot procedure in a human melanoma xenograft model. *J Pathol* 1998, 184:136-143

155. Airley RE, Loncaster J, Raleigh JA, Harris AL, Davidson SE, Hunter RD, West CM, Stratford IJ. GLUT-1 and CAIX as intrinsic markers of hypoxia in carcinoma of the cervix: relationship to pimonidazole binding. *Int J Cancer* 2003, 104:85-91

156. Abbott NJ. Dynamics of CNS barriers: evolution, differentiation, and modulation. *Cell Mol Neurobiol* 2005, 25:5-23

157. Keyt BA, Berleau LT, Nguyen HV, Chen H, Heinsohn H, Vandlen R, Ferrara N. The carboxyl-terminal domain (111-165) of vascular endothelial growth factor is critical for its mitogenic potency. *J Biol Chem* 1996, 271:7788-7795

158. Plouet J, Moro F, Bertagnolli S, Coldeboeuf N, Mazarguil H, Clamens S, Bayard F. Extracellular cleavage of the vascular endothelial growth factor 189-amino acid form by urokinase is required for its mitogenic effect. *J Biol Chem* 1997, 272:13390-13396

159. Lee S, Jilani SM, Nikolova GV, Carpizo D, Iruela-Arispe ML. Processing of VEGF-A by matrix metalloproteinases regulates bioavailability and vascular patterning in tumors. *J Cell Biol* 2005, 169:681-691

160. Bates DO, Cui TG, Doughty JM, Winkler M, Sugiono M, Shields JD, Peat D, Gillatt D, Harper SJ. VEGF165b, an inhibitory splice variant of vascular endothelial growth factor, is down-regulated in renal cell carcinoma. *Cancer Res* 2002, 62:4123-4131

161. Hutchings H, Ortega N, Plouet J. Extracellular matrix-bound vascular endothelial growth factor promotes endothelial cell adhesion, migration, and survival through integrin ligation. *FASEB J* 2003, 17:1520-1522

162. Pittman RN. Oxygen transport and exchange in the microcirculation. *Microcirculation* 2005, 12:59-70

163. Soker S, Gollamudi-Payne S, Fidder H, Charmahelli H, Klagsbrun M. Inhibition of vascular endothelial growth factor (VEGF)-induced endothelial cell proliferation by a peptide corresponding to the exon 7-encoded domain of VEGF165. *J Biol Chem* 1997, 272:31582-31588

164. Blancher C, Moore JW, Robertson N, Harris AL. Effects of ras and von Hippel-Lindau (VHL) gene mutations on hypoxia-inducible factor (HIF)-1alpha, HIF-2alpha, and vascular endothelial growth factor expression and their regulation by the phosphatidylinositol 3'-kinase/Akt signaling pathway. *Cancer Res* 2001, 61:7349-7355

165. Leenders WP. Targetting VEGF in anti-angiogenic and anti-tumour therapy: where are we now? *Int J Exp Pathol* 1998, 79:339-346

166. Eichhorn ME, Strieth S, Dellian M. Anti-vascular tumor therapy: recent advances, pitfalls and clinical perspectives. *Drug Resist Updat* 2004, 7:125-138

167. Vermeulen PB, Colpaert C, Salgado R, Royers R, Hellemans H, Van Den HE, Goovaerts G, Dirix LY, Van Marck E. Liver metastases from colorectal adenocarcinomas grow in three patterns with different angiogenesis and desmoplasia. *J Pathol* 2001, 195:336-342

168. Dome B, Paku S, Somlai B, Timar J. Vascularization of cutaneous melanoma involves vessel co-option and has clinical significance. *J Pathol* 2002, 197:355-362

169. Posey JA, Khazaeli MB, DelGrosso A, Saleh MN, Lin CY, Huse W, LoBuglio AF. A pilot trial of Vitaxin, a humanized anti-vitronectin receptor (anti alpha v beta 3) antibody in patients with metastatic cancer. *Cancer Biother Radiopharm* 2001, 16:125-132

170. Tamagnone L, Artigiani S, Chen H, He Z, Ming GI, Song H, Chedotal A, Winberg ML, Goodman CS, Poo M, Tessier-Lavigne M, Comoglio PM. Plexins are a large family of receptors for transmembrane, secreted, and GPI-anchored semaphorins in vertebrates. *Cell* 1999, 99:71-80

171. Fujisawa H. Discovery of semaphorin receptors, neuropilin and plexin, and their functions in neural development. *J Neurobiol* 2004, 59:24-33

172. Pasterkamp RJ and Kolodkin AL. Semaphorin junction: making tracks toward neural connectivity. *Curr Opin Neurobiol* 2003, 13:79-89

173. Takahashi T, Fournier A, Nakamura F, Wang LH, Murakami Y, Kalb RG, Fujisawa H, Strittmatter SM. Plexin-neuropilin-1 complexes form functional semaphorin-3A receptors. *Cell* 1999, 99:59-69

174. van der Zwaag B, Hellemons AJ, Leenders WP, Burbach JP, Brunner HG, Padberg GW, van Bokhoven H. PLEXIN-D1, a novel plexin family member, is expressed in vascular endothelium and the central nervous system during mouse embryogenesis. *Dev Dyn* 2002, 225:336-343

175. Torres-Vazquez J, Gitler AD, Fraser SD, Berk JD, Van N Pham, Fishman MC, Childs S, Epstein JA, Weinstein BM. Semaphorin-plexin signaling guides patterning of the developing vasculature. *Dev Cell* 2004, 7:117-123

176. Gitler AD, Lu MM, Epstein JA. PlexinD1 and semaphorin signaling are required in endothelial cells for cardiovascular development. *Dev Cell* 2004, 7:107-116

177. Gu C, Yoshida Y, Livet J, Reimert DV, Mann F, Merte J, Henderson CE, Jessell TM, Kolodkin AL, Ginty DD. Semaphorin 3E and plexin-D1 control vascular pattern independently of neuropilins. *Science* 2005, 307:265-268

178. Raats JM, Wijnen EM, Pruijn GJ, van den Hoogen FH, van Venrooij WJ. Recombinant human monoclonal autoantibodies specific for citrulline-containing peptides from phage display libraries derived from patients with rheumatoid arthritis. *J Rheumatol* 2003, 30:1696-1711

179. van Koningsbruggen S, de Haard H, de Kievit P, Dirks RW, van Remoortere A, Groot AJ, van Engelen BG, den Dunnen JT, Verrips CT, Frants RR, van der Maarel SM. Llama-derived phage display antibodies in the dissection of the human disease oculopharyngeal muscular dystrophy. *J Immunol Methods* 2003, 279:149-161

180. Kreis TE. Microinjected antibodies against the cytoplasmic domain of vesicular stomatitis virus glycoprotein block its transport to the cell surface. *EMBO J* 1986, 5:931-941

181. Kristensen P and Winter G. Proteolytic selection for protein folding using filamentous bacteriophages. *Fold Des* 1998, 3:321-328

182. Raats J, van Bree N, van Woezik J, Pruijn G. Generating recombinant anti-idiotypic antibodies for the detection of haptens in solution. *J Immunoassay Immunochem* 2003, 24:115-146

183. Kusters B, Westphal JR, Smits D, Ruiter DJ, Wesseling P, Keilholz U, de Waal RM. The pattern of metastasis of human melanoma to the central nervous system is not influenced by integrin alpha(v)beta(3) expression. *Int J Cancer* 2001, 92:176-180

184. Nakamura F, Kalb RG, Strittmatter SM. Molecular basis of semaphorin-mediated axon guidance. *J Neurobiol* 2000, 44:219-229

185. Adams GP, Schier R, McCall AM, Simmons HH, Horak EM, Alpaugh RK, Marks JD, Weiner LM. High affinity restricts the localization and tumor penetration of single-chain fv antibody molecules. *Cancer Res* 2001, 61:4750-4755

186. Horton MA. Arg-gly-Asp (RGD) peptides and peptidomimetics as therapeutics: relevance for renal diseases. *Exp Nephrol* 1999, 7:178-184

187. Christensen CR, Klingelhofer J, Tarabykina S, Hulgaard EF, Kramerov D, Lukanidin E. Transcription of a novel mouse semaphorin gene, M-semaH, correlates with the metastatic ability of mouse tumor cell lines. *Cancer Res* 1998, 58:1238-1244

188. Elder DE. Pathology of melanoma. *Clin Cancer Res* 2006, 12:2308s-2311s

189. Guerry D, Synnestvedt M, Elder DE, Schultz D. Lessons from tumor progression: the invasive radial growth phase of melanoma is common, incapable of metastasis, and indolent. *J Invest Dermatol* 1993, 100:342S-345S

190. Barnhill RL, Fandrey K, Levy MA, Mihm MC, Jr., Hyman B. Angiogenesis and tumor progression of melanoma. Quantification of vascularity in melanocytic nevi and cutaneous malignant melanoma. *Lab Invest* 1992, 67:331-337

191. Erhard H, Rietveld FJ, van Altena MC, Brocker EB, Ruiter DJ, de Waal RM. Transition of horizontal to vertical growth phase melanoma is accompanied by induction of vascular endothelial growth factor expression and angiogenesis. *Melanoma Res* 1997, 7 Suppl 2:S19-S26

192. Clark WH, From L, Bernardino EA, Mihm MC. The histogenesis and biologic behavior of primary human malignant melanomas of the skin. *Cancer Res* 1969, 29:705-727

193. Ruiter DJ and van Muijen GN. Markers of melanocytic tumour progression. *J Pathol* 1998, 186:340-342

194. Johnson JP. Cell adhesion molecules in the development and progression of malignant melanoma. *Cancer Metastasis Rev* 1999, 18:345-357

195. Alonso SR, Ortiz P, Pollan M, Perez-Gomez B, Sanchez L, Acuna MJ, Pajares R, Martinez-Tello FJ, Hortelano CM, Piris MA, Rodriguez-Peralto JL. Progression in cutaneous malignant melanoma is associated with distinct expression profiles: a tissue microarray-based study. *Am J Pathol* 2004, 164:193-203

196. Bosserhoff AK. Novel biomarkers in malignant melanoma. *Clin Chim Acta* 2006, 367:28-35

197. Gherardi E, Love CA, Esnouf RM, Jones EY. The sema domain. *Curr Opin Struct Biol* 2004, 14:669-678

198. Rohm B, Ottemeyer A, Lohrum M, Puschel AW. Plexin/neuropilin complexes mediate repulsion by the axonal guidance signal semaphorin 3A. *Mech Dev* 2000, 93:95-104

199. Perala NM, Immonen T, Sariola H. The expression of plexins during mouse embryogenesis. *Gene Expr Patterns* 2005, 5:355-362

200. Behar O, Golden JA, Mashimo H, Schoen FJ, Fishman MC. Semaphorin III is needed for normal patterning and growth of nerves, bones and heart. *Nature* 1996, 383:525-528

201. Roodink I, Raats J, van der Zwaag B, Verrijp K, Kusters B, van Bokhoven H, Linkels M, de Waal RM, Leenders WP. Plexin D1 expression is induced on tumor vasculature and tumor cells: a novel target for diagnosis and therapy? *Cancer Res* 2005, 65:8317-8323

202. Toyofuku T, Yabuki M, Kamei J, Kamei M, Makino N, Kumanogoh A, Hori M. Semaphorin-4A, an activator for T-cell-mediated immunity, suppresses angiogenesis via Plexin-D1. *EMBO J* 2007, 26:1373-1384

203. Kusters B, Kats G, Roodink I, Verrijp K, Wesseling P, Ruiter DJ, de Waal RM, Leenders WP. Micronodular transformation as a novel mechanism of VEGF-A-induced metastasis. *Oncogene* 2007, 26:5808-5815

204. Span PN, Grebenchtchikov N, Geurts-Moespot J, Westphal JR, Lucassen AM, Sweep CG. EORTC Receptor and Biomarker Study Group Report: a sandwich enzyme-linked immunosorbent assay for vascular endothelial growth factor in blood and tumor tissue extracts. *Int J Biol Markers* 2000, 15:184-191

205. Livak KJ and Schmittgen TD. Analysis of relative gene expression data using real-time quantitative PCR and the 2(-Delta Delta C(T)) Method. *Methods* 2001, 25:402-408

206. Kashani-Sabet M, Shaikh L, Miller JR, III, Nosrati M, Ferreira CM, Debs RJ, Sagebiel RW. NF-kappa B in the vascular progression of melanoma. *J Clin Oncol* 2004, 22:617-623

207. Christensen C, Ambartsumian N, Gilestro G, Thomsen B, Comoglio P, Tamagnone L, Guldberg P, Lukanidin E. Proteolytic processing converts the repelling signal Sema3E into an inducer of invasive growth and lung metastasis. *Cancer Res* 2005, 65:6167-6177

208. Chauvet S, Cohen S, Yoshida Y, Fekrane L, Livet J, Gayet O, Segu L, Buhot MC, Jessell TM, Henderson CE, Mann F. Gating of Sema3E/PlexinD1 signaling by neuropilin-1 switches axonal repulsion to attraction during brain development. *Neuron* 2007, 56:807-822

209. Galvin NJ, Vance PM, Dixit VM, Fink B, Frazier WA. Interaction of human thrombospondin with types I-V collagen: direct binding and electron microscopy. *J Cell Biol* 1987, 104:1413-1422

210. Aho S and Uitto J. Two-hybrid analysis reveals multiple direct interactions for thrombospondin 1. *Matrix Biol* 1998, 17:401-412

211. Trotter MJ, Colwell R, Tron VA. Thrombospondin-1 and cutaneous melanoma. *J Cutan Med Surg* 2003, 7:136-141

212. Straume O and Akslen LA. Expresson of vascular endothelial growth factor, its receptors (FLT-1, KDR) and TSP-1 related to microvessel density and patient outcome in vertical growth phase melanomas. *Am J Pathol* 2001, 159:223-235

213. Han Z, Ni J, Smits P, Underhill CB, Xie B, Chen Y, Liu N, Tylzanowski P, Parmelee D, Feng P, Ding I, Gao F, Gentz R, Huylebroeck D, Merregaert J, Zhang L. Extracellular matrix protein 1 (ECM1) has angiogenic properties and is expressed by breast tumor cells. *FASEB J* 2001, 15:988-994

214. Wang L, Yu J, Ni J, Xu XM, Wang J, Ning H, Pei XF, Chen J, Yang S, Underhill CB, Liu L, Liekens J, Merregaert J, Zhang L. Extracellular matrix protein 1 (ECM1) is over-expressed in malignant epithelial tumors. *Cancer Lett* 2003, 200:57-67

215. Neufeld G, Shraga-Heled N, Lange T, Guttmann-Raviv N, Herzog Y, Kessler O. Semaphorins in cancer. *Front Biosci* 2005, 10:751-760

216. Xiang R, Davalos AR, Hensel CH, Zhou XJ, Tse C, Naylor SL. Semaphorin 3F gene from human 3p21.3 suppresses tumor formation in nude mice. *Cancer Res* 2002, 62:2637-2643

217. Nasarre P, Constantin B, Rouhaud L, Harnois T, Raymond G, Drabkin HA, Bourmeyster N, Roche J. Semaphorin SEMA3F and VEGF have opposing effects on cell attachment and spreading. *Neoplasia* 2003, 5:83-92

218. Giordano S, Corso S, Conrotto P, Artigiani S, Gilestro G, Barberis D, Tamagnone L, Comoglio PM. The semaphorin 4D receptor controls invasive growth by coupling with Met. *Nat Cell Biol* 2002, 4:720-724

219. Conrotto P, Corso S, Gamberini S, Comoglio PM, Giordano S. Interplay between scatter factor receptors and B plexins controls invasive growth. *Oncogene* 2004, 23:5131-5137

220. Escudier B, Pluzanska A, Koralewski P, Ravaud A, Bracarda S, Szczylik C, Chevreau C, Filipek M, Melichar B, Bajetta E, Gorbunova V, Bay JO, Bodrogi I, Jagiello-Gruszfeld A, Moore N. Bevacizumab plus interferon alfa-2a for treatment of metastatic renal cell carcinoma: a randomised, double-blind phase III trial. *Lancet* 2007, 370:2103-2111

221. Hurwitz H, Fehrenbacher L, Novotny W, Cartwright T, Hainsworth J, Heim W, Berlin J, Baron A, Griffing S, Holmgren E, Ferrara N, Fyfe G, Rogers B, Ross R, Kabbinavar F. Bevacizumab plus irinotecan, fluorouracil, and leucovorin for metastatic colorectal cancer. *N Engl J Med* 2004, 350:2335-2342

222. Herbst RS, O'Neill VJ, Fehrenbacher L, Belani CP, Bonomi PD, Hart L, Melnyk O, Ramies D, Lin M, Sandler A. Phase II study of efficacy and safety of bevacizumab in combination with chemotherapy or erlotinib compared with chemotherapy alone for treatment of recurrent or refractory non small-cell lung cancer. *J Clin Oncol* 2007, 25:4743-4750

223. Roodink I, van der Laak J, Kusters B, Wesseling P, Verrijp K, de Waal R, Leenders W. Development of the tumor vascular bed in response to hypoxia-induced VEGF-A differs from that in tumors with constitutive VEGF-A expression. *Int J Cancer* 2006, 119:2054-2062

224. Trepel M, Arap W, Pasqualini R. In vivo phage display and vascular heterogeneity: implications for targeted medicine. *Curr Opin Chem Biol* 2002, 6:399-404

225. Joyce JA, Laakkonen P, Bernasconi M, Bergers G, Ruoslahti E, Hanahan D. Stage-specific vascular markers revealed by phage display in a mouse model of pancreatic islet tumorigenesis. *Cancer Cell* 2003, 4:393-403

226. van Kempen LC and Leenders WP. Tumours can adapt to anti-angiogenic therapy depending on the stromal context: lessons from endothelial cell biology. *Eur J Cell Biol* 2006, 85:61-68

227. Zhang Y, Singh MK, Degenhardt KR, Lu MM, Bennett J, Yoshida Y, Epstein JA. Tie2Cre-mediated inactivation of plexinD1 results in congenital heart, vascular and skeletal defects. *Dev Biol* 2009, 325:82-93

228. Roodink I, Kats G, van Kempen L, Grunberg M, Maass C, Verrijp K, Raats J, Leenders W. Semaphorin 3E Expression Correlates Inversely with Plexin D1 During Tumor Progression. *Am J Pathol* 2008, 173:1873-1881

229. Kigel B, Varshavsky A, Kessler O, Neufeld G. Successful inhibition of tumor development by specific class-3 semaphorins is associated with expression of appropriate semaphorin receptors by tumor cells. *PLoS ONE* 2008, 3:e3287

230. Rafii S, Avecilla ST, Jin DK. Tumor vasculature address book: identification of stage-specific tumor vessel zip codes by phage display. *Cancer Cell* 2003, 4:331-333

231. Kuroda H, Tamaru J, Sakamoto G, Ohnisi K, Itoyama S. Immunophenotype of lymphocytic infiltration in medullary carcinoma of the breast. *Virchows Arch* 2005, 446:10-14

232. Saravanamuthu J, Reid WM, George DS, Crow JC, Rolfe KJ, MacLean AB, Perrett CW. The role of angiogenesis in vulvar cancer, vulvar intraepithelial neoplasia, and vulvar lichen sclerosus as determined by microvessel density analysis. *Gynecol Oncol* 2003, 89:251-258

233. Gambino LS, Wreford NG, Bertram JF, Dockery P, Lederman F, Rogers PA. Angiogenesis occurs by vessel elongation in proliferative phase human endometrium. *Hum Reprod* 2002, 17:1199-1206

234. Kerbel RS. Tumor angiogenesis. *N Engl J Med* 2008, 358:2039-2049

235. Bergers G and Hanahan D. Modes of resistance to anti-angiogenic therapy. *Nat Rev Cancer* 2008, 8:592-603

236. Norden AD, Drappatz J, Wen PY. Antiangiogenic therapy in malignant gliomas. *Curr Opin Oncol* 2008, 20:652-661

237. Holig P, Bach M, Volkel T, Nahde T, Hoffmann S, Muller R, Kontermann RE. Novel RGD lipopeptides for the targeting of liposomes to integrin-expressing endothelial and melanoma cells. *Protein Eng Des Sel* 2004, 17:433-441

238. Kolonin MG, Sun J, Do KA, Vidal CI, Ji Y, Baggerly KA, Pasqualini R, Arap W. Synchronous selection of homing peptides for multiple tissues by in vivo phage display. *FASEB J* 2006, 20:979-981

239. Rajotte D, Arap W, Hagedorn M, Koivunen E, Pasqualini R, Ruoslahti E. Molecular heterogeneity of the vascular endothelium revealed by in vivo phage display. *J Clin Invest* 1998, 102:430-437

240. Valadon P, Garnett JD, Testa JE, Bauerle M, Oh P, Schnitzer JE. Screening phage display libraries for organ-specific vascular immunotargeting in vivo. *Proc Natl Acad Sci U S A* 2006, 103:407-412

241. Hoogenboom HR. Selecting and screening recombinant antibody libraries. *Nat Biotechnol* 2005, 23:1105-1116

242. Cortez-Retamozo V, Backmann N, Senter PD, Wernery U, De Baetselier P, Muyldermans S, Revets H. Efficient cancer therapy with a nanobody-based conjugate. *Cancer Res* 2004, 64:2853-2857

243. Huang L, Gainkam LO, Caveliers V, Vanhove C, Keyaerts M, De Baetselier P, Bossuyt A, Revets H, Lahoutte T. SPECT imaging with 99mTc-labeled EGFR-specific nanobody for in vivo monitoring of EGFR expression. *Mol Imaging Biol* 2008, 10:167-175

244. van Laarhoven HW, Bussink J, Lok J, Punt CJ, Heerschap A, van der Kogel AJ. Effects of nicotinamide and carbogen in different murine colon carcinomas: immunohistochemical analysis of vascular architecture and microenvironmental parameters. *Int J Radiat Oncol Biol Phys* 2004, 60:310-321

245. Roepman R, Schick D, Ferreira PA. Isolation of retinal proteins that interact with retinitis pigmentosa GTPase regulator by interaction trap screen in yeast. *Methods Enzymol* 2000, 316:688-704

246. Reijerkerk A, Kooij G, van der Pol SM, Khazen S, Dijkstra CD, de Vries HE. Diapedesis of monocytes is associated with MMP-mediated occludin disappearance in brain endothelial cells. *FASEB J* 2006, 20:2550-2552

247. Vaughan KT. Microtubule plus ends, motors, and traffic of Golgi membranes. *Biochim Biophys Acta* 2005, 1744:316-324

248. Askham JM, Vaughan KT, Goodson HV, Morrison EE. Evidence that an interaction between EB1 and p150(Glued) is required for the formation and maintenance of a radial microtubule array anchored at the centrosome. *Mol Biol Cell* 2002, 13:3627-3645

249. Shaw RM, Fay AJ, Puthenveedu MA, von Zastrow M, Jan YN, Jan LY. Microtubule plus-end-tracking proteins target gap junctions directly from the cell interior to adherens junctions. *Cell* 2007, 128:547-560

250. Rondaij MG, Bierings R, Kragt A, Gijzen KA, Sellink E, van Mourik JA, Fernandez-Borja M, Voorberg J. Dynein-dynactin complex mediates protein kinase A-dependent clustering of Weibel-Palade bodies in endothelial cells. *Arterioscler Thromb Vasc Biol* 2006, 26:49-55

251. Wu S, Chen H, Alexeyev MF, King JA, Moore TM, Stevens T, Balczon RD. Microtubule motors regulate ISOC activation necessary to increase endothelial cell permeability. *J Biol Chem* 2007, 282:34801-34808

252. Dixit R, Levy JR, Tokito M, Ligon LA, Holzbaur EL. Regulation of dynactin through the differential expression of p150Glued isoforms. *J Biol Chem* 2008, 283:33611-33619

253. Tokito MK, Howland DS, Lee VM, Holzbaur EL. Functionally distinct isoforms of dynactin are expressed in human neurons. *Mol Biol Cell* 1996, 7:1167-1180

254. Nguyen VK, Hamers R, Wyns L, Muyldermans S. Camel heavy-chain antibodies: diverse germline V(H)H and specific mechanisms enlarge the antigen-binding repertoire. *EMBO J* 2000, 19:921-930

255. Schroer TA. Dynactin. *Annu Rev Cell Dev Biol* 2004, 20:759-779

256. Dvorak AM and Feng D. The vesiculo-vacuolar organelle (VVO). A new endothelial cell permeability organelle. *J Histochem Cytochem* 2001, 49:419-432

257. Roesli C, Borgia B, Schliemann C, Gunthert M, Wunderli-Allenspach H, Giavazzi R, Neri D. Comparative analysis of the membrane proteome of closely related metastatic and nonmetastatic tumor cells. *Cancer Res* 2009, 69:5406-5414

258. Zemskov EA, Janiak A, Hang J, Waghray A, Belkin AM. The role of tissue transglutaminase in cell-matrix interactions. *Front Biosci* 2006, 11:1057-1076

259. Deregibus MC, Cantaluppi V, Calogero R, Lo IM, Tetta C, Biancone L, Bruno S, Bussolati B, Camussi G. Endothelial progenitor cell derived microvesicles activate an angiogenic program in endothelial cells by a horizontal transfer of mRNA. *Blood* 2007, 110:2440-2448

260. Ruoslahti E and Rajotte D. An address system in the vasculature of normal tissues and tumors. *Annu Rev Immunol* 2000, 18:813-827

261. Koning GA, Schiffelers RM, Wauben MH, Kok RJ, Mastrobattista E, Molema G, ten Hagen TL, Storm G. Targeting of angiogenic endothelial cells at sites of inflammation by dexamethasone phosphate-containing RGD peptide liposomes inhibits experimental arthritis. *Arthritis Rheum* 2006, 54:1198-1208

262. Hu P, Yan J, Sharifi J, Bai T, Khawli LA, Epstein AL. Comparison of three different targeted tissue factor fusion proteins for inducing tumor vessel thrombosis. *Cancer Res* 2003, 63:5046-5053

263. Hamers-Casterman C, Atarhouch T, Muyldermans S, Robinson G, Hamers C, Songa EB, Bendahman N, Hamers R. Naturally occurring antibodies devoid of light chains. *Nature* 1993, 363:446-448

264. Tijink BM, Laeremans T, Budde M, Stigter-van WM, Dreier T, de Haard HJ, Leemans CR, van Dongen GA. Improved tumor targeting of anti-epidermal growth factor receptor Nanobodies through albumin binding: taking advantage of modular Nanobody technology. *Mol Cancer Ther* 2008, 7:2288-2297

265. van Koningsbruggen S, de Haard H, de Kievit P, Dirks RW, van Remoortere A, Groot AJ, van Engelen BG, den Dunnen JT, Verrips CT, Frants RR, van der Maarel SM. Llama-derived phage display antibodies in the dissection of the human disease oculopharyngeal muscular dystrophy. *J Immunol Methods* 2003, 279:149-161

266. Ebos JM, Lee CR, Cruz-Munoz W, Bjarnason GA, Christensen JG, Kerbel RS. Accelerated metastasis after short-term treatment with a potent inhibitor of tumor angiogenesis. *Cancer Cell* 2009, 15:232-239

267. Paez-Ribes M, Allen E, Hudock J, Takeda T, Okuyama H, Vinals F, Inoue M, Bergers G, Hanahan D, Casanovas O. Antiangiogenic therapy elicits malignant progression of tumors to increased local invasion and distant metastasis. *Cancer Cell* 2009, 15:220-231

268. St.Croix B, Rago C, Velculescu V, Traverso G, Romans KE, Montgomery E, Lal A, Riggins GJ, Lengauer C, Vogelstein B, Kinzler KW. Genes expressed in human tumor endothelium. *Science* 2000, 289:1197-1202

269. Davies J and Riechmann L. Single antibody domains as small recognition units: design and in vitro antigen selection of camelized, human VH domains with improved protein stability. *Protein Eng* 1996, 9:531-537

270. Cortez-Retamozo V, Lauwereys M, Hassanzadeh GG, Gobert M, Conrath K, Muyldermans S, De Baetselier P, Revets H. Efficient tumor targeting by single-domain antibody fragments of camels. *Int J Cancer* 2002, 98:456-462

271. Lauwereys M, Arbabi GM, Desmyter A, Kinne J, Holzer W, De Genst E, Wyns L, Muyldermans S. Potent enzyme inhibitors derived from dromedary heavy-chain antibodies. *EMBO J* 1998, 17:3512-3520

272. van der Linden RH, Frenken LG, de Geus B, Harmsen MM, Ruuls RC, Stok W, de Ron L, Wilson S, Davis P, Verrips CT. Comparison of physical chemical properties of llama VHH antibody fragments and mouse monoclonal antibodies. *Biochim Biophys Acta* 1999, 1431:37-46

273. Dumoulin M, Conrath K, Van Meirhaeghe A, Meersman F, Heremans K, Frenken LG, Muyldermans S, Wyns L, Matagne A. Single-domain antibody fragments with high conformational stability. *Protein Sci* 2002, 11:500-515

274. Muyldermans S. Single domain camel antibodies: current status. *J Biotechnol* 2001, 74:277-302

275. Nguyen VK, Su C, Muyldermans S, van der Loo W. Heavy-chain antibodies in Camelidae; a case of evolutionary innovation. *Immunogenetics* 2002, 54:39-47

List of publications

Roodink I, Raats J, van der Zwaag B, Verrijp K, Kusters B, van Bokhoven H, Linkels M, de Waal RM, Leenders WP. Plexin D1 expression is induced on tumor vasculature and tumor cells: a novel target for diagnosis and therapy? *Cancer Res* 2005, 65:8317-8323

Roodink I, van der Laak J, Kusters B, Wesseling P, Verrijp K, de Waal R, Leenders W. Development of the tumour vascular bed in response to hypoxia-induced VEGF-A differs from that in tumors with constitutive VEGF-A expression. *Int J Cancer* 2006, 119:2054-2062

Kusters B, Kats G, **Roodink I**, Verrijp K, Wesseling P, Ruiter DJ, de Waal RM, Leenders WP. Micronodular transformation as a novel mechanism of VEGF-A-induced metastasis. *Oncogene* 2007, 26:5808-5815

Roodink I, Kats G, van Kempen L, Grunberg M, Maass C, Verrijp K, Raats J, Leenders W. Semaphorin 3E Expression Correlates Inversely with Plexin D1 During Tumor Progression. *Am J Pathol* 2008, 173:1873-1881

Roodink I, Verrijp K, Raats J, Leenders WP. Plexin D1 is ubiquitously expressed on tumor vessels and tumor cells in solid malignancies. *BMC Cancer* 2009, 9:297

Kats-Ugurlu G, **Roodink I**, de Weijer M, Tiemessen D, Maass C, Verrijp K, van der Laak J, de Waal R, Mulders P, Oosterwijk E, Leenders W. Circulating tumor tissue fragments in patients with pulmonary metastasis of clear cell renal cell carcinoma. In press, *J Pathol*

Roodink I, Roepman R, van Wijk E, Letteboer S, Hermsen R, Frederix G, Verrijp K, Raats J, Leenders W. Dynactin-1-p150^{glued} as a specific and targetable marker on tumor endothelial cells. Submitted

Roodink I, Franssen M, Zuidscherwoude M, Verrijp K, van der Donk T, Raats J, Leenders W. Isolation of targeting nanobodies against co-opted tumor vasculature. In press, *Lab Invest*

Curriculum Vitae

De auteur van dit proefschrift werd geboren op 3 februari 1980 te Ede en groeide op in Ellecom. Na het behalen van haar VWO diploma aan ’t Rhedens te Rozendaal is ze in 1998 begonnen met de studie Biomedische Gezondheidswetenschappen aan de Katholieke Universiteit Nijmegen. Als onderdeel van haar hoofdvak Toxicologie heeft ze reproductietoxicologisch onderzoek uitgevoerd bij het Rijksinstituut voor Volksgezondheid en Milieu, Laboratorium voor Effectenonderzoek. Onder begeleiding van Dr. A. Piersma is gedurende zes maanden de invloed van antioxidanten op reactieve zuurstof species-geïnduceerde teratogeniteit in ratten bestudeerd. In het kader van het hoofdvak Pathobiologie heeft ze gedurende vijf maanden onderzoek verricht bij de afdeling Pathologie van het Universitair Medisch Centrum Nijmegen, waar ze onder begeleiding van Dr. W. Leenders de expressie van verschillende VEGF-A isovormen en hun relatie tot vasculaire fenotypes in humane hersentumoren in kaart heeft gebracht. In september 2002 heeft ze het doctoraal examen Biomedische Gezondheidswetenschappen met de ontvangst van het diploma afgesloten.

Van februari 2003 tot augustus 2008 heeft ze als junior onderzoeker op de afdeling Pathologie van het Universitair Medisch Centrum Nijmegen onder begeleiding van Dr. W. Leenders het in dit proefschrift beschreven onderzoek verricht. Ze presenteerde haar resultaten op verschillende nationale en internationale bijeenkomsten. Tevens was ze tijdens haar promotieonderzoek betrokken bij de begeleiding van verscheidene stagiaires. Sinds november 2008 is ze werkzaam als onderzoeker op de afdeling Pathologie van het Universitair Medisch Centrum Nijmegen onder begeleiding van Dr. W. Leenders, waar ze het werk beschreven in dit proefschrift voortzet.

Gedurende haar studententijd en promotieonderzoek is Ilse actief geweest in verenigingsbesturen. Van 1998 tot 2002 is ze secretaris geweest van Paardensportvereniging De Loenermarkruiters te Loenen, waar ze sinds 2002 voorzitter van is. Tevens is ze van 2002 tot 2006 voorzitter geweest van de Vereniging van Eigenaren van Vinkenlaan 1-23 te Dieren.

Dankwoord

Daar is ie dan, HET boekje waar een groot deel van mijn werk van de afgelopen jaren in beschreven staat. Uiteraard zou dit proefschrift niet tot stand zijn gekomen zonder de inzet en betrokkenheid van verschillende mensen, die ik hierbij graag wil bedanken.

Uiteraard wil ik als eerste mijn copromotor Dr. William Leenders bedanken. Via Rob de Waal ben ik in 2002 bij jou stage komen lopen, wat een erg leerzame periode is geweest. Ook voor jou, want je was ineens van mening dat het begeleiden van studenten toch niet zo'n kwelling was (ook al ben je inmiddels weer meermaals van gedachten veranderd). Daaropvolgend heb ik dankzij Rob en jou de mogelijkheid gekregen om op de afdeling Pathologie aan de slag te gaan als junior onderzoeker. Hoewel er in eerste instantie onvoldoende financiering was voor een volledig promotietraject heb jij je erg ingespannen om dit toch rond te krijgen en zoals iedereen nu kan lezen met succes door o.a. een samenwerking met N.V. Organon. Daarnaast heb je met je creatieve ideeën, wetenschappelijk denken en enorme enthousiasme een essentieel aandeel gehad in dit proefschrift. William, ik heb ontzettend veel van je geleerd de afgelopen jaren! Toen je de subsidie van Stichting Vanderes toegekend kreeg, ben je me komen polsen of ik op dat project wilde gaan werken want je vond "dat we wel goed konden samenwerken", nou William, ik ben het (een keer) geheel met je eens.

Professor van Krieken, beste Han, bedankt dat ik op de afdeling Pathologie mijn promotieonderzoek heb mogen verrichten en voor het aanvaarden van het promotorschap.

Kiek, zoals je jezelf al had omschreven in het concept dankwoord wat jij en Fieke voor dit proefschrift hadden geschreven, je bent een super collega. Je hebt me vele technieken geleerd, we hebben veel gepraat en gelachen en gelukkig weinig (ik bedoel eigenlijk nooit, maar dan zijn we weer van die koele kikkers) gehuild. Samen met Fieke en An hebben we als "de vier musketiers" ook buiten het werk de nodige gezelligheid gehad tijdens feestjes in Nijmegen, Kranenburg en Loenen (of Klarenbeek als je na een avondje feesten op de fiets stapt). Kiek, ik ben erg blij dat jij mijn paranimf wilt zijn.
Fieke, je bent toch een beetje mijn lab-soulmate geweest. We houden beiden van werken met een muziekje erbij, gezelligheid en goede grappen uithalen (met als hoogtepunt onze "lepeltje-lepeltje" act). Met name met dit laatste hebben we onze naaste collega's toch wel regelmatig het bloed onder de nagels vandaan gehaald (of niet Kiek?). Thnx voor de gezelligheid de afgelopen jaren zowel op het werk als daarbuiten. Ik vind het fijn dat je mijn getuige bent.

Ja An, de volgende van de vier musketiers, ook jou wil ik bedanken voor de gezelligheid en leuke gesprekken. Hoewel mijn Belgisch nog steeds te wensen overlaat, doe ik hierbij toch een poging. Ik heb het altijd erg plezant gevonden om met jou een werkkamer te delen, hoewel ik ook wel eens onnozel van jou werd. An-viseerdag was altijd toppie! Ik wens je heel veel succes met je studie Geneeskunde.

Cathy, ik wil je bedanken voor de goede gesprekken. Je kijk op dingen, openheid, interesse in je medemens en spraakzaamheid hebben me altijd erg aangesproken. Verder wil ik van de Agiogenese-groep Rob, Benno, Gürsah en natuurlijk alle stagiares (Leonie, Anjo, Ton, Tom, Jouk, Roel, Geert, Iris, Meritha, Eric, Gaby, Maarten, Corine, Anke, Jori, Melvin en Martijn) bedanken voor de vruchtbare werkbesprekingen en goede samenwerking.

Beste Léon, je deur stond altijd open als ik weer eens wat te vragen had, bedankt!
(Ex-)Kamergenoten Anke, Lieke en Yvonne, allen bedankt voor de hulpvaardigheid en gezelligheid. Gelukkig vonden jullie de radio geen probleem! (Voormalige) Promovendi Jack, Bart, Margit, Corine, Miriam, Jolien, Martijn en Anneke bedankt voor de leuke tijd en nodige adviezen. Allen veel succes met jullie verdere carrière.
Verder wil ik alle andere medewerkers van de afdeling Pathologie bedanken voor de goede werksfeer, nuttige werkoverleggen en gezellige labuitjes.

Ook wil ik een aantal mensen bedanken van de afdeling Biomoleculaire Chemie en Modiquest B.V. waar ik een deel van mijn onderzoek heb ik verricht.
Jos, dankzij jou kennis heb ik veel ervaring op mogen doen met faagdisplay. Het eerste jaar heb je mij samen met Daniëlle wegwijs gemaakt in deze veel omvattende techniek, beiden dank hiervoor. Jos, ik ben blij dat jij met je bedrijf Modiquest nog steeds betrokken bent bij ons onderzoek. Tevens wil ik Tom, Kalok, Reinout, Angelique en Carla bedanken voor de samenwerking, gastvrijheid en gezelligheid de afgelopen jaren.

Beste Hans, de (financiële) ondersteuning van N.V. Organon heeft een groot aandeel gehad in de totstandkoming van dit proefschrift. Ik wil je bedanken voor de nuttige besprekingen in het kader van onze samenwerking en hoop dat we deze in de toekomst kunnen voortzetten.

Tenslotte wil ik mijn (schoon)familie en vrienden bedanken die door de nodige gezelligheid, ontspanning, vriendschap en steun indirect hebben bijgedragen aan dit proefschrift. In het bijzonder wil ik mijn ouders bedanken. Pap, je hebt erg uitgekeken naar het verschijnen van dit proefschrift en hebt min of meer gesolliciteerd naar het “baantje” paranimf. Ik ben erg blij dat ik je heb aangenomen voor deze taak. Moeders,

toen ik naar de middelbare school ging heb je je meermaals afgevraagd hoe mijn rapportje er uit zou zien, want ik zat toch alleen maar “op m’n peerd te hobbelen”. Hoewel er wat dat betreft nog weinig veranderd is ligt er nu toch een mooi boekje, iets waar jij en pap ook trots op mogen zijn. Dat Maarten en ik toch nog gaan trouwen heeft je aangenaam verrast en ik hoop dat jij net zo verheugd bent als ik dat je mijn getuige bent.

Lieve Maarten, je was er toen ik mijn VWO-diploma in ontvangst mocht nemen en gelukkig ben je er nu nog steeds. Ik ben je dankbaar voor alle steun en liefde in de afgelopen jaren. Ik hoop dat we er straks als getrouwd stel ook een hele mooie tijd van maken!

Ilse

Color figures

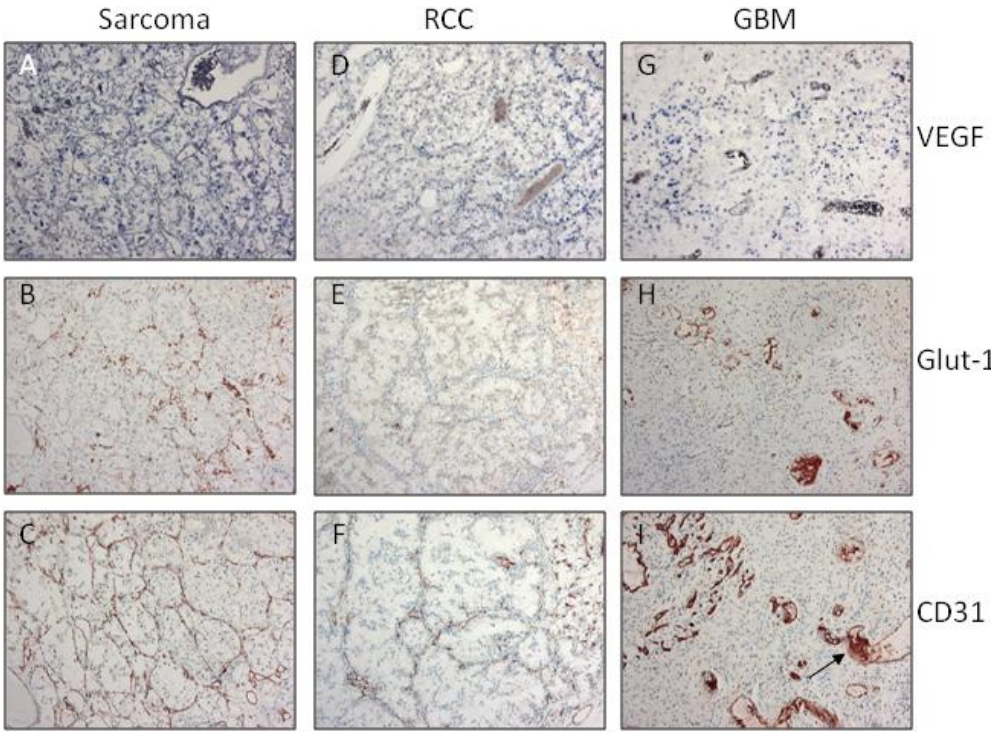

Chapter2, Figure 1. Representative examples of spatial distribution of VEGF-A expression (A,D,G), hypoxia (B,E,H) and blood vessels (C,F,I) in brain metastases of sarcoma (A-C) and renal cell carcinoma (D-F) and in glioblastoma multiforme (G-I). VEGF-A transcripts were highlighted by in situ hybridization with an antisense VEGF-A RNA probe, hypoxia was demonstrated by immunohistochemistry using an anti-Glut-1 antibody, vessels were stained with an antibody against CD31. Note in B, E and H that no Glut-1 positive tumor cells are present. The positivity in these sections is due to erythrocytes in dilated vessels. In the GBM some blood vessels also stain positive, indicating that these are in fact pre-existent capillaries with a functional blood brain barrier. The arrow in I points at a glomeruloid proliferation. These stainings show that in this group of tumors there is no correlation between hypoxia and VEGF-expression.

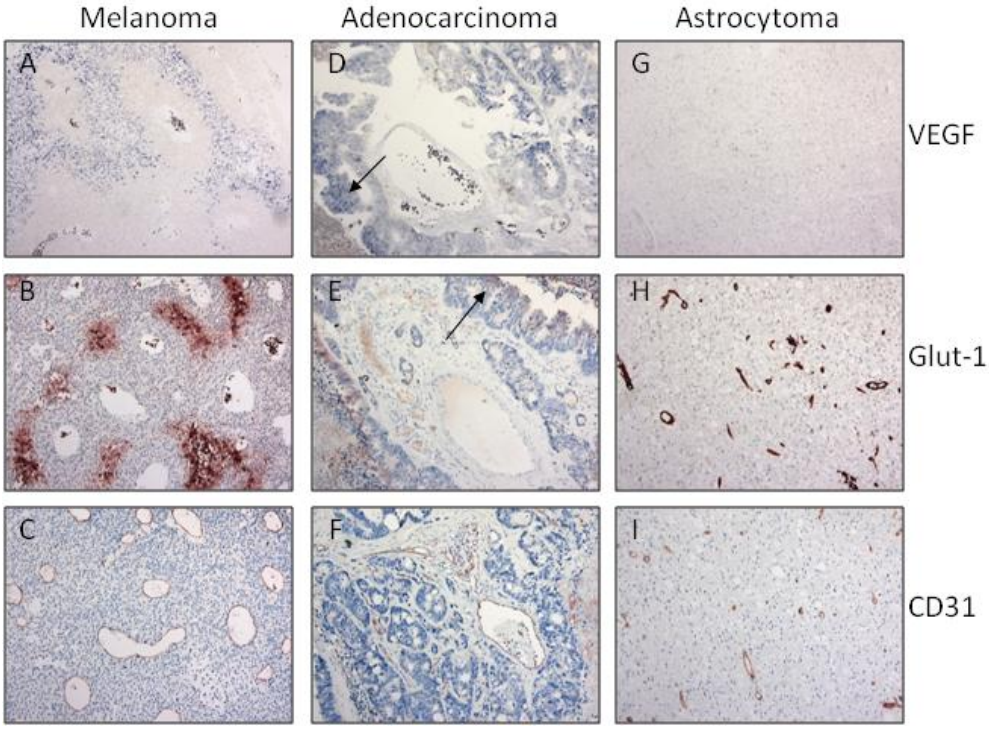

Chapter 2, Figure 2. Spatial distribution of VEGF-A expression as determined by VEGF-A ISH (A,D,G), hypoxia (Glut-1 immunostaining, B,E,H) and blood vessels (CD31 immunostaining, C,F,I) in brain metastases of melanoma (A-C), adenocarcinoma (D-F), and in low grade glioma. In melanoma and adenocarcinoma metastases, there is a clear co-localization of Glut-1 expression and VEGF-A expression, suggesting that in these tumor types VEGF-A is expressed as a response to hypoxia. In melanoma the hypoxic areas are confined to concentric regions at regular distances from dilated blood vessels, in the adenocarcinoma metastases the hypoxia and VEGF-A expression occurred primarily in epithelial cells distant from the fibrovascular regions (arrows). The blood vessels in the low grade astrocytoma are positive for Glut-1, indicating that these are pre-existent brain capillaries with a functional blood brain barrier. Note that the sections shown are obtained from the same tumor regions. Due to technical reasons, however, these are not exact serial sections.

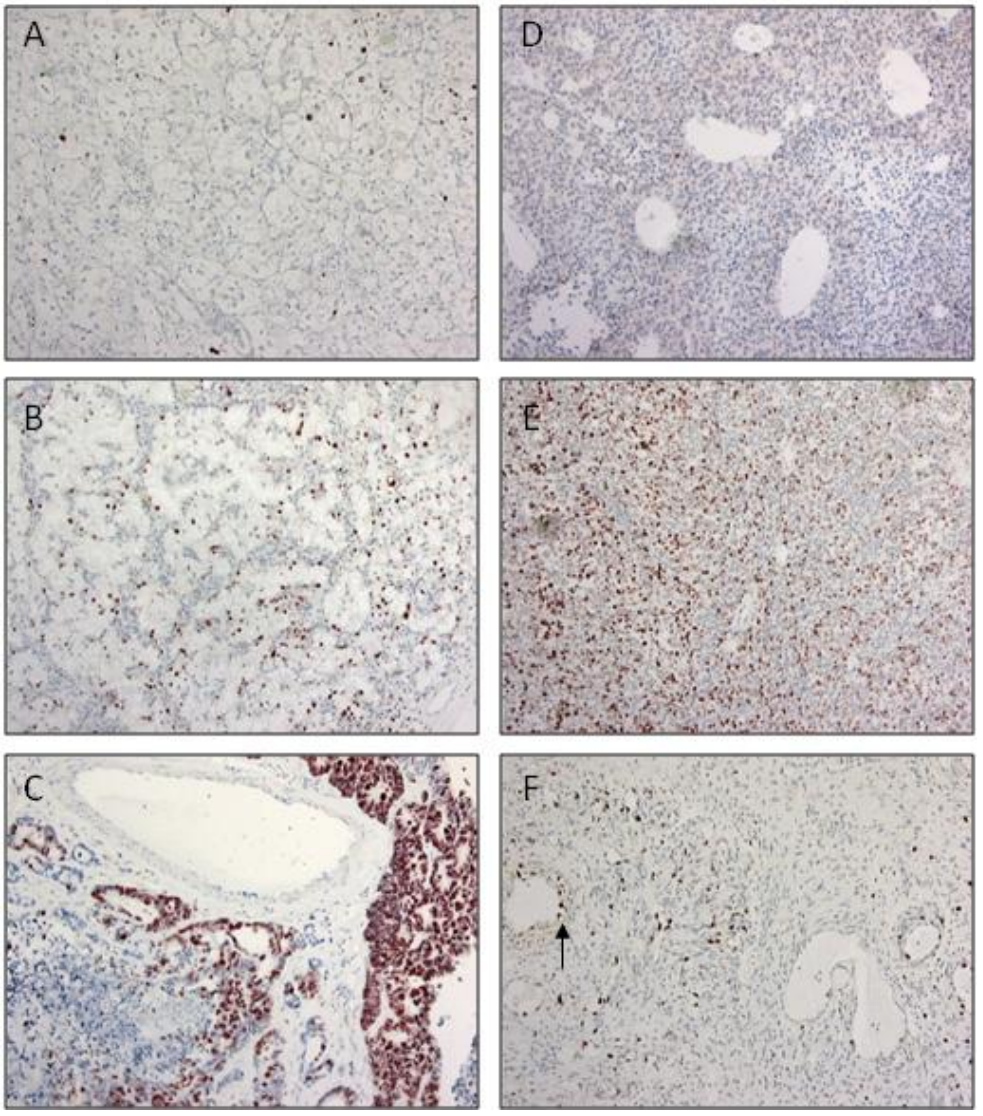

Chapter 2, Figure 5. Proliferation indices of tumors as revealed by MIB-1 staining. Shown are brain metastases of sarcoma (A), renal cell carcinoma (B), adenocarcinoma (C), melanoma (D,E) and a GBM (F).

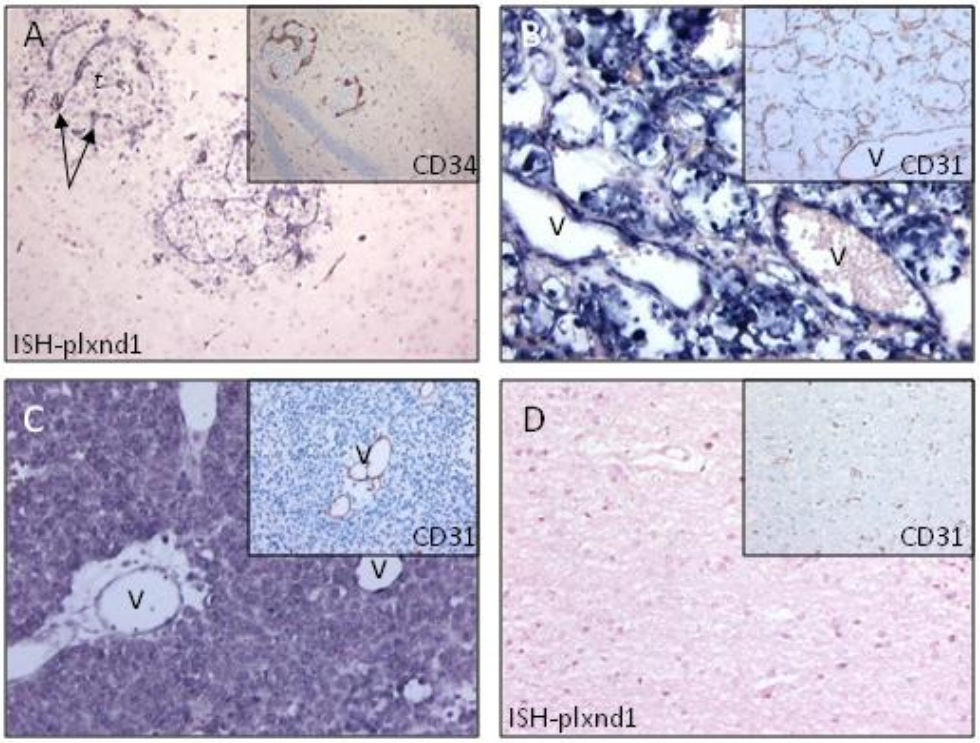

Chapter 3, Figure 1. A) ISH analysis of a cerebral Mel57-VEGF lesion using a mouse-specific *plxnd1* RNA probe. Note the strong positivity of tumor vessels (arrows) whereas brain capillaries, distant from the lesions, are negative (compare the ISH profile with the CD34 staining in the inset). B-D) Human PLXND1-specific ISH analyses of a brain metastasis of sarcoma (B), melanoma (C) and normal brain (D). Insets show CD31 stainings of serial sections. Control ISH using sense probes were negative (not shown). Note in B and C that *PLXND1* expression is not confined to the blood vessels: also in tumor cells high levels of the *PLXND1* transcript are found. *t*=tumor, V=vessel

In normal human brain, no vessel-associated expression of *PLXND1* was detected (Figure 1D). ISH revealed that tumor cells themselves also were often strongly positive for PLXND1 (compare ISH profiles with the CD31 stainings in the insets in Figure 1B and 1C). Also primary brain tumors were found to be positive for *PLXND1* both on blood vessels and tumor cells (not shown).

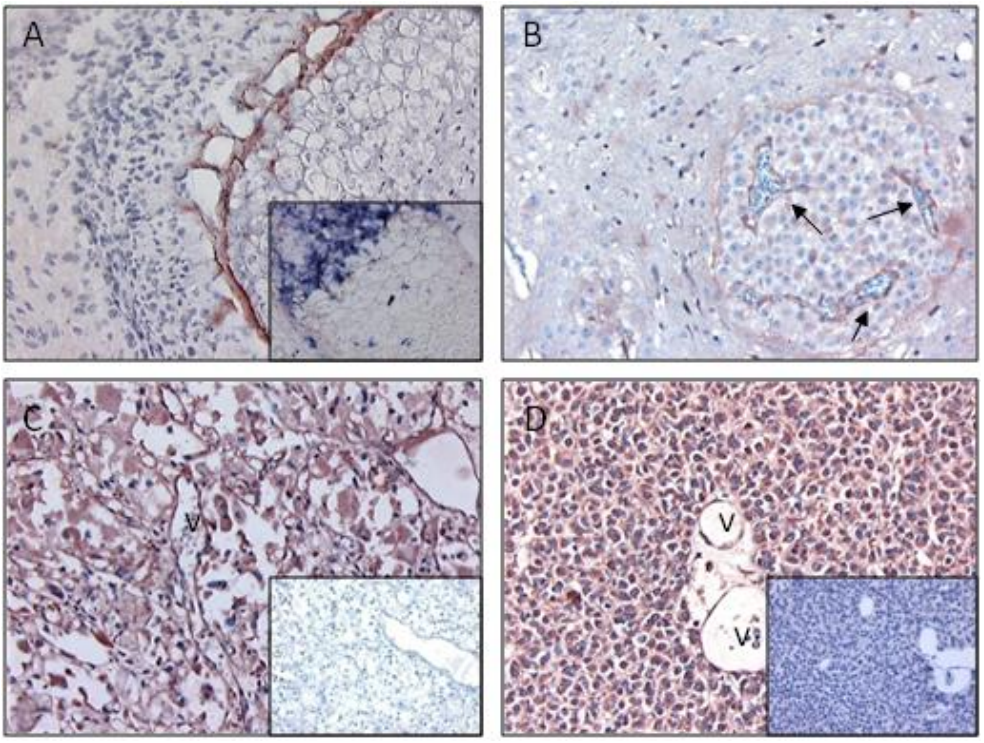

Chapter 3, Figure 3. Immunohistochemistry using sdab A12 and F8. A) Growth plate of a trabecular bone in a mouse embryo (E16.5), stained with sdab A12. Note the immunoreactivity in the blood vessels which is consistent with ISH for *plxnd1* (inset). B) Immunostaining with sdab F8 of a Mel57-VEGF-A_{165} lesion in mouse brain. A similar expression profile is seen as in the ISH depicted in figure 1A. Vessels stain positive (arrows) while tumor cells are moderately positive. C) and D) show immunostainings with sdab A12 of the sarcoma (C) and melanoma (D) brain metastases, of which *PLXND1* ISHs are shown in Figure 1. The insets in C and D show control stainings with anti-VSV antibody only. V=vessel.

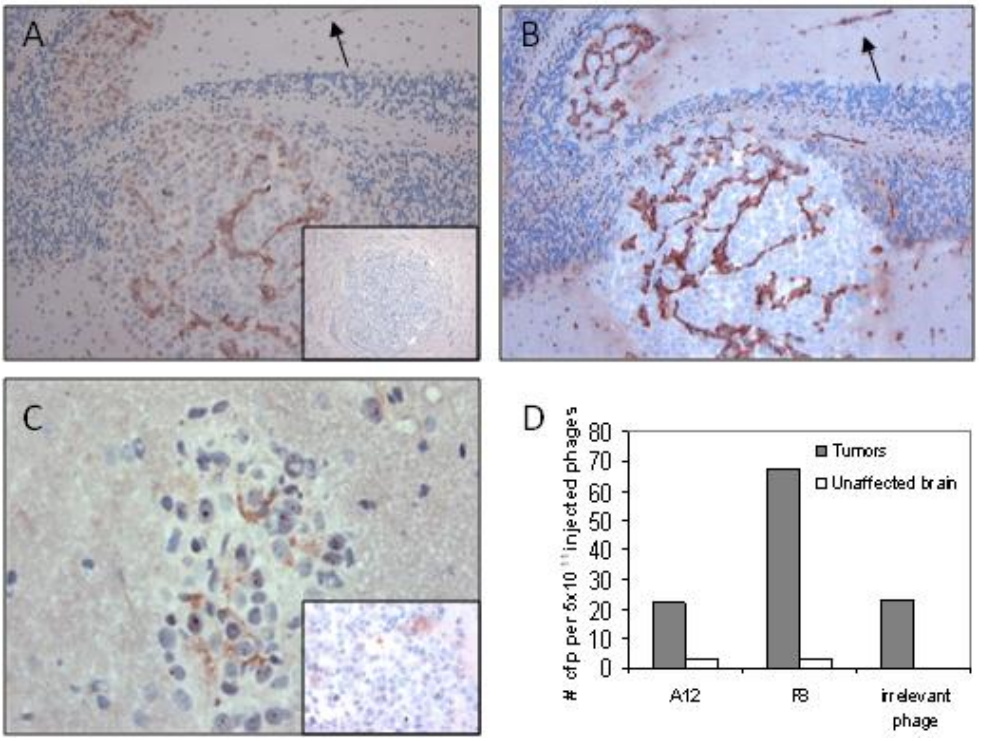

Chapter 3, Figure 4. *In vivo* targeting: homing of phage A12, F8 or an irrelevant phage to Mel57-$VEGF_{165}$ brain lesions. Tumor-bearing mice were injected with 10^{12} phages in the tail vein as described in the text. Mice were sacrificed, brains removed and frozen sections were analyzed for phage content and distribution. A) M13 staining of a frozen section of brain Mel57-$VEGF_{165}$ lesions. Phages are clearly vessel-associated, as evidenced by the anti-CD31 immunostaining on a serial section, shown in B). The arrows point at a CD34-positive vessel, distant from the lesion, which is not highlighted by anti-M13 staining. The inset in (A) shows a control experiment where an irrelevant phage was injected. C) Distribution of sdab F8 after intravenous injection in tumor bearing mice. Sdabs are visualized by immunohistochemistry using an anti-VSV antibody. Note that the sdab is detected in tumor vessels but not in normal brain capillaries. The inset shows the control experiment where an irrelevant sdab was injected. An interstitial localization was observed, consistent with the leaky nature of the vessels in these tumors. D) Quantification of phage homing. Tumor tissue was dissected from 10 µm frozen sections using laser capture dissection microscopy. Number of colony-forming phages (cfp) were counted after infection of TG1 cells. Twenty-fold more F8 phages were eluted from tumors than from comparable areas of unaffected brain tissue.

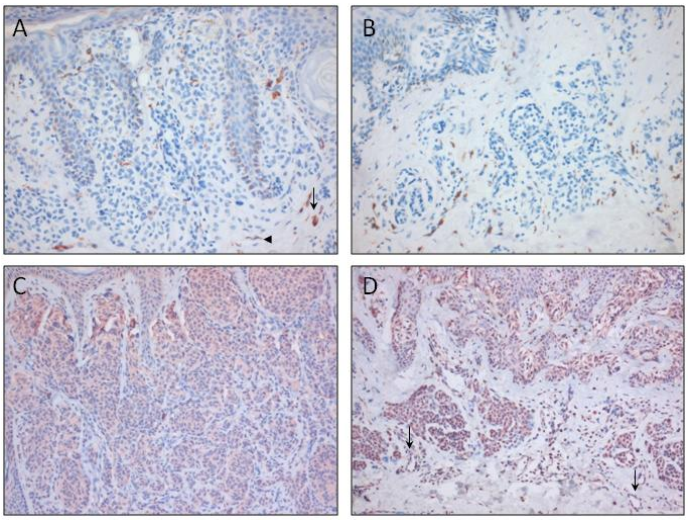

Chapter 4, Figure 1. Immunohistochemical analysis of PLXND1 and Sema3E expression in naevi. PLXND1 is not detected in melanocytes in naevocellular (A) and dysplastic (B) naevi. Note the PLXND1-positivity of macrophage- (arrow in A) and fibroblast-like (arrowhead in A) cells. Melanocytes in naevocellular (C) and dysplastic (D) naevi abundantly express Sema3E. Note that vessels in a dysplastic naevus express Sema3E (arrows in D).

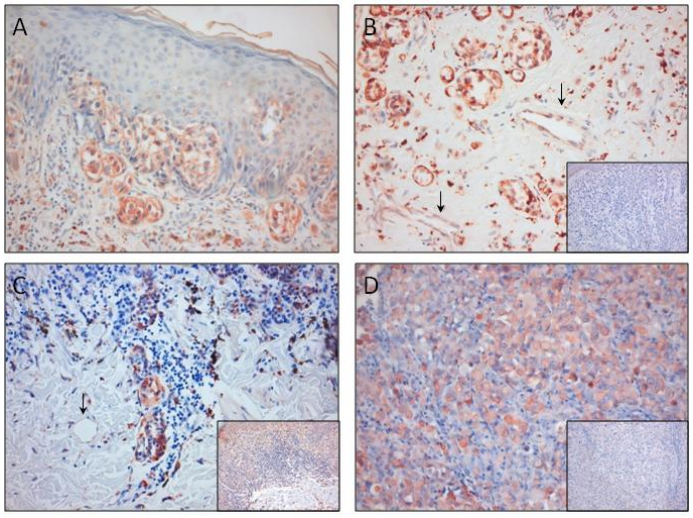

Chapter 4, Figure 2. PLXND1 expression in primary melanomas and a melanoma metastasis as revealed by immunostaining with single domain antibody A12. Shown are PLXND1 positive tumor cells in a Clark II melanoma (A), Clark IV melanomas (B and C) and a lymph node metastasis (D). Note in B that tumor vessels in a melanoma with a Breslow thickness of 3.2 mm express PLXND1 (arrows), while PLXND1 is absent in the vasculature of a Clark IV melanoma with a Breslow thickness of 0.65 mm (arrow in C). The insets in B, C and D show Sema3E staining in a Clark IV melanoma (B), a Clark II melanoma (C) and a lymph node metastasis (D).

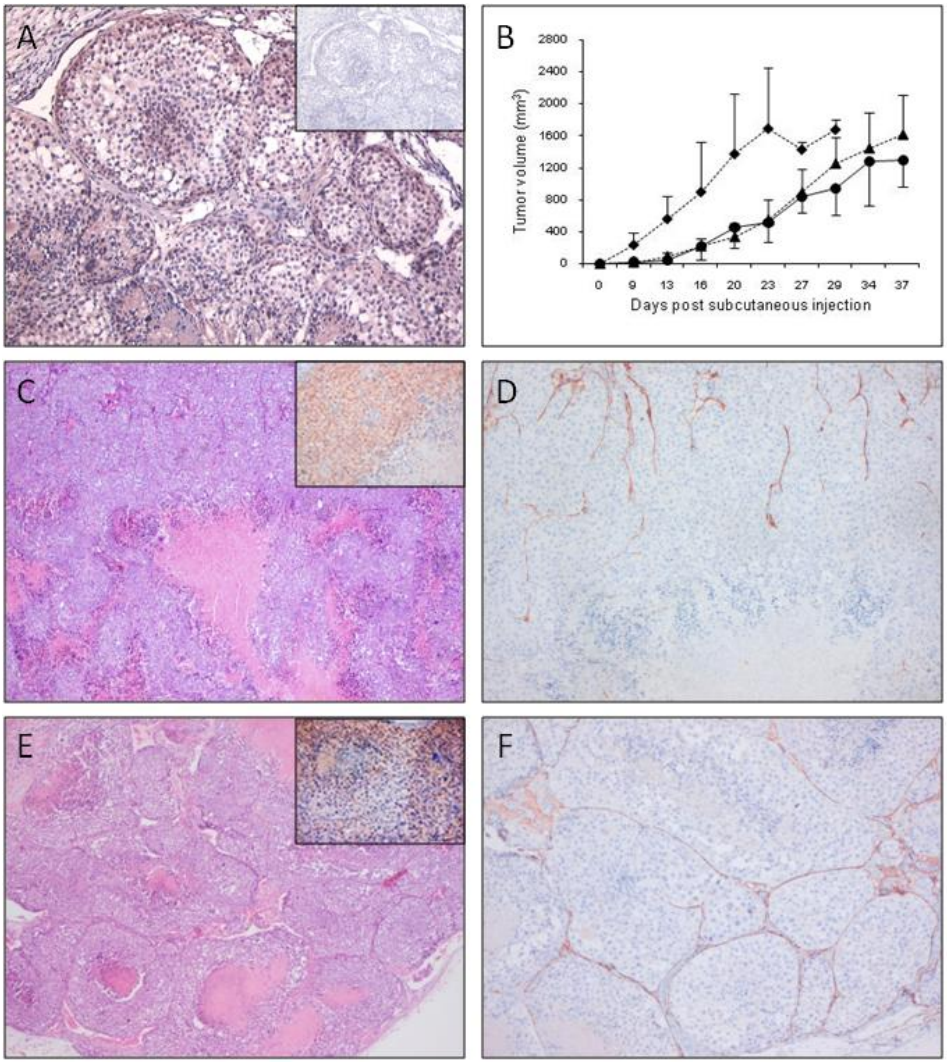

Chapter 4, Figure 3. Analysis of subcutaneous Mel57-VEGF-A xenografts co-expressing Sema3E or Sema3C. A) shows PLXND1 expression in subcutaneous Mel57-VEGF-A xenografts as revealed by immunohistochemistry using single domain antibody A12. Both Mel57-VEGF-A cells and endothelium express PLXND1 (the inset shows a negative control staining with anti-VSV-G antibody). B) Tumor growth curves of Sema3E (●) and Sema3C(▲)-expressing Mel57-VEGF-A xenografts and control Mel57-VEGF-A/EGFP lesions (◆). Tumor volumes are calculated as height x depth x width. Note that the xenografts co-expressing Sema3(C/E) show comparable growth rates. Histological analysis of subcutaneous Mel57-VEGF-A/Sema3E and -/Sema3C tumors by H&E staining (C and E) and anti-CD34 staining (D and F). Note the absence of micronodular transformation in Sema3E-expressing tumors (C and D), while Mel57-VEGF-A/Sema3C xenografts show the typically VEGF-A induced micronodular growth pattern (E and F). In contrast to Mel57-VEGF-A/Sema3C xenografts, Sema3E-expressing tumors only show a well vascularized tumor rim. The insets in C and E show Sema3E and Sema3C immunostainings on Mel57-VEGF-A/Sema3E (C) and -/Sema3C (E) xenografts respectively.

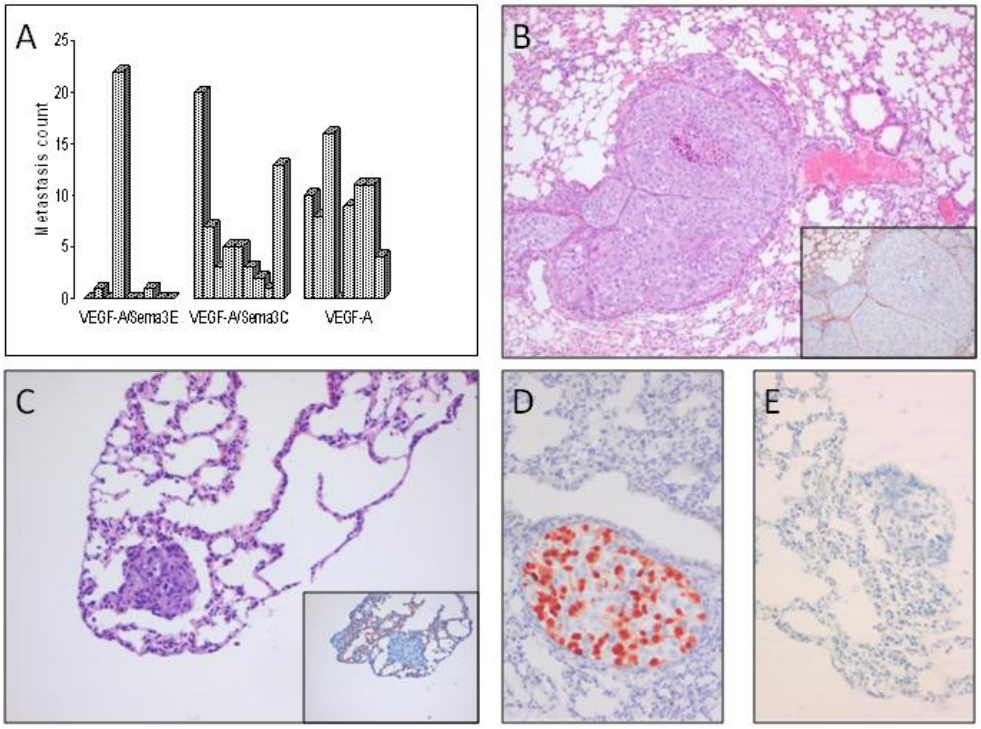

Chapter 4, Figure 4. Analysis of metastatic burden, localization and composition. A) Metastasis count of mice carrying different subcutaneous Mel57-VEGF-A xenografts. Lung lesions were counted after H&E staining. Note that in mice carrying subcutaneous Mel57-VEGF-A/Sema3E xenografts metastatic burden is significantly reduced compared to Mel57-VEGF-A/EGFP (p=0.022) and -/Sema3C tumors (p=0.006). In contrast, metastatic load in mice carrying Sema3C expressing tumors is not significantly different from Mel57-VEGF-A/EGFP xenografts (p=0.289). Histochemical analysis of lung metastases by H&E staining (B and C) and anti-CD34 staining (insets) show that lung metastases derived from Mel57-VEGF-A/Sema3C xenografts (B) are predominantly located in the larger branches of the pulmonary vessels. Note in C that the small lesion in the tip of the lung derived from a Mel57-VEGF-A/Sema3E tumor is not surrounded by endothelial cells (inset in C). EGFP immunostainings on lung metastases derived from Mel57-VEGF-A/Sema3C (D) and -/Sema3E (E) xenografts tagged with EGFP-expressing tumor cells. Note that most lung metatases derived from Mel57-VEGF-A/Sema3C xenografts are of multicellular origin with both Mel57-VEGF-A/Sema3C and Mel57-EGFP cells (D), while the EGFP-negative lung lesion in a mice carrying a subcutaneous Mel57-VEGF-A/Sema3E xenograft likely originates from clonal expansion of a single tumor cell (E).

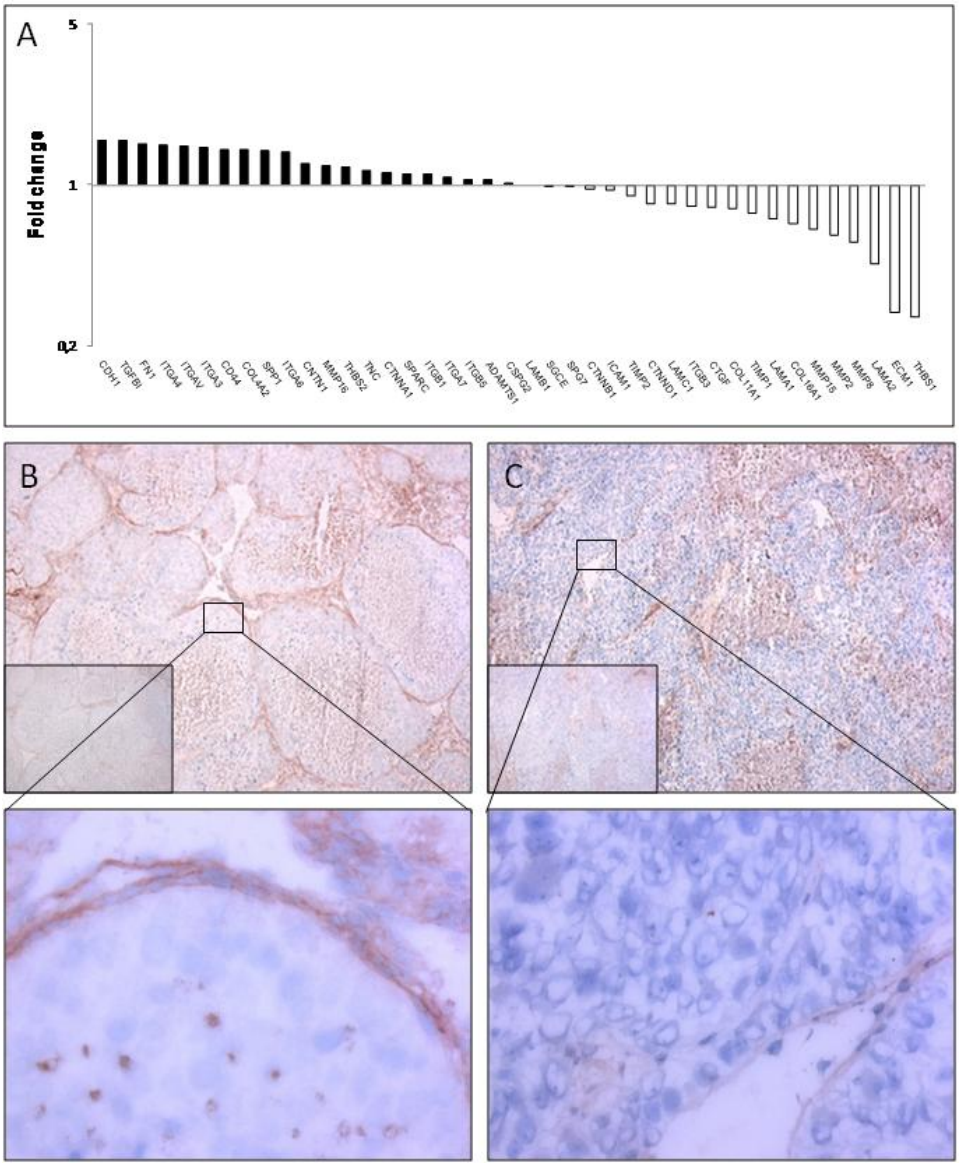

Chapter 4, Figure 5. Fold-changes in mRNA expression of extracellular matrix and adhesion molecules in Sema3E overexpressing tumors relative to the control subcutaneous Mel57-VEGF-A lesions as revealed by RT-PCR array analysis (A). Columns represent fold changes in expression in Sema3E-expressing tumors relative to subcutaneous Mel57-VEGF-A lesions. Upper columns (>1.00) represent molecules whose mRNA expression is up-regulated, lower columns (<1.00) molecules whose expression is down-regulated. Immunohistochemical analysis of THBS expression in subcutaneous Mel57-VEGF-A (B) and Mel57-VEGF-A/Sema3E xenografts (C). In contrast to Mel57-VEGF-A/Sema3E lesions THBS is abundantly expressed in Mel57-VEGF-A tumors (the insets show negative control stainings with anti-mouse antibody). Note in B that THBS expression is clearly associated with the network of vessel wall elements and tumor cells.

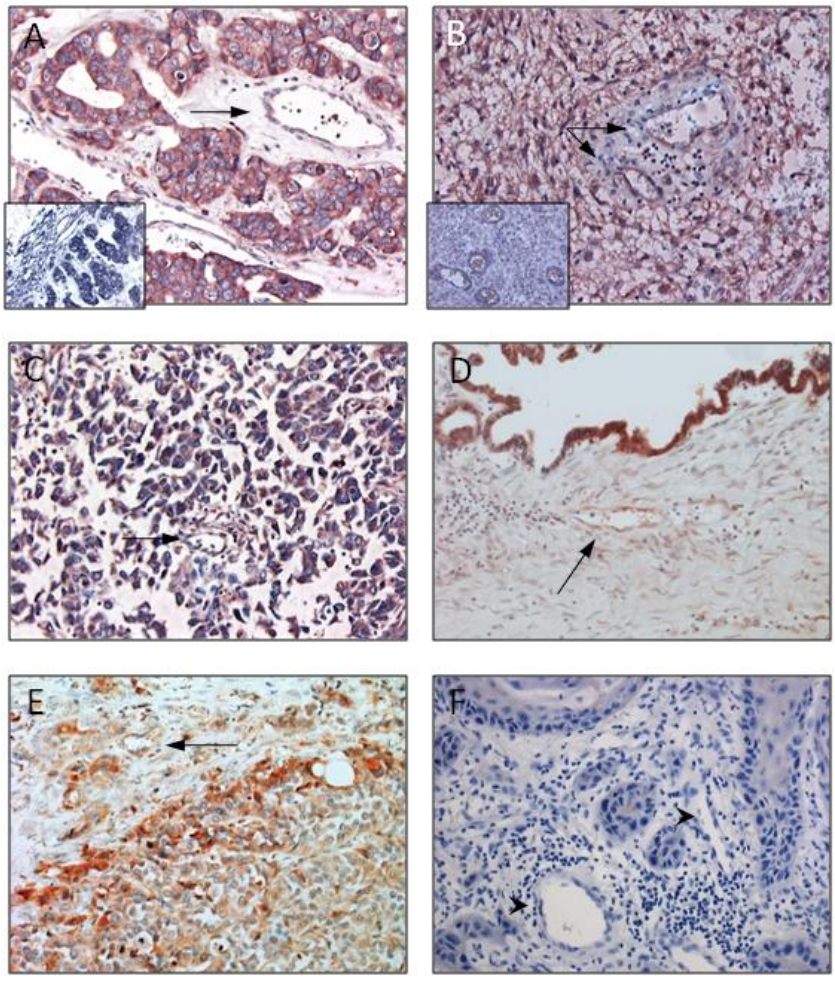

Chapter 5, Figure 1. Immunohistochemical analysis of PLXND1 expression in representative clinical tumor samples. PLXND1 is abundantly expressed in adenocarcinoma brain metastases (A), glioblastomas multiforme (B), neuro-endocrine lung tumors (C), an ovarian adenocarcinoma (D), and prostatic urothelial cell carcinomas (E). The arrows point at PLXND1-positive vasculature. PLXND1 is absent in both tumor vasculature (arrowheads) and tumor cells in vulvar squamous cell carcinomas (F). The insets in A and B show corresponding PLXND1 mRNA *in situ* hybridization analyses.

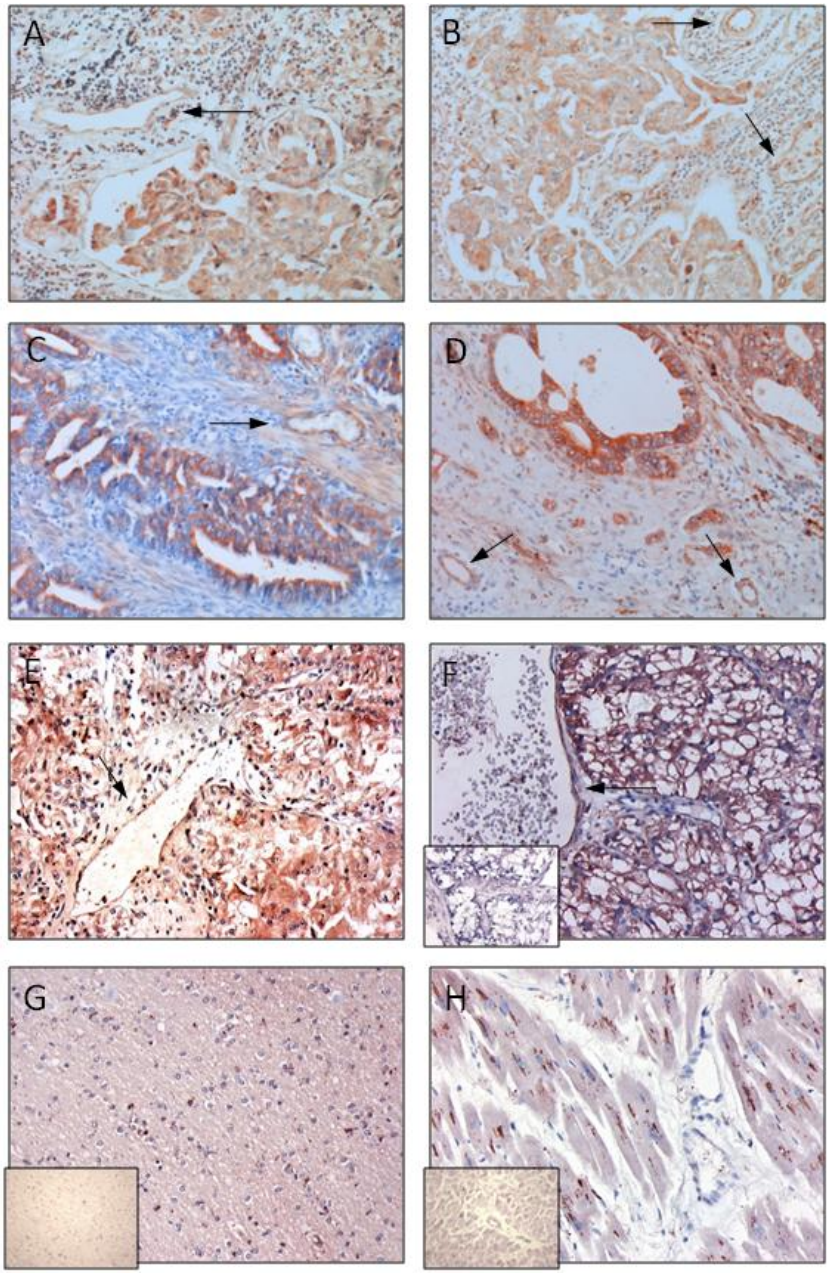

Chapter 5, Figure 2. Immunohistochemical analysis of PLXND1 expression in representative clinical tumor samples. PLXND1 is expressed at high levels in primary ductal breast carcinomas (A) and corresponding lymph node metastases (B), colon adenocarcinomas (C) and corresponding liver metastases (D) and a renal cell carcinoma (E) and corresponding brain metastasis (F). The arrows point at PLXND1-expressing tumor vessels. PLXND1 is not detected in normal human cerebral cortex (G) and heart (H) tissue samples. The insets in F, G and H show corresponding PLXND1 mRNA *in situ* hybridization analyses.

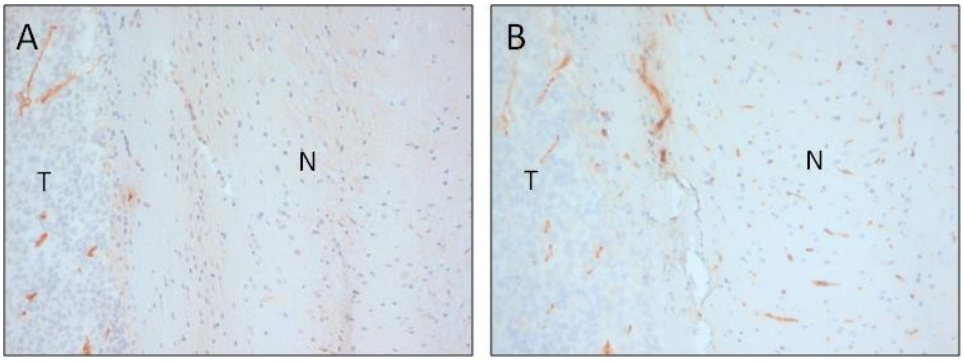

Chapter 6, Figure 1. Phage distribution in orthotopic glioma xenografts after *in vivo* biopanning. Procedures are described in Materials and Methods. After sacrifice, brains were removed and serial frozen sections of E98 glioma xenografts were analyzed for phage distribution by anti-M13 (A) or anti-CD31 (B) immunostaining. Note that phages are clearly more associated with tumor vasculature than normal vessels. N=normal, T=tumor

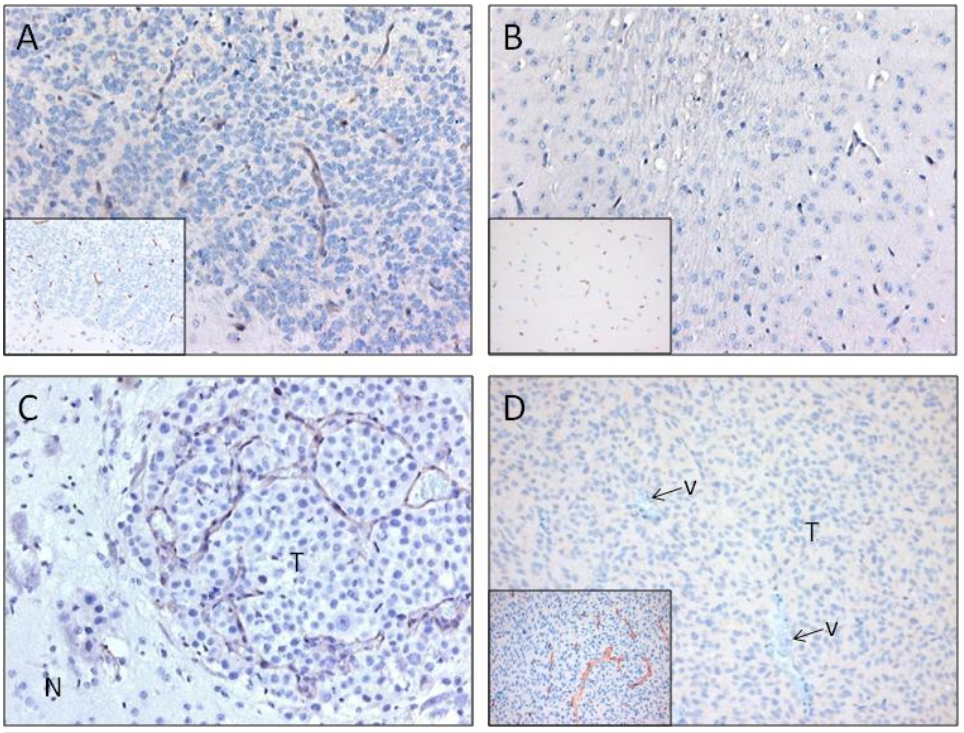

Chapter 6, Figure 2. Immunohistochemical analysis of nanobody C-C7 reactivity in cerebral E98 xenografts (A), unaffected mouse brain parenchyma (B), a brain metastasis of Mel57-$VEGF_{165}$ melanoma (C) and a cerebral U87 xenograft (D). C-C7 recognizes subsets of tumor vessels in both diffuse infiltrative E98 tumor, while normal mouse brain vessels and the vasculature of intracerebral U87 glioma are negative. Insets in A, B and D show CD34 immunostainings of serial sections. N=normal, T=tumor, V=vessel.

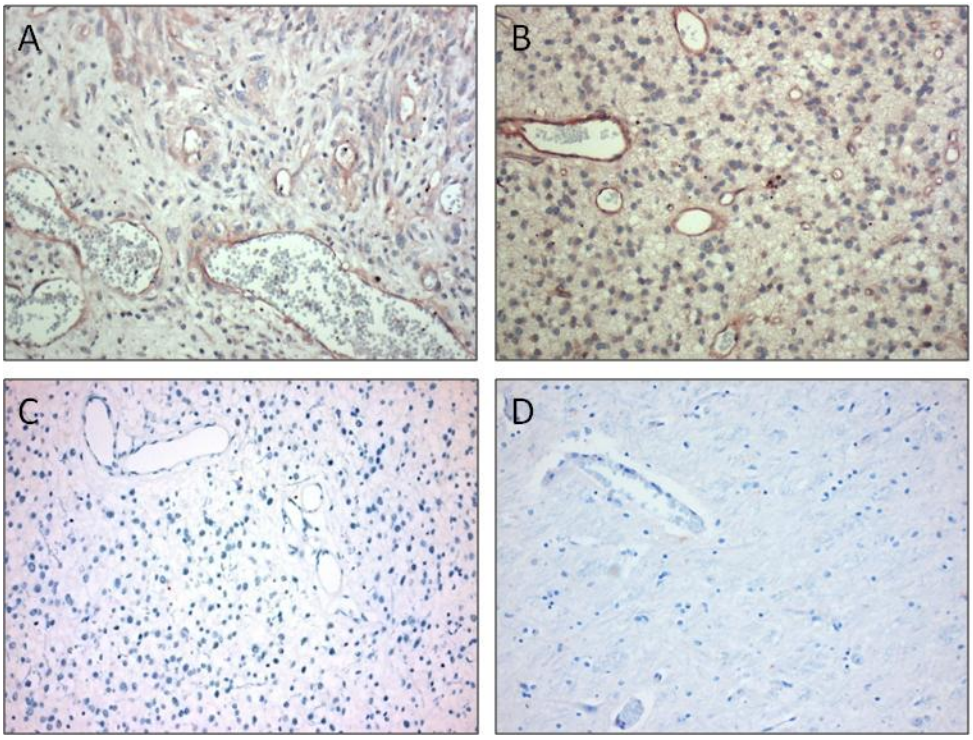

Chapter 6, Figure 3. C-C7 also recognizes human tumor blood vessels. Shown are immunostaining with nanobody C-C7 of human GBM (A), low grade glioma (B,C) and normal brain (D). Subsets of vessels are strongly positive for C-C7 (A-B), while C-C7 reactivity is absent in the vasculature of a low grade glioma (C) and normal brain endothelium (D).

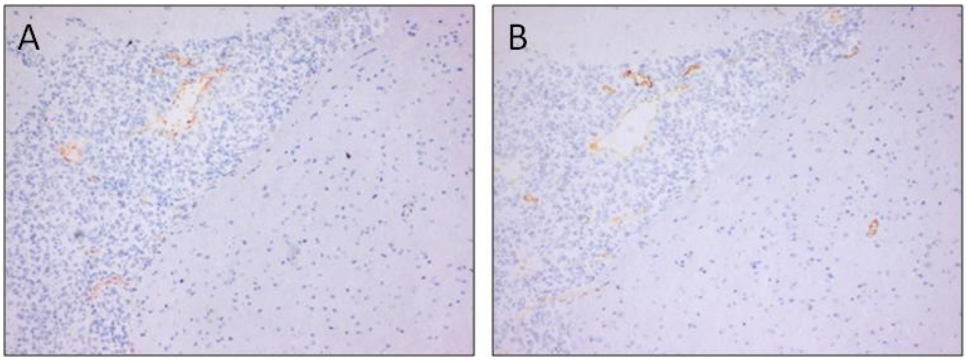

Chapter 6, Figure 4. *In vivo* targeting of phages displaying C-C7 to cerebral E98 xenografts. Monoclonal C-C7 phages were injected in mice with orthotopic E98 xenografts and phage distribution analyzed by M13 staining after cardiac perfusion. (A) Frozen brain sections stained for M13 phages. Phages displaying C-C7 home to a subset of tumor vessels in E98 xenografts, but not to normal brain vessels, as evidenced by the anti-CD31 immunostaining on a serial section (B).

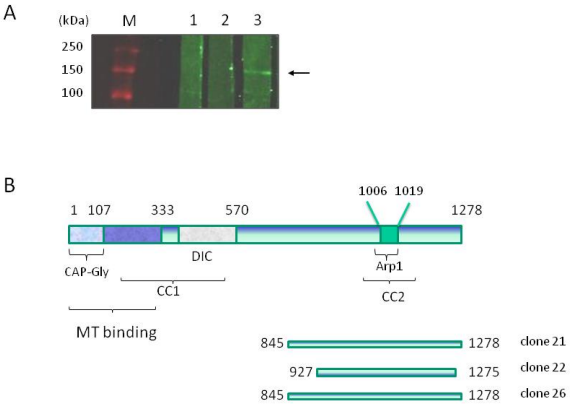

Chapter 6, Figure 5. Identification of dynactin-1 p150^{glued} as the C-C7 ligand. A) Western blot analysis of GP8 cell extract with C-C7. Nanobody C-C7 (lane 3) but not two irrelevant single domain antibodies (lanes 1 and 2) recognizes an endothelial protein of approximately 150 kDa (arrow). B) Structural domains in p150^{glued} and recognized domains of C-C7. The aminoterminal domains contain a CAP-Gly domain and and a coiled-coil domain which are responsible for microtubule (MT) binding and dynein binding (DIC=dynein intermediate chain). A second coiled-coil domain, encompassing a binding site for Arp1, is present in the carboxyterminal part of the protein and mediates binding to membrane components.

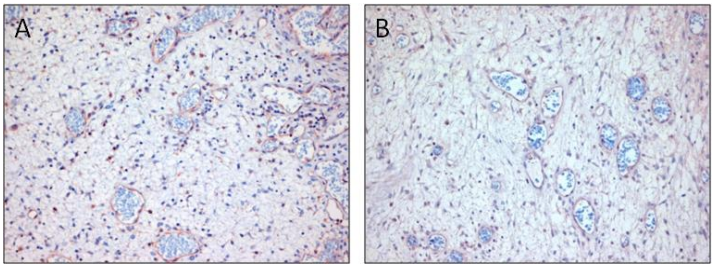

Chapter 6, Figure 6. Comparative immunohistochemistry with a commercial anti-dynactin-1-p150^{glued} antibody (A) and C-C7 (B) on serial sections of a high grade glioma. Note that both antibodies react similarly in these tissues. Control stainings were negative (not shown).

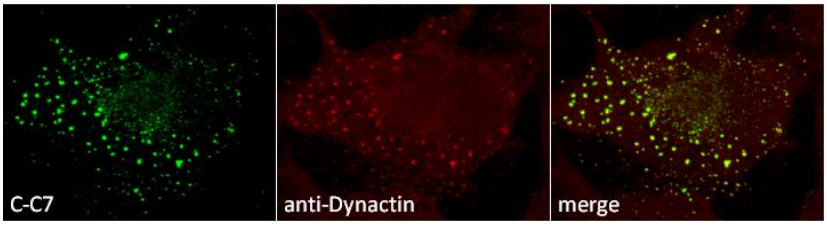

Chapter 6, Figure 7. Immunolocalization of the carboxyterminal domain of dynactin-1-p150^{glued} in transfected COS-1 cells, as illustrated by costaining with C-C7 (green) and commercial anti-dynactin (red). Cells were transiently transfected with p3xflg-CMV-dyn-2532-3837 and analysed two days later with a confocal microscope. Both antibodies colocalize as shown in the merged figure.

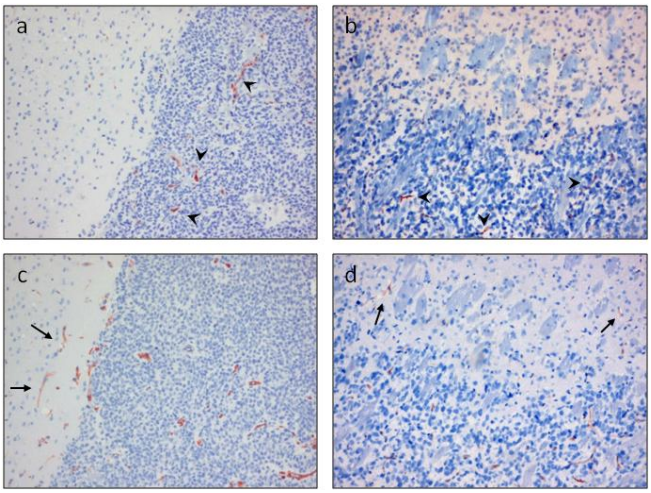

Chapter 7, Figure 1. Phage distribution in cerebral glioma xenografts after *in vivo* biopanning of an immune Llama phage library. Paraffin-embedded sections of E98 (a) and E434 (b) xenografts were analyzed for phage localization by M13 immunostainings. As evidenced by anti-CD34 immunostainings on serial sections of E98 (c) and E434 (d) xenografts phages are clearly associated with the tumor vasculature (arrowheads in figure 1a and 1b), whereas vessels in unaffected brain parenchyma are not highlighted by anti-M13 staining (arrows in figure 1c and 1d). Note the CD34 up-regulation on tumor-associated endothelial cells compared to normal brain capillaries (c and d).

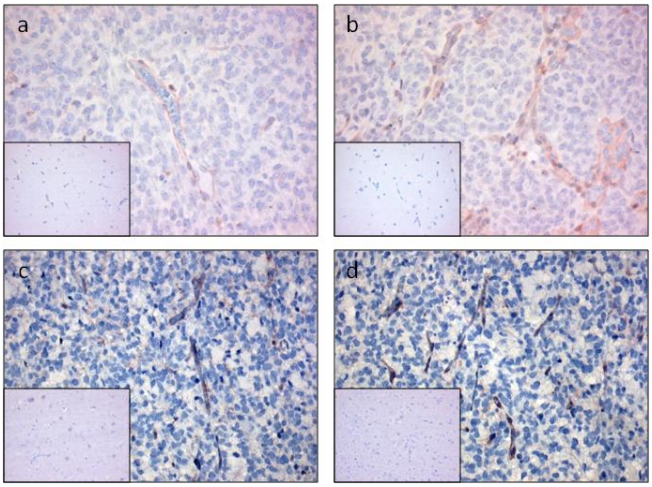

Chapter 7, Figure 2. Immunohistochemical analysis of the reactivity of selected nanobodies in glioma xenografts. Clones obtained from group A (a) and D (b) are representative for nanobodies which specifically recognized subsets of glioma vessels in immunostainings on paraffin-embedded sections of E98 xenografts. Nanobodies produced by clones from group IX (c) and VIII (d) demonstrate representative immunoreactivity on E434 vasculature. Note the absence of immunoreactivity on vessels in unaffected brain areas (insets).